

**Impact of deglacial and Holocene AMOC changes on the
mixed layer and deepwater hydrography of the subtropical
North Atlantic**

Dissertation zur Erlangung des Doktorgrades
der Mathematisch-Naturwissenschaftlichen Fakultät
der Christian-Albrechts-Universität zu Kiel

**vorgelegt von
Janne Repschläger
Kiel, Juli 2013**

1. Gutachterin und Betreuerin:

PD Dr. Mara Weinelt

2. Gutachter:

Prof. Dr. Ralph Schneider

Tag der Disputation:

28.08.2013

Zum Druck genehmigt:

03.08.2014

Der Dekan:

Prof. Dr. Wolfgang J. Duschl

Erklärung

Hiermit erkläre ich von Eides statt, dass die vorliegende Arbeit, abgesehen von der Beratung durch meine akademischen Lehrer, in Inhalt und Form meine eigene Arbeit darstellt. Ferner habe ich weder diese noch eine ähnliche Arbeit an einer anderen Hochschule im Rahmen eines Prüfungsverfahrens vorgelegt. Diese Arbeit ist unter Einhaltung der Regeln guter wissenschaftlicher Praxis der Deutschen Forschungsgemeinschaft entstanden.

Kiel, den 18.07.2013

Janne Repschläger

Abstract

The Atlantic meridional overturning circulation (AMOC) transports warm saline water from low to high northern latitudes where it cools, sinks down and returns southward as deepwater flow. By the heat transfer from low to high latitudes, AMOC contributes in balancing the global energy budget and thus is an important part of global climate system.

Within this study the impact of AMOC changes on surface and deepwater hydrography of the subtropical North Atlantic is investigated by the use of high-resolution sediment cores from a coring site located south of the Azores at the eastern flank of the Mid Atlantic Ridge. The Azores coring site is situated in the subtropical eastern North Atlantic (NA) at the boundary between warm Subtropical Gyre Water (STG) and temperate East North Atlantic Water (ENAW) at the surface. At depth the site is located at the interface between southern sourced Lower Deep Water (LDW) and North East Atlantic Deep Water (NEADW) that consists of a mixture of northern sourced Iceland-Scotland Overflow Water (ISOW) and Labrador Sea Water (LSW). Due to its location at water mass boundaries the coring position is ideal to reconstruct coupled surface and deepwater changes. Deglacial records in centennial to decadal resolution of changes in the mixed layer and the deepwater are established.

Multiproxy sea surface temperature (SST) reconstructions using Mg/Ca surface of planktonic surface and subsurface dwelling foraminifera, the alkenone undersaturation index U_{37}^K and foraminifera transfer function (SIMMAX) are used to gain a reliable deglacial SST records from the subtropical NA and to decipher environmental imprints other than temperature on SST reconstructions. The combination of these SST records with stable oxygen isotope records ($\delta^{18}\text{O}$) from planktonic surface and subsurface dwelling foraminifera are used to derive changes in the mixed layer salinity ($^{18}\text{O}_{\text{w-ice}}$). Additionally, variations in the STG position are reconstructed by the use of foraminifera abundance data. Deglacial changes in deepwater composition are traced by its ventilation, temperature and salinity by the coupled use of stable isotope ($\delta^{18}\text{O}$ and $\delta^{13}\text{C}$) and Mg/Ca bottom water temperature (BWT) reconstructions from benthic foraminifera.

This new data indicates that the position of the NA subtropical Gyre (STG) was coupled with AMOC strength over the last deglaciation and the early to mid Holocene (16 -7 ka BP). During cold deglacial and Holocene weak AMOC phases (Heinrich event 1 (H1), Younger Dryas (YD), Preboreal and 8.2 event) the STG was displaced southward. This STG displacement most probably was driven by meltwater that reached southward to the Azores coring site (38°N) as indicated by salinity reconstructions ($^{18}\text{O}_{\text{w-ice}}$) that indicate at least a salinity decrease of 1‰ Standard Mean Ocean Water (SMOW) for the H1 and 8.2 events. Additionally a southward extension of temperate ENAW led to a SST cooling of 4.5-6°C in comparison to modern values. On the contrary the presence of relatively warm subsurface water (14°C) during the YD might indicate subsurface heat storage during this event.

The new high-resolution BWT, ventilation and $\delta^{18}\text{O}_{\text{w-ice}}$ record from the subtropical eastern NA indicates that the deepwater composition in the eastern North Atlantic basin changed over the last 15 ka BP in parallel to deglacial changes in surface water hydrography. A general evolution toward a warmer better ventilated deepwater was disrupted during the H1 event, the YD and the early Holocene by a less ventilated ($\delta^{13}\text{C}$ values between 0-0.5‰), cool (1.5°C minimum BWT) and freshened water (0.5 ‰ $\delta^{18}\text{O}_{\text{w-ice}}$ depletion). The parallel evolution of BWT, $\delta^{13}\text{C}$ and $\delta^{18}\text{O}_{\text{w-ice}}$ with changes in deep- and surface water compositions in the subpolar NA and with the Greenland ice core record NGRIP indicates that variations in deepwater composition over the last 15 ka BP were triggered by high northern latitude climatic processes. This new results contradict the idea that southern sourced deepwater entered the subpolar NA during cold events. In consequence the new results would imply that the NA changes contributed even to deglacial changes in the Antarctic bottom water composition and finally had an impact on changes in the deepwater stratification mode as is discussed in a new conceptual model.

Zusammenfassung

Die meridionale Umwälzkirkulation im Atlantik (engl. AMOC) transportiert warmes und salzreiches Wasser aus den Tropen in die hohen nördlichen Breiten, wo es abkühlt, absinkt und als Tiefenwasser in den Süden zurück fließt. Durch den Wärmetransport von niedrigen zu hohen Breiten trägt die AMOC zum Erhalt des globalen Energiehaushalts bei und ist daher ein wichtiger Bestandteil des globalen Klimasystems.

Diese Studie befasst sich mit dem Einfluss von AMOC- Veränderungen auf die Oberflächen- und Tiefenwasser Hydrographie des subtropischen Nordatlantiks. Diese Veränderungen werden anhand von hochauflösenden Zeitreihen von Sedimentkernen rekonstruiert. Die Sedimentkerne stammen von einer Kernposition südlich der Azoren an der östlichen Flanke des Mittelatlantischen Rückens. Die Oberflächenwasserzirkulation in diesem Teil des subtropischen östlichen Nordatlantik (NA) wird von der warmen subtropischen Gyre (STG) bestimmt, die im Norden von gemäßigttem Ost-Nordatlantik Wasser (engl. ENAW) begrenzt wird. Die Kernposition liegt an der Grenze dieser zwei Wassermassen. An der Azoren Kernposition treffen zwei Tiefenwassermassen aufeinander, Unteren Tiefenwasser (engl. LDW), welches im südlichen subpolaren Atlantik gebildet wird und das Nord-Ostatlantische Tiefenwasser (engl. NEADW). Letzteres wird im subpolaren Nordatlantik gebildet und besteht aus der Mischung zwei weiterer Wassermassen, dem Island-Schottland „Overflow“ Wasser (engl. ISOW) und dem Labrador Seewasser (engl. LSW).

Aufgrund der Position an den Grenzen der Oberflächen- und Tiefenwassermassen ist die Azoren Kernposition ideal dazu geeignet gekoppelte Deckschicht- und Tiefenwasser- Veränderungen zu rekonstruieren. Diese Veränderungen werden mit Hilfe von Datensätzen mit zehn- bis hundertjähriger Auflösung untersucht.

Veränderungen der Deckschichttemperatur werden mit Hilfe verschiedener Proxies, der Foraminiferentransferfunktionen (SIMMAX), dem Alkenonuntersättigungs- Index $U^{K'}_{37}$ sowie Mg/Ca Messungen an den Gehäusen von Oberflächen- und Zwischenwasser bewohnenden planktischen Foraminiferen rekonstruiert. Der Vergleich dieser verschiedenen Proxy- Temperaturen wird dazu genutzt, potentielle Überprägungen des Temperaturdatensatzes zu erkennen und somit eine verlässliche Temperaturrekonstruktion aus dem subtropischen Nordatlantik über das letzte Deglazial zu erhalten. Des weiteren wurden stabilen Sauerstoffisotopenwerten ($\delta^{18}O$) an den Gehäusen von Oberflächen- und Zwischenwasser bewohnenden planktischen Foraminiferen gemessenen. Die Kombination der Temperaturrekonstruktionen mit den stabilen Sauerstoffisotopenwerten ($\delta^{18}O$) wird dazu genutzt Veränderungen im Salzgehalt ($^{18}O_{w-ice}$) der Wassermassen zu rekonstruieren. Zusätzlich werden Veränderungen der STG Position mit Hilfe der Häufigkeitsverteilungen planktonischer Foraminiferen rekonstruiert.

Die Änderungen in der Tiefenwasserzusammensetzung im Deglazial wurden durch Ventilations-, Temperatur- und Salinitätsrekonstruktionen mit Hilfe von stabilen Isotopen ($\delta^{18}\text{O}$ and $\delta^{13}\text{C}$) und Mg/Ca Bodenwassertemperatur Rekonstruktionen an benthischen Foraminiferen nachverfolgt.

Diese neuen Daten zeigen, eine Kopplung zwischen der Position der NA subtropischen Gyre (STG) und der AMOC Stärke im Deglazials und dem frühen bis mittleren Holozän (16 -7 ka BP). In deglaziale Kaltphasen (Heinrich Ereignis 1, Jüngere Dryas, Präboreal und 8.2 Ereignis), in denen AMOC schwach war, verschob sich der Nordrand der STG südwärts. Salzgehaltsabnahmen von 1‰ SMOW, die für das Heinrich 1 und 8.2 Ereignis rekonstruiert wurden, deuten darauf hin, dass diese Verschiebung der STG durch Schmelzwasser verursacht wurden, welches sich bis zur Azoren Kernposition (38°N) ausdehnte. Ein gleichzeitiges Vordringen von temperiertem ENAW führte zu einer Abkühlung des Oberflächenwassers an der heute subtropischen Position von 4.5-6°C gegenüber heutigen Werten. Im Gegensatz dazu deuten relativ stabile Zwischenwassertemperaturen in der Jüngeren Dryas auf eine Wärmespeicherung im Zwischenwasser hin.

Neue Tiefenwassertemperatur, -ventilations- und $\delta^{18}\text{O}_w$ Daten in zehn- bis hundertjähriger Auflösung aus dem östlichen subpolaren NA zeigen, dass sich die Tiefenwasserzusammensetzung im östlichen NA Becken während der letzten 15 000 Jahre verändert hat. Diese Veränderung ereigneten sich gleichzeitig mit den Veränderungen in der Oberflächenwasserhydrografie. Während dem Deglazial erwärmte sich das Tiefenwasser und die Tiefenwasserventilation verbesserte sich. Diese generelle Evolution zu einem wärmeren, besser ventilerten Tiefenwasser wurde durch das Vordringen von schlechter ventilertem ($\delta^{13}\text{C}$ Werte zwischen 0-0.5‰), kühlerem (Minimalwert für BWT 1.5°C) und weniger salzreichem Wasser (‰ $\delta^{18}\text{O}_{w\text{-Eis}}$ Abnahme) während des H1 Ereignis, der YD und dem frühen Holozän unterbrochen. Die parallele Evolution von BWT, $\delta^{13}\text{C}$ und $\delta^{18}\text{O}_{w\text{-Eis}}$ an den Azoren mit Veränderungen im Tiefen –und Oberflächenwasser im subpolaren NA deuten darauf hin, dass die Veränderungen in der Tiefenwasserzusammensetzung über die letzten 15 000 Jahre von klimatischen Prozessen in den hohen nördlichen Breiten gesteuert wurden. Diese neuen Ergebnisse widersprechen der Annahme, dass in Kaltphasen AABW bis in den subpolaren NA vordrang. Eine Konsequenz dieser Ergebnisse wäre, dass Veränderungen im NA auch zu deglazialen Veränderungen des Antarktischen Bodenwassers beitragen und somit zu Änderungen in der atlantischen Tiefenwasserstratifizierung führen könnten. Dieser Zusammenhang wird mit Hilfe eines neuen Begriffmodells diskutiert.

Danksagung

So ganz alleine schreibt niemand...

Mara Weinelt danke ich herzlich für die Vergabe Betreuung der Arbeit. Ihre zahlreichen Anregungen und Korrekturen haben zum Erfolg dieser Arbeit beigetragen. Des Weiteren ermöglichten ihre aufwendigen Zählungen der Foraminiferenvergesellschaftungen eine erweiterte Diskussion meiner Ergebnisse.

Ralph Schneider möchte ich für die Bereitstellung des Arbeitsplatzes und die Übernahme der Endkorrekturen und des Zweitgutachtens danken.

Hanno Kinkel danke ich für seine konstruktiven Beiträge zur Interpretation und Darstellung der Ergebnisse. Prof. Dr. M. Sarnthein eröffnete mir mit seinem Enthusiasmus und Diskussionen immer wieder die Schönheit der Wissenschaft.

Meinem "Mitbewohner" Christian Schwab danke ich für die zahlreichen Diskussionen und das Korrekturlesen.

Ein ganz herzlicher Dank geht an die Techniker und Laborleiter, die an der Messung der Daten maßgeblich beteiligt waren: Dr. Thomas Blanz für die Messung der Alkenone; Nils Andersen für die Isotopenmessungen; Karin Kissling, Sabine Lange, Karen Bremer, Ulrike Westernstroer und Dieter Garbe Schönberg für die Messung der Mg/Ca Proben; Rik Tjallingii für die Einführung in die Welt des XRF Scannens.

Meinen Hiwis Julie Schindelbeck, Ines Irion, Gitta von Rönn und Oliver Mautner danke ich für ihre Hilfe bei der Beprobung der Sedimentkerne und der Probenaufbereitung.

Ich möchte mich ganz herzlich bei allen ehemaligen und derzeitigen Mitarbeitern der Arbeitsgruppe Marine Klimaforschung and der CAU für ihre Unterstützung danken. Insbesondere danke ich Uta Krebs-Kanzow für Bereitstellung der Modellierungsdaten und die Diskussionen über AMOC Variabilität. Sven Balmer danke ich für die zusätzlichen Isotopendaten. Guillaume Leduc danke ich für zahlreiche Diskussionen über den derzeitigen Stand der Forschung. Marcus Regenberd danke ich für gemeinsame Arbeit im Mg/Ca Labor und zahlreiche Diskussionen über Mg/Ca Messungen und Korrektur lesen. Seine ruhige, gelassene Art hat mir sehr geholfen.

Bernard Danielou vom Ifremer danke ich für die Bereitstellung der GEOFAR KF16 Proben.

Die hier präsentierten Ergebnisse stammen teilweise von Kernen, die an Bord der R.V. Marion Dufresne (French Polar Institute, IPEV) während der IMAGES-AMOCINT MD168-Expedition im Rahmen des 06-EuroMARC-FP-006 Project entnommen wurden. Ich danke dem Kapitän, der Crew und den Kollegen an Bord für ihre Hilfe. Dieses Projekt wurde von der European Science Foundation (ESF) im EUROCORES Programm EuroMARC, mit der Projektnummer No. ERAS-

CT-2003-980409 der Europäischen Kommission, gefördert. Für diese Förderung und finanzielle Unterstützung des Projektes bedanke ich mich bei der DFG.

Beim Gleichstellungsbüro der CAU bedanke ich mich für die unkomplizierte und prompte Bereitstellung von Mitteln zur Beendigung dieser Dissertation.

Für die moralische Unterstützung und zahlreiche angeregte Gespräche über Vereinbarkeit von Familie und Wissenschaft danke ich Friedericke, Uta K., Katharina, Ina, Christiane und Andrea.

Des Weiteren möchte ich mich ganz herzlich beim Team der Kita Olshausenstrasse für die hervorragende Kinderbetreuung bedanken die eine Grundvoraussetzung für das Gelingen dieser Arbeit war. Ebenso danke ich den Hardenbergzwerge und unseren Babysittern Mathilde und Julie.

... außerdem bedanke ich mich ganz herzlich bei meiner Familie, die so manche schlechte Laune und lange Arbeitstage geduldig ertragen hat.

Content

1	Introduction	1
1.1	The Atlantic Meridional Overturning circulation	3
1.2	The interaction between global climate change and AMOC	4
1.3	Objectives and Approach of this thesis	8
1.4	Modern hydrography of the North Atlantic and Azores region	9
1.4.1	NA Surface water currents	9
1.4.2	Surface water hydrography of the coring site	11
1.4.3	NA Deep water currents	12
1.4.4	Deepwater hydrography in the Azores region	12
1.5	References	13
1.6	Thesis Outline	19
2	Material and Methods	21
2.1	Coring site and Cores	23
2.2	XRF core scanning	26
2.3	Core sampling and sample preparation	27
2.4	Stable isotope analyses	27
2.4.1	Sample preparation and measurement	27
2.4.2	Correction of $\delta^{18}\text{O}$ values for vital effects	28
2.5	Abundance of selected foraminifera and its use in water mass reconstruction	31
2.5.1	Habitat preferences of selected planktonic foraminifera species	31
2.6	SST reconstructions	34
2.6.1	SST reconstructions using Modern Analogue Technique SIMMAX	34
2.6.2	SST reconstructions using the Alkenone undersaturation index U^K_{37}	35
2.6.3	Water temperature reconstructions using Mg/Ca in planktonic foraminifera (<i>G. ruber w.</i> and <i>G. bulloides</i> and <i>G. truncatulinoides</i>)	36
2.6.4	Mg/Ca calibrations for planktonic foraminifera	37
2.7	BWT reconstructions using Mg/Ca in benthic foraminifera	39
2.7.1	Mg/Ca calibrations for benthic foraminifera	39
	$\delta^{18}\text{O}_{\text{w-ice}}$ reconstructions	41
2.8	References	41
3	Age Model	45
3.1	References	49
4	Disentangling multiproxy temperature reconstructions in the subtropical North Atlantic	51
4.1	Introduction	53
4.2	Hydrology	55
4.3	Material and Methods	56
4.4	Results	57

4.5 Discussion	60
4.5.1 Differences between SIMMAX SST and $U^{K_{37}}$ temperatures.....	61
4.5.2 Differences in reconstructed SST during cold events.....	61
4.5.3 Younger Dryas subsurface influence on the SIMMAX SST record.....	66
4.5.4 Comparison of the strong deglacial cold events with the Preboreal “flickering” phase.....	67
4.5.5 Influence of SST on derived salinity reconstructions.....	68
4.6 Summary and Conclusion	69
4.7 References	70
5 Response of the subtropical North Atlantic surface hydrography on Deglacial and Holocene AMOC changes	73
Key points	75
5.1 Abstract	75
5.2 Introduction	75
5.3 Oceanographic setting and study location	78
5.4 Material and methods	80
5.4.1 Coring site and cores.....	80
5.4.2 Sample preparation.....	81
5.4.3 Stable isotope analyses.....	81
5.4.4 Temperature reconstructions.....	82
5.4.5 Foraminifera assemblages	83
5.4.6 $\delta^{18}O_{\text{water}}$ reconstructions	83
5.5 Age model	84
5.6 Results	85
5.7 Discussion	91
5.7.1 Deglacial evolution of AMOC state and its coupling with subtropical gyre position	91
5.7.2 The influence of subpolar meltwater on the Azores coring site	92
5.7.3 Bølling/Allerød heat storage.....	94
5.7.4 Subtropical subsurface heat storage and AMOC resumption during YD	96
5.8 Summary and conclusion	100
5.9 Acknowledgements	100
5.10 References	101
6 Coccolithophore paleoproductivity and ecology response to deglacial and Holocene changes in the Azores Current System	107
6.1 Comment on Chapter 6	127
7 Deglacial and early Holocene evolution of deepwater composition in the Eastern North Atlantic Basin	129
7.1 Key points	131
7.2 Abstract	131
7.3 Introduction	132
7.4 Approach	134

7.5	Hydrographic Setting	135
7.6	Material and Methods	137
7.6.1	Material	137
7.6.2	Methods.....	137
7.6.3	Stable isotopes	137
7.6.4	Mg/Ca BWT reconstructions	138
7.6.5	Calibration and error assessment	138
7.6.6	Possible overprint by carbonate ion concentration	138
7.6.7	$\delta^{18}\text{O}_w$ reconstructions	139
7.7	Results	139
7.8	Discussion	141
7.8.1	Deglacial deepwater composition and distribution changes.....	141
7.9	NADW freshening as a driver for deglacial AABW composition changes	146
7.10	Holocene instabilities in the deepwater composition	148
7.11	Conclusion	149
7.12	Acknowledgements	150
7.13	References	150
7.14	Supplementary information	153
7.14.1	Calibration of benthic Mg/Ca data.....	153
7.14.2	Potential overprint by carbon ion saturation.....	155
7.14.3	Potential overprinted of $\delta^{13}\text{C}$ signals by productivity changes.....	156
7.14.4	References.....	157
8	Summary and conclusion	159
8.1	Multiproxy temperature reconstructions	161
8.2	Coupled AMOC and surface water hydrography evolution over Holocene and deglacial 162	
8.3	Deglacial deepwater composition changes	162
9	Outlook	163
9.1	The 6.5 ka BP event – a “new” Holocene cold event?.....	165
9.2	Core MD08-3181- a midocean sediment core with decadal resolution?.....	167
10	Appendix	169

List of figures

Figure 1.1 The Global Ocean Conveyor belt	3
Figure 1.2 Deglacial climate records from the NA	5
Figure 1.3 Hydrographic overview of the NA surface water currents	9
Figure 1.4 The global wind patterns [picture from NASA Earth Observatory]	11
Figure 1.5 Hydrographic overview of the NA deep water currents	13
Figure 2.1 Bathymetric map of the coring area with the coring site	23
Figure 2.2 Sample preparations for foraminifera analyses	27
Figure 2.4 Modern distribution patterns of common planktonic foraminifera species in the NA using the dataset of <i>Pflaumann et al.</i> [1996]	32
Figure 2.3 Cleaning protocol for Mg/Ca analyses	37
Figure 3.1 Age model for cores GEOFAR KF16 and MD08-3180	47
Figure 3.2 Comparison between <i>G. ruber</i> w. abundance data and Greenland ice core data	48
Figure 3.3 Comparison between benthic $\delta^{13}\text{C}$ records	49
Figure 4.1 Comparison of SST reconstructions as based on different proxies over the last deglacial	58
Figure 4.2 Relative abundance records of subtropical species	59
Figure 4.3 Model output from KCM	65
Figure 4.4. Model output from KCM	65
Figure 4.5 Comparison between SIMMAX su SST and the relative abundance of <i>N. pachyderma d.</i>	67
Figure 4.6 Comparison between different $\delta^{18}\text{O}_{\text{sw-ice}}$ reconstructions	68
Figure 5.1 Modern surface water hydrography of the NA	79
Figure 5.2 Age model for cores GEOFAR KF16 and MD08-3180	85
Figure 5.3 Overview over the results from stacked cores GEOFAR KF16 and MD08-3180,	87
Figure 5.4 Deglacial and Holocene foraminiferal fauna abundances of selected foraminifera species from the Azores coring site and core SU90-03 [Chapman et al., 2000]	88
Figure 5.5 Comparison of SST records from the NA region	93
Figure 5.6 Conceptual model for the deglacial changes (from bottom to top) of the subtropical gyre position and heat storage patterns	98
Figure 7.1 Overview of the modern deepwater hydrography at the Azores coring site	136
Figure 7.2 Results	140
Figure 7.3 Comparison between the benthic marine records and ice core records	142
Figure 7.4 five deglacial time slices showing $\delta^{18}\text{O}/\delta^{13}\text{C}$ cross plots comparing cores GEOFAR KF16/MD08-3180 from the Azores coring site with cores obtained from the eastern Atlantic basin	143
Figure 7.5 Influence of brine water on deglacial deepwater evolution	144
Figure 7.6 Comparison between the deglacial benthic $\delta^{18}\text{O}$ records	147
Figure 7.S1 multispecies benthic Mg/Ca BWT records using different calibrations	154
Figure 7.S2 Comparison of benthic BWT and $\delta^{13}\text{C}$ records from our coring site with NA $[\text{CO}_3]^{2-}$ records [Yu et al., 2008] from site BOFS10K at 2777 m water depth (red line) and BOFS 8K at 4045 m water depth.	155
Figure 7.S3 Possible overprint Comparison of the benthic foraminifera $\delta^{13}\text{C}$ record with by productivity changes	156
Figure 7.S4 versus δ^{13} (Ba/Ti) cross plot	157
Figure 9.1 Various surface and deepwater records indicating the 6.5 ka BP event	166

List of tables

Table 2.1 Cores used in this study	24
Table 2.2 a analysed parameters and analyse intervals	24
Table 2.2 b analysed parameters and analyse intervals	25
Table 2.3 Elements measured with the XRF core scanner and its detection limits	26
Table 2.4 sample size and fraction prepared for stable isotope and Mg/Ca analyses	28
Table 2.5 Offsets between different planktonic species	29
Table 2.6 Offsets between different benthic species	30
Table 2.7 Mg/Ca calibrations for planktonic foraminifera used in this study	38
Table 2.8 Mg/Ca calibrations for reductive cleaned benthic foraminifera used in this study.....	40
Table 2.9 Offsets between Mg/Ca ratios obtained from parallel measurements of different benthic species.....	41
Table 4.1 Overview of habitat preferences of planktonic foraminifera used as indicator species in this study	55
Table 5.1 Different Mg/Ca calibrations for planktonic foraminifera	82
Table 7.1: modern Atlantic water mass properties	135

List of abbreviations

AABW	Antarctic Bottom Water
AC	Azores current
AF	Azores front
BA	Bølling-Allerød
BWT	Bottom Water Temperature
DSOW	Denmark-Strait Overflow Water
ENAB	Eastern North Atlantic Basin
ENACW	East North Atlantic Central Water
H1	Heinrich event 1
IACP	Inter Allerød Cold Period
IBCP	Inter Bølling Cold Period
ISOW	Iceland Scotland-Overflow Water
LDW	Lower Deep Water
LGM	Last Glacial Maximum
LSW	Labrador Sea Water
MAR	Mid Atlantic Ridge
MOW	Mediterranean Overflow Water
NA	North Atlantic
NADW	North Atlantic Deep Water
NEADW	North East Atlantic Deep Water
NH	Northern Hemisphere
OD	Older Dryas
PB	Preboreal
PBO	Preboreal Oscillation
SST	Sea Surface Temperature
SST _{su}	SIMMAX summer Sea Surface Temperature
SST _{wi}	SIMMAX winter Sea Surface Temperature
YD	Younger Dryas
$\delta^{18}\text{O}$	$\delta^{18}\text{O}$ of foraminifera calcite
$\delta^{18}\text{O}_w$	temperature corrected $\delta^{18}\text{O}$ value
$\delta^{18}\text{O}_{w\text{-ice}}$	temperature and ice volume corrected $\delta^{18}\text{O}$

Chapter 1

Introduction

1 Introduction

1.1 The Atlantic Meridional Overturning circulation

The oceans have a strong influence on the global climate as its huge heat capacity allows them to store, to transport and to redistribute heat and to exchange heat, moisture and momentum with the atmosphere. The oceans transport and redistribute heat through the global conveyor belt, a global network of warm and surface and cold intermediate and deepwater currents [e.g. *Broecker et al.*, 1990; *Rahmsdorf*, 2002] (Figure 1.1).

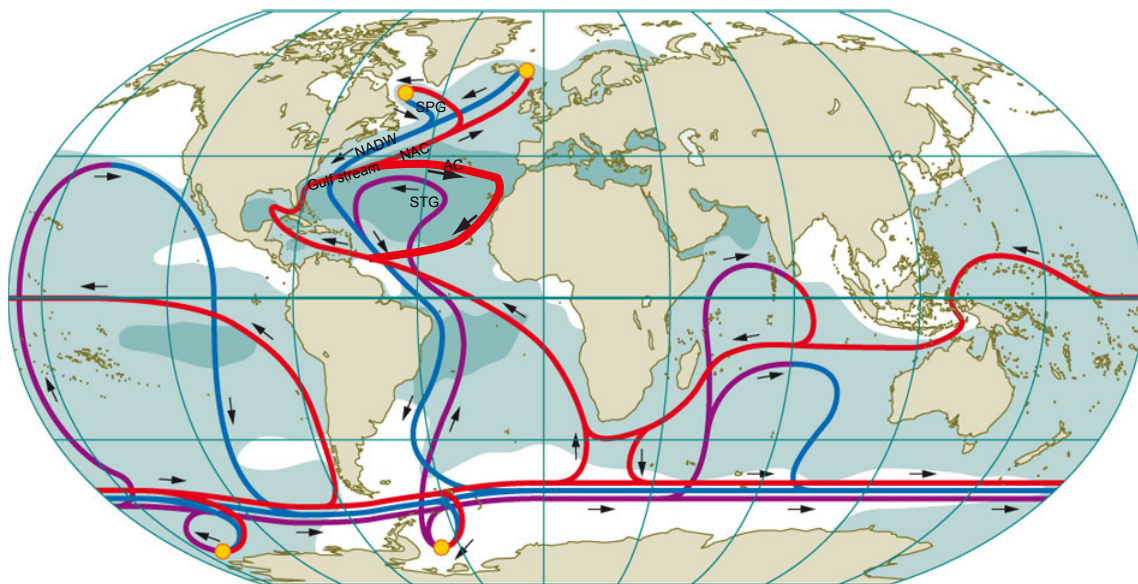


Figure 1.1 The Global Ocean Conveyor belt

Schematic picture of the global conveyor belt and AMOC modified after *Rahmsdorf* [2002] warm surface currents are shown in red, cold intermediate (violet) and deepwater (blue) and , subpolar deepwater convection sites are indicated with yellow circles.

One of the main drivers of the global conveyor belt is the Atlantic Meridional Overturning Circulation (AMOC). In the North Atlantic (NA) AMOC transports warm and highly saline surface water from the subtropics to convection sites in the subpolar NA. There, the water gains density by cooling and evaporation, sinks down to form the North Atlantic Deepwater (NADW) that flows back southwards as a deepwater return flow. As the density gain of the surface water depends on the water temperature and salinity, the NADW formation is highly sensitive to changes in the heat exchange between surface water and atmosphere and the freshwater budget at the deepwater convection sites. A reduced heat flux and freshening at the convection sites lead to a weakening of AMOC that is associated with a cooling of the subpolar NA [*Bailey et al.*, 2005; *Kageyama et al.*, 2010; *Liu et al.*, 2009; *Otto-Bliesner and Brady*, 2010] and a heat storage within the tropical NA [e.g. *Lea et al.*, 2003; *Rühlemann et al.*, 1999] which extension into the subtropics is still unknown.

1.2 The interaction between global climate change and AMOC

In connection to the recent global warming, a freshening of the NA has been observed [e.g. *Curry et al.*, 2003; *Karcher et al.*, 2011]. Modeling studies [e.g. *Gregory et al.*, 2005; *Jansen et al.*, 2007] predict that a further increase of atmospheric greenhouse gas concentrations over the next century will lead to further warming of another 4-5°C. This warming includes a warming of the NA surface water and further melting of the Greenland ice sheet, increasing the freshwater content at the NA deepwater convection sites and subsequently weakening the AMOC. The exact rate of AMOC reduction and NA temperature increase and its impact on the subtropical NA, however, differ significantly among different climate models and thus are still intensively debated and subject to large uncertainties [*Jansen et al.*, 2007]. Climate models can be improved by comparison with paleoceanographic proxy data. Therefore phases of severe climatic change, as marking the transition from the last glacial to the current interglacial, can be used to identify driving components on long-term climate changes and responses in the AMOC system to climatic perturbations. Research on interglacial climate variability on the other hand, can help us to disentangle the effect of the recent anthropogenic climate change from natural climate variability. The understanding of the impact of climatic perturbations on the subtropical NA and its interaction with AMOC changes is sparse, due to low sedimentation rates within this region. Hence, the purpose of this study is to reconstruct changes in AMOC and the surface water hydrology of the subtropical NA over the last deglaciation and the Holocene.

The last deglaciation lasted from 19 to 10.5 ka BP and comprises an 8.5 ka period of the transition between the cold last glacial into the warm modern interglacial (Holocene) time. In general the last deglaciation is associated with a warming of the Northern Hemisphere and the adjacent oceans. This general warming trend was interrupted by several drawbacks to more glacial conditions that have been defined as cold events in the Greenland ice core record [*Andersen et al.*, 2006; *Steffensen et al.*, 2008; *Svensson et al.*, 2008] and in terrestrial records (Appendix table 1) and are also evident in high-resolution time series of climate proxy data from marine archives [e.g. *Bard et al.*, 2000; *Benway et al.*, 2010; *Duplessy et al.*, 1992; *Peck et al.*, 2008; *Sarnthein et al.*, 1995; *Thornalley et al.*, 2011a] (Figure 1.2).

To explain the deglacial and early Holocene evolution of climate change several hypotheses have been developed including short-term and longer-term forcing and feedback mechanisms. The deglacial warming is thought to be driven by changes in the Earth orbital parameters [*Berger et al.*, 2006; *Lisiecki and Raymo*, 2005], which control the net income of solar radiation (insolation) on the Earth's surface. The Northern Hemisphere summer insolation started to increase at 19 ka BP and reached its maximum at 10 ka BP [*Berger et al.*, 2006; *Clark et al.*, 2009]. The insolation changes were amplified by various feedback mechanisms including changes in vegetation, atmospheric aerosol and greenhouse gas content, sea ice extent and ice sheets, as well as atmospheric and ocean

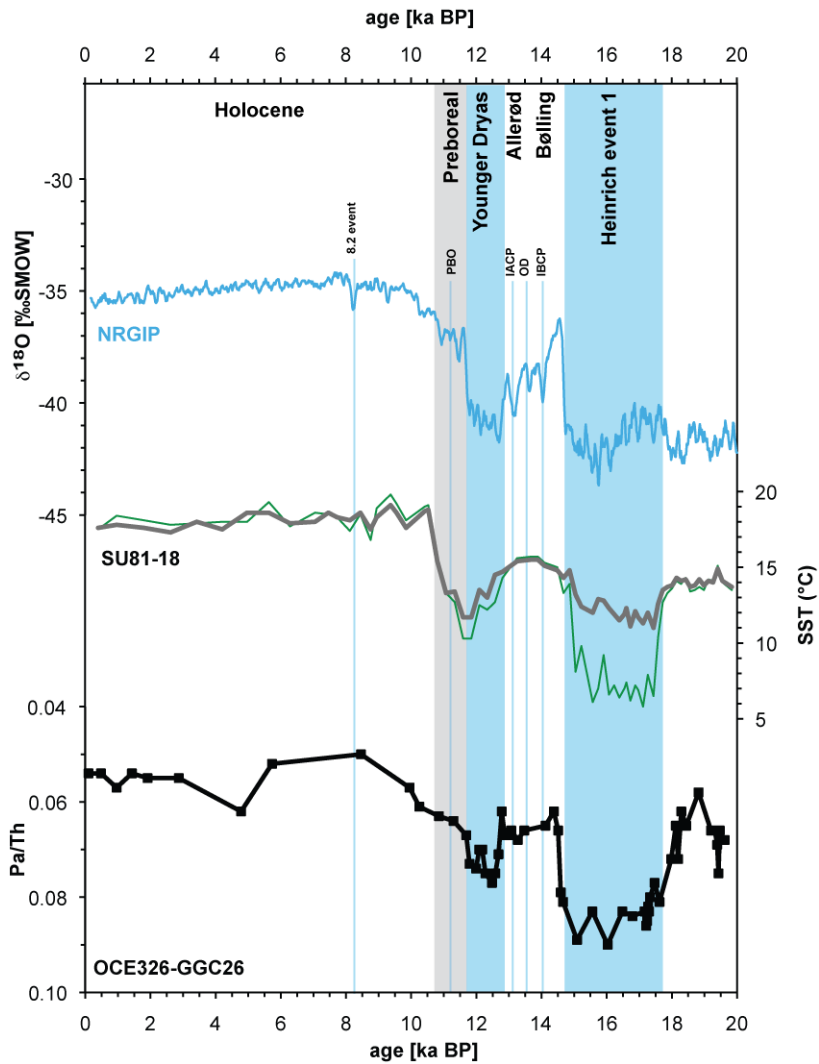


Figure 1.2 Deglacial climate records from the NA

Showing the succession of the deglacial warming and deepwater reorganization in the Greenland ice core record (blue) [Andersen *et al.*, 2006], temperature reconstruction using the alkenone understuation index U^{K}_{37} (green) [Schwab *et al.*, 2012] and U^{K}_{37} (grey) from the Iberian Margin sediment core SU81-18 [Bard *et al.*, 2000] and the reconstructions of the AMOC rate by the kinematic proxy Pa/Th ratios, obtained from sediment core OCE326-GGC28 from the Bermuda rise [McManus *et al.*, 2004]

circulation changes [e.g. Allen *et al.*, 2011; Alley and Clark, 1999; Clark *et al.*, 1999; Manabe and Stouffer, 1997; Shakun and Carlson, 2010].

The ocean circulation during the last deglaciation is characterized by a strengthening and deepening of AMOC [Barker *et al.*, 2010; Came *et al.*, 2008; Gherardi *et al.*, 2005; Gherardi *et al.*, 2009; Labeyrie *et al.*, 2005; McManus *et al.*, 2004; Sarnthein *et al.*, 1994; Thornalley *et al.*, 2011a; Thornalley *et al.*, 2011b; Waelbroeck *et al.*, 2011], that was coupled with a surface warming in the NA. This warming led to the Bølling-Allerød (BA) warm period (14.65-12.65 ka BP) [Lowe *et al.*, 2008; Yu and Eicher, 2001] and the in north Europe termed [Björck *et al.*, 1996] Preboreal warming (PB) (11.6-10.5 ka BP) [e.g. Aagaard-Sørensen *et al.*, 2010; Björck and Wastegård, 1999; Björck *et al.*, 1996; Bos *et al.*, 2007; Fisher *et al.*, 2002; Hald *et al.*, 2007; Kobashi *et al.*, 2008] that ended

with the warm Holocene optimum that began at 10.5 ka BP and was followed by the late Holocene warm climate.

The warming subsequently induced a melting of the vast continental ice sheets that covered the Northern Hemisphere during the last glacial [Clark *et al.*, 2009; Björck *et al.*, 1998; Björck *et al.*, 1996; Bodén *et al.*, 1997; Carlson *et al.*, 2008b; Duplessy *et al.*, 1981]. The resulting huge amount of meltwater temporarily flushed the NA via different pathways e.g. the Mackenzie Valley, Hudson, St. Lawrence and Mississippi river [Aharon, 2003; Bond *et al.*, 1992; Carlson *et al.*, 2008b; Obbink *et al.*, 2010; Teller, 1995; Teller *et al.*, 2002; Thornalley *et al.*, 2010]. In the subpolar NA the freshwater lens capped the surface and prevented deepwater convection and leading to a weakening of AMOC and caused well known deglacial cold events that are the cold Heinrich event 1 (H1) (17.9-14.9 ka BP) [Stanford *et al.*, 2011]; three major cold interruptions during the warm BA, termed the Inter Bølling Cold Period (IBCP), the Older Dryas (OD) and the Inter Allerød Cold Period (IACP) [Lowe *et al.*, 2008; Yu and Eicher, 2001] (for age boundaries see Appendix table 1) as well as the cool Preboreal Oscillation (PO) [e.g. Aagaard-Sørensen *et al.*, 2010; Björck and Wastegård, 1999; Björck *et al.*, 1996; Bos *et al.*, 2007; Fisher *et al.*, 2002; Hald *et al.*, 2007; Kobashi *et al.*, 2008] and the early to mid-Holocene interglacial variability [Andersson *et al.*, 2010; Calvo *et al.*, 2002; Came *et al.*, 2007; Giraudeau *et al.*, 2010; Hald *et al.*, 2007; Jansen *et al.*, 2009; Marchal *et al.*, 2002; Moros *et al.*, 2006] with the cold 8.2 event being the most pronounced [e.g. Daley *et al.*, 2011; Keigwin *et al.*, 2005; Kleiven *et al.*, 2008].

The ultimate trigger for AMOC reduction, that caused the Younger Dryas (YD) cold event (12.85-11.7 ka BP), a 1200 years lasting cold period that followed the BA [e.g. Broecker *et al.*, 2010; Broecker *et al.*, 1988; Lowe *et al.*, 2008], however is still discussed controversially [e.g. Broecker *et al.*, 2010; Hillaire-Marcel *et al.*; Tarasov and Peltier, 2005]. The suggestions range from a meltwater flood event to a volcanic eruption or even an extraterrestrial impact.

As part of recent paleoceanographic research, special emphasis has been given to solid reconstructions of regional patterns of past ocean temperature changes that are associated to deglacial climate changes. In this purpose multiproxy SST records were used, that were obtained from alkenones, Mg/Ca ratios of planktonic foraminifera and planktonic foraminifera transfer functions [e.g. CLIMAP and Members, 1981; Kucera *et al.*, 2005; Leduc *et al.*, 2010; MARGO, 2009; Shakun and Carlson, 2010]. However, inconsistencies between the SST reconstructions obtained from different proxies are still a matter of discussion [e.g. Leduc *et al.*, 2010; Sicre *et al.*, 2013; Telford *et al.*, 2012], especially in regions with low data coverage as the subtropical NA.

The cooling of the SST in the subpolar NA, however, is well constrained for the deglacial cold events and is assumed to be coupled with changes in the latitudinal wind pattern, upwelling regimes and the displacement of oceanic and atmospheric fronts [e.g. Chiang and Bitz, 2005; Haug *et al.*, 2001; Lea *et al.*, 2003; Mix *et al.*, 1986]. Yet, it remains unclear whether the front displacements

were associated with a displacement of its characteristic strong SST gradients *Barker et al.* [2009] or whether the most pronounced cooling during cold events appeared in the northern high latitudes (6-8°C) and gradually vanished southwards [*Shakun and Carlson* 2010].

The reduced northward heat transport during weak AMOC phases has been suggested to have led to the retention of warm saline water in southern ocean and thereby inducing a see-saw like pattern with warming in the southern hemisphere and cooling in the Northern hemisphere [e.g. *Broecker*, 1998; *Crowley*, 1992; *Schmittner and Clement*, 2002]. This is supported by observations of heat storage within the tropics and subtropical NA [e.g. *Rühlemann et al.*, 2004; *Schmidt et al.*, 2004; *Weldeab et al.*, 2006]. The extension of the warm water sphere and associated warm water storage patterns within the subtropical NA are still not well constrained. Possible storage scenarios comprise a warm water storage within the surface of the western subtropical NA, in the surface tropical NA, or the intermediate subtropical water mass [*Bakke et al.*, 2009; *Carlson*, 2008; *Rühlemann et al.*, 2004; *Schmidt et al.*, 2004; *Weldeab et al.*, 2006]. The release and transport of stored warm waters into the NA convection areas via different pathways are assumed to have played a major role in the resumption of AMOC [*Carlson*, 2008; *Schmidt et al.*, 2004; *Bakke et al.*, 2009; *Krebs and Timmermann*, 2007].

Paleoceanographic reconstructions not only need to assess warming and cooling trends on centennial to millennial timescales, but are also required for robust salinity estimates, in order to assess the impact of surface water freshening on AMOC and the extension of freshwaters into the NA. This still is unknown for the eastern NA basin, although data from sediment cores indicate that meltwater fluxes extended far into the subpolar NA [*Bond et al.*, 1992] and during H1 even reached into the Mediterranean Basin [*Eynaud et al.*, 2009; *Voelker et al.*, 2006]. Freshwater housing experiments with general ocean circulation models predict a range of different extensions of these freshwater plumes in the open NA and thus a related change in the extension of the subtropical warm water pool [*Stouffer et al.*, 2006].

Several studies that reconstruct the deglacial deepwater evolution [*Gherardi et al.*, 2005; *McManus et al.*, 2004; *Oppo et al.*, 2003; *Sarnthein et al.*, 1994; *Skinner et al.*, 2003] suggest that weak AMOC phases experienced an increased influence of southern sourced deep water that flushed the NA basin. Thereby a see-saw like pattern between deepwater masses of northern and southern origin was induced [e.g. *Skinner et al.*, 2003]. However, recent studies suggest a more complex situation due to the influence of NA brine waters that may overprint the isotopic signature during the H1 and the YD [*Labeyrie et al.*, 2005; *Meland et al.*, 2008; *Thornalley et al.*, 2010; *Waelbroeck et al.*, 2011]. Thus the regional deglacial deepwater distribution in the NA remains uncertain as the case is in the eastern NA basin. Furthermore, still little is known about the impacts on Holocene climate by shifts in the NA deepwater source area from the Nordic seas to the Labrador Sea [*Hoogakker et al.*, 2011; *Roberts et al.*, 2010; *Skinner et al.*, 2003].

1.3 Objectives and Approach of this thesis

This study has been conducted within the framework of the European Science Foundation (ESF) project AMOCINT (Atlantic Meridional Overturning Circulation during Interglacials). AMOCINT was launched with the overall aim to identify and survey sites for a future IODP campaign. The project aimed to investigate the interglacial variability of AMOC, in order to better assess its impact on climate. In this purpose, high-resolution marine sediment cores were obtained from high sedimentation key sites to produce time series of NA circulation parameters in centennial scale resolution in order to gain data from marine archives that are comparable to the high-resolution ice core archives. The key sites are situated along the NA warm water routes and include sites within the subtropical recirculation. Coring was carried out during the Marion Dufresne 168/AMOCINT IMAGES XVII 2008 campaign, including a calypso coring device that provides extremely long sediment cores (up to 60 m) in order to core sediments that reach back from the Holocene to older interglacials.

A major aim of this thesis is to better investigate the impact of AMOC changes on the surface water hydrology of the eastern subtropical NA. In addition the impact of AMOC changes on North East Atlantic Deepwater (NEADW) composition is discussed from 15 ka BP to 7 ka BP, comprising the last deglaciation and the early current interglacial. In this investigations the cores MD08-3180 / GEOFAR KF16 taken at the same coring site south of the Azores islands at the eastern flank of the MAR were used. Under modern conditions the coring site is situated at the boundary between subtropical and transitional NA water and thus is ideal to trace deglacial changes in the surface water hydrology. At depth, the coring site is influenced by southern sourced Lower Deep Water (LDW), and NEADW of northern origin, and thus is suitable to trace deglacial changes in the deepwater distribution. The main objectives of the thesis are

- To assess the deglacial magnitude of SST change and frontal movements in the subtropical NA. Therefore independent high-resolution geochemical and marine plankton based multi proxy SST reconstructions provided by the $U^{K'}_{37}$, Mg/Ca, and SIMMAX paleothermometry methods are compared. Additionally, the abundance of foraminiferal indicator species is used to reconstruct changes in the mixed layer, including the position of the northern STG boundary to explain the discrepancies between different SST reconstructions.
- It is of particular interest how the STG surface hydrology responds to freshwater pulses under different deglacial AMOC modes to identify the mechanisms and patterns of subtropical heat retention. For this assessment multi proxy SST estimates, $\delta^{18}O$ measurements and $\delta^{18}O_{w-ice}$ (SSS) reconstructions from surface and subsurface dwelling foraminifera as well as foraminiferal abundance and deepwater ventilation records (benthic $\delta^{13}C$ records) are used.

- To reconstruct deglacial and Holocene changes in the sources of the deepwater that occupies the East Atlantic Basin addressing the question whether the source changed between a southern and northern hemisphere origin over the deglacial and whether these changes were triggered in the southern or northern hemisphere. The deepwater changes are reconstructed using bottom water temperatures (BWT) as derived from Mg/Ca ratios of benthic foraminifera and stable isotope analyses ($\delta^{13}\text{C}$ and $\delta^{18}\text{O}$) of benthic foraminifera.

1.4 Modern hydrography of the North Atlantic and Azores region

1.4.1 NA Surface water currents

The main elements of the upper AMOC limb in the NA are the Gulf Stream, the North Atlantic Current (NAC), the Subtropical Gyre (STG) and the Subpolar Gyre (SPG). The Gulf Stream transports warm saline water northwards from the Caribbean and is termed North Atlantic current (NAC) as soon as it separates from the continental American shelf (Figure 1.1, and 1.3).

In the subtropical NA, the STG circulates warm NAC waters between 10 and 40°N. The northern STG boundary between 34 and 38°N consists of the Azores Current (AC), which branches off the

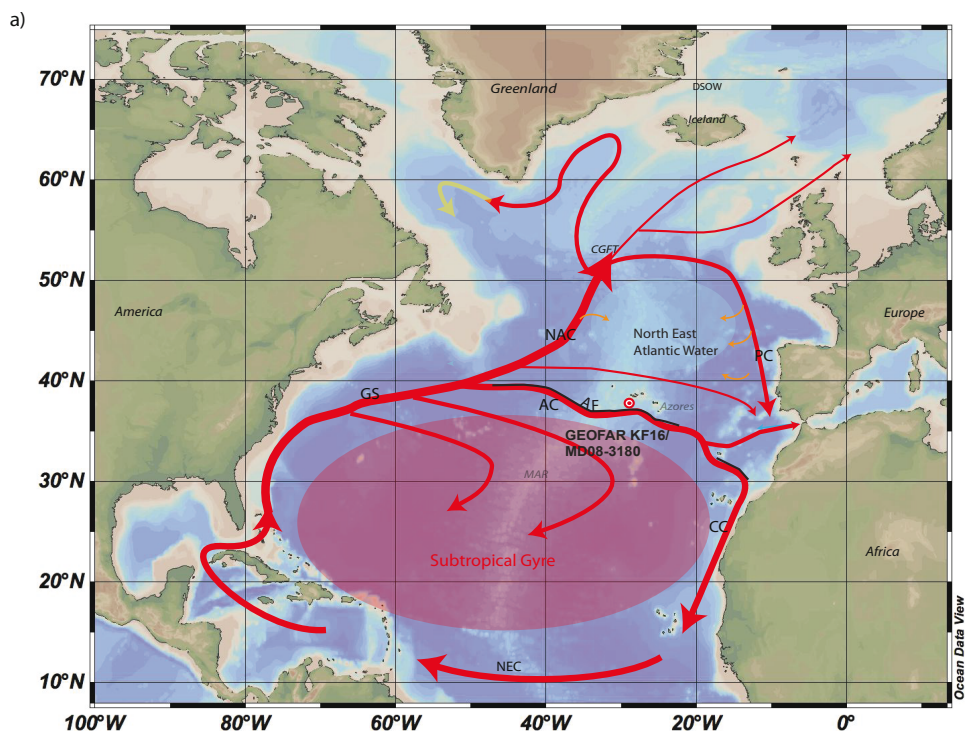


Figure 1.3 Hydrographic overview of the NA surface water currents modified after Schott et al. [2004] and Lherminier et al. [2010] map obtained from Ocean data view [Schlitzer, 2012]

Abbreviations: GC Gulf Stream; NAC North Atlantic Current; AC Azores Current; AF Azores front ; CC Canary Current; PC Portugal Current; NEC North Equatorial Current; CGFT Charlie- Gibbs-Fracture-Zone; MAR Mid Atlantic Ridge

NAC between 35 and 40°N and flows eastward towards the Mediterranean Sea [e.g. *Alves and de Verdière*, 1999; *Alves et al.*, 2002; *Stramma and Siedler*, 1988; *Volkov and Fu*, 2010, 2011]. The eastern and southern boundaries of the STG are composed of the Canary Current and the Eastern Equatorial Current, and the western part of the STG is framed by the Gulf Stream. Due to the circulation of warm nutrient depleted waters, the STG is a zone of low productivity [*Longhurst*, 2007]. The subpolar gyre (SPG) is situated to the Northwest of the STG. The SPG rotates counterclockwise in the western subpolar NA basin. The cold East and West Greenland Current, the West Greenland Current, and the Labrador Current transport cold waters along the east coast of Greenland [*Higginson et al.*, 2011] and to the east the SPG is bordered by the warm Irminger Current that separates at 50°N from the NAC and flows in northwesterly direction.

To the northeast of the STG, the northeastern Atlantic basin is filled with Eastern North Atlantic Water (ENAW), a mixture of the northern most eastward branch of NAC, Mediterranean Overflow water (MOW) and Western North Atlantic Water (WNAW) [*Pollard et al.*, 1996]. To the east this basin is bordered by the Portugal Current (PC) that transports a mixture of NAC and subpolar waters southward along the Iberian Margin [*Eynaud et al.*, 2009; *Pérez et al.*, 2001].

The position of the STG is governed by changes in the NAC and the AC, which are mainly forced by the strength of the westerly wind belt wind, that causes a frictional drag on the ocean surface [*Bearman*, 2004]. This wind belt is part of the atmospheric Ferrel cell (Figure 1.4) that is characterized by a southward air transport within the upper atmosphere and a northward transport of warm air within the lower atmosphere. On its northward path the warm air is deflected eastward by the coriolis force and thus induce the westerly wind belt [*Bearman*, 2004]. Strengthening of the westerlies leads to a southward movement of the AC and a contraction of the STG, while decreasing wind strength lead to a relaxation and northward expansion of the gyre [*Volkov and Fu*, 2010, 2011]. Furthermore the westerly wind belt has a strong influence on the European climate by transporting moist warm air from the Atlantic towards the continent.

On the contrary the SPG is forced by the strength of the polar easterlies that are part of the polar cell (Figure 1.4). Within these cell warm air is transported pole ward within the upper atmosphere where it cools sinks down. The southward return flow is deflected eastward by the coriolis force and is named polar easterlies. As the polar easterlies induce the Greenland Current, its strength governs the strength of the SPG with increasing wind strength induces a strengthening of the SPG.

Due to the atmospheric connection, the westerly wind belt changes coevally with in the polar cell. Recent oceanographic data and modeling studies suggested, that increasing SPG strength and a weakening of the STG lead to enhanced transport of warm saline waters into the deepwater convection areas and results in increasing overturning in the SPG and AMOC strength [*Born and Levermann*, 2010; *Häkkinen et al.*, 2011; *Hátún et al.*, 2005; *Lozier et al.*, 2010] Therefore AMOC strength and the changing extension and strength of the STG and SPG are coupled on decadal time scales.

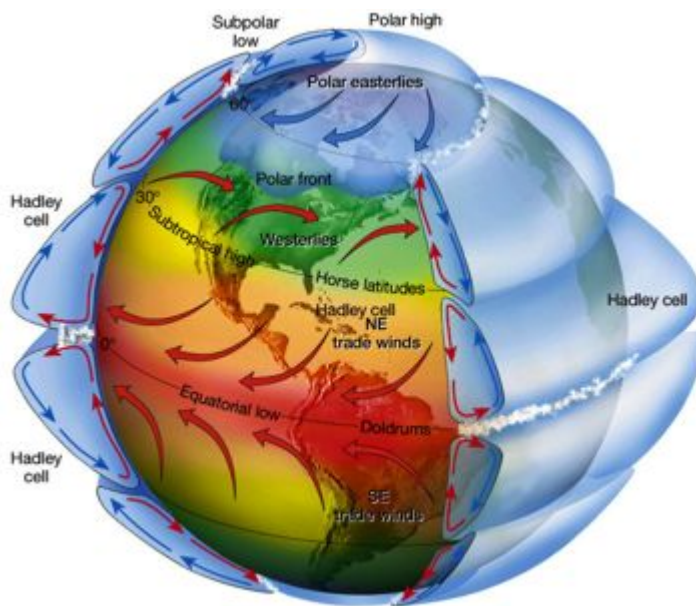


Figure 1.4 The global wind patterns [picture from NASA Earth Observatory]

Furthermore, the AC strength is considered to be driven by the strength of MOW through the entrainment of surface waters into the MOW cascading from the Mediterranean into the eastern NA basin at the Strait of Gibraltar, according to the β -plume formation theory, suggesting that overflows induce a upper layer motion due to baroclinic instability [Kida *et al.*, 2008; Lamas *et al.*, 2010; Volkov and Fu, 2010]. Modeling studies suggest that increasing MOW strength and an associated increase of the exchange transport from 0.5 (recent value) to 2 Sv, would lead to an increase of the eastward transport from 3 to 12.5 Sv within the area between 34–37°N and 10–25°W.

1.4.2 Surface water hydrography of the coring site

The study area is situated at the northern boundary of the low productivity STG (Figure 1.3) that is delineated by the AC. The AC is about 50 km wide and penetrates at least to 1000 m depths and is situated between 32° and 36°N at present [Rogerson *et al.*, 2004; Volkov and Fu, 2011]. Its extensive meanders induce mesoscale eddies of 100-200 km width at both sides of the AC that reach a latitude of 38°N [Alves and de Verdière, 1999; Dickson *et al.*, 1985; Gould, 1985; Käse and Siedler, 1982; Pingree, 1997; Rogerson *et al.*, 2004]. Within the AC system warm STG (19°C) water and cool subpolar ENAW (14°C), are separated by the Azores front (AF). The AF position is defined by the strongest dip in the 15°C isotherm, situated above 200 m north of the front and dipping below 300 m south of the front [Gould, 1985]. Although the thermal contrast remains at the subsurface and most time of the year it is not expressed at the surface [Alves *et al.*, 2002], this boundary can be traced by a distinct shift in planktonic and coccolithophoride fauna [*e.g.* Rogerson *et al.*, 2004; Schiebel *et al.*, 2002].

1.4.3 NA Deep water currents

At depth below 500-1000m the North Atlantic is filled with deepwater from different sources, the Antarctic bottom water (AABW) and its derivative Lower Deep Water (LDW) are formed in Antarctic region. AABW and LDW are the densest water masses in the NA and fill the bottom of the western and eastern NA basin. The overlying North Atlantic deepwater (NADW) originates from the subpolar North Atlantic convection sites that are situated in the Nordic seas and Labrador Sea (Figure 1.1 and 1.5).

The Nordic seas deepwater enters the NA via the overflows through Denmark Strait [e.g. *Dickson and Brown, 1994*] and over the Iceland-Scotland Ridge forming Denmark-Strait-Overflow Water (DSOW) and Iceland-Scotland Ridge Overflow Water (ISOW). With an overall transport of 16 -18 Sv, the major part of the southward return flow consists of these water masses [e.g. *Pickart and Spall, 2007; Sarafanov et al., 2012*]. Labrador Sea Water (LSW) is formed in the SPG by winter mixing that induces deep water convection [e.g. *Pickart and Spall, 2007*]. Although the LSW contribution to the deepwater export is minor (newest results 1-2 Sv) [*Pickart and Spall, 2007* and citations therein] it is important for the ventilation of the deep Atlantic. The newly formed LSW propagates southward in the western Atlantic Basin. A smaller portion enters the eastern NA basin via the Charlie Gibbs Fracture Zone and thereby ventilates the deep eastern NA [*Bower et al.; Bower et al., 2009; Gary et al.; van Sebille et al., 2011*]. The composition of the NADW differs between the eastern and western basin due to different contribution of LSW and Overflow water and thus is named North East Atlantic Deep Water (NEADW) in the eastern NA basin and North West Atlantic Deep Water (NWADW) in the western NA basin.

1.4.4 Deepwater hydrography in the Azores region

The deep eastern Atlantic basin is filled with LDW that originates from Antarctic bottom water that enters the eastern NA basin through the Vema Fracture Zone at 11°N [*van Aken, 2000; Van Aken and De Boer, 1995*], extends northwards along the eastern flank of Mid Atlantic Ridge (MAR) up to 30°N, then continuing northward on a more eastern route and intruding subpolar latitudes [*Frew et al., 2000*] and citations therein].

The LDW is overlain NEADW, which typically occupies water depths between 2.0 and 3.5 km [*van Aken, 2000; Van Aken and De Boer, 1995*]. NEADW is formed from Iceland- Scotland Overflow Water (ISOW) that originates from the Greenland-Iceland-Norwegian (GIN) Seas [*Hansen and Østerhus, 2000; Van Aken and De Boer, 1995*]. The ISOW flows through the Iceland-Faroer-Channel into the eastern NA basin. Thereby it entrains Subpolar Mode Water (SPMW) and a small proportion of LSW that enters the East Atlantic Basin via Charlie Gibbs Fracture Zone (CGFZ) [*Talley and McCartney, 1981; [Curry et al., 2003]*]. After crossing the CGFZ a small northward branch circulates within the North Atlantic basin whereas the major part of LSW propagates

southward along the MAR. Due to its relatively high temperatures and low salinities it is lower in density than NEADW and its southward branch occupies the water depth between 200 and 2200 m [Frew *et al.*, 2000; van Sebille *et al.*, 2011]. Sandwiched between NEADW and ENAW (between 1200 and 1500 m wd.) small portions of MOW enter the East Atlantic Basin up to 45°N via the Strait of Gibraltar [Curry *et al.*, 2003].

The study site is situated at the eastern flank of the MAR at the boundary between NEADW and LDW.

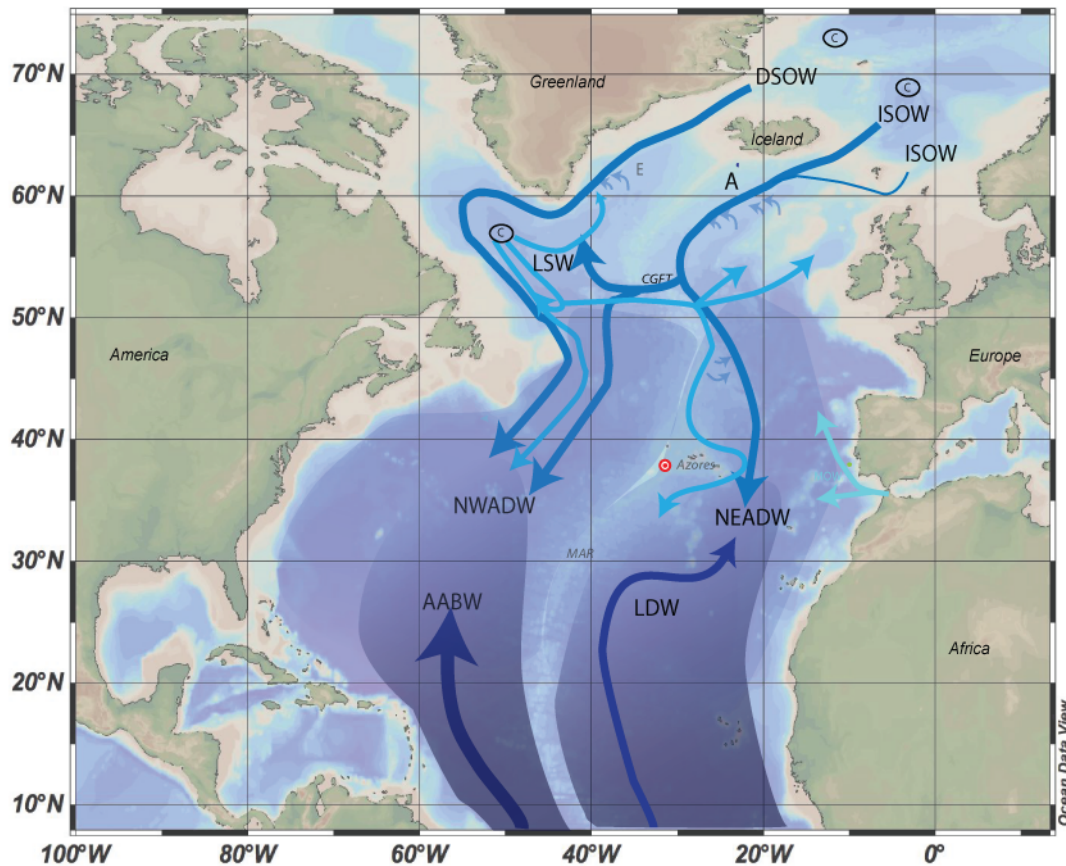


Figure 1.5 Hydrographic overview of the NA deep water currents

modified after Schott *et al.* [2004] and Lherminier *et al.* [2010] map obtained from Ocean data view [Schlitzer, 2012] Abbreviations: NAC North Atlantic Current; ISOW Iceland-Scotland Overflow Water; DSOW Denmark-Strait-Overflow-Water; LSW Labrador-Sea Water; MOW Mediterranean Overflow Water; NEADW North East Atlantic Deep Water; NWADW North-West Atlantic Deep Water; LDW Lower Deep Water; AABW Antarctic Bottom Water, CGFT Charlie- Gibbs-Fracture-Zone

1.5 References

- Aagaard-Sørensen, S., K. Husum, M. Hald, and J. Knies (2010), Paleooceanographic development in the SW Barents Sea during the Late Weichselian-Early Holocene transition, *Quaternary Science Reviews, In Press, Corrected Proof*.
- Aharon, P. (2003), Meltwater flooding events in the Gulf of Mexico revisited: Implications for rapid climate changes during the last deglaciation, *Paleoceanography*, 18(4), 1079.
- Allen, C. S., J. Pike, and C. J. Pudsey (2011), Last glacial-interglacial sea-ice cover in the SW Atlantic and its potential role in global deglaciation, *Quaternary Science Reviews, In Press, Corrected Proof*.
- Alley, R. B., and P. U. Clark (1999), The deglaciation of the northern hemisphere: A global perspective, *Annu. Rev. Earth Planet. Sci.*, 27, 149-182.
- Alves, M., and A. de Verdière (1999), Instability Dynamics of a Subtropical Jet and Applications to the Azores Front Current System: Eddy-Driven Mean Flow, *Journal of Physical Oceanography*, 29(5), 837-864.

- Alves, M., F. Gaillard, M. Sparrow, M. Knoll, and S. Giraud (2002), Circulation patterns and transport of the Azores Front-Current system, *Deep Sea Research Part II: Topical Studies in Oceanography*, 49(19), 3983-4002.
- Andersen, K. K., et al. (2006), The Greenland Ice Core Chronology 2005, 150-0 ka. Part 1: constructing the time scale, *Quaternary Science Reviews*, 25(23-24), 3246-3257.
- Andersson, C., F. S. R. Pausata, E. Jansen, B. Risebrobakken, and R. J. Telford (2010), Holocene trends in the foraminifer record from the Norwegian Sea and the North Atlantic Ocean, *Clim. Past.*, 6, 179-193.
- Bailey, D., P. Rhines, and S. Häkkinen (2005), Formation and pathways of North Atlantic Deep Water in a coupled ice-ocean model of the Arctic-North Atlantic Oceans, *Climate Dynamics*, 25(5), 497-516.
- Bakke, J., O. Lie, E. Heegaard, T. Dokken, G. H. Haug, H. H. Birks, P. Dulski, and T. Nilsen (2009), Rapid oceanic and atmospheric changes during the Younger Dryas cold period, *Nature Geosci.*, 2(3), 202-205.
- Bard, E., and R. E. M. Rickaby (2009), Migration of the subtropical front as a modulator of glacial climate, *Nature*, 460(7253), 380-383.
- Bard, E., F. Rostek, J.-L. Turon, and S. Gendreau (2000), Hydrological Impact of Heinrich Events in the Subtropical Northeast Atlantic, *Science*, 289(5483), 1321-1324.
- Bard, E., M. Arnold, P. Maurice, J. Duprat, J. Moyes, and J.-C. Duplessy (1987), Retreat velocity of the North Atlantic polar front during the last deglaciation determined by ^{14}C accelerator mass spectrometry, *Nature*, 328(6133), 791-794.
- Barker, P. Diz, M. J. Vautravers, J. Pike, G. Knorr, I. R. Hall, and W. S. Broecker (2009), Interhemispheric Atlantic seesaw response during the last deglaciation, *Nature*, 457(7233), 1097-1102.
- Barker, S., G. Knorr, M. J. Vautravers, P. Diz, and L. C. Skinner (2010), Extreme deepening of the Atlantic overturning circulation during deglaciation, *Nature Geosci.*, 3(8), 567-571.
- Bearman, G. B. E. C. A. (2004), *Ocean circulation*, Butterworth-Heinemann [u.a.], Oxford.
- Benway, H. M., J. F. McManus, D. W. Oppo, and J. L. Cullen (2010), Hydrographic changes in the eastern subpolar North Atlantic during the last deglaciation, *Quaternary Science Reviews*, 29(23-24), 3336-3345.
- Berger, A., M. F. Loutre, and J. L. M $\sqrt{\text{lice}}$ (2006), Equatorial insolation: from precession harmonics to eccentricity frequencies, *Clim. Past Discuss.*, 2(4), 519-533.
- Björck, J., and S. Wastegård (1999), Climate oscillations and tephrochronology in eastern middle Sweden during the last glacial-interglacial transition, *Journal of Quaternary Science*, 14(5), 399-410.
- Björck, S., M. J. C. Walker, L. C. Cwynar, S. Johnsen, K.-L. Knudsen, J. J. Lowe, and B. Wohlfarth (1998), An event stratigraphy for the Last Termination in the North Atlantic region based on the Greenland ice-core record: a proposal by the INTIMATE group, *Journal of Quaternary Science*, 13(4), 283-292.
- Björck, S., et al. (1996), Synchronized Terrestrial/Atmospheric Deglacial Records Around the North Atlantic, *Science*, 274(5290), 1155-1160.
- Bodén, P., R. G. Fairbanks, J. D. Wright, and L. H. Burckle (1997), High-Resolution Stable Isotope Records From Southwest Sweden: The Drainage of the Baltic Ice Lake and Younger Dryas Ice Margin Oscillations, *Paleoceanography*, 12(1), 39-49.
- Bond, G., et al. (1992), Evidence for massive discharges of icebergs into the North Atlantic ocean during the last glacial period *Nature*, 360, 245-249.
- Born, A., and A. Levermann (2010), The 8.2 ka event: Abrupt transition of the subpolar gyre toward a modern North Atlantic circulation, *Geochem. Geophys. Geosyst.*, 11(6), Q06011.
- Bos, J. A. A., B. van Geel, J. van der Plicht, and S. J. P. Bohncke (2007), Preboreal climate oscillations in Europe: Wiggle-match dating and synthesis of Dutch high-resolution multi-proxy records, *Quaternary Science Reviews*, 26(15-16), 1927-1950.
- Bower, A., S. Lozier, and S. Gary Export of Labrador sea water from the subpolar north Atlantic: A Lagrangian perspective, *Deep Sea Research Part II: Topical Studies in Oceanography*, In Press, Accepted Manuscript.
- Bower, A. S., M. S. Lozier, S. F. Gary, and C. W. Boning (2009), Interior pathways of the North Atlantic meridional overturning circulation, *Nature*, 459(7244), 243-247.
- Broecker, W. S. (1998), Paleocean circulation during the Last Deglaciation: A bipolar seesaw?, *Paleoceanography*, 13(2), 119-121.
- Broecker, W. S., G. Bond, M. Klas, G. Bonani, and W. Wolfli (1990), A salt oscillator in the glacial Atlantic? 1. The concept, *Paleoceanography*, 5(4), 469-477.
- Broecker, W. S., G. H. Denton, R. L. Edwards, H. Cheng, R. B. Alley, and A. E. Putnam (2010), Putting the Younger Dryas cold event into context, *Quaternary Science Reviews*, 29(9-10), 1078-1081.
- Broecker, W. S., M. Andree, W. Wolfli, H. Oeschger, G. Bonani, J. Kennett, and D. Peteet (1988), The chronology of the last Deglaciation: Implications to the cause of the Younger Dryas Event, *Paleoceanography*, 3(1), 1-19.
- Calvo, E., J. Grimalt, and E. Jansen (2002), High resolution U37K sea surface temperature reconstruction in the Norwegian Sea during the Holocene, *Quaternary Science Reviews*, 21(12-13), 1385-1394.
- Came, R. E., D. W. Oppo, and J. F. McManus (2007), Amplitude and timing of temperature and salinity variability in the subpolar North Atlantic over the past 10 k.y., *Geology*, 35(4), 315-318.
- Came, R. E., D. W. Oppo, W. B. Curry, and J. Lynch-Stieglitz (2008), Deglacial variability in the surface return flow of the Atlantic meridional overturning circulation, *Paleoceanography*, 23(1), PA1217.
- Carlson, A. E. (2008), Why there was not a Younger Dryas-like event during the Penultimate Deglaciation, *Quaternary Science Reviews*, 27(9-10), 882-887.
- Carlson, A. E., D. W. Oppo, R. E. Came, A. N. LeGrande, L. D. Keigwin, and W. B. Curry (2008a), Subtropical Atlantic salinity variability and Atlantic meridional circulation during the last deglaciation, *Geology*, 36(12), 991-994.
- Carlson, A. E., A. N. LeGrande, D. W. Oppo, R. E. Came, G. A. Schmidt, F. S. Anslow, J. M. Licciardi, and E. A. Obbink (2008b), Rapid early Holocene deglaciation of the Laurentide ice sheet, *Nature Geosci.*, 1(9), 620-624.

- Chiang, J. H., and C. Bitz (2005), Influence of high latitude ice cover on the marine Intertropical Convergence Zone, *Climate Dynamics*, 25(5), 477-496.
- Clark, P. U., R. B. Alley, and D. Pollard (1999), Northern Hemisphere Ice-Sheet Influences on Global Climate Change, *Science*, 286(5442), 1104-1111.
- Clark, P. U., A. S. Dyke, J. D. Shakun, A. E. Carlson, J. Clark, B. Wohlfarth, J. X. Mitrovica, S. W. Hostetler, and A. M. McCabe (2009), The Last Glacial Maximum, *Science*, 325(5941), 710-714.
- CLIMAP, and P. Members (1981), Seasonal reconstruction of the earth's surface at the last glacial maximum, *Geological Society of America, Map and Chart Series*, 36, 18 pp.
- Crowley, T. J. (1992), North Atlantic Deep Water cools the southern hemisphere, *Paleoceanography*, 7(4), 489-497.
- Curry, R., B. Dickson, and I. Yashayaev (2003), A change in the freshwater balance of the Atlantic Ocean over the past four decades, *Nature*, 426(6968), 826-829.
- Daley, T. J., et al. (2011), The 8200 yr BP cold event in stable isotope records from the North Atlantic region, *Global and Planetary Change*, 79(3-4), 288-302.
- Dickson, R. R., and J. Brown (1994), The production of North Atlantic Deep Water: Sources, rates, and pathways, *Journal of Geophysical Research: Oceans*, 99(C6), 12319-12341.
- Dickson, R. R., W. J. Gould, T. J. Müller, and C. Maillard (1985), Estimates of the mean circulation in the deep (>2,000m) layer of the Eastern North Atlantic, *Progress in Oceanography*, 14, 103-127.
- Duplessy, J. C., I. Delibrias, J. L. Turon, C. Pujol, and J. Duprat (1981), Deglacial warming of the northeastern Atlantic Ocean. correlation with the paleoclimatic evolution of the european continent, *Palaeoecology, Palaeoecology*, 35, 121-144.
- Duplessy, J. C., L. Labeyrie, M. Arnold, M. Paterne, J. Duprat, and T. C. E. van Weering (1992), Changes in surface salinity of the North Atlantic Ocean during the last deglaciation, *Nature*, 358(6386), 485-488.
- Eynaud, F., et al. (2009), Position of the Polar Front along the western Iberian margin during key cold episodes of the last 45 ka, *Geochem. Geophys. Geosyst.*, 10(7), Q07U05.
- Fisher, T. G., D. G. Smith, and J. T. Andrews (2002), Preboreal oscillation caused by a glacial Lake Agassiz flood, *Quaternary Science Reviews*, 21(8-9), 873-878.
- Frew, R. D., P. F. Dennis, K. J. Heywood, M. P. Meredith, and S. M. Boswell (2000), The oxygen isotope composition of water masses in the northern North Atlantic, *Deep Sea Research Part I: Oceanographic Research Papers*, 47(12), 2265-2286.
- Gary, S. F., M. Susan Lozier, C. W. Böning, and A. Biastoch Deciphering the pathways for the deep limb of the Meridional Overturning Circulation, *Deep Sea Research Part II: Topical Studies in Oceanography*, In Press, Accepted Manuscript.
- Gherardi, J.-M., L. Labeyrie, J. F. McManus, R. Francois, L. C. Skinner, and E. Cortijo (2005), Evidence from the Northeastern Atlantic basin for variability in the rate of the meridional overturning circulation through the last deglaciation, *Earth and Planetary Science Letters*, 240, 710-723.
- Gherardi, J. M., L. Labeyrie, S. Nave, R. Francois, J. F. McManus, and E. Cortijo (2009), Glacial-interglacial circulation changes inferred from 231Pa/230Th sedimentary record in the North Atlantic region, *Paleoceanography*, 24(2), n/a-n/a.
- Giraudeau, J., M. Grelaud, S. Solignac, J. T. Andrews, M. Moros, and E. Jansen (2010), Millennial-scale variability in Atlantic water advection to the Nordic Seas derived from Holocene coccolith concentration records, *Quaternary Science Reviews*, 29(9-10), 1276-1287.
- Gould, W. J. (1985), Physical oceanography of the Azores front, *Progress in Oceanography*, 14, 167-190.
- Gregory, J. M., et al. (2005), A model intercomparison of changes in the Atlantic thermohaline circulation in response to increasing atmospheric CO₂ concentration, *Geophysical Research Letters*, 32(12), L12703.
- Häkkinen, S., P. B. Rhines, and D. L. Worthen (2011), Warm and saline events embedded in the meridional circulation of the northern North Atlantic, *J. Geophys. Res.*, 116(C3), C03006.
- Hald, M., C. Andersson, H. Ebbesen, E. Jansen, D. Klitgaard-Kristensen, B. Risebrobakken, G. R. Salomonsen, M. Samthein, H. P. Sejrup, and R. J. Telford (2007), Variations in temperature and extent of Atlantic Water in the northern North Atlantic during the Holocene, *Quaternary Science Reviews*, 26(25-28), 3423-3440.
- Hansen, B., and S. Østerhus (2000), North Atlantic - Nordic Seas exchanges, *Prog. Oceanogr.*, 45, 109-208.
- Hátún, H., A. B. Sandö, H. Drange, B. Hansen, and H. i. Valdimarsson (2005), Influence of the Atlantic Subpolar Gyre on the Thermohaline Circulation, *Science*, 309(5742), 1841-1844.
- Haug, G. H., K. A. Hughen, D. M. Sigman, L. C. Peterson, and U. Röhl (2001), Southward Migration of the Intertropical Convergence Zone Through the Holocene, *Science*, 293, 1304-1308.
- Higginson, S., K. R. Thompson, J. Huang, M. Véronneau, and D. G. Wright (2011), The mean surface circulation of the North Atlantic subpolar gyre: A comparison of estimates derived from new gravity and oceanographic measurements, *J. Geophys. Res.*, 116(C8), C08016.
- Hillaire-Marcel, C., J. Maccali, C. Not, and A. Poirier Geochemical and isotopic tracers of Arctic sea ice sources and export with special attention to the Younger Dryas interval, *Quaternary Science Reviews*(0).
- Hoogakker, B. A. A., M. R. Chapman, I. N. McCave, C. Hillaire-Marcel, C. R. W. Ellison, I. R. Hall, and R. J. Telford (2011), Dynamics of North Atlantic Deep Water masses during the Holocene, *Paleoceanography*, 26(4), PA4214.
- Jansen, E., C. Andersson, M. Moros, K. H. Nisancioglu, B. F. Nyland, and R. J. Telford (2009), The Early to Mid-Holocene Thermal Optimum in the North Atlantic, in *Natural Climate Variability and Global Warming*, edited, pp. 123-137, Wiley Blackwell.

- Jansen, E., et al. (Eds.) (2007), *Climate Change 2007: The Physical Science Basis. Contribution of Working Group I to the Fourth Assessment Report of the Intergovernmental Panel on Climate Change*, Cambridge University Press, Cambridge, United Kingdom and New York, NY, USA.
- Kageyama, M., A. Paul, D. M. Roche, and C. J. Van Meerbeeck (2010), Modelling glacial climatic millennial-scale variability related to changes in the Atlantic meridional overturning circulation: a review, *Quaternary Science Reviews*, 29(21-22), 2931-2956.
- Karcher, M., A. Beszczynska-Möller, F. Kauker, R. Gerdes, S. Heyen, B. Rudels, and U. Schauer (2011), Arctic Ocean warming and its consequences for the Denmark Strait overflow, *J. Geophys. Res.*, 116(C2), C02037.
- Käse, R. H., and G. Siedler (1982), Meandering of the subtropical front south-east of the Azores, *Nature*, 300(5889), 245-246.
- Keigwin, L. D., J. P. Sachs, Y. Rosenthal, and E. A. Boyle (2005), The 8200 year B.P. event in the slope water system, western subpolar North Atlantic, *Paleoceanography*, 20(2), PA2003.
- Kida, S., J. F. Price, and J. Yang (2008), The Upper-Oceanic Response to Overflows: A Mechanism for the Azores Current, *Journal of Physical Oceanography*, 38(4), 880-895.
- Kleiven, H. K. F., C. Kissel, C. Laj, U. Ninnemann, T. O. Richter, and E. Cortijo (2008), Reduced North Atlantic deep water coeval with the glacial Lake Agassiz freshwater outburst, *Science*, 319, 60-64.
- Kobashi, T., J. P. Severinghaus, and J.-M. Barnola (2008), 4 ± 1.5 °C abrupt warming 11,270 yr ago identified from trapped air in Greenland ice, *Earth and Planetary Science Letters*, 268(3-4), 397-407.
- Krebs, U., and A. Timmermann (2007), Fast advective recovery of the Atlantic meridional overturning circulation after a Heinrich event, *Paleoceanography*, 22, PA1220.
- Kucera, M., A. Rosell-Melé, R. Schneider, C. Waelbroeck, and M. Weinelt (2005), Multiproxy approach for the reconstruction of the glacial ocean surface (MARGO), *Quaternary Science Reviews*, 24(7-9), 813-819.
- Labeyrie, L., C. Waelbroeck, E. Cortijo, E. Michel, and J.-C. Duplessy (2005), Changes in deep water hydrology during the Last Deglaciation, *C. R. Geoscience*, 337, 919-927.
- Lamas, L., Á. Peliz, I. Ambar, A. Barbosa Aguiar, N. Maximenko, and A. Teles-Machado (2010), Evidence of time-mean cyclonic cell southwest of Iberian Peninsula: The Mediterranean Outflow-driven beta-plume?, *Geophys. Res. Lett.*, 37(12), L12606.
- Lea, D. W., D. K. Pak, L. C. Peterson, and K. A. Hughen (2003), Synchronicity of Tropical and High-Latitude Atlantic Temperatures over the Last Glacial Termination, *Science*, 301(5638), 1361-1364.
- Leduc, G., R. Schneider, J. H. Kim, and G. Lohmann (2010), Holocene and Eemian sea surface temperature trends as revealed by alkenone and Mg/Ca paleothermometry, *Quaternary Science Reviews*, 29(7-8), 989-1004.
- Lisiecki, L. E., and M. E. Raymo (2005), A Pliocene-Pleistocene stack of 57 globally distributed benthic $\delta^{18}O$ records, *Paleoceanography*, 20, PA1003.
- Liu, Z., et al. (2009), Transient Simulation of Last Deglaciation with a New Mechanism for Bolling-Allerod Warming, *Science*, 325(5938), 310-314.
- Longhurst, A. R. (2007), *Ecological geography of the sea*, Amsterdam: Academic Press.
- Lowe, J. J., S. O. Rasmussen, S. Björck, W. Z. Hoek, J. P. Steffensen, M. J. C. Walker, and Z. C. Yu (2008), Synchronisation of palaeoenvironmental events in the North Atlantic region during the Last Termination: a revised protocol recommended by the INTIMATE group, *Quaternary Science Reviews*, 27(1-2), 6-17.
- Lozier, M. S., V. Roussinov, M. S. C. Reed, and R. G. Williams (2010), Opposing decadal changes for the North Atlantic meridional overturning circulation, *Nature Geosci.*, 3(10), 728-734.
- Manabe, S., and R. J. Stouffer (1997), Coupled Ocean-Atmosphere Model Response to Freshwater Input: Comparison to Younger Dryas Event, *Paleoceanography*, 12(2), 321-336.
- Marchal, O., et al. (2002), Apparent long-term cooling of the sea surface in the northeast Atlantic and Mediterranean during the Holocene, *Quaternary Science Reviews*, 21(4-6), 455-483.
- MARGO (2009), Constraints on the magnitude and patterns of ocean cooling at the Last Glacial Maximum, *Nature Geosci.*, 2(2), 127-132.
- McManus, J. F., R. Francois, J. M. Gherardi, L. D. Keigwin, and S. Brown-Leger (2004), Collapse and rapid resumption of Atlantic meridional circulation linked to deglacial climate changes, *Nature*, 428(6985), 834-837.
- Meland, M. Y., T. M. Dokken, E. Jansen, and K. Hevroy (2008), Water mass properties and exchange between the Nordic seas and the northern North Atlantic during the period 23-6 ka: Benthic oxygen isotopic evidence, *Paleoceanography*, 23(1), 19.
- Mix, A. C., W. F. Ruddiman, and A. McIntyre (1986), Late Quaternary paleoceanography of the Tropical Atlantic, 1: Spatial variability of annual mean sea-surface temperatures, 0-20,000 years B.P., *Paleoceanography*, 1(1), 43-66.
- Moros, M., J. T. Andrews, D. D. Eberl, and E. Jansen (2006), Holocene history of drift ice in the northern North Atlantic: Evidence for different spatial and temporal modes, *Paleoceanography*, 21(2), 10.
- Mulitza, S., A. Dürkoop, W. Hale, G. Wefer, and H. Stefan Niebler (1997), Planktonic foraminifera as recorders of past surface-water stratification, *Geology*, 25(4), 335-338.
- Obbink, E. A., A. E. Carlson, and G. P. Klinkhammer (2010), Eastern North American freshwater discharge during the Bolling-Allerod warm periods, *Geology*, 38(2), 171-174.
- Oppo, D. W., J. F. McManus, and J. L. Cullen (2003), Palaeo-oceanography: Deepwater variability in the Holocene epoch, *Nature*, 422(6929), 277-277.
- Otto-Bliesner, B. L., and E. C. Brady (2010), The sensitivity of the climate response to the magnitude and location of freshwater forcing: last glacial maximum experiments, *Quaternary Science Reviews*, 29(1-2), 56-73.
- Peck, V. L., I. R. Hall, R. Zahn, and H. Elderfield (2008), Millennial-scale surface and subsurface paleothermometry from the northeast Atlantic, 55-8 ka BP, *Paleoceanography*, 23(3), PA3221.

- Peltier, W. R. (2002), On eustatic sea level history: Last Glacial Maximum to Holocene, *Quaternary Science Reviews*, 21(1-3), 377-396.
- Pérez, F. F., C. G. Castro, X. A. Álvarez-Salgado, and A. F. Ríos (2001), Coupling between the Iberian basin -- scale circulation and the Portugal boundary current system: a chemical study, *Deep Sea Research Part I: Oceanographic Research Papers*, 48(6), 1519-1533.
- Pickart, R. S., and M. A. Spall (2007), Impact of Labrador Sea Convection on the North Atlantic Meridional Overturning Circulation, *Journal of Physical Oceanography*, 37(9), 2207-2227.
- Pingree, R. D. (1997), The eastern Subtropical gyre (North Atlantic): flow rings recirculations structure and subduction., *Journal of Marine Biological Association of the United Kingdom*, 77, 573-624.
- Pollard, R. T., M. J. Griffiths, S. A. Cunningham, J. F. Read, F. F. Pérez, and A. F. Ríos (1996), Vivaldi 1991 - A study of the formation, circulation and ventilation of Eastern North Atlantic Central Water, *Progress in Oceanography*, 37(2), 167-172.
- Rahmsdorf, S. (2002), Ocean circulation and climate during the past 120000 years, *Nature*, 419, 207-214.
- Roberts, N. L., A. M. Piotrowski, J. F. McManus, and L. D. Keigwin (2010), Synchronous Deglacial Overturning and Water Mass Source Changes, *Science*, 327(5961), 75-78.
- Rogerson, M., E. J. Rohling, P. P. E. Weaver, and J. W. Murray (2004), The Azores Front since the Last Glacial Maximum, *Earth and Planetary Science Letters*, 222(3-4), 779-789.
- Rühlemann, C., S. Mulitza, P. J. Muller, G. Wefer, and R. Zahn (1999), Warming of the tropical Atlantic Ocean and slowdown of thermohaline circulation during the last deglaciation, *Nature*, 402(6761), 511-514.
- Rühlemann, C., S. Mulitza, G. Lohmann, A. Paul, M. Prange, and G. Wefer (2004), Intermediate depth warming in the tropical Atlantic related to weakened thermohaline circulation: Combining paleoclimate data and modeling results for the last deglaciation, *Paleoceanography*, 19(1), n/a-n/a.
- Sarafanov, A., A. Falina, H. Mercier, A. Sokov, P. Lherminier, C. Gourcuff, S. Gladyshev, F. Gaillard, and N. Danialt (2012), Mean full-depth summer circulation and transports at the northern periphery of the Atlantic Ocean in the 2000s, *J. Geophys. Res.*, 117(C1), C01014.
- Sarnthein, M., K. Winn, S. J. A. Jung, J.-C. Duplessy, L. Labeyrie, H. Erlenkeuser, and G. Ganssen (1994), Changes in east Atlantic deepwater circulation over the last 30000 years: Eight time slice reconstructions, *Paleoceanography*, 9(2), 209-267.
- Sarnthein, M., et al. (1995), Variations in Atlantic Surface Ocean Paleoceanography, 50°-80°N: A Time-Slice Record of the Last 30,000 Years, *Paleoceanography*, 10(6), 1063-1094.
- Schiebel, R., J. Waniek, A. Zeltner, and M. Alves (2002), Impact of the Azores Front on the distribution of planktic foraminifers, shelled gastropods, and coccolithophorids, *Deep Sea Research Part II: Topical Studies in Oceanography*, 49(19), 4035-4050.
- Schlitzer, R. (2012), Ocean Data View, <http://odv.awi.de>.
- Schmidt, M. W., H. J. Spero, and D. W. Lea (2004), Links between salinity variation in the Caribbean and North Atlantic thermohaline circulation, *Nature*, 428(6979), 160-163.
- Schmittner, A., and A. C. Clement (2002), Sensitivity of the thermohaline circulation to tropical and high latitude freshwater forcing during the last glacial-interglacial cycle, *Paleoceanography*, 17(2), 1017.
- Schwab, C., H. Kinkel, M. Weinelt, and J. Repschläger (2012), Coccolithophore paleoproductivity and ecology response to deglacial and Holocene changes in the Azores Current System, *Paleoceanography*, 27(3), PA3210.
- Shakun, J. D., and A. E. Carlson (2010), A global perspective on Last Glacial Maximum to Holocene climate change, *Quaternary Science Reviews*, 29(15-16), 1801-1816.
- Skinner, L. C., N. J. Shackleton, and H. Elderfield (2003), Millennial-scale variability of deep-water temperature and $\delta^{18}\text{O}_{\text{dw}}$ indicating deep-water source variations in the Northeast Atlantic, 0-34 cal. ka BP, *Geochem. Geophys. Geosyst.*, 4(12), 1098.
- Stanford, J. D., E. J. Rohling, S. Bacon, A. P. Roberts, F. E. Grousset, and M. Bolshaw (2011), A new concept for the paleoceanographic evolution of Heinrich event 1 in the North Atlantic, *Quaternary Science Reviews*, 9-10, 1047-1066.
- Steffensen, J. r. P., et al. (2008), High-Resolution Greenland Ice Core Data Show Abrupt Climate Change Happens in Few Years, *Science*, 321(5889), 680-684.
- Stouffer, R. J., et al. (2006), Investigating the Causes of the Response of the Thermohaline Circulation to Past and Future Climate Changes, *Journal of Climate*, 19(8), 1365-1387.
- Stramma, L., and G. Siedler (1988), Seasonal Changes in the North Atlantic Subtropical Gyre, *JOURNAL OF GEOPHYSICAL RESEARCH*, 93(C7), 8111-8118.
- Svensson, A., et al. (2008), A 60 000 year Greenland stratigraphic ice core chronology, *Clim. Past*, 4(1), 47-57.
- Tarasov, L., and W. R. Peltier (2005), Arctic freshwater forcing of the Younger Dryas cold reversal, *Nature*, 435(7042), 662-665.
- Teller, J. T. (1995), History and drainage of large ice-dammed lakes along the Laurentide Ice Sheet, *Quaternary International*, 28(0), 83-92.
- Teller, J. T., D. W. Leverington, and J. D. Mann (2002), Freshwater outbursts to the oceans from glacial Lake Agassiz and their role in climate change during the last deglaciation, *Quaternary Science Reviews*, 21(8-9), 879-887.
- Thornalley, D., H. Elderfield, and I. N. McCave (2010), Intermediate and deep water paleoceanography of the northern North Atlantic over the past 21,000 years, *Paleoceanography*, 25(1), n/a-n/a.
- Thornalley, D., H. Elderfield, and I. N. McCave (2011a), Reconstructing North Atlantic deglacial surface hydrography and its link to the Atlantic overturning circulation, *Global and Planetary Change*, 79(3-4), 163-175.
- Thornalley, D., S. Barker, W. S. Broecker, H. Elderfield, and I. N. McCave (2011b), The Deglacial Evolution of North Atlantic Deep Convection, *Science*, 331(6014), 202-205.

- Thornalley, D. J. R., I. N. McCave, and H. Elderfield (2010), Freshwater input and abrupt deglacial climate change in the North Atlantic, *Paleoceanography*, 25(PA1201).
- van Aken, H. M. (2000), The hydrography of the mid-latitude northeast Atlantic Ocean: I: The deep water masses, *Deep Sea Research Part I: Oceanographic Research Papers*, 47(5), 757-788.
- Van Aken, H. M., and C. J. De Boer (1995), On the synoptic hydrography of intermediate and deep water masses in the Iceland Basin, *Deep Sea Research Part I: Oceanographic Research Papers*, 42(2), 165-189.
- van Sebille, E., M. O. Baringer, W. E. Johns, C. S. Meinen, L. M. Beal, M. F. de Jong, and H. M. van Aken (2011), Propagation pathways of classical Labrador Sea water from its source region to 26°N, *J. Geophys. Res.*, 116(C12), C12027.
- Voelker, A. H. L., S. M. Lebreiro, J. Schönfeld, I. Cacho, H. Erlenkeuser, and F. Abrantes (2006), Mediterranean outflow strengthening during northern hemisphere coolings: A salt source for the glacial Atlantic?, *Earth and Planetary Science Letters*, 245(1-2), 39-55.
- Volkov, D. L., and L.-L. Fu (2010), On the Reasons for the Formation and Variability of the Azores Current, *Journal of Physical Oceanography*, 40(10), 2197-2220.
- Volkov, D. L., and L.-L. Fu (2011), Interannual variability of the Azores Current strength and eddy energy in relation to atmospheric forcing, *J. Geophys. Res.*, 116(C11), C11011.
- Waelbroeck, C., L. C. Skinner, L. Labeyrie, J. C. Duplessy, E. Michel, N. Vazquez Riveiros, J. M. Gherardi, and F. Dewilde (2011), The timing of deglacial circulation changes in the Atlantic, *Paleoceanography*, 26(3), PA3213.
- Weldeab, S., R. R. Schneider, and M. Kölling (2006), Deglacial sea surface temperature and salinity increase in the western tropical Atlantic in synchrony with high latitude climate instabilities, *Earth and Planetary Science Letters*, 241(3-4), 699-706.
- Yu, Z., and U. Eicher (2001), Three ampho-Atlantic century-scale cold events during the Bølling-Allerød warm period, *Géographie physique et Quaternaire*, 55(2), 171-179.

1.6 Thesis Outline

Chapter 1: Introduction

Gives a general overview of ocean and atmospheric circulation in the NA region. Respectively, AMOC changes and its impact on the subtropical NA for the deglacial transition and the Holocene warm climate are summarized. This chapter relies on my own literature studies and synthesis. The aims and objective of the thesis are defined and an overview of the thesis structure is given.

Chapter 2: Material and Methods

Gives an overview of the sediment material and describes the methods used in this study

Chapter 3: Age model

Introduces the age models for cores MD08-3180 and GEOFAR KF16 and discusses its uncertainties. The age models as published earlier [Schwab *et al.*, 2012] have been established with contribution of C. Schwab.

Chapter 4: Disentangling Multiproxy SST reconstructions in the subtropical North Atlantic

Compares reconstructions as obtained with different temperature proxies and discusses observed differences apparent at the Azores coring site in context with the deglacial changes in the reconstructed STG position.

I conducted all sampling of the sediment cores and sample preparation with the technical assistance of students. The samples for Mg/Ca analyses were prepared by myself, and the measurements were carried out with technical assistance of the ICP-OES lab technicians. D. Garbe-Schönberg provided assistance for the assessment of Mg/Ca data quality. I counted the fauna assemblages in 10 cm resolution; M. Weinelt provided the high-resolution record. C. Schwab prepared the samples for the alkenone analyses that were analyzed by T. Blanz. U. Krebs-Kanzow provided me with the data from Kiel Climate Model. I interpreted the data, together with my supervisor M. Weinelt and some additional ideas concerning the model data from U. Krebs-Kanzow.

Chapter 5: Response of the central subtropical North Atlantic surface hydrography on Deglacial and Holocene AMOC changes

Represents a manuscript with me as the leading author that will be resubmitted to Paleoceanography after final proof reading of my revised text by the co-authors M. Weinelt, N. Andersen, H. Kinkel, C. Schwab, and D. Garbe-Schönberg. The manuscript deals with the response of the subtropical NA under different AMOC weakening and strengthening scenarios. Thereby changes in the position of the STG, the influence of meltwater pulses on the STG, heat storage patterns at different mixed layers depth and the coupling between the STG and the European Climate are addressed.

I conducted all sampling of the sediment cores and sample preparation with the technical assistance of students. For this manuscript, all samples for isotope analyses were prepared by myself and

complemented with two samples that were prepared by S. Balmer. N. Andersen analyzed all samples were at the Leibniz Laboratory for Radiometric Dating and Stable Isotope Research. The samples for Mg/Ca analyses were conducted as for Chapter 4 as is the case for the fauna assemblages and the alkenone analyses. I wrote the manuscript with the help of my supervisor M. Weinelt. Myself, M. Weinelt, C. Schwab and H. Kinkel, interpreted the data.

Chapter 6: Coccolithophore paleoproductivity and ecology response to deglacial and Holocene changes in the Azores Current System

Consists of a published article in *Paleoceanography* (Schwab et al., 2012). This chapter deals with last deglacial and Holocene changes in productivity and hydrography in the Azores region. The article is written by C. Schwab, my contributions include the discussion of the data as well as the generation of XRF core scanner and all stable isotope data and the age model.

Chapter 7: Deglacial and Holocene evolution of deepwater composition in the eastern North Atlantic basin

Presents the manuscript with me as the leading author and co-authors are A. Andersen, D. Garbe-Schönberg and M. Weinelt. Prepared for submission to a peer-reviewed journal. The manuscript requires final proof reading of the co-authors before submission. It deals with the changes of the deepwater origin from a southern to a northern source over the deglacial period and the changing composition of North East Atlantic Deep Water (NEADW) over the Holocene.

For this manuscript I prepared all samples for stable isotope analyses. N. Andersen at the Leibniz Laboratory for Radiometric Dating and Stable Isotope Research analyzed all samples. The samples for Mg/Ca analyses were prepared by me and were measured with the technical assistance of the ICP-OES lab technicians. D. Garbe-Schönberg provided assistance for the assessment of Mg/Ca data quality. I wrote the manuscript and interpreted the data with help of my supervisor M. Weinelt. The other co-authors contributed with data analyses.

Chapter 8: Summary and Conclusion

Summarizes the outcomes of Chapter 3-6

Chapter 9: Outlook

This chapter gives short overview of the work in progress and possible future work based on my own experience and ideas resulting from this thesis work furthermore it includes additional data that is not incorporated and discussed in any of the other chapters designed for actual submission.

As for the previous chapters, I prepared all samples for isotope analyses that were measured by N. Andersen at the Leibniz Laboratory for Radiometric Dating and Stable Isotope Research. The samples for Mg/Ca analyses were prepared by me and were measured with the technical assistance of the ICP-MOES lab technicians. D. Garbe-Schönberg provided assistance for the assessment of Mg/Ca data quality. C. Schwab prepared the sample for radiocarbon age dating that was carried out in the Leibniz Laboratory for Radiometric Dating and Stable Isotope Research and prepared the samples for $U^{K'}_{37}$ measurements that were conducted by T. Blanz.

Chapter 2

Materials and Methods

2 Material and Methods

2.1 Coring site and Cores

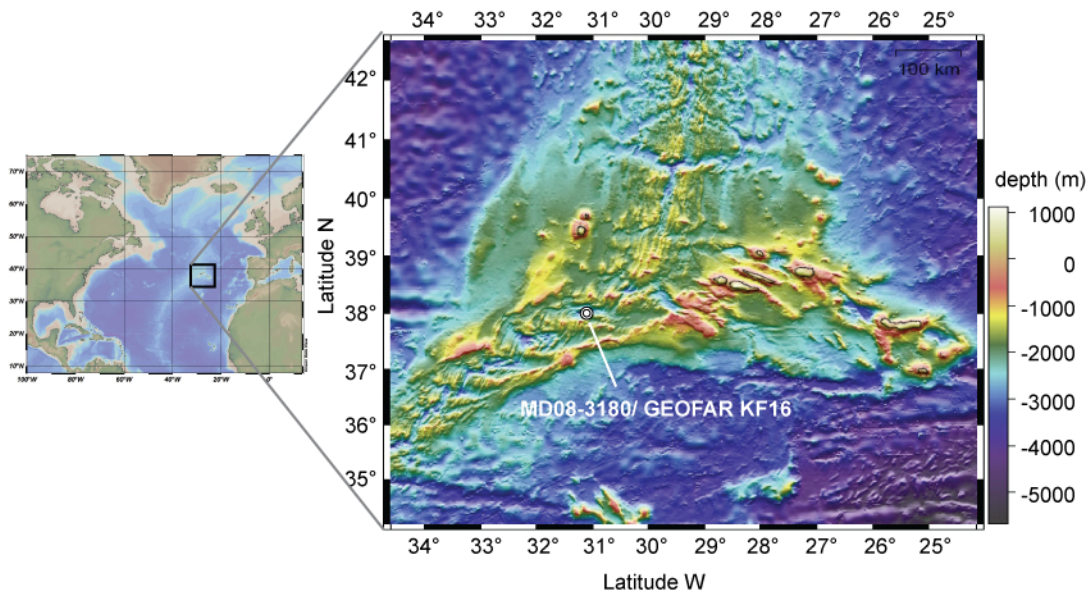


Figure 2.1 Bathymetric map of the coring area with the coring site

The coring location used in this study is situated south of the Azores Islands east of the Mid Atlantic Ridge (MAR) (Figure 2.1). In this area, second order ridge elements that spread in NNE-SSW direction are separated by non-transform discontinuities that form narrow basins with steep flanks [Richter, 1998]. These basins act as sediment traps and thus provide partly laminated sediments with exceptionally high sedimentation rates that reach up to 120 cm /ka and allow high-resolution sampling. The pelagic sediments with a carbonate content of up to 85% consist of nanofossil ooze with foraminifera [Richter, 1998]. A more detailed investigation of the sediments by Scanning Electron Microscopy (SEM) [Schwab, 2013] and the reflected-light microscope reveals that the sediments are composed of calcareous coccolithophores, foraminifera and dinoflagellates, as well as siliceous diatoms and silicoflagellates. Although the coring site lies in the vicinity of the hydrothermal active Menez Gwen field, a geochemical overprint of the sediments by the venting was not observed [Richter, 1998].

Three cores that were taken at the same location (table 2.1) were used in this study. Piston Core GEOFAR KF16 [Richter, 1998] was taken during GEOFAR cruise of RV Le Noroit 1993 and partially sampled and analyzed for previous studies [Richter, 1998]. The residuals of the working half were provided from Ifremer (courtesy of B. Danniellou). Calypso square core (Casq) MD08-3180 and Calypso piston core MD08-3181 were taken during

Table 2.1 Cores used in this study

Core	Latitude [°N]	Longitude [°W]	Water Depth [m]	Core length [m]	Coring device	Reference
GEOFAR KF16	37.984	31.1178	3050	8.0	Piston corer	Richter et al. [1998]
MD08-3180	37.9998	31.1345	3064	10.5	Calypso square core	Kissel et al. [2008]
MD08-3181	38.000	31.1346	3059	23.36	Calypso piston core	Kissel et al. [2008]

MD168 / AMOCINT IMAGES XVII 2008 cruise on board the vessel Marion Dufresne [Kissel et al., 2008].

Core MD08-3181 was extremely bend, and had to be cut open on deck. This resulted in a hiatus of at least 23 cm between 1251 and 1274 cm core depth [Kissel et al., 2008]. Calypso square MD08-3180 and piston core MD08-3181 were sampled aboard with 6 cm wide U-tubes, thereby six core series (A-G) were obtained [Kissel et al., 2008]. For this study series A and series B were used. Foraminifera analyses were conducted on samples of Series B, bulk sediment samples were taken from series A and used for alkenone analyses and nannofossil analyses [Schwab et al., 2012]. XRF core scans were obtained from MD08-3180 series A and MD08-3181A (Achieve half) (table 2.2). Table 2.2 gives an overview of the methods and sample density employed on the individual cores.

Table 2.2 a analysed parameters and analyse intervals

Following initials are used: J.R. Janne Repschläger, M.W. Mara Weinelt, C.S. Christian Schwab, T.B. Thomas Blanz

core	Method	Parameter	species	Analyses interval	Analysed
GEOFAR KF16	Stable isotope measurement	$\delta^{18}\text{O}$, $\delta^{13}\text{C}$	<i>G. ruber w.</i>	every cm	J.R.
			<i>G. truncatulinoides</i>		
			<i>C. wuellerstorfi</i> , <i>M. affinis</i> , <i>M. barleanum</i>		
	Mg/Ca	SST	<i>G. truncatulinoides</i>	70-197 cm every 5-10 cm	J.R.
Foraminiferal transfer functions (SIMMAX)	SST	PF assemblages	Every 5-10 cm Every 1-5 cm	J.R. M.W	
Mg/Ca	BWT	<i>C. wuellerstorfi</i> , <i>M. affinis</i> , <i>M. barleanum</i>	every cm	J.R.	

Table 2.2 b analysed parameters and analyse intervals

core	Method	Parameter	Species	Analyses interval	Analyse
MD08-3180 CQ	Stable isotope measurement	$\delta^{18}\text{O}$, $\delta^{13}\text{C}$	<i>G. ruber w.</i>	1-5 cm	J.R.
			<i>G. bulloides</i>	1-5 cm	
			<i>G. truncatulinoides</i>	1-5 cm	
			<i>C. wuellerstorfi</i> , <i>M. affinis</i> , <i>M. barleanum</i>	1-5 cm	
	Mg/Ca	SST	<i>G. ruber w.</i>	1-5 cm	J.R.
	Mg/Ca	SST	<i>G. bulloides</i>	1-5 cm	J.R.
	Mg/Ca	SST thermocline	<i>G. truncatulinoides</i>	1-2 cm YD and BA	J.R.
	Foraminiferal transfer functions (SIMMAX)	SST	PF assemblages	every 5-10 cm every 1-5 cm	J.R. M.W
Alkenone (U^{k}_{37}) measurements	SST		every 5 cm	T.B, C. S.	
Mg/Ca	BWT	<i>C. wuellerstorfi</i> , <i>M. affinis</i> , <i>M. barleanum</i>	1-5 cm	J.R.	
XRF core scanning	Al, Si, P, S, Cl, K, Ca, Ti, Mn, Fe, Sr, Zr, Ba		0.5 cm	J.R.	
MD08-3181	Stable isotope measurement	$\delta^{18}\text{O}$, $\delta^{13}\text{C}$	<i>G. ruber w.</i>	1cm interval 1900-2236 cm 10 cm interval 100-1900cm	J.R.
			<i>G. bulloides</i>	10 cm interval 100-1900cm	
			<i>C. wuellerstorfi</i> <i>G. affinis</i> ,	1cm - interval 1900- 2236 cm	
	Mg/Ca	BWT	<i>C. wuellerstorfi</i> , <i>M. affinis</i> , <i>M. barleanum</i>	1cm - interval 1900- 2236 cm	J.R.
XRF core scanning	Al, Si, P, S, Cl, K, Ca, Ti, Mn, Fe, Sr, Zr, Ba		0.5 cm	J.R.	

2.2 XRF core scanning

XRF core scanning is a non-destructive technique to measure the chemical composition of sediments cores including the elements from Aluminum (Al, atomic number 13) to Uranium (U, atomic number 92). This method is based on the ionization of the elements by X-ray beam, which induces the emission of element specific fluorescence energy. The measured element intensities (in counts per seconds) are proportional to the chemical concentration. Within this study Ba/Ca ratios are used to assess the paleoproductivity at the coring site.

Table 2.3 Elements measured with the XRF core scanner and its detection limits

Element	Detection limit	Element	Detection limit
Al	2000	Ti	<1000
Si	1000	Mn	100
P	<5000	Fe	50
S	<5000	Sr	5
Cl	n.a.	Zr	?
K	400	Ba	50
Ca	200		

In this study cores MD08-3180 and MD08-3181 were measured in 0.5 cm resolution, with a sampling time of 30 s and a generator setting of 10 kV and 50 kV. With these settings the elements Al, Si, P, S, Cl, K, Ca, Ti, Mn, Fe (10 kV) and Sr, Zr and Ba (50 kV) were measured. The detection limits for the elements are given in table 2.3.

Before analyses the surface of the spliced cores were carefully cleaned and covered with a 4 μ m thin SPEXCerti Prep Ultralene® to avoid dissociation and contamination of the core and the scanner, for technical details see [Tjallingii *et al.*, 2007]. Additionally the cores were covered with a mask of strong plastic foil that left a slit for the scanner detector to prevented the scanner from sinking into the soft sediments and piling it up. For the measurement, a generator slit adjustment was chosen that produced dead times between 20 % and 40 % to achieve the highest possible element intensities. To define this setting test runs on the “lithological extremes of the sediment core (e.g. darkest and brightest intervals)” [Tjallingii *et al.*, 2007; Weltje and Tjallingii, 2008] were used.

To allow the comparison with data from cores measured with different generator settings and core scanners with different measurement geometry, element ratios were used for data interpretation.

2.3 Core sampling and sample preparation

The cores were sampled (Appendix table A 2) in 0.5 to 10 cm intervals in 0.5 to 1 cm wide slices and analyzed according to table 2.2. For foraminifera analyses all sediment samples were freeze dried, weighted, washed over a 63 μm sieve and the residual oven dried at 40°C, weighted and sieved according to the flow chart in Figure 2.2. From core GEOFAR KF16 and MD08-3181 a split of the dry samples was taken for nannofossil analyses.

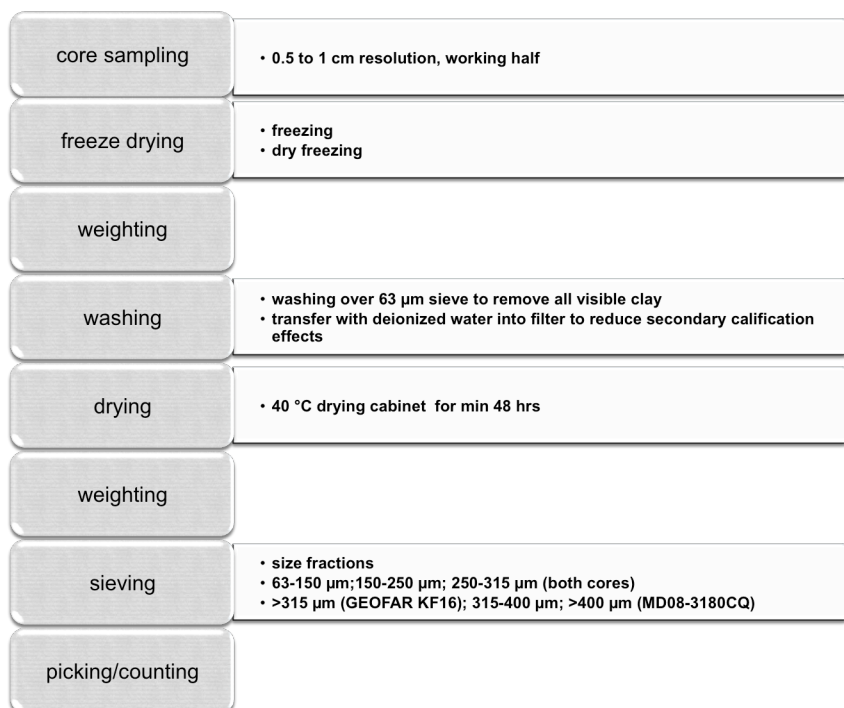


Figure 2.2 Sample preparations for foraminifera analyses

2.4 Stable isotope analyses

The shells of planktonic and benthic foraminifera incorporate the stable oxygen and carbon isotope signal of the ambient seawater. As these signals are related to fractionation temperature, local salinity and global sea ice volume ($\delta^{18}\text{O}$ signal) and to the distribution of dissolved inorganic carbon and its remediation in the ocean ($\delta^{13}\text{C}$ signal), stable isotope signals of foraminifera shells can be used to reconstruct changes in past water masses and are vulnerable proxy to reconstruct past ocean changes.

2.4.1 Sample preparation and measurement

Parallel analyses of surface dwelling (0-100 m) *Globigerinoides ruber w.* [Hemleben *et al.*, 1989; Schiebel *et al.*, 2002b] and deep-dwelling (100-200 m) *Globorotalia truncatulinoides* [Hemleben *et al.*, 1989; Schiebel *et al.*, 2002b] were conducted for core MD08-3180 / GEOFAR KF16. *G. ruber*

w. shows changing abundances over the course of the last 18 ka BP in core MD08-3180 and MD08-3181 and partially even is absent during cold events. In order to obtain a continuous surface water record the *G. ruber* w. record was supplemented with stable isotope measurements on *Globigerina bulloides* (0-300 m) [Hemleben et al., 1989; Schiebel et al., 2002b]. In core MD08-3181 a continuous stable isotope record of *G. truncatulinoides* was hindered by limited numbers of this species. For all stable isotope analyses monospecific samples of planktonic foraminifera were handpicked, cracked, ethanol cleaned, decanted and dried at 40°C (Figure 2.2). To get statistically robust data, average sample sizes between 15 and 30 specimens were used. This number was only undergone when the species abundance was too low (table 2.3).

In order to avoid size related offsets [Friedrich et al., 2012] specimens were obtained from the larger size fractions (>250/315 µm) on which the size fraction effect is assumed to be stable [Friedrich et al., 2012]. For the benthic stable isotope record epibenthic foraminifera of *Cibicidoides wuellerstorfi* was used and supplemented with *Melonis affinis*, *Melonis barleanum* and *Globobulimina sp.*, where *C.wuellerstorfi* was limited; size fractions and sample sizes are summarized in table 2.4. All stable isotope analyses were carried out at the Leibniz Laboratory for Radiometric Dating and Stable Isotope Research in Kiel using a Finnigan MAT 253 mass spectrometer coupled with a Kiel IV carbonate preparation device and calibrated to the V-PDB scale. The analytic precision is better 0.1 ‰ for $\delta^{18}\text{O}$ and better 0.05 ‰ for $\delta^{13}\text{C}$.

Table 2.4 sample size and fraction prepared for stable isotope and Mg/Ca analyses
numbers in brackets indicate the smallest sample size that was used for measurements in samples with low foraminifera abundances

species	Stable isotope analyses ($\delta^{13}\text{C}$, $\delta^{18}\text{O}$)		Mg/Ca analyses	
	Size fraction [µm]	Number	Size fraction [µm]	Number
<i>Globigerinoides ruber</i> w.	>315	25 (8)	>315	25 (15)
<i>Globigerina bulloides</i>	>315	20 (11)	>315	25 (15)
<i>Globorotalia truncatulinoides</i>	>315	15	>315	30 (11)
<i>Cibicidoides wuellerstorfi</i>	>250µm	1-3	>250µm	4-10
<i>Melonis affinis</i>	315-400µm	4-10	>250µm	30 (7)
<i>Melonis barleanum</i>	315-400µm	4-10	>250µm	30 (7)
<i>Globobulimina sp.</i>	315-400µm	6-10	No data	No data

2.4.2 Correction of $\delta^{18}\text{O}$ values for vital effects

Some species fractionate the oxygen isotopes in disequilibrium with the ambient seawater. In order to use stacked species records the $\delta^{18}\text{O}$ values have to be corrected for these so called vital effect

that is most probably related to different metabolic behavior of the species and assumed to be stable over time [Duplessy *et al.*, 1984; Jansen *et al.*, 1988; Shackleton, 1987].

2.4.2.1 $\delta^{18}\text{O}$ vital effect correction for planktonic foraminifera

Ganssen and Kroon [2000] provide an extensive study of changing vital effects in surface and subsurface water $\delta^{18}\text{O}$ of planktonic species on a North Atlantic (NA) transect. This dataset indicates a stable offset of 0.73 to 0.6 ‰ between *G. bulloides* and *G. ruber w.* between 45 and 38°N, south of this area the difference is however increasing. 27 parallel measurements on *G. bulloides* and *G. ruber w.* in core MD08-3180 indicate an average offset of 0.88 ‰, with a standard deviation of 0.27 ‰. This offset is close to the correction of Ganssen and Kroon [2000] (table 2.5). Nevertheless the difference between both species fluctuates between 1.4 and 0.34 ‰ at the transition between warm and cold events as at the onset of the BA, the YD and the Holocene. Therefore the stacked record from these intervals has to be regarded with care.

Table 2.5 Offsets between different planktonic species

Species offset	test size	Offset $\delta^{13}\text{C}$ [‰]	STD [‰]	Offset $\delta^{18}\text{O}$ [‰]	STD [‰]	Reference
<i>G. bulloides</i> - <i>G. ruber w.</i>	2	Not used		0.73-0.60		Ganssen and Kroon [2000]
<i>G. bulloides</i> - <i>G. ruber w.</i>	65	Not used		0.88	0.27	this study core MD08-3180 and MD08-3181

2.4.2.2 $\delta^{18}\text{O}$ vital effect correction for benthic foraminifera

First efforts in correcting benthic species vital effects has been made by Duplessy *et al.* [1984] Jansen *et al.* [1988] Shackleton *et al.* [1987] and Shackleton and Opdyke [1973], comparing the $\delta^{18}\text{O}$ signal of *C. wuellerstorfi* and *Uvigerina sp.*. Those authors assume that *Uvigerina sp.* is recording the signal of the seawater without fractionation, whereas *C. wuellerstorfi* incorporates the $\delta^{18}\text{O}$ signal with a constant offset of 0.64 ‰ to *Uvigerina sp.* and thus is a faithful recorder of seawater $\delta^{18}\text{O}$. This offset of 0.64 ‰ has proved to be robust [Hoogakker *et al.*, 2011] and is used in this study to correct *C. wuellerstorfi* $\delta^{18}\text{O}$ values.

Furthermore a variety on studies included offsets between different other benthic species [Fontanier *et al.*, 2006; Jansen *et al.*, 1988; Schmiedl and Mackensen, 2006] of which the most recent study with the largest data set from the NA region is the study of Hoogakker *et al.* [2011]. Their work provides a compilation of datasets comparing epifaunal and infaunal species and giving correction factors for species-species offsets including the interspecies offset between *M. barleanum* and *C. wuellerstorfi*. No study was published yet specifically considering the vital effects of *M. affinis*.

Here the species specific offset between *M. affinis*, *M. barleeanum* and *C. wuellerstorfi* was investigated by 8 parallel measurements on *M. affinis* and *C. wuellerstorfi*. The observed average offset of -0.2 ‰ between *C. wuellerstorfi* and *M. affinis* matches the observed offset for *M. barleeanum* and *C. wuellerstorfi* of Hoogakker *et al.*[2011] (0.24 ‰) (table 2.6).

Table 2.6 Offsets between different benthic species

Species offset	test size	Offset $\delta^{13}\text{C}$ [‰]	STD +/- [‰]	Offset $\delta^{18}\text{O}$ [‰]	STD +/- [‰]	Reference
<i>C. wuellerstorfi</i> - <i>M. affinis</i>	8	1.5	0.3	-0,2	0.2	this study core GEOFAR KF16
<i>C. wuellerstorfi</i> - <i>M. barleeanum</i>		Not used		-0.18	0.24	<i>Hoogakker et al.</i> 2011

2.5 Abundance of selected foraminifera and its use in water mass reconstruction

Foraminifera assemblages have a long history in its use to reconstruct paleoceanographic changes [Bé and Tolderlund, 1971; CLIMAP and Members, 1981; Darling and Wade, 2008; Kucera et al., 2005; McIntyre et al., 1972; Mix et al., 1986a, b; Pflaumann et al., 1996; Pflaumann et al., 2003; Prell, 1985; Vincent and Berger, 1981] Foraminifera distribution patterns are related to the specialization of foraminifera species on different ecological environments. Due to this specialization on e.g. nutrient and light availability, temperatures, salinity and oxygen content, foraminifera distribution patterns are closely linked to the properties of different water masses. Thus foraminifera assemblages are typical indicators for water masses and can be used to distinguish between polar to tropical water masses (Figure 2.4) [Bé and Tolderlund, 1971; Pflaumann et al., 1996; Schiebel et al., 2002a]. This approach recently was reevaluated using RNA analyses of planktonic foraminifera [Darling and Wade, 2008]. Furthermore the NA datasets were refined by studies of local water mass and foraminifera assemblage distributions [Ottens, 1991; Rogerson et al., 2004; Schiebel et al., 2002a; Schiebel et al., 2002b].

2.5.1 Habitat preferences of selected planktonic foraminifera species

In the following ecological preferences and occurrences of single species, used in this study are explained in detail.

2.5.1.1 *Globigerinoides ruber w. (d'Orbigny, 1839)*

G. ruber w. is a oligotrophic, symbiont bearing spinose species [Bé and Tolderlund, 1971; Hemleben et al., 1989]. Due to photosynthesis performing symbionts, *G. ruber* dwells within the photic zone (0-50 m wd.) preferentially within the uppermost 10 m [Lombard et al., 2011]. In northern subtropical oceans its abundance maximum occurs in august [Lombard et al., 2011]. *G. ruber w.* is the most successful warm water species in terms of distribution and abundance. Its distribution is limited to water temperatures above 14°C and *G. ruber w.* tolerates salinities above 36 PSU or below 34 PSU [Bé and Tolderlund, 1971]. This subtropical to tropical species has a distinct distribution pattern that is limited to latitudes south of 40°N. Its 10% abundance sharply delineates the northern STG boundary [Lombard et al., 2011; Schiebel et al., 2002b]. Thus *G. ruber w.* is an ideal indicator species to track changes in the position of the STG, with values below 10 % indicating a southward retraction of the STG boundary and abundances above 20 % indicate a northward extension of the warm STG.

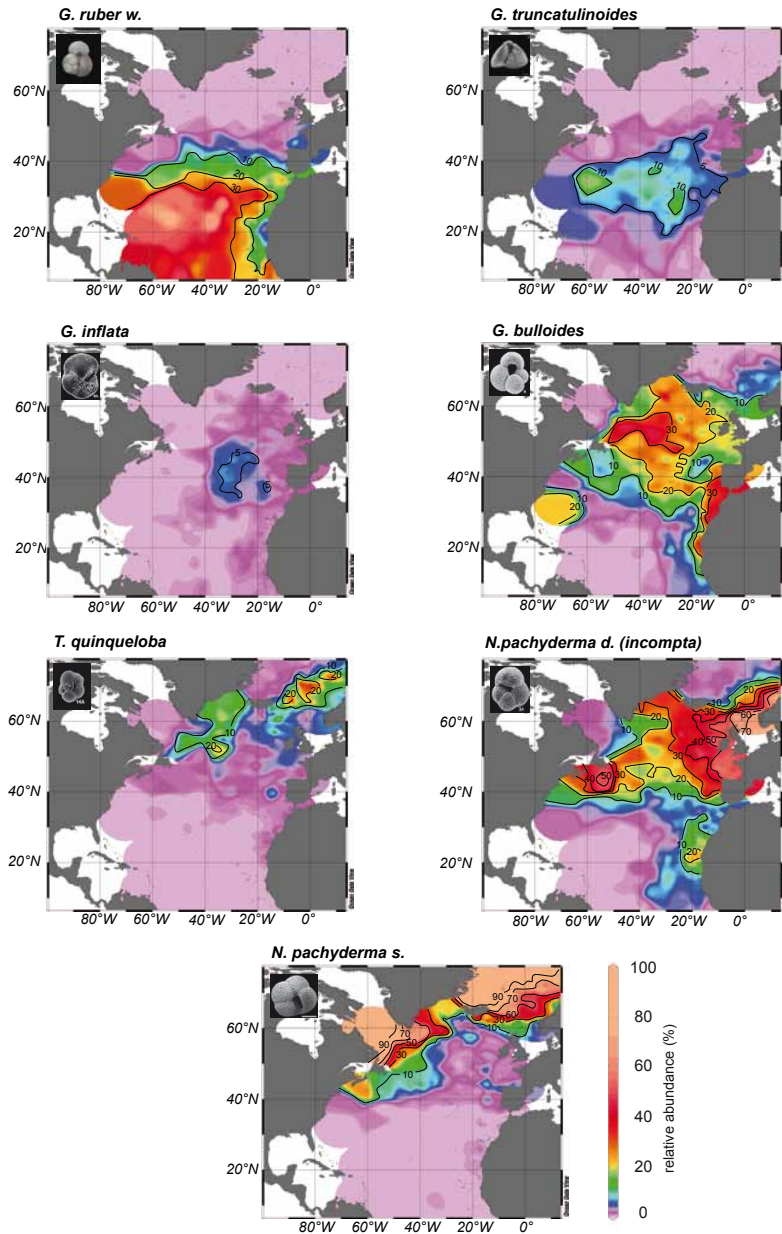


Figure 2.4 Modern distribution patterns of common planktonic foraminifera species in the NA using the dataset of Pflaumann *et al.* [1996]

2.5.1.2 *Globorotalia truncatulinoides*

G. truncatulinoides is a asymbiotic and non-spinose deep-dwelling species that usually feeds on phytoplankton prey [Hemleben *et al.*, 1989]. *G. truncatulinoides* dwells in and below the thermocline [Mulitza *et al.*, 1997]. This species is observed down to 800 m wd in the Caribbean region [Schmuker and Schiebel, 2002], in water masses of temperatures below 16°C it preferentially lives at the basis of the summer thermocline. In the NA north of 35°N the summer thermocline typically evolves at 100 m water depth and thus defines the dwelling depth of *G. truncatulinoides* [Cl  roux *et al.*, 2007]. This observations match with a plankton tow study of

Schiebel et al. [2002a] observing the majority of *G. truncatulinoides* at 0-100 m wd during January and suggest that *G. truncatulinoides* lives in greater water depth throughout the year and emerges to a shallower water depth for reproduction. *G. truncatulinoides* has its distribution maximum within the northern part of the STG between 25 and 40°N. Its 10 % abundance exceeds the northern rim of the STG by 2°N. In analogy to transport pathways in the Caribbean [*Deuser and Ross*, 1989; *Schmuker and Schiebel*, 2002] *Schiebel et al.* [2002a] furthermore suggest that *G. truncatulinoides* is transported by the AC from the Sargasso Sea towards the Azores and thus can be used as indicator for the AC strength.

2.5.1.3 *Globigerina bulloides* (d'Orbigny 1938)

G. bulloides is a non symbiotic, spinose planktonic foraminifera that is associated to temperate to subpolar water masses and probably clustering several genetically distinct opportunistic populations [*Darling and Wade*, 2008]. In latitudes between 40-60°N its maximum abundance occurs in summer (July-August) in subtropical areas in spring [*Lombard et al.*, 2011]. Furthermore it is characteristic and dominant in sediments of upwelling environments in lower latitudes [*Bé*, 1980; *Bé and Tolderlund*, 1971] and tolerating a broad temperature range (0-27°C with peak abundance from 3-19°C) [*Bé and Tolderlund*, 1971].

2.5.1.4 *Globorotalia scitula*

G. scitula is a non spinose, subsurface dwelling species. It is typically found at depth between 100 and 700 m in the NA. Its distribution maximum is situated north of the STG (Figure 2.4) [*Ottens*, 1991; *Pflaumann et al.*, 1996; *Schiebel et al.*, 2002a]. Although *Schiebel et al.* [2002b] stated that the maximum abundance of *G. scitula* delineates the AF, the modern distribution pattern [*Pflaumann et al.*, 1996] (Figure 2.4) indicates a major abundance peak between 37 and 50°N within the ENATW. Therefore peak abundances in *G. scitula* can be associated with an increasing influence of transitional water on the Azores coring site.

2.5.1.5 *Turborotalita quinqueloba* (Natland)

T. quinqueloba is a spinose, symbiont bearing shallow dwelling species (25-75 m) [*Hemleben et al.*, 1989; *Simstich et al.*, 2003]. Its main bloom occurs during the summer season when a pronounced stratification occurs [*Jonkers et al.*, 2010]. *T. quinqueloba* tolerates a range of SST from 1-21°C but predominantly lives in waters with SST below 12°C [*Bé and Tolderlund*, 1971; *Darling and Wade*, 2008]. Accordingly *T. quinqueloba* is predominantly found in subarctic and subantarctic waters. Its modern distribution maximum in the NA is south and east of Iceland and in the Nordic Seas [*Bé and Tolderlund*, 1971; *Pflaumann et al.*, 1996; *Simstich et al.*, 2003]. Due to its predominance in the Arctic front, *T. quinqueloba* is ideal to trace subpolar meltwater and/or even an extreme southward movement of Arctic front to the Azores coring site.

2.5.1.6 *Neoglobigerina pachyderma dextral (N. incompta)*

Is a subpolar non symbiotic, non spinose species [Darling and Wade, 2008]. It mainly dwells at depth below 50 m with a maximum summer dwelling depth of 100-200 m wd.. In latitudes between 40-60°N its maximum abundance occurs in summer (july-august) in subtropical areas in spring [Lombard et al., 2011]. It is one of the major components of the subpolar to transitional water masses of the NA [Darling and Wade, 2008 and citations therein; Pflaumann et al., 1996] with a recent distribution maximum in the eastern subpolar NA. Thus high abundances of *N. pachyderma d* can be used as indicator of ENATW at the Azores coring site.

2.5.1.7 *Neoglobigerina pachyderma sinistral*

Is a non symbiotic, non spinose, carnivore species. It is the only polar species and is the dominant species (>90 %) in sediment assemblages in Polar Regions [Imbrie and Kipp, 1971; Pflaumann et al., 1996]. Its high abundance north of the Arctic front is used to track changes of the Arctic front position over the glacial-interglacial times [McIntyre et al., 1972; Pflaumann et al., 1996]. Its highest abundances are associated with the chlorophyll maximum that occurs between 20 and 80 m wd, where its primary food source is available [Kohfeld et al., 1996]. In latitudes between 40-60°N its abundance maximum occurs in spring [Lombard et al., 2011]. *N. pachyderma s.* tolerates a wide range of temperatures (-1.4 to 10°C) and salinity variation between 30.5 and 50 ‰ [Bé and Tolderlund, 1971] and is most abundant in dense, cold, low salinity surface waters.

2.6 SST reconstructions

Within this study, three different independent methods are used to reconstruct past ocean mixed layer temperatures in the Azores region. Those comprise PF based transfer functions, alkenone based, and Mg/Ca based proxies.

2.6.1 SST reconstructions using Modern Analogue Technique SIMMAX

Modern analogue techniques are used in paleoceanography to quantitatively relate and interpret faunal changes of deep-sea sediment cores in terms of modern oceanographic conditions like temperatures [Hutson, 1980; Imbrie and Kipp, 1971; Pflaumann et al., 1996; Prell, 1985]. Thereby modern calibration data sets link modern core top assemblage data with surface ocean conditions [Imbrie and Kipp, 1971; Pflaumann et al., 1996; Prell, 1985]. In this study the advanced Modern Analogue Technique (MAT) SIMMAX program [Pflaumann et al., 1996] is used. This program optionally includes a geographical weighting that favors modern analogue samples that lie within a range of 100/200 km to the fossil sample site [Pflaumann et al., 2003]. Although this method can induce a smoothing of signals from non- analogue situations [Weinelt et al., 2003], it also avoids the inclusion of spurious or biased analogues from distant regions [Pflaumann et al., 1996; Weinelt et al., 2003].

Analyzed samples were spliced to count 300-1000 individuals from size fraction >150 μm following the taxonomy of *Pflaumann et al. [1996]* which is based on *Bé and Tolderlund [1974]*. The used reference database SIMMAX28 consists of 947 core top samples that are linked to Sea Surface Temperatures (SST) from the Levitus database [*Levitus and T. P. Boyer, 1994*]. To calculate distant and non-distant weighted summer and winter SST the best 10 analogues were used. The minimum correlation coefficient of the default SIMMAX setting was reduced from 0.9 to 0.7 as the use of default setting resulted in non-analogue situations for more than 30 % of the samples. For this adjusted setting the correlation coefficient is >0.92 for all samples except samples between 13.1 and 12.9 ka BP that show correlations between 0.7 and 0.9. Within this study only non-distant weighted results are shown, the difference to the distant weighted method does not exceed 0.5°C. The standard deviation of the SIMMAX SST reconstruction is +/-1°C.

2.6.2 SST reconstructions using the Alkenone undersaturation index U'_{37}

Alkenones are long-chain di-,tri- and tetra-unsaturated ketones that are widely distributed in marine sediments [e.g *Brassell et al., 1986; Müller et al., 1998; Prahl et al., 1988*]. They are produced by the phytoplanktonic coccolithophorid species *Emiliania huxley* and *Gephyrocapsa oceanica*. As these species built more saturated compounds [37:3] and [37:4] in colder water the relationship between the unsaturated components can be used as proxy for SST.

The original global index of [*Brassell et al., 1986*]

$$(1) U'_{37} = [C_{37:2}] - [C_{37:4}] / [C_{37:2} + C_{37:3} + C_{37:4}]$$

has been simplified for the use in temperate to tropical waters by *Prahl et al. [1988]* to

$$(2) U'_{37} = [C_{37:2}] / [C_{37:2} + C_{37:3}]$$

Prahl et al. [1988] state that a content of less than 5 % [37:4] does not influence the SST estimation. As the tetra-unsaturated compound only becomes significant in cold waters (<15°C), the U'_{37} index is used in most studies of tropical to subpolar sediment cores. The global 60°N-60°S calibration (3) of *Müller et al. [1998]* that is used in this study is based on the assumption of *Prahl et al. [1988]*.

$$(3) U'_{37} = 0.033 * SST + 0.044$$

Alkenones were extracted from 2 g of freeze-dried bulk pestled sediment samples by the procedure described in *Etourneau et al. [2010]* using an Accelerator Solvent Extraction system (Dionex ASE 200). Analyses were carried out by multidimensional, double-column gas chromatography using two Agilent 6890 gas chromatographs as described by *Etourneau et al. [2010]*.

Following the assumption of *Prahl et al.* [1998], the influence of [37:4] on low latitudes SST would only be minor and thus would not affect SST reconstructions for the Azores coring site. Though *Rosell-Melé et al.* [1998] however suggest that in the subpolar NA [37:4] are not controlled by temperature but by freshened water as soon as the [37:4] content is increasing above 5 %. Only minor [37:4] (1-2 %) peaks were identified for the H1 event, for the residual record they are absent. Thus for Alkenone SST reconstructions the U^{K}_{37} index was used.

U^{K}_{37} measurements at the Kiel Biomarker Lab have a precision of +/- 0.05 U and were converted to SST by applying the global core top calibration of *Müller et al.* [1998] with an overall uncertainty of +/-1°C.

2.6.3 Water temperature reconstructions using Mg/Ca in planktonic foraminifera (*G. ruber w.* and *G. bulloides* and *G. truncatulinoides*)

Mg/Ca paleothermometry is a widely used proxy for the reconstruction of past ocean temperatures. This method uses species-specific exponential relationship between temperature and Mg/Ca incorporation in $CaCO_2$ shells of marine organisms as planktonic and benthic foraminifera and ostracodes [e.g. *Dwyer et al.*, 1995; *Nürnberg et al.*, 1996]. The advantage of this method using foraminifera shells is that reconstructions of the Mg/Ca temperature and $\delta^{18}O$ measurements can be obtained from the same specimens. Thereby changes in past $\delta^{18}O$ seawater can be estimated without additional errors due to offsets between different proxies.

Monospecific samples of planktonic *G. ruber w.*, *G. bulloides*, and *G. truncatulinoides* in size fractions and sample sizes according to table 2.4 have been used for Mg/Ca analyses. The samples were cracked gently between two glass plates, transferred into pre leached safe lock tubes and cleaned following the protocol of *Martin and Lea* [2002] (Figure 2.3) that includes a reductive and an oxidative cleaning step. After cleaning and dilution, the samples were measured in a simultaneous ICPM-OES instrument with radial plasma observation at the IfG Kiel. Analytical error for Mg/Ca analyses was 0.1% RSD, standard deviations obtained by double measurements on 13 samples are 0.04-0.2 μmol Mg/Ca. Possible shell contamination or coatings by heavy minerals were controlled by additional trace element measurements as suggested by *Barker et al.* [2003].

Several studies have tested different cleaning methods for Mg/Ca analyses including or excluding a reduction step [*Barker et al.*, 2003], that is applied to minimize the effect of authigenic heavy mineral coatings. The results indicate that different cleaning methods affect the Mg/Ca ratios. Thereby reductive treatment causes dissolution of the sample and might result in a 10-15 % decrease of the Mg/Ca ratios [*Barker et al.*, 2003] that translates to 1.2-1.7°C difference in SST estimation. In order to avoid systematical errors based on different cleaning methods, calibrations based on reductive cleaned samples were chosen to convert Mg/Ca ratios into temperatures.

water rinse 3x	<ul style="list-style-type: none"> •n-pure H₂O •ultra sonic bath 20 s
methanol rinse 2x	<ul style="list-style-type: none"> •200 µl ultrapure methanol •ultra sonic bath 20 s
wash 3x	<ul style="list-style-type: none"> •n-pure H₂O
reductive cleaning	<ul style="list-style-type: none"> •100 µl solution Hydrazine + Ammonium Citrate + Ammonium Hydroxide •hot waterbath 30 min with ultrasound every 2 min
wash 3x	<ul style="list-style-type: none"> •n-pure H₂O
oxidative cleaning	<ul style="list-style-type: none"> •250 µl NaOH + H₂O₂ solution •hot water bath 10 min with ultrasound 2x
wash 3x	<ul style="list-style-type: none"> •n-pure H₂O
sample transfer	<ul style="list-style-type: none"> •into leached vials
weak acid leach	<ul style="list-style-type: none"> •100 µl of 0.001 N HNO₃
wash 1x	<ul style="list-style-type: none"> •n-pure H₂O
dissolution	<ul style="list-style-type: none"> •in 500 µl 0.1 N HNO₃
dilution	<ul style="list-style-type: none"> •dilute with 0.1 N HNO₃
analyses with the ICPM-OES	

Figure 2.3 Cleaning protocol for Mg/Ca analyses

2.6.4 Mg/Ca calibrations for planktonic foraminifera

For the calculation of SST from planktonic Mg/Ca ratios a wide range of calibrations is available. Most of describe the relationship between the Mg/Ca ratio and SST by an exponential function in the form of

$$\text{Mg/Ca} = T \cdot b \cdot \exp a$$

with varying parameters a and b (table 2.7 and 2.8).

Early Mg/Ca calibrations mostly relied on culturing experiments with single species. This approach was followed by multispecies [Anand *et al.*, 2003] and single species [e.g. Cléroux *et al.*, 2008; Elderfield and Ganssen, 2000; Regenberg *et al.*, 2009] calibrations based on core top and plankton tow samples. Multispecies calibrations have the advantage that they even can be applied on extinct species and thus mainly are used for reconstructions on longer time scales [Anand *et al.*, 2003].

Recently the awareness of secondary effects on the Mg/Ca ratios as salinity or $[\text{CO}_3^{2-}]$ changes led to the establishment of calibration data sets that include a salinity correction [Ferguson *et al.*, 2008; Hoogakker *et al.*, 2009; Kisakürek *et al.*, 2008] and even a $[\text{CO}_3^{2-}]$ correction [Arbuszewski *et al.*, 2010]. The dwelling depth of planktonic foraminifera may considerably change with variations in the water mass properties as stratification and temperature. Therefore core top calibrations are established taking the advantage of cross calibrations between foraminifera Mg/Ca ratios and calcification temperatures obtained from oxygen isotope ($\delta^{18}\text{O}$) data. These temperature reconstructions are used to estimate the calcification depth and associated calcification temperature from modern ocean datasets [for detail see e.g. Cléroux *et al.*, 2008; Regenberg *et al.*, 2009]. Given the large differences in foraminifera dwelling depth in different water masses, large regional differences exist within the core top calibration data set. To avoid offsets due to this regional bias, here we used the regional species specific calibration of Cléroux [2008] based on NA core tops for surface dwelling *G. bulloides* and *G. ruber w.*. Subsurface dwelling *G. truncatulinoides* were calibrated with the mixed subsurface dweller calibration of Cléroux [2008]. Thereby late Holocene temperature reconstructions rather well match modern temperatures at the Azores coring site. A potential salinity effect on Mg/Ca of *G. ruber* was tested using the equation of Arbuszewski *et al.* [2010], resulting in unrealistic high salinity estimations (39 PSU). The main influence of a salinity overprint is expected to occur at temperatures above 25°C and salinities between 35.5 and 37.7 PSU these temperatures exceed modern temperatures at the Azores coring site (summer 22°C). We therefore assume that Mg/Ca reconstructions at Azores coring site are not influenced by a salinity effect.

Table 2.7 Mg/Ca calibrations for planktonic foraminifera used in this study
The general form of equation is $\text{Mg/Ca} = b \exp(a \cdot T)$

Species	source	B	a	Cleaning method	Reference
<i>G. ruber w.</i>	Core tops North Atlantic	0.78±0.12	0.082±0.01	Reductive	Cléroux <i>et al.</i> [2008]
<i>G. bulloides</i>	Core tops North Atlantic	0.78±0.12	0.082±0.01	Reductive	Cléroux <i>et al.</i> [2008]
Subsurface dweller	Core tops North Atlantic	0.78±0.04	0.052±0.003	Reductive	Cléroux <i>et al.</i> [2008]

2.7 BWT reconstructions using Mg/Ca in benthic foraminifera

Analogously to SST, BWT can be reconstructed using the Mg/Ca ratio of benthic foraminifera. As benthic species live stationary on the sea ground, no offset due to different dwelling depth exist and core top calibrations are established using the bottom water temperatures at the coring site.

For BWT reconstruction from benthic foraminifera, monospecific samples of 11-52 *M. affinis*, *M. barleeanum* (size fraction 250-400 μm) and 7-40 *C. wuellerstorfi* (size fraction 250-400 μm) size fractions and sample sizes according to table 2.3. were used for the Mg/Ca analyses. Sample preparation and measurement followed the same protocol as planktonic foraminifera (Figure 2.3). Down core double measurements on 26 samples gave a standard deviation of 0.1 mmol/mol Mg/Ca for *C. wuellerstorfi*, 0.05 mmol/mol Mg/Ca for *M. barleeanum* and 0.04 mmol/mol Mg/Ca for *M. affinis*.

2.7.1 Mg/Ca calibrations for benthic foraminifera

Several calibration functions for benthic species using different cleaning methods (with and without reductive step) and analyses methods (laser ablation and bulk foraminifera analyses) exist [Bryan and Marchitto, 2008; Elderfield et al., 2006; Healey et al., 2008; Kristj nsd ttir et al., 2007; Lear et al., 2002; Marchitto et al., 2007; Raitzsch et al., 2008; Russell et al., 2004; Segev and Erez, 2006; Skinner et al., 2003; Tachikawa and Elderfield, 2004; Tisserand et al., 2013; Yu and Elderfield, 2008]. Mg/Ca ratio in the benthic foraminifera *C. wuellerstorfi* is influenced by the calcification temperature [Lear et al., 2002; Martin et al., 2002] and the carbonate ion concentration [CO_3^{2-}] of the ambient seawater [Elderfield et al., 2006; Healey et al., 2008; Raitzsch et al., 2008; Yu and Elderfield, 2008]. Various calibrations exist for the Mg/Ca- temperature relationship of *C. wuellerstorfi*, which are adjusted to different temperature ranges [Elderfield et al., 2006; Healey et al., 2008; Lear 2002; Martin et al., 2002; Raitzsch et al., 2008; Russell et al., 2004; Yu and Elderfield, 2008]. At temperatures below 4 C the Mg/Ca uptake is more sensitive to changes in temperature [Elderfield et al., 2006; Healey et al., 2008; Martin et al., 2002; Yu and Elderfield, 2008] than in warmer environments. Elderfield et al. [2006] and [Yu and Elderfield, 2008] attribute this elevated sensitivity to a response of foraminiferal Mg/Ca uptake to changes in the [CO_3^{2-}] saturation. To assess this effect Yu and Elderfield [2008] estimated the [CO_3^{2-}] change over the last deglaciation and Healey et al. [2008] established a new linear calibration for the cold end of the calibration and adding a formula to correct for the carbonate ion effect. Whereas Tisserand et al. [2013] choose a depth transect at the Brasil margin with stable [CO_3^{2-}] conditions at all depth to establish a new calibration exclusively influenced by changes in the BWT. These potential effects on the Azores coring site are discussed in detail in chapter 7.

Neither *C. wuellerstorfi* nor *M. barleeanum* are present in sufficient numbers over the whole record the benthic *M. barleeanum* Mg/Ca record was supplemented with *M. affinis*. Due to the lack of a

calibration for this species, the Mg/Ca offset between *M. affinis* and the species *C. wuellerstorfi* and *M. barleeanum* with established calibrations was tested by parallel measurements (table 2.9). They revealed a constant offset of 0.177 mmol/mol between Mg/Ca values of *M. barleeanum* and *M. affinis* ($\Delta\text{Mg/Ca}$) that was added on the *M. affinis* Mg/Ca values before applying the known calibrations.

Regional benthic multispecies calibrations [Lear *et al.*, 2002] are available for the subpolar NA. At the Azores site however, these calibrations seem to overestimate late Holocene deepwater temperatures by 2°C. Follow the argument of Lear *et al.* [2002] who detect no large Mg/Ca differences between *M. barleeanum* and *C. wuellerstorfi*, we assume that the calibration of Healey *et al.* [2008] that was established for *C. wuellerstorfi* can be used on all three benthic species. This approach might induce systematic error that have to be considered for the intervals where *G. affinis* was used.

Table 2.8 Mg/Ca calibrations for reductive cleaned benthic foraminifera used in this study
General form of equation $\text{Mg/Ca} = b \exp(a \cdot T)$

Species	source	B	a	T range [°C]	Reference
<i>C. wuellerstorfi</i>	Core tops Atlantic, Indian, and Pacific Oceans	0.781	0.23	0.95-3.8	[Healey <i>et al.</i> , 2008]
<i>C. wuellerstorfi</i>	core tops Hawaii, Little Bahama Bank, Sea of Okhotsk, Gulf of California, NE Atlantic, Ceara Rise, Sierra Leone Rise, the Ontong Java Plateau, and the Southern Ocean	0.652	0.28	1.7-4.4	[Lear <i>et al.</i> , 2002]
<i>C. wuellerstorfi</i> <i>Cibicides sp.</i>	core tops (see above)	0.867	0.109	0.8-18	[Lear <i>et al.</i> , 2002]
<i>M. barleeanum</i> <i>M. pompilioides</i> (<i>M. affinis</i>)	core tops (see above)	0.982	0.101	0.8–18.4	(Lear, et al. 2002)
<i>M. barleeanum</i>	core tops Atlantic Ocean	0.658	0.137	0-7	[Kristjánsdóttir <i>et al.</i> , 2007]

Table 2.9 Offsets between Mg/Ca ratios obtained from parallel measurements of different benthic species

Species offset	Core	test size [number]	Offset Mg/Ca	STD +/-	Comment
<i>M. affinis</i> - <i>M. barleanum</i>	GEOFAR KF16	8	-0.30	0.10	Assumed to be constant
<i>C. wuellerstorfi</i> - <i>M. barleanum</i>	GEOFAR KF16	4	0.01	0.22	No clear dependency
<i>C. wuellerstorfi</i> - <i>M. affinis</i>	GEOFAR KF16	3	0.24	0.02	Assumed to be constant

$\delta^{18}\text{O}_{\text{w-ice}}$ reconstructions

Salinity changes in the seawater can be reconstructed from the $\delta^{18}\text{O}$ signal of planktonic and benthic foraminifera by removing the temperature and ice volume effect.

In this study the equations of *Shackleton* [1974] and *Bemis et al.* [1998] are used to remove the temperature effect and calculate the $\delta^{18}\text{O}_{\text{w}}$ values. Additionally the ice volume correction of *Waelbroeck et al.* [2002] is applied, the results are shown as $\delta^{18}\text{O}_{\text{w-ice}}$ record. For details see chapter 4, 5 and 7.

2.8 References

- Anand, P., H. Elderfield, and M. H. Conte (2003), Calibration of Mg/Ca thermometry in planktonic foraminifera from a sediment trap time series, *Paleoceanography*, 18(2), 1050.
- Arbuszewski, J., P. deMenocal, A. Kaplan, and E. C. Farmer (2010), On the fidelity of shell-derived $\delta^{18}\text{O}_{\text{seawater}}$ estimates, *Earth and Planetary Science Letters*, 300(3-4), 185-196.
- Barker, S., M. Greaves, and H. Elderfield (2003), A study of cleaning procedures used for foraminiferal Mg/Ca paleothermometry, *Geochemistry, Geophysics, Geosystems*, 4(9), 8407.
- Bé, A. W. H. (1980), Gametogenic calcification in a spinose planktonic foraminifer, *Globigerinoides sacculifer* (BRADY), *Marine Micropaleontology* 5, 283-310.
- Bé, A. W. H., and D. S. Tolderlund (1971), Distribution and ecology of living planktonic foraminifera in surface waters of the Atlantic and Indian oceans, In: *Funnell, B.M., Riedel, W.R. (Eds.), Micropaleontology of the Oceans. Cambridge Univ. Press, London*, 105-149.
- Bemis, B. E., H. J. Spero, J. Bijma, and D. W. Lea (1998), Reevaluation of the Oxygen Isotopic Composition of Planktonic Foraminifera: Experimental Results and Revised Paleotemperature Equations, *Paleoceanography*, 13(2), 150-160.
- Brassell, S. C., G. Eglinton, I. T. Marlowe, U. Pflaumann, and M. Sarnthein (1986), Molecular stratigraphy: a new tool for climatic assessment, *Nature*, 320(6058), 129-133.
- Bryan, S. P., and T. M. Marchitto (2008), Mg/Ca-temperature proxy in benthic foraminifera: New calibrations from the Florida Straits and a hypothesis regarding Mg/Li, *Paleoceanography*, 23(2), PA2220.
- Cléroux, C., E. Cortijo, J.-C. Duplessy, and R. Zahn (2007), Deep-dwelling foraminifera as thermocline temperature recorders, *G3*, 8(4), Q04N11.
- Cléroux, C., E. Cortijo, P. Anand, L. Labeyrie, F. Bassinot, N. Caillon, and J.-C. Duplessy (2008), Mg/Ca and Sr/Ca ratios in planktonic foraminifera: Proxies for upper water column temperature reconstruction, *Paleoceanography*, 23(3), n/a-n/a.
- CLIMAP, and P. Members (1981), Seasonal reconstruction of the earth's surface at the last glacial maximum, *Geological Society of America, Map and Chart Series*, 36, 18 pp.
- Darling, K. F., and C. M. Wade (2008), The genetic diversity of planktic foraminifera and the global distribution of ribosomal RNA genotypes, *Marine Micropaleontology*, 67(3,4), 216-238.
- Deuser, W. G., and E. H. Ross (1989), Seasonally abundant planktonic foraminifera of the Sargasso Sea; succession, deep-water fluxes, isotopic compositions, and paleoceanographic implications, *The Journal of Foraminiferal Research*, 19(4), 268-293.

- Duplessy, J.-C., N. J. Shackleton, R. K. Matthews, W. Prell, W. F. Ruddiman, M. I. Caralp, and C. H. Hendy (1984), 13C Record of benthic foraminifera in the last interglacial ocean: Implications for the carbon cycle and the global deep water circulation, *Quaternary Research*, 21(2), 225-243.
- Dwyer, G. S., T. M. Cronin, P. A. Baker, M. E. Raymo, J. S. Buzas, and T. Corége (1995), North Atlantic Deepwater Temperature Change During Late Pliocene and Late Quaternary Climatic Cycles, *Science*, 270(5240), 1347-1351.
- Elderfield, H., and G. Ganssen (2000), Past temperature and $\delta^{18}\text{O}$ of surface ocean waters inferred from foraminiferal Mg/Ca ratios, *Nature*, 405, 442-445.
- Elderfield, H., J. Yu, P. Anand, T. Kiefer, and B. Nyland (2006), Calibrations for benthic foraminiferal Mg/Ca paleothermometry and the carbonate ion hypothesis, *Earth and Planetary Science Letters*, 250(3-4), 633-649.
- Etourneau, J., R. Schneider, T. Blanz, and P. Martinez (2010), Intensification of the Walker and Hadley atmospheric circulations during the Pliocene-Pleistocene climate transition, *Earth and Planetary Science Letters*, 297(1-2), 103-110.
- Ferguson, J. E., G. M. Henderson, M. Kucera, and R. E. M. Rickaby (2008), Systematic change of foraminiferal Mg/Ca ratios across a strong salinity gradient, *Earth and Planetary Science Letters*, 265(1-2), 153-166.
- Fontanier, C., A. Mackensen, F. Jorissen, P. Anschutz, L. Licari, and C. Griveaud (2006), Stable oxygen and carbon isotopes of live benthic foraminifera from the Bay of Biscay: Microhabitat impact and seasonal variability, *Marine Micropaleontology*, 58(3), 159-183.
- Friedrich, O., R. Schiebel, P. A. Wilson, S. Weldeab, C. J. Beer, M. J. Cooper, and J. Fiebig (2012), Influence of test size, water depth, and ecology on Mg/Ca, Sr/Ca, $\delta^{18}\text{O}$ and $\delta^{13}\text{C}$ in nine modern species of planktic foraminifers, *Earth and Planetary Science Letters*, 319, 1320(0), 133-145.
- Ganssen, G. M., and D. Kroon (2000), The isotopic signature of planktonic foraminifera from NE Atlantic surface sediments: implications for the reconstruction of past oceanic conditions, *Journal of The Geological Society*, 157(3), 693-699.
- Healey, S. L., R. C. Thunell, and B. H. Corliss (2008), The Mg/Ca-temperature relationship of benthic foraminiferal calcite: New core-top calibrations in the $<4^{\circ}\text{C}$ temperature range, *Earth and Planetary Science Letters*, 272(3-4), 523-530.
- Hemleben, C., M. Spindler, and O. R. Anderson (1989), Modern Planktonic Foraminifera, *Springer, Berlin*, 363pp.
- Hoogakker, B., H. Elderfield, K. Oliver, and S. Crowhurst (2011), Benthic foraminiferal oxygen isotope offsets over the last glacial-interglacial cycle, *Paleoceanography*, 25(4), PA4229.
- Hoogakker, B. A. A., G. P. Klinkhammer, H. Elderfield, E. J. Rohling, and C. Hayward (2009), Mg/Ca paleothermometry in high salinity environments, *Earth and Planetary Science Letters*, 284(3-4), 583-589.
- Hutson, W. H. (1980), The Agulhas Current During the Late Pleistocene: Analysis of Modern Faunal Analogs, *Science*, 207(4426), 64-66.
- Imbrie, J., and N. G. Kipp (1971), A new micropaleontological method for paleoclimatology: Application to a Late Pleistocene Caribbean core, *The Late Cenozoic Glacial Ages. New Haven, Yale University Press.*, 71-181.
- Jansen, E., U. Bleil, R. Henrich, L. Kringstad, and B. Slettemark (1988), Paleoenvironmental Changes in the Norwegian Sea and the Northeast Atlantic During the Last 2.8 m.y.: Deep Sea Drilling Project/Ocean Drilling Program Sites 610, 642, 643 and 644, *Paleoceanography*, 3(5), 563-581.
- Jonkers, L., G.-J. A. Brummer, F. J. C. Peeters, H. M. van Aken, and M. F. De Jong (2010), Seasonal stratification, shell flux, and oxygen isotope dynamics of left-coiling *N. pachyderma* and *T. quinqueloba* in the western subpolar North Atlantic, *Paleoceanography*, 25(2), PA2204.
- Kisakürek, B., A. Eisenhauer, F. Böhm, D. Garbe-Schönberg, and J. Erez (2008), Controls on shell Mg/Ca and Sr/Ca in cultured planktonic foraminifera, *Globigerinoides ruber* (white), *Earth and Planetary Science Letters*, 273(3/4), 260-269.
- Kissel, C., H. Kleiven, X. Morin, and t. S. S. Party (2008), MD168-AMOCINT/1079 XVII IMAGES cruise report, *Les rapports de campagne à la mer, IPEV, 1080 OCE/2008/02*.
- Kohfeld, K. E., R. G. Fairbanks, S. L. Smith, and I. D. Walsh (1996), *Neogloboquadrina pachyderma* (sinistral coiling) as paleoceanographic tracers in polar oceans: evidence from Northeast Water Polynya plankton tows, sediment traps, and surface samples, *Paleoceanography*, 11(6), 679-699.
- Kristjánssdóttir, G. B., D. W. Lea, A. E. Jennings, D. K. Pak, and C. Belanger (2007), New spatial Mg/Ca-temperature calibrations for three Arctic, benthic foraminifera and reconstruction of north Iceland shelf temperature for the past 4000 years, *Geochem. Geophys. Geosyst.*, 8.
- Kucera, M., A. Rosell-Melé, R. Schneider, C. Waelbroeck, and M. Weinelt (2005), Multiproxy approach for the reconstruction of the glacial ocean surface (MARGO), *Quaternary Science Reviews*, 24(7-9), 813-819.
- Lear, C. H., Y. Rosenthal, and N. Slowey (2002), Benthic foraminiferal Mg/Ca-paleothermometry: A revised core-top calibration, *Geochimica et Cosmochimica Acta*, 66(19), 3375-3387.
- Levitus, S., and T. P. Boyer (1994), World Ocean Atlas, NOAA Atlas DIS, Natl. Oceanogr. Data Cent., Ocean Clim. Lab., Washington, D. C., vol. 4, Temperature, 117.
- Lombard, F., L. Labeyrie, E. Michel, L. Bopp, E. Cortijo, S. Retailleau, H. Howa, and F. Jorissen (2011), Modelling planktic foraminifer growth and distribution using an ecophysiological multi-species approach, *Biogeosciences*, 8, 853-873.
- Mackensen, A., H. W. Hubberten, T. Bickert, G. Fischer, and D. K. Fütterer (1993), The $\delta^{13}\text{C}$ in benthic foraminiferal tests of *Fontbotia wuellerstorfi* (Schwager) Relative to the $\delta^{13}\text{C}$ of dissolved inorganic carbon in Southern Ocean Deep Water: Implications for glacial ocean circulation models, *Paleoceanography*, 8(5), 587-610.
- Marchitto, T. M., S. P. Bryan, W. B. Curry, and D. C. McCorkle (2007), Mg/Ca temperature calibration for the benthic foraminifer *Cibicidoides pachyderma*, *Paleoceanography*, 22, PA1203.

- Martin, P. A., and D. W. Lea (2002), A simple evaluation of cleaning procedures on fossil benthic foraminiferal Mg/Ca, *Geochemistry, Geophysics, Geosystems*, 3(10), 8401.
- Martin, P. A., D. W. Lea, Y. Rosenthal, N. J. Shackleton, M. Sarnthein, and T. Papenfuss (2002), Quaternary deep sea temperature histories derived from benthic foraminiferal Mg/Ca, *Earth and Planetary Science Letters*, 198(1-2), 193-209.
- McIntyre, A., W. F. Ruddiman, and R. Jantzen (1972), Southward penetrations of the North Atlantic polar front: faunal and floral evidence of large-scale surface water mass movements over the last 225,000 years, *Deep Sea Research and Oceanographic Abstracts*, 19(1), 61-77.
- Mix, A. C., W. F. Ruddiman, and A. McIntyre (1986), Late Quaternary paleoceanography of the Tropical Atlantic, 1: Spatial variability of annual mean sea-surface temperatures, 0-20,000 years B.P., *Paleoceanography*, 1(1), 43-66.
- Mulitza, S., A. DÅ¼rkoop, W. Hale, G. Wefer, and H. Stefan Niebler (1997), Planktonic foraminifera as recorders of past surface-water stratification, *Geology*, 25(4), 335-338.
- Müller, P. J., G. Kirst, G. Ruhland, I. von Storch, and A. Rosell-Melé (1998), Calibration of the alkenone paleotemperature index U37K' based on core-tops from the eastern South Atlantic and the global ocean (60°N-60°S), *Geochimica et Cosmochimica Acta*, 62(10), 1757-1772.
- Nürnberg, D., J. Bijma, and C. Hemleben (1996), Assessing the reliability of magnesium in foraminiferal calcite as a proxy for water mass temperature *Geochimica et Cosmochimica Acta*, 60(5), 803-814.
- Ottens, J. J. (1991), Planktic foraminifera as North Atlantic water mass indicators, *Oceanologica Acta*, 14(2), 123-140.
- Pflaumann, U., J. Duprat, C. Pujol, and L. D. Labeyrie (1996), SIMMAX: A Modern Analog Technique to Deduce Atlantic Sea Surface Temperatures from Planktonic Foraminifera in Deep-Sea Sediments, *Paleoceanography*, 11(1), 15-35.
- Pflaumann, U., et al. (2003), Glacial North Atlantic: Sea-surface conditions reconstructed by GLAMAP 2000, *Paleoceanography*, 18(3), 1065.
- Prahl, F. G., L. A. Muehlhausen, and D. L. Zahnle (1988), Further evaluation of long-chain alkenones as indicators of paleoceanographic conditions, *Geochimica et Cosmochimica Acta*, 52(9), 2303-2310.
- Prell, W. L. (1985), The stability of low-latitude sea-surface temperatures: An evaluation of the CLIMAP reconstruction with emphasis on the positive SST anomalies, *Washington, D. C. Department of Energy*, 60p.
- Raitzsch, M., H. Kuhnert, J. Groeneveld, and T. Bickert (2008), Benthic foraminifer Mg/Ca anomalies in South Atlantic core top sediments and their implications for paleothermometry, *Geochem. Geophys. Geosyst.*, 9(Q05010).
- Regenberg, M., S. Steph, D. Nürnberg, R. Tiedemann, and D. Garbe-Schönberg (2009), Calibrating Mg/Ca ratios of multiple planktonic foraminiferal species with $\delta^{18}\text{O}$ -calcification temperatures: Paleothermometry for the upper water column, *Earth and Planetary Science Letters*, 278(3,4), 324-336.
- Richter, T. (1998), Sedimentary fluxes at the mid-atlantic ridge - sediment sources, accumulation rates, and geochemical characterisation, *GEOMAR Report, GEOMAR Research Center for Marine Geosciences, Christian Albrechts University in Kiel*(73), 173.
- Richter, T. O., S. van der Gaast, B. Koster, A. Vaars, R. Gieles, H. C. de Stigter, H. De Haas, and T. C. E. van Weering (2006), The Avaatech XRF Core Scanner: technical description and applications to NE Atlantic sediments, *Geological Society, London, Special Publications*, 267(1), 39-50.
- Rogerson, M., E. J. Rohling, P. P. E. Weaver, and J. W. Murray (2004), The Azores Front since the Last Glacial Maximum, *Earth and Planetary Science Letters*, 222(3-4), 779-789.
- Rosell-Melé, A. (1998), Interhemispheric appraisal of the value of alkenone indices as temperature and salinity proxies in high-latitude locations, *Paleoceanography*, 13(6), 694-703.
- Russell, A. D., B. Hönisch, H. J. Spero, and D. W. Lea (2004), Effects of seawater carbonate ion concentration and temperature on shell U, Mg, and Sr in cultured planktonic foraminifera, *Geochimica et Cosmochimica Acta*, 68(21), 4347-4361.
- Schiebel, R., B. Schmuker, M. Alves, and C. Hemleben (2002a), Tracking the Recent and late Pleistocene Azores front by the distribution of planktic foraminifers, *Journal of Marine Systems*, 37(1-3), 213-227.
- Schiebel, R., J. Waniek, A. Zeltner, and M. Alves (2002b), Impact of the Azores Front on the distribution of planktic foraminifers, shelled gastropods, and coccolithophorids, *Deep Sea Research Part II: Topical Studies in Oceanography*, 49(19), 4035-4050.
- Schmiedl, G., and A. Mackensen (2006), Multispecies stable isotopes of benthic foraminifers reveal past changes of organic matter decomposition and deepwater oxygenation in the Arabian Sea, *Paleoceanography*, 21(4), n/a-n/a.
- Schmuker, B., and R. Schiebel (2002), Planktic foraminifers and hydrography of the eastern and northern Caribbean Sea, *Marine Micropaleontology*, 46(3-4), 387-403.
- Schwab, C. (2013), Late Quaternary changes in paleoproductivity and hydrography in the Azores region deduced from coccolithophore assemblages, *Eldiss. University Kiel*.
- Schwab, C., H. Kinkel, M. Weinelt, and J. Repschläger (2012), Coccolithophore paleoproductivity and ecology response to deglacial and Holocene changes in the Azores Current System, *Paleoceanography*, 27(3), PA3210.
- Segev, E., and J. Erez (2006), Effect of Mg/Ca ratio in seawater on shell composition in shallow benthic foraminifera, *Geochemistry, Geophysics, Geosystems (G3)*, 7(2).
- Shackleton, N. J. (1987), Oxygen isotopes, ice volume and sea level, *Quaternary Science Reviews*, 6(3-4), 183-190.
- Shackleton, N. J., and N. D. Opdyke (1973), Oxygen isotope and palaeomagnetic stratigraphy of Equatorial Pacific core V28-238: Oxygen isotope temperatures and ice volumes on a 105 year and 106 year scale, *Quaternary Research*, 3(1), 39-55.
- Simstich, J., M. Sarnthein, and H. Erlenkeuser (2003), Paired $\delta^{18}\text{O}$ signals of *Neogloboquadrina pachyderma* (s) and *Turborotalita quinqueloba* show thermal stratification structure in Nordic Seas, *Marine Micropaleontology*, 48, 107-125.

- Skinner, L. C., N. J. Shackleton, and H. Elderfield (2003), Millennial-scale variability of deep-water temperature and $\delta^{18}\text{O}_{\text{dw}}$ indicating deep-water source variations in the Northeast Atlantic, 0-34 cal. ka BP, *Geochem. Geophys. Geosyst.*, 4(12), 1098.
- Tachikawa, K., and H. Elderfield (Eds.) (2004), Chemistry of benthic foraminiferal shells for recording ocean environments: Cd/Ca, $\delta^{13}\text{C}$ and Mg/Ca, 249-263 pp., TERRAPUB.
- Tisserand, A. A., T. M. Dokken, C. Waelbroeck, J.-M. Gherardi, V. Scao, C. Fontanier, and F. Jorissen (2013), Refining benthic foraminiferal Mg/Ca-temperature calibrations using core-tops from the western tropical Atlantic: Implication for paleotemperature estimation, *Geochemistry, Geophysics, Geosystems*, 14(4), 929-946.
- Tjallingii, R., U. Röhl, M. Kölling, and T. Bickert (2007), Influence of the water content on X-ray fluorescence core-scanning measurements in soft marine sediments, *Geochemistry, Geophysics, Geosystems*, 8(2), Q02004.
- Vincent, E., and W. Berger (1981), Planktonic foraminifera and their use in paleoceanography, *n: Emiliani C (ed) The Sea*, 7, pp 1025-1119.
- Waelbroeck, C., L. Labeyrie, E. Michel, J. C. Duplessy, J. F. McManus, K. Lambeck, E. Balbon, and M. Labracherie (2002), Sea-level and deep water temperature changes derived from benthic foraminifera isotopic records, *Quaternary Science Reviews*, 21, 295-305.
- Weinelt, M., E. Vogelsang, M. Kucera, U. Pflaumann, M. Sarnthein, A. Voelker, H. Erlenkeuser, and B. A. Malmgren (2003), Variability of North Atlantic heat transfer during MIS 2, *Paleoceanography*, 18(3), 1071.
- Weltje, G. J., and R. Tjallingii (2008), Calibration of XRF core scanners for quantitative geochemical logging of sediment cores: Theory and application, *Earth Planet. Sci. Lett.*
- Yu, J., and H. Elderfield (2008), Mg/Ca in the benthic foraminifera *Cibicides wuellerstorfi* and *Cibicides mundulus*: Temperature versus carbonate ion saturation, *Earth and Planetary Science Letters*, 276(1-2), 129-139.

Foraminifera fotos obtained from

http://commons.wikimedia.org/wiki/File:Neoglobobulimina-pachyderma_hg.jpg

<http://www.google.de/imgres?q=N.pachyderma&start=99&client=safari&sa=X&rls=en&biw=1129&bih=619&tbn=isch&tbnid=aN1rdumKO07QbM:&imgrefurl=http://webpersonal.uma.es/~fsl/publicaciones.html&docid=egoAiarFGQHIRM&imgurl=http://webpersonal.uma.es/~fsl/imag/N.pachyderma.jpg&w=150&h=158&ei=kdS5UbSkI-O14ATEzIC4DQ&zoom=1&iact=hc&vpx=359&vpy=271&dur=721&hovh=126&hovw=120&tx=73&ty=66&page=5&tbnh=126&tbnw=106&ndsp=30&ved=1t:429,r:1,s:100,i:7>

http://www.google.de/imgres?imgurl=http://1.bp.blogspot.com/_vIFjCB2JdF8/TGJLnIHYR7I/AAAAAAAAANE/-1pF-sXIdQs/s1600/globorotalia-truncatulinoidea1-heb214.jpg&imgrefurl=http://foraminifer.blogspot.com/2010/08/globorotalia-truncatulinoidea.html&h=1600&w=1600&sz=51&tbnid=fdxEHHce-Ne3CM:&tbnh=87&tbnw=87&prev=/search%3Fq%3Dtruncatulinoidea%2Bphoto%26tbn%3Disch%26tbo%3Du&zoom=1&q=truncatulinoidea+photo&usq=__3DMHF-IRGK9-G244WmrBXf27h4U=&docid=IA4PcqyBHIWcqM&sa=X&ei=kSnbUc-VCITQtaA3soCgBQ&ved=0CCwQ9QEwAA&dur=347

<http://www.ucl.ac.uk/GeolSci/micropal/images/fora/fora003.gif>

Chapter 3

Age Model

3 Age Model

The age models of the spliced cores MD08-3180 / GEOFAR KF16 are based on ^{14}C AMS Accelerator Mass spectrometer (AMS) measurements that were analyzed at the Leibniz-Laboratory for Radiometric Dating and Isotope Research at Kiel University. All ages were converted into calendar ages using Calib 6.0 software [Stuiver and Reimer, 1986] with marine09 calibration curve [Reimer et al., 2009] assuming a constant reservoir age of 400 years. Accordingly changes in the *G. ruber w.* $\delta^{18}\text{O}$ record and U^{K}_{37} SST coincided well in timing with changes in the Greenland $\delta^{18}\text{O}$ record NGRIP [Andersen et al., 2006] for warm periods and justify the assumption that atmospheric northern hemisphere (NH) temperatures coincide with subtropical SST changes. Therefore, in addition to ^{14}C age depth markers the surface $\delta^{18}\text{O}$ record and U^{K}_{37} SST record were fine-tuned against Greenland ice core NGRIP [Andersen et al., 2006] using the AnalySeries computer program [Paillard et al., 1996], resulting in additional 10 markers (Figure 3.1).

Based on this tuning, reservoir ages of up to 1000 years were observed for the Younger Dryas, which are consistent with other findings from the North Atlantic [e.g. Waelbroeck et al., 2001].

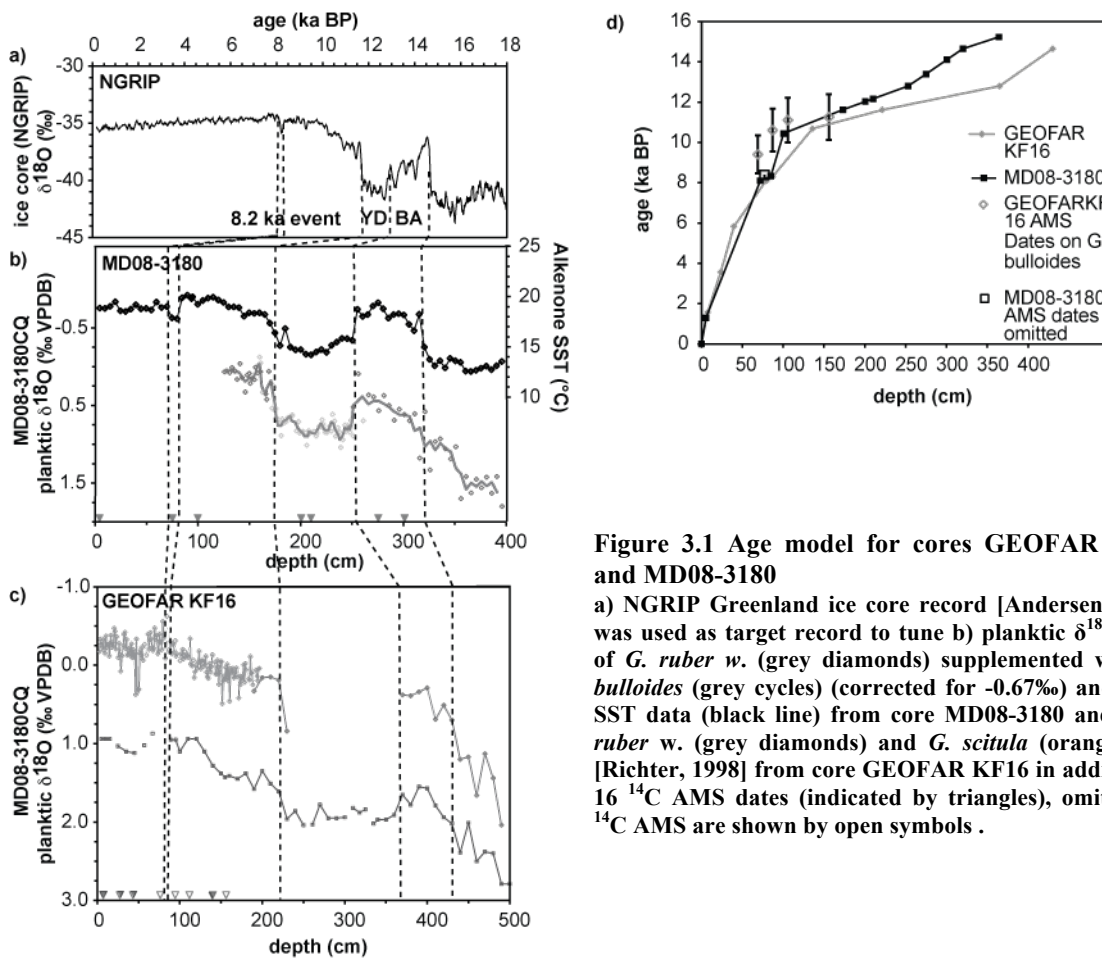


Figure 3.1 Age model for cores GEOFAR KF16 and MD08-3180

a) NGRIP Greenland ice core record [Andersen, 2007] was used as target record to tune b) planktic $\delta^{18}\text{O}$ data of *G. ruber w.* (grey diamonds) supplemented with *G. bulloides* (grey cycles) (corrected for -0.67‰) and U^{K}_{37} SST data (black line) from core MD08-3180 and c) *G. ruber w.* (grey diamonds) and *G. scitula* (orange line) [Richter, 1998] from core GEOFAR KF16 in addition to 16 ^{14}C AMS dates (indicated by triangles), omitted 16 ^{14}C AMS are shown by open symbols.

Accordingly our proxy records cover the deglacial transition from 16 ka BP to 6 ka BP in 200 to 20 year resolution with particular high-resolution over the deglacial sequence. For core GEOFAR KF16 three age points during the Preboreal (9800-10600 ka) measured on *G. bulloides* fall apart from the isotope stratigraphy based on *G. ruber w.*, and the sedimentology of both cores (Figure 3.1). Those ages rather seem to be influenced by the upwelling of an older intermediate water mass at the coring site and are therefore ignored for the age model.

An alternative tuning approach uses the abundances of *G. ruber w.*. This record closely matches the Greenland ice core record from 16-10 ka BP and thus might be related to NH atmospheric temperatures. Accordingly, the start of the YD would be 300 years earlier as compared to the $U^{K'}_{37}$ and $\delta^{18}O$ record. This mismatch might be explained by an overprint of the signal by freshwater and/or failure of the $U^{K'}_{37}$ in freshwater influenced environments.

This tuning method would imply reservoir ages of less than 200 years at the end of BA that are neither consistent with the findings of *Waelbroeck et al.* [2001] nor with the findings of *Thornalley et al.* [2011b], who observed reservoir age of 400-800 years ages in the end of BA.

The similarity between *G. ruber w.* abundance and the Greenland ice core is limited to the Bølling-Allerød and the YD interval reveals strong mismatches over the Holocene (Figure 3.2). These mismatches question the reliability of the linkage between the *G. ruber w.* record and the Greenland ice core record. The benthic $\delta^{13}C$ record matches well-dated records from Iberian Margin and subpolar NA within dating accuracy (Figure 3.3) [Skinner et al., 2003; Thornalley et al., 2011a].

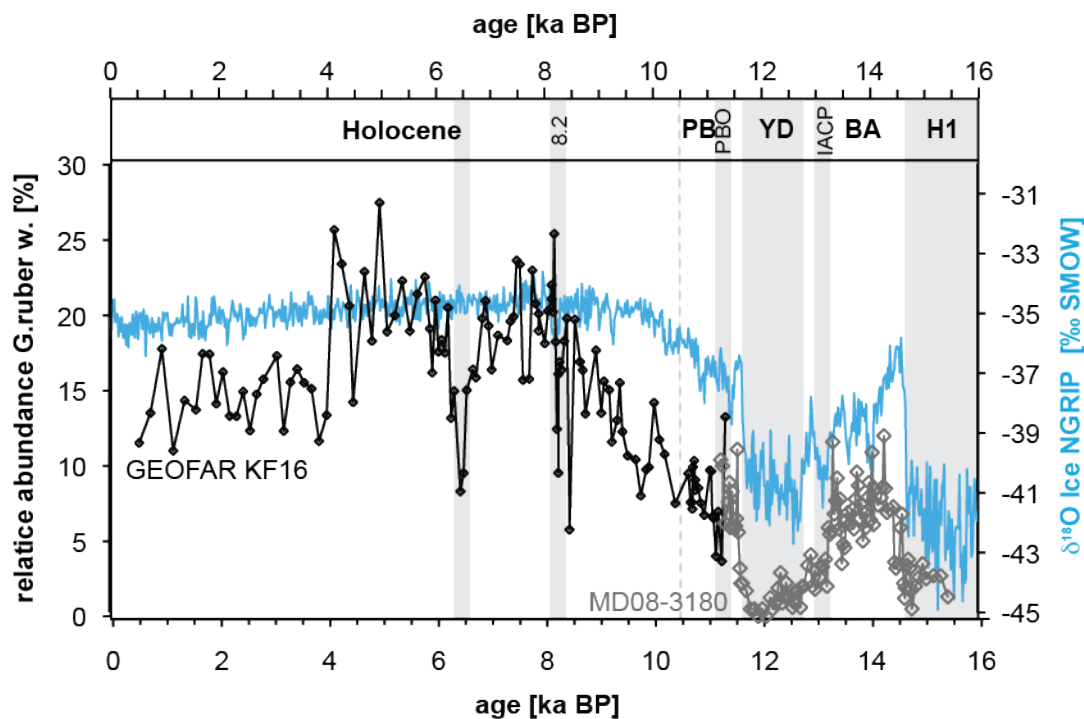


Figure 3.2 Comparison between *G. ruber w.* abundance data and Greenland ice core data shows close relation between the relative abundance of *G. ruber w.* (black GEOFAR KF16; grey MD08-3180) and NGRIP data [Andersen, 2007] during BA but lower correlation over the Holocene

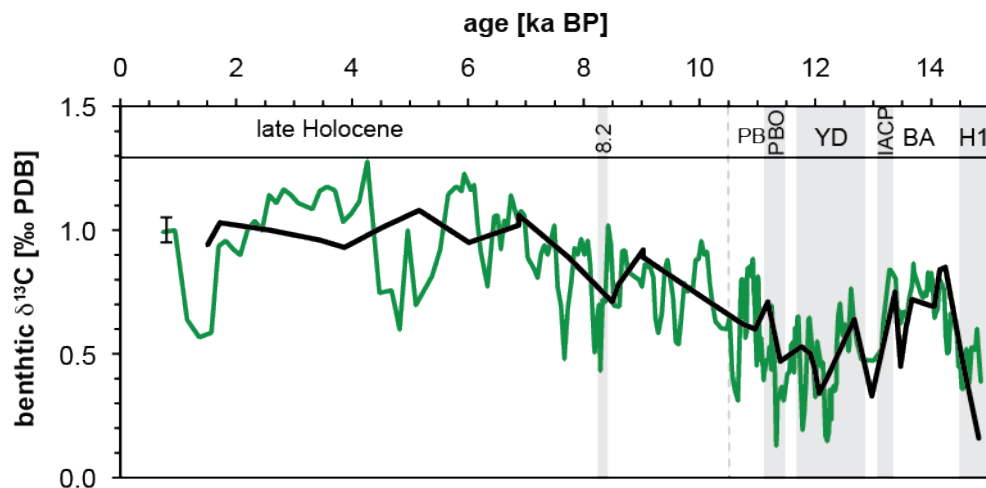


Figure 3.3 Comparison between benthic $\delta^{13}\text{C}$ records from the Azores coring site (green line) and the Iberian Margin [Skinner *et al.*, 2003] (black line) show a close correlation.

The age model of Schwab *et al.* [2012] is furthermore supported by additional ^{14}C AMS data points obtained from the transition between the BA and the YD by Balmer (pers. communication). Therefore we keep the age model of Schwab *et al.* [2012].

Nevertheless, observed offsets between different SST proxies in timing [Sicre *et al.*, 2013] indicate that the tuning of SST records with the Greenland ice core record might imply systematic errors and requires further investigation.

3.1 References

- Andersen, K. K., *et al.* (2006), The Greenland Ice Core Chronology 2005, 150-0 ka. Part 1: constructing the time scale, *Quaternary Science Reviews*, 25(23-24), 3246-3257.
- Paillard, D., L. Labeyrie, and P. Yiou (1996), Macintosh program performs time-series analysis, *Eos Trans. AGU*, 77.
- Reimer, P., *et al.* (2009), IntCal09 and Marine09 Radiocarbon Age Calibration Curves, 0-50,000 Years cal BP, *Radiocarbon*, 51(4), 1111-1150.
- Schwab, C., H. Kinkel, M. Weinelt, and J. Repschlager (2012), Coccolithophore paleoproductivity and ecology response to deglacial and Holocene changes in the Azores Current System, *Paleoceanography*, 27(3), PA3210.
- Sicre, M. A., G. Siani, D. Genty, N. Kallel, and L. Essallami (2013), Seemingly divergent sea surface temperature proxy records in the central Mediterranean during the last deglacial, *Clim. Past Discuss.*, 9(1), 683-701.
- Skinner, L. C., N. J. Shackleton, and H. Elderfield (2003), Millennial-scale variability of deep-water temperature and $\delta^{18}\text{O}_{\text{dw}}$ indicating deep-water source variations in the Northeast Atlantic, 0-34 cal. ka BP, *Geochem. Geophys. Geosyst.*, 4(12), 1098.
- Stuiver, M., and P. J. Reimer (1986), A computer program for radiocarbon age calibration, *Radiocarbon*, 28, 022-1030.
- Thornalley, D., H. Elderfield, and I. N. McCave (2011a), Reconstructing North Atlantic deglacial surface hydrography and its link to the Atlantic overturning circulation, *Global and Planetary Change*, 79(3-4), 163-175.
- Thornalley, D., S. Barker, W. S. Broecker, H. Elderfield, and I. N. McCave (2011b), The Deglacial Evolution of North Atlantic Deep Convection, *Science*, 331(6014), 202-205.
- Waelbroeck, C., J.-C. Duplessy, E. Michel, L. Labeyrie, D. Paillard, and J. Duprat (2001), The timing of the last deglaciation in North Atlantic climate records, *Nature*, 412(6848), 724-727.

Chapter 4

Disentangling multiproxy temperature reconstructions in the subtropical North Atlantic

4 Disentangling multiproxy temperature reconstructions in the subtropical North Atlantic

4.1 Introduction

Reliable reconstructions of the sea surface temperature (SST) variability that is associated with global climate changes are needed to improve the climate models that predict the anthropogenic forced future climate change. In order to robustly assess the full range of glacial to interglacial temperature changes in paleoceanography, multiple proxies records were used to better approximate the SST [Kucera *et al.*, 2005; MARGO, 2009]. This approach includes microfossil and geochemical based SST reconstructions. The microfossil proxies consist of transfer functions (e.g. as Modern Analogue Techniques (MAT) and Artificial Neural Networks (ANN)) that are mostly based on planktonic foraminifera (PF) and complemented with diatom, dinoflagellate cyst and radiolarian abundances. Geochemical “paleothermometers” are obtained from Mg/Ca measurements on planktonic foraminifera and the alkenone undersaturation index U_{37}^k that is produced by coccolithophores (for details see chapter 3). The multiproxy approach reveals strong mismatches between single SST estimates [Jansen *et al.*, 2009; Leduc *et al.*, 2010; Schneider *et al.*, 2010; Sicre *et al.*, 2013; Steinke *et al.*, 2008] and thus allows a wide range of possible SST scenarios. These differences become for example evident in the results of the CLIMAP [1981] and the MARGO [2009] projects that provided glacial temperature maps of the last Glacial Maximum with different results. While CLIMAP [1981] reconstructed a glacial warming of the subtropical regions by the use of MAT, the results of the MARGO [2009] multiproxy approach indicate a slight glacial cooling (2°C) for that region.

It is generally reasoned that discrepancies between different proxy reconstructions are caused by differential reactions of the signal bearing organisms on the ecological changes that went along with the SST change [Leduc *et al.*, 2010; Sicre *et al.*, 2013; Telford *et al.*, 2012]. Those are for example changes in the vertical and horizontal position of water mass boundaries, changes in nutrient availability and salinity changes [Kisakürek *et al.*, 2008; Pérez-Folgado *et al.*, 2003; Sabbatini *et al.*, 2011a; Sicre *et al.*, 2013; Storz *et al.*, 2009; Telford *et al.*, 2012]. The impact of these variations in water mass conditions on the marine biota may have a larger effect on the proxy than the SST change. Thereby the assumption of a constant relationship between the water mass conditions and the SST proxy may be violated [Telford *et al.*, 2012]. Due to this various effects, different biases are observed for SST reconstructions that are specified in the following.

Pérez-Folgado *et al.* [2003] and Sicre *et al.* [2013] report a bias between SST calculated by Modern Analogue Technique (MAT) and U_{37}^k SST reconstructions from the Mediterranean Sea that might be caused by seasonal changes of the coccolithophore bloom. Such seasonal offsets are also suggested to cause different interglacial evolutions of U_{37}^k records between low and high

latitudes [Leduc *et al.*, 2010; Sicre *et al.*, 2013]. Furthermore U^{K}_{37} SST reconstructions and SST reconstructions based on foraminifera shells might be biased by a strong transport of coccolithophores with oceanic currents [Ohkouchi *et al.*, 2002] and by bioturbation that effects the coccolithophore containing fine fraction ($< 63\mu\text{m}$) stronger than the foraminifera bearing ($>150\mu\text{m}$) fraction [Bard, 2001] as used in PF transfer functions.

SST reconstructions with the modern analogue technique using the SIMMAX calculation [Pflaumann *et al.*, 1996], though calibrated to defined water depths (here 10 m) might be influenced by a strong imprint of subsurface water mass conditions [Adloff *et al.*, 2011; Telford *et al.*, 2012]. This is caused by the integration of specimens from different water depth into core top fauna assemblages, thus integrating the thermal structure of the whole upper water column. Once the thermal structure of the ocean changes over time foraminifera assemblages suggests a SST change according to the modern structures. Thereby most severe changes are not restricted to the upper 10 m water of the water column that are used for the SIMMAX calibrations but may occur within the upper 100 m. The resulting temperature signal may therefore be biased towards a subsurface water signal. This bias is especially important in regions with pronounced oceanographic changes between glacial and interglacial times that lack analogue situations in the calibration data sets [Adloff *et al.*, 2011; Storz *et al.*, 2009; Telford *et al.*, 2012]. This situation also applies to the North Atlantic Subtropical Gyre (STG).

Mg/Ca temperature reconstructions in turn are particularly prone to changes in the growing season and depth habitat of the foraminifera [Lohmann *et al.*, 2012; Lombard *et al.*, 2011; Schneider *et al.*, 2010], as well as changes in the chemistry of the ambient seawater including salinity changes [Kisakürek *et al.*, 2008; Sabbatini *et al.*, 2011b] and changes in the carbonate ion concentration [Arbuszewski *et al.*, 2010]. Furthermore, heavy mineral coatings of the foraminifera shells can strongly affect the Mg/Ca content of the shells [Barker *et al.*, 2003; Bian and Martin, 2010]. Reduced reliability of the Mg/Ca-temperature calibration at the cold end of the calibration data set [Kozdon *et al.*, 2009; Meland *et al.*, 2005] might lead to an overestimation of the SST during cold periods.

The Azores coring site is positioned at the northern boundary of the subtropical gyre, at the interface between cool temperate, nutrient rich subpolar and warm, oligotrophic subtropical water. The position of this water mass boundary is expected to have changed on glacial to interglacial time scales [Schiebel *et al.*, 2002] as well as during interglacials [Schwab *et al.*, 2012]. Thus it is particularly well suited to disentangle the performance of SST proxies, under changing water mass properties and thus, to better assess subtropical SST variability on multi-centennial to millennial-scale AMOC variability.

We compare independent geochemical (Mg/Ca and U^{K}_{37}) SST reconstructions and microfossil (SIMMAX MAT) based SST reconstructions. Abundances of foraminiferal indicator species with well known ecological preferences are used to explain discrepancies between single SST

reconstructions and gain better insight into the deglacial and the Holocene changes in surface hydrology of the AC. Furthermore our SST estimates are compared with fresh water forced modeling run using the Kiel Climate Model in order to assess the plausibility of the SST reconstructions.

4.2 Hydrology

The surface hydrography at the Azores coring site is governed by the Azores current system (see also chapter 1.6). The main feature of this system is the AC current, that branches off the NAC between 30 and 40°N and flows eastward towards the Mediterranean Sea. On its pathway it induces mesoscale eddies that can reach the width of 200 km. Within this current system the Azores front (AF) separates oligotrophic subtropical and nutrient rich transitional Eastern North Atlantic Central Water (ENACW) and is defined by the strongest dipping 15°C isotherm. Although it is not distinguishable by the surface SST distribution [Alves *et al.*, 2002], the AF separates distinctly different fauna assemblages [Ottens, 1991; Rogerson *et al.*, 2004; Schiebel *et al.*, 2002] that can be used to track deglacial changes in the AF position.

Table 4.1 Overview of habitat preferences of planktonic foraminifera used as indicator species in this study

SPECIES	WATER MASS	TEMPERATURE TOLERANCE [°C]	LATITUDE	DWELLING DEPTH [M]	BLOOM
<i>N. pachyderma s.</i>	Polar ¹⁾²⁾³⁾⁵⁾	0-10 ³⁾⁸⁾ d.max	40-90°N	50-300 ²⁾	May ²⁾¹⁾
<i>T. quinqueloba</i>	Polar to subpolar ¹⁾⁵⁾³⁾ typically living in polar and subpolar front ⁶⁾		40-90°N	25-75 ¹⁾²⁾	Summer ¹⁾
<i>N. pachyderma d.</i>	Transitional, NE Atlantic water ⁶⁾⁵⁾		40-60°N 30-40°N	30 ²⁾ -100 ²⁾ 50 ²⁾ -200 ²⁾	June-July ²⁾ May-June ²⁾
<i>G. bulloides</i>	Transitional ⁵⁾⁶⁾⁷⁾		40-60°N 30-40°N	20 ²⁾ 50 ²⁾	June-July ²⁾ May-June ²⁾
<i>G. scitula</i>	Transitional, typically occurring in small band N of AF ⁷⁾⁶⁾	10-30 ³⁾⁸⁾	North of Azores front	100-700 ⁴⁾	April-May ¹²⁾
<i>G. truncatulinoides</i>	Subtropical to tropical, indicator for AC transport strength ⁴⁾	8-30 ³⁾⁸⁾	40-60°N 30-40°N	100-150 ⁹⁾ 200-800 ⁹⁾	Annual cycle ⁴⁾⁹⁾ Annual cycle ⁴⁾⁹⁾
<i>G. ruber w.</i>	Subtropical to tropical limited to warm oligotrophic STG ⁵⁾	>14 ³⁾⁸⁾ d.max>24	0-40°N	0-10 max 50 ²⁾	August ²⁾¹¹⁾
Alkenone producing coccolithophorides	global		40-60°N 30-40°N	0-10 assumed 0-10 assumed	Late spring ¹⁰⁾ Early spring ¹⁰⁾

References ¹⁾ Simstich *et al.* [2003] ²⁾ Lombard *et al.* [2011] ³⁾ Bé and Tolderlund, [1971] ⁴⁾ Schiebel *et al.* [2002] ⁵⁾ Pflaumann *et al.* [1996] ⁶⁾ Ottens [1991] ⁷⁾ [2004] ⁸⁾ Darling and Wade [2008] ⁹⁾ Cléroux *et al.* [2007] ¹⁰⁾ Longhurst [2007], ¹¹⁾ Anand *et al.* [2003] ¹²⁾ Storz *et al.* [2009]

G. ruber w. and *G. truncatulinoides* are most abundant south of the AF, *G. scitula* and *N. pachyderma d.* typically occur north of the front within the ENACW. Whereas the species *T. quinqueloba* and *N. pachyderma s.* today are dominant in the Nordic seas and at the polar front and thus are valid indicators for subpolar to polar conditions (for more detailed information see Chapter 3). Habitat and seasonal preferences for these species are given in table 4.1.

Under modern conditions the main coccolithophore bloom at the vicinity of the Azores occurs during spring [Longhurst, 2007] when the first stratification of the surface water occurs after winter mixing has increased the nutrient content of the mixed layer. In the transitional to subpolar NA (40 and 60°N) high nutrient availability prevails all year long and the coccolithophore bloom occurs during the summer months, when a strong stratification evolves [Longhurst, 2007].

4.3 Material and Methods

For this study a high-resolution deglacial record of the spliced cores GEOFAR KF16 / MD08-3180 from the Azores coring site are used (for age model see chapter 3; 5; 6). This core interval spans the last 16 ka BP in multidecadal to centennial resolution, that were governed by the last deglaciation with warm Bølling-Allerød (BA) and the warm Holocene and the cold Heinrich 1 (H1) event, the Younger Dryas (YD) event. The short term cold IACP and 8.2 interrupted the warm BA and Holocene. The sediments are well preserved as shown by the occurrence of pteropodes during the YD and samples from throughout the core showing pristine calcite shells when analyzed under a scanning electron microscope (SEM).

SST reconstructions from three different methods that are foraminiferal transfer functions (SIMMAX) [Pflaumann *et al.*, 1996], the alkenone undersaturation index $U_{37}^{K'}$ and Mg/Ca SST reconstruction from surface (*G. ruber w.*, *G. bulloides*) and subsurface dwelling (*G. truncatulinoides*) foraminifera calibrated with the calibration of Cléroux *et al.* [2008] are compared. Additionally single foraminifera indicator species abundances are used to get an insight into the hydrological changes at the Azores coring site as summarized in table 4.1. Thereby *G. ruber w.* is assumed to be an indicator for the influence of oligotrophic STG waters and its abundance changes reflect changes in the STG position. *G. truncatulinoides* is suggested to be an indicator for transport strength within the AC [Schiebel *et al.*, 2002]. *G. scitula* and *N. pachyderma d.* typically occur north of the front within the ENACW [Ottens, 1991; Rogerson *et al.*, 2004]. The subpolar and polar species *T. quinqueloba* and *N. pachyderma s.* indicate the influence of subpolar water on the coring site (for more details see Chapter 2.5).

Changes in salinity over time can be reconstructed from the surface foraminiferal $\delta^{18}\text{O}_{\text{carbonate}}$ record by removing the temperature effect, known from the SST. To assess the impact of different SST reconstruction on the salinity reconstructions the $\delta^{18}\text{O}_w$ record was established using the formula of Bemis *et al.* [1998] and $\delta^{18}\text{O}_{\text{carbonate}}$ records of *G. ruber w.* and *G. bulloides* and combined with the

SIMMAX, $U^{K'}_{37}$ and SST records. To correct this $\delta^{18}O_w$ record for ice volume, we used the relative sea level composite curve of *Waelbroeck et al.* [2002].

For the modeling study a fully coupled Atmosphere Ocean General Circulation Model (AOGCM), the Kiel Climate Model (KCM) (for further details see *Schneider et al.* [2010]) was used. For the transient experimental setup a continuous 1 Sv meltwater input into the NA was applied on the pre-industrial (0 ka) model setting following the experimental setup of *Stouffer et al.* [2006] (pers. communication Krebs-Kanzow).

4.4 Results

Deglacial temperature records based on $U^{K'}_{37}$, SIMMAX calculations and Mg/Ca ratios (Figure 4.1) from *G. bulloides* and *G. ruber w.* show the well-known deglacial sequence consisting of the cold H1 (12°C), YD (14°C) and 8.2 event (6-18°C) and the warm BA (19°C) and Holocene (19-20°C).

SIMMAX SST reconstructions indicate warm temperatures over the Holocene similar to modern summer SST (23°C) and winter SST (16°C). The difference between both seasons amounts to 6°C over the Holocene. During BA warm period, SIMMAX summer SST (SST_{su}) fluctuate around the modern annual mean SST (19°C), whereas SIMMAX winter SST (SST_{wi}) are 5°C colder. During early to mid YD (12.8-12.1 ka BP) SST_{su} are warm and reach 17-18°C that are close to modern annual mean SST, during the late YD SST_{su} cool down by 4°C to 14°C. Over the entire YD SST_{wi} are 4°C colder than SST_{su} . Three major short-time cold events, the H1 event, the IACP and the 8.2 event are indicated within the SIMMAX SST record with extreme cooling rates of 9°C during H1 event and 11°C during the IACP and the 8.2 event. Similar absolute SST_{su} values of about 10°C are reached during all three events with the SST_{wi} even reaching down to 6°C. These cold events are thus by far colder than modern winter SST of 16°C. During the Preboreal SIMMAX SST are generally rising by 5°C. This Preboreal warming trend is characterized by pronounced fluctuations in both SST_{su} and SST_{wi} with a magnitude of about 4°C (Figure 4.1a).

The $U^{K'}_{37}$ SST record (Figure 4.1) indicates warm SST for the Bølling-Allerød (19°C) and the Holocene (19-20°C) that match the modern annual mean SST. Colder temperatures are indicated during the H1, the YD and the 8.2 event. With respect to modern annual mean the cooling rates for these events amount to 6°C during the H1 and the YD and 1.5°C during the 8.2 event (Figure 4.1b). The cooling during the IACP hardly exceeds the error of the calibration (1°C).

Surface water Mg/Ca reconstructions are restricted to the interval of late BA to the end of the YD. During the BA, the *G. bulloides* Mg/Ca SST record oscillates between modern winter and summer SST, reaching modern winter SST between 14.4-14.2 and at 13.3 ka BP and summer SST at 13.85, 13.7 and 13.22 ka BP. Mg/Ca SST obtained from *G. bulloides* (Figure 4.1c) indicate a warming to

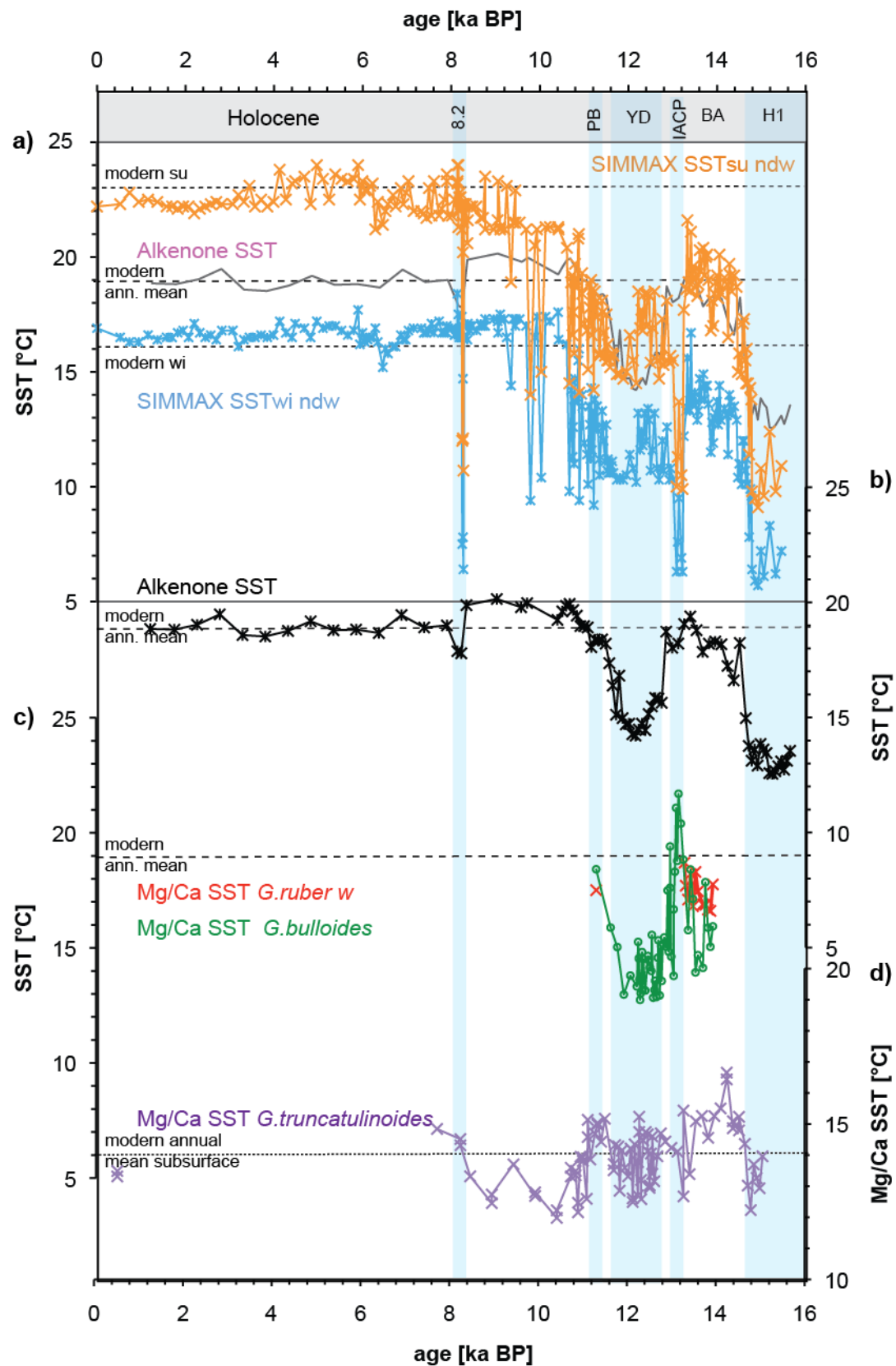


Figure 4.1 Comparison of SST reconstructions as based on different proxies over the last deglacial

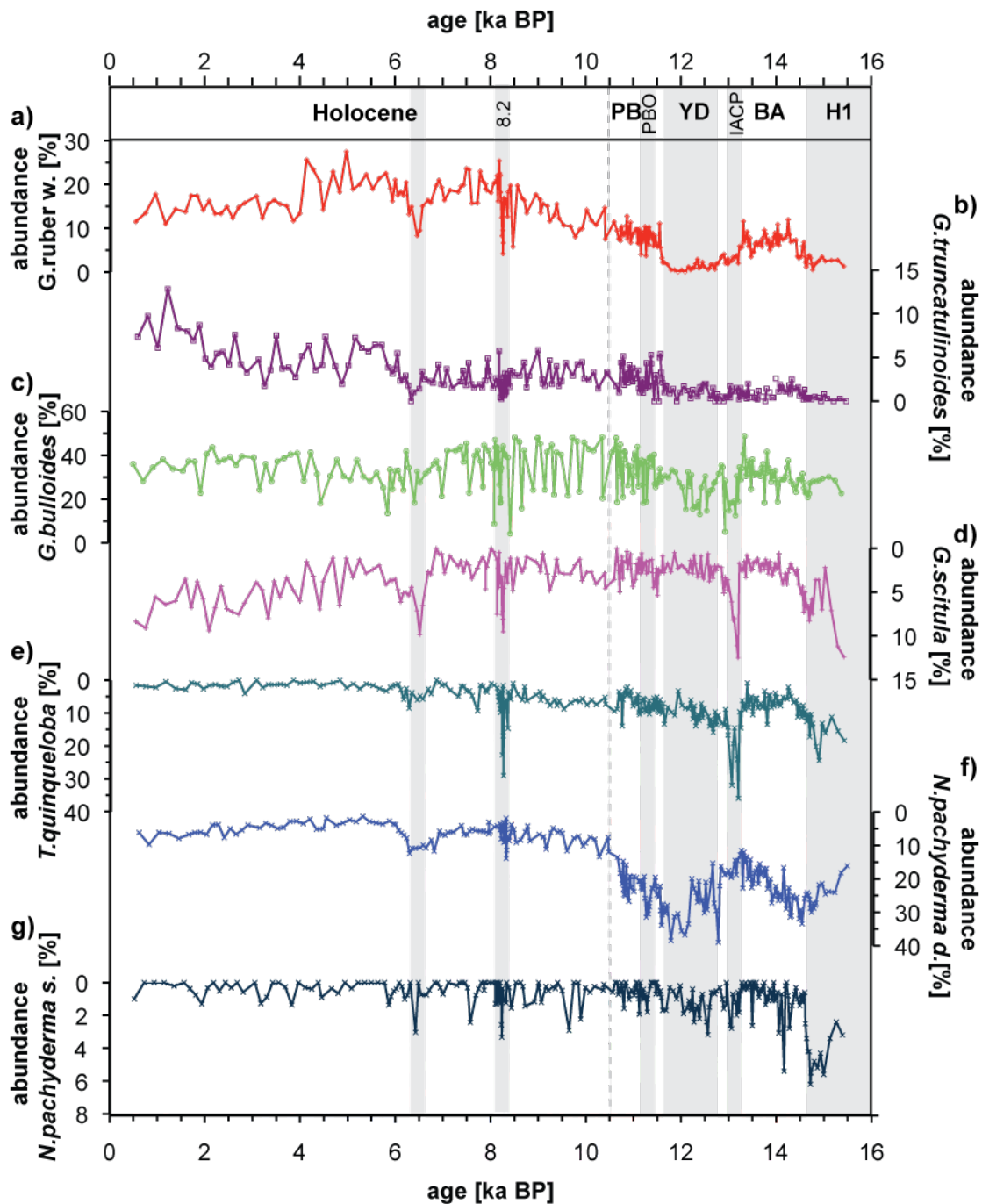


Figure 4.2 Relative abundance records of subtropical species

G. ruber w. (red), *G. truncatulinoides* (violet), transitional species *G. scitula* (pink), *G. bulloides* (green), *N. pachyderma d.* (light blue) and sub/polar species *T. quinqueloba* (green-blue) and *N. pachyderma s.* (dark blue). Note that scale of the transitional and subpolar species *G. scitula*, *T. quinqueloba*, *N. pachyderma d.* and *N. pachyderma s.* is inverted.

21°C for the IACP. This warming coincides with high Fe/Ca values. During the YD *G. bulloides* Mg/Ca SST indicate cold SST that fluctuate between 13 and 15°C and rise during the Preboreal to modern annual mean SST (19°C).

Subsurface temperatures obtained from *G. truncatulinoides* Mg/Ca measurements are decreasing from 16°C at the beginning of the BA to 14°C at the onset of the IACP. During the early YD and the Preboreal *G. truncatulinoides* Mg/Ca temperatures are warm (14°C) with an unstable phase

during the mid YD when Mg/Ca SST indicate temperatures of 13°C. The coldest Mg/Ca temperatures of 12°C are reached during H1 and the Preboreal periods with long term gradual increase into the 8.2 event close to modern surface winter SST.

The distribution of *G. ruber w.* is in general following the SST evolution with very low relative abundances close to 0 during the YD and the H1 event, intermediate abundances (10 %) during the BA and the Preboreal, reaching maximum abundances (25 %) between 8 and 4 ka BP. After 4 ka BP the abundances stabilize during the late Holocene (14-18 %).

The relative abundances of *N. pachyderma d.* pattern (Figure 4.2f) is roughly inverse to the distribution of *G. ruber w.*. *N. pachyderma d.* shows two abundance peaks (30-35%), one occurring at the onset of BA and one in the YD. During Preboreal the abundance of *N. pachyderma d.* decreases and reaches Holocene values of about 10 % at 10 ka BP.

During BA the relative abundances of the polar/subpolar and transitional species *T. quinqueloba* (Figure 4.2e), *N. pachyderma s.* (Figure 4.2g) species and *G. scitula* (Figure 4.2d) (2-4 %) are slightly elevated as compared to the late Holocene (0-3%). The three short term cold events H1, IACP and 8.2 are marked by a sharp retreat of subtropical species and an increase of subpolar and temperate species as indicated by high relative abundances of the subpolar species *T. quinqueloba* (25-35 %) and *G. scitula* (9.5-12.5 %) and low abundances of the subtropical *G. ruber w.* (2.5 % during H1, 3.5 during IACP and 7 % during 8.2 event) (Figure 4.2e,d.a).

4.5 Discussion

The general evolution of the SIMMAX and $U^{K'}_{37}$ SST records is following the known deglacial succession, with warm BA and Holocene and the cold H1 event and YD, yet distinct differences are observed between both records.

- 1) The reconstructed SIMMAX are close to modern summer and winter SST, while the $U^{K'}_{37}$ SST record resemble the annual mean SST during Holocene. In contrast, from H1 toward the end of the YD $U^{K'}_{37}$ temperatures in general are quite similar to the SST_{su} . For the BA both, $U^{K'}_{37}$ and SST_{su} , match modern annual mean SST.
- 2) Decadal to centennial events, are indicated by most pronounced cooling during H1, IACP and 8.2 event in the SIMMAX SST records. These events are only poorly visible or even absent in the $U^{K'}_{37}$ record.
- 3) In contrast, SST_{su} are by 4°C warmer than the $U^{K'}_{37}$ SST during the YD.
- 4) Even shorter scale climate variability is indicated by SIMMAX SST revealing rapid decadal changes between cold and warm SST during the Preboreal, which is not visible in the $U^{K'}_{37}$ record. Such kind of short term variability might also be reflected in the Mg/Ca record of *G. bulloides* and *G. truncatulinoides* but not as pronounced as in the SIMMAX records due to lower resolution.

In the following these different phases are discussed in order to understand the causes for these mismatches and to assess a solid reconstruction of the deglacial SST change at the Azores coring site and to investigate its impact on salinity reconstructions.

4.5.1 Differences between SIMMAX SST and $U^{K'}_{37}$ temperatures on long time scales

The better match between SST_{su} and $U^{K'}_{37}$ SST (Figure 4.1a,b) during H1 into the Preboreal followed by the divergence of the $U^{K'}_{37}$ signal towards annual mean SST values within the Holocene can be explained with a shift in the growing season of the alkenone producing coccolithophorides. A similar shift in the alkenone signal with respect to SIMMAX SST, has been observed by *Sicre et al.* [2013] in the Mediterranean Sea.

A shift in the ecology of the alkenone producing coccolithophorides at the Azores coring site can be explained by the enhanced influence of nutrient rich transitional ENATW that is indicated by high relative abundances of *N. pachyderma d.* (10-30 %) (Figure 4.2f) during the BA and the YD. Within these water masses that also prevail at 40°N in the modern ocean, the coccolithophore bloom occurs during late spring/summer [*Longhurst, 2007*] (for detail see Chapter 5).

After 10.5 ka BP increasing relative abundance of *G. ruber w.* (Figure 4.2a) and decreasing relative abundance of *N. pachyderma d.* (Figure 4.2f) indicate that the modern hydrological situation established. Consequently, as defined by the calibration of both methods Holocene SIMMAX and $U^{K'}_{37}$ SST reflect modern SST_{su}/SST_{wi} and annual mean SST. This assumption is in agreement with the concept of *Schneider et al.* [2010] and *Leduc et al.* [2010] suggesting that during interglacial periods the $U^{K'}_{37}$ record is recording the warm stratified season in high latitudes and cold nutrient rich season in low latitudes.

Mg/Ca SST reconstructions of *G. ruber w.* match the SST_{su} and $U^{K'}_{37}$ SST during BA and thus are assumed to also reflect summer SST. This agrees well with foraminifera ecological models that suggest that the main growth of *G. ruber w.* in the subtropical NA occurs in late summer under modern conditions as well as during glacial and interglacial times [*Anand et al., 2003; Fraile et al., 2009; Lombard et al., 2011*].

4.5.2 Differences in reconstructed SST during cold events

The centennial to decadal scale cold event (e.g. H1, IACP and 8.2 event) are associated with similar extreme cooling signals in the SIMMAX SST record (Figure 4.1a). Especially during short-term IACP and 8.2 cold events, the cooling is exceeding the cooling signal from the $U^{K'}_{37}$ SST record by factor 5-6 (Figure 4.1b). This mismatch might either be caused by a bias of $U^{K'}_{37}$ towards the warm temperatures or by non-analogue situation causing anomalously low SIMMAX SST for the cold events.

An overestimation of the $U^{K'}_{37}$ SST, caused by an extreme increase in the abundance of the 37:4 component during cold events is not likely and already was excluded in Chapter 2.4.1. The weaker cooling suggested by this record however, could be caused by its lower sampling resolution compared to that of the foraminifera counts not resolving decadal scale variability. Moreover it is common sense that the alkenone temperature signal is smoothing out short scale SST variability. This smoothing might either be related to the high amount of specimens contributing to the alkenones fossilized in the sediments [Leduc *et al.*, 2010], while only about 400 foraminifera are considered for the SIMMAX estimation, or to different magnitudes of influence by oceanic current transport responses on coccolithophores and foraminifera [Ohkouchi *et al.*, 2002] and bioturbation [Bard, 2001].

A serpentinite layers that occurred during IACP as observed during the SEM analyses (Schwab *et al.* pers. communication) and 8.2 [Richter, 1998] coincide with an extreme increase in sedimentation rates and might be related to a pronounced winnowing of fine fraction sediments that could have diminished the $U^{K'}_{37}$ cooling signal. But parallel changes in coccolithophore [Schwab *et al.*, 2012] and foraminifera species assemblages, both showing pronounced abundance peaks of transitional to subpolar species during IACP, indicate that a transport related bias between coccolithophores and foraminifera is unlikely. These coinciding records also exclude bioturbation to have affected the $U^{K'}_{37}$ SST and SIMMAX record in a different manner. Therefore we tend to address the missing cooling for the short scale events in the alkenone record to a smoothing and under sampling effect, which is seen also in many other records.

The most pronounced divergence between Mg/Ca SST and SIMMAX SST is apparent for the IACP. In principal two effects could explain such warm Mg/Ca estimates in contrast to the SIMMAX extreme cooling. The very high Mg/Ca values could be caused by a strong increase in salinity [Arbuszewski *et al.*, 2010; Kisakürek *et al.*, 2008; Sabbatini *et al.*, 2011b] and /or Mg rich antigenic coating on the foraminifera shells [Barker *et al.*, 2003]. An overestimation of Mg/Ca SST by a salinity overprint most probably would be related to the advection of warm saline subtropical water into the subtropical gyre. Such an advection can be excluded since an increasing contribution of subpolar species and decreasing subtropical species indicate the presence of subpolar water at the coring site. As the subpolar NA water is at least 0.5 PSU lower in salinity than the STG water such a salinity reduction from 36 PSU (modern) to 35.5 PSU would reduce the temperature signal by at least 1°C and thus can not contribute to an SST overestimation.

G. bulloides Mg/Ca ratios between (2.3 and 4.7 $\mu\text{mol/mol}$) temperature above 20°C are extremely high and coincide with high Fe/Ca (0.9-1.2 $\mu\text{mol/mol}$) values in the samples. Thus we assume that the foraminifera these samples are affected by a Fe-Mg rich coating and thus exclude those samples from the discussion following the protocol of [Barker *et al.*, 2003].

Additionally it might be worth to regard the possible sources of the Fe enrichment. The serpentinite that is deposited during IACP interval might be a source for the high Fe and Mg content.

Furthermore is the cold IACP known to be caused by a strong meltwater pulse from the Laurentian ice sheet [Obbink *et al.*, 2010; Thornalley *et al.*, 2010]. As sub glacial meltwater can be highly enriched with dissolved iron [Bhatia *et al.*, 2013] the transport of those iron rich meltwater from the Laurentian ice sheet /Greenland ice sheet down to the Azores coring site might also have caused the high iron concentrations. But would not increase the Mg content of the water and thus can be excluded as a source for the high Mg phase. Thus the bias seems to be related to the serpentinite.

Despite the reasonable arguments for an overestimation of surface SST by the alkenone and Mg/Ca measurements also the possibility of calculating too cold temperatures with the SIMMAX method should be explored. Such an underestimation of the SIMMAX SST might either be caused by missing analogue samples within the calibration data set [Storz *et al.*, 2009; Telford *et al.*, 2012] or by the integration of a cooler subsurface signal into the calculations. However, the Mg/Ca estimates from *G. truncatulinoides* suggesting relatively warm temperatures at 14°C for the IACP and 8.2 events counter argue a subsurface cooling effect.

So far mixed faunal assemblages representative for oceanographic frontal conditions are underrepresented in the SIMMAX calibration data set [Storz *et al.*, 2009]. This may yield non-analogue situations for the down core data from the Azores site and becomes evident in low similarities of 0.7-0.85 for the SIMMAX SST calculation over the IACP interval. Similarity values of 0.7-0.85 are significantly lower than the majority within the record leveling at (>0.89), according to Pflaumann *et al.* [1996] SST estimates from samples with similarities smaller than 0.9 should be regarded only with caution. On the other hand since the cooling of the SIMMAX SST record (Figure 4.1a) for the IACP event is paralleled by high abundances of *T. quinqueloba* (Figure 4.2e) and the temperate species *G. scitula* (Figure 4.2d) it is likely that the abundance of these subpolar to transitional species are responsible for the cold excursion of the SST record during the IACP. In fact today *T. quinqueloba* is most common in the Arctic front thus its high abundances might indicate a strong change in the frontal system of the subtropical NA. This would argue against the alkenone temperatures remaining at quite warm temperatures but is ground truthing of the SIMMAX SST calculation implying such an extreme cooling.

4.5.2.1 Plausibility of strong SIMMAX SST cooling events

The plausibility of extreme cooling is tested in the following under the basic assumption that the STG was displaced southward during the deglacial cold events (H1, IACP and 8.2 event).

In the modern NA *T. quinqueloba* abundances of 30-35 % are observed in the Nordic seas (65°N) and south east of Greenland (52°N), and maximum *G. scitula* abundance of 7 % prevails between 40 and 43°N. Therefore we assume that the high abundances of these species during IACP and 8.2 event are associated with a strong influence of subpolar waters on the coring site. This most probably is associated with a southward displacement of the STG rim as further discussed in

Chapter 5 and 6 and might even be coupled with an extreme southward displacement of the Arctic front, to which the abundance of *T. quinqueloba* is associated [Simstich *et al.*, 2003]. These events most probably were caused by massive meltwater outbursts from the Laurentian ice sheets that penetrated the NA via Hudson Strait (Chapter 5).

Assuming that subpolar conditions prevailed at the Azores coring site during cold events, SST at the Azores coring site would be expected to match SSTs observed in the NA. *G. bulloides* and *N. pachyderma s.* Mg/Ca SST calculations from subpolar NA (52-62°N), indicate a cooling down to 6-7°C for the 8.2 event and IACP [Benway *et al.*, 2010; Came *et al.*, 2007; Peck *et al.*, 2008; Thornalley *et al.*, 2010]. SIMMAX SST reconstructions indicate that summer SST cooled down to 8°C at 50°N (site BOFS 5K) [Maslin *et al.*, 1995]. During H1 the cooling was even stronger with SST_{su} of 3°C at 50°N [Maslin *et al.*, 1995], down to 7°C with MAT and 9-10°C with U^K₃₇ SST is described for Heinrich events [Pérez-Folgado *et al.*, 2003], thus are even lower than our SIMMAX SST_{su} of 10°C.

Furthermore abundance peaks of *T. quinqueloba* resemble those observed in glacial records from the Mediterranean Sea [Pérez-Folgado *et al.*, 2003], supporting very cold SST_{su} estimates reconstructed for our coring site. However, such cold SST_{su} estimates would argue for about 4°C colder SST_{wi} and about 2°C colder annual mean estimates, which represent the common seasonal contrast and annual mean difference to SST_{su}, respectively, for the entire record at the Azores site.

An alternative way to test the feasibility of such SST estimates during sub-millennial scale cold events is to compare our result with those of appropriate climate simulations. In coupled ocean atmosphere model experiments with a freshwater induced AMOC collapse, SST cools by up to 13°C in the subpolar region whereas the cooling outside the subpolar region does not exceed 5°C [Kageyama *et al.*, 2010; Liu *et al.*, 2009; Stouffer *et al.*, 2006]. For example the Kiel Climate Model (KCM) predicts only a SST cooling by 2.5°C at 38°N, when forced by a continuous freshwater pulse of 1 Sv under preindustrial boundary conditions (Figure 4.3) (pers. communication Krebs-Kanzow). But a shift in the position of the Azores front is also indicated in the KCM. This displacement reaches its maximum east of the Azores coring site (Figure 4.4) resulting in a surface water cooling of 5°C including a frontal shift. Within the uncertainty of the coarse resolution a 5°C at the Azores coring site thus is reasonable. This cooling can even exceed the 5°C magnitude under deglacial or glacial boundary conditions (Krebs –Kanzow personal communication).

However a cooling by about 10-12°C as observed in the SIMMAX reconstructions resulting in absolute temperatures that are similar in all three cold events (H1, IACP, 8.2 event) is unlikely because of the different climatic background conditions before during and after the deglacial warming and ice sheet melting. Such a similar signal is neither observed in the subpolar nor polar NA. Therefore we assume that temperature amplitudes of 12°C reconstructed by SIMMAX SST reconstructions at the Azores coring site are slightly overestimated.

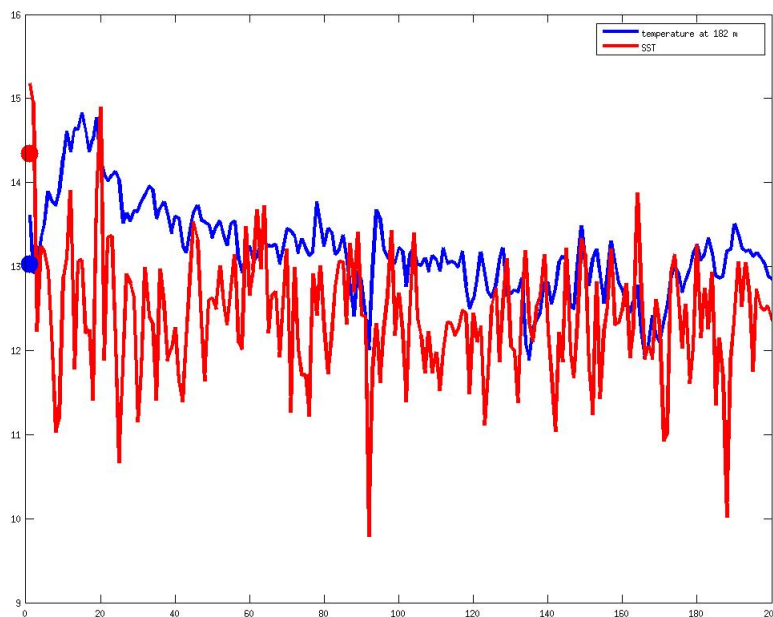


Figure 4.3 Model output from KCM using a transient model run applying a continuous 1Sv meltwater anomaly N of 60°N into the NA, red lines indicate the temperature evolution of the SST at the Azores coring site and the blue line indicates the subsurface temperature evolution.

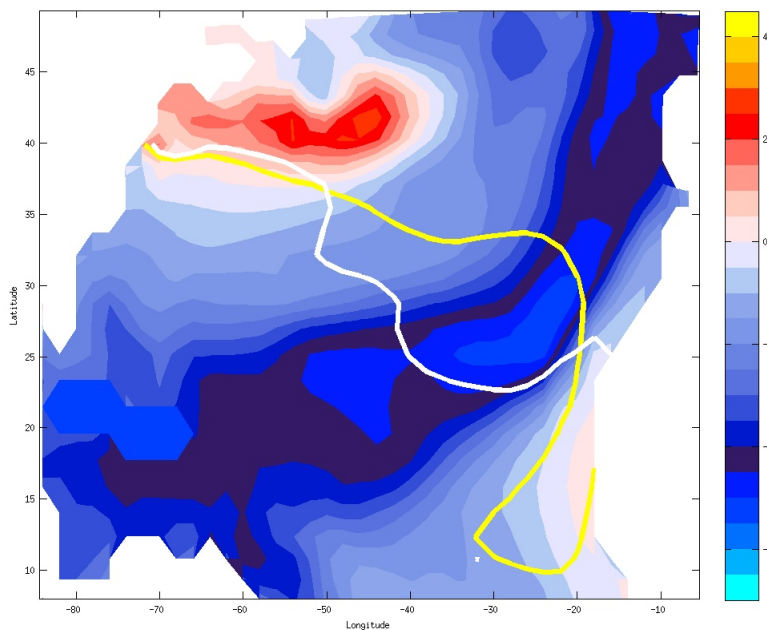


Figure 4.4. Model output from KCM using a transient model run applying a continuous 1Sv meltwater anomaly N of 60°N into the NA, the colors indicate the SST difference the temperature anomaly between undisturbed and meltwater disturbed circulation (THC-off –THC_on mode), the position AF is indicated by the position of the 15° isotherm, yellow for THC_on white for the THC_off mode.

4.5.3 Younger Dryas subsurface influence on the SIMMAX SST record

The SIMMAX SST signal and the $U^{K'}_{37}$ SST signal are decoupled over the YD (Figure 4.1a,b), with SIMMAX SST suggesting a short-term warming event shortly after the beginning of the YD cooling while $U^{K'}_{37}$ SST remain at cold YD like temperatures. Thus either $U^{K'}_{37}$ reconstructions do not account for this short warming or in the SIMMAX SST record or the YD cooling is masked. SIMMAX SST might reflect subsurface SST rather than sea surface conditions due to high relative abundances of subsurface dwelling foraminifera as suggested by *Telford et al.* [2012].

The $U^{K'}_{37}$ SST cooling to 15°C at the onset of the YD is also evident in the Mg/Ca reconstruction from *G. bulloides* (Figure 4.1c). The Mg/Ca SST record fluctuates stronger than the $U^{K'}_{37}$ SST record and partially indicates 2°C colder SST than $U^{K'}_{37}$ SST. These fluctuations might be missed in the lower resolved $U^{K'}_{37}$ SST record. Furthermore might changes in the dwelling depth of *G. bulloides* account for these changes. The close match between the $U^{K'}_{37}$ and the *G. bulloides* SST temperature record however indicates that both temperatures reflect the same season and roughly the same water depth. In agreement with the previous argumentation (chapter 4.5.1), we assume that during the YD $U^{K'}_{37}$ and *G. bulloides* Mg/Ca temperature reflect summer SST.

A strong impact of the subsurface dwelling species *N. pachyderma d.* on the SIMMAX SST record becomes evident in the close match between the SIMMAX SST record and the inverse *N. pachyderma d.* abundance record (Figure 4.5). This record shows an increasing abundance of the subsurface dwelling species *N. pachyderma d.* during the cold YD, whereas the surface dwelling species *G. ruber w.* becomes nearly absent (>4 %) (Figure 4.2a). Thus *N. pachyderma d.* becomes one of the dominating species during the YD and most probably strongly influences the SIMMAX SST. As *N. pachyderma d.* is dwelling within the shallow subsurface water (100-150 m wd.) [*Lombard et al.*, 2011], the SIMMAX SST may reflect a subsurface water mass signal as suggested by *Telford et al.* [2012].

If it is assumed that SIMMAX SST reflects subsurface temperatures for this short interval within the YD, it might be surprising that the subsurface temperatures during the early YD period are warmer than the surface temperatures calculated by the alkenones and Mg/Ca of *G. bulloides*. These warm temperatures might either be an effect of the non-analogue situation for the SIMMAX calculations or might be related to warm water storage within the subsurface. This potential subsurface warming was tested, using the Mg/Ca temperatures from the subsurface dweller *G. truncatulinoides*. This record indicates temperatures of 15°C that average the SIMMAX SST_{su/wi} and show a similar pattern as SIMMAX SST. The absolute temperatures match the $U^{K'}_{37}$ and *G. bulloides* Mg/Ca SST but a cooling as indicated in the surface water is missing in the subsurface SST record at the beginning of the YD.

As the living depth of *G. truncatulinoides* is bound to the thermocline depth [*Caroline Cléroux et al.*, 2007; *Cléroux et al.*, 2008] we assume that the corresponding SST evolution between

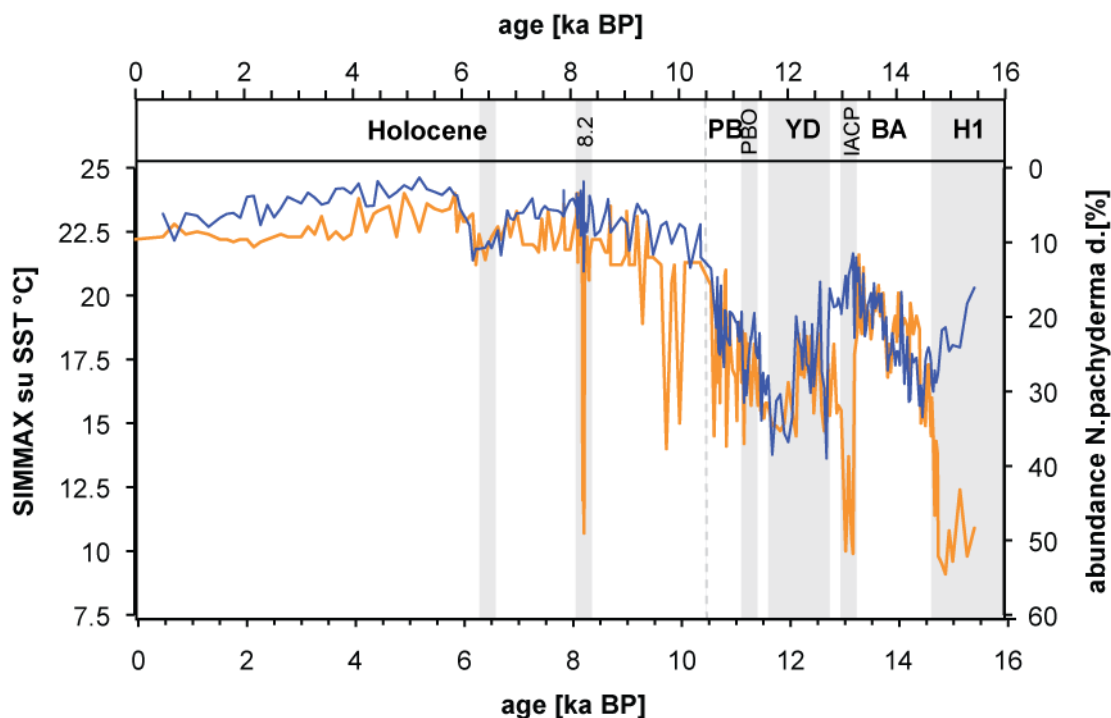


Figure 4.5 Comparison between SIMMAX su SST and the relative abundance of *N. pachyderma d*
 The comparison between SIMMAX su SST (orange) and the relative abundance of *N. pachyderma d.* (blue) indicates a strong influence of the *N. pachyderma d.* on the SIMMAX SST reconstructions

SIMMAX and *G. truncatulinoides* Mg/Ca SST indeed reflect deeper mixed layer temperatures during the YD. Thus a strong subsurface warming at the Azores coring site seems to be real and can be explained with change in the hydrology at the Azores coring site (see Chapter 5). Thus SIMMAX SST cannot be exclusive regarded as a surface water signal in this part of the YD record given the complex hydrographic situation at the Azores front.

During the late YD SIMMAX SST and Mg/Ca subsurface temperature records still match rather well, indicating that SIMMAX reflects subsurface temperatures. Within this interval no subsurface heat storage is observed. As soon as the abundance of *G. ruber w.* recovers at the onset of Preboreal, SIMMAX SST seems to reflect surface temperatures again.

4.5.4 Comparison of the strong deglacial cold events with the Preboreal “flickering” phase

During the Preboreal and the early Holocene a series of minor cold-warm oscillations is evident within the SIMMAX SST record (Figure 4.1a). The cold events within these oscillations cannot be related to an increase of the subpolar species *G. scitula* and *T. quinqueloba* (Figure 4.2e,f) and the 4°C cooling is much lesser than during the H1, IACP, 8.2 event. This “flickering” temperature signal in the SIMMAX SST record might be related to minor changes in the faunal assemblage that are related to changes in the position or structure of the AF. Due to underrepresentation of frontal fauna assemblages [Storz *et al.*, 2009] in the calibration, these minor compositional changes might lead to a pronounced switch of the SIMMAX equation based considering either subpolar or transitional samples to calculate the SST.

The cold events however match the period of several subordinate meltwater pulses of the Laurentian Ice sheet draining via the St. Lawrence River [Teller *et al.*, 2002]. We suggest that those waters had a less strong impact on the STG than the main meltwater drainage events (H1, IACP, 8.2 event) that are related to meltwater pulses from the Hudson Bay [Teller *et al.*, 2002] (Chapter 5). This hypothesis needs to be tested with independent high-resolution $\delta^{18}\text{O}_{\text{w-ice}}$ reconstructions by combined planktonic Mg/Ca SST and $\delta^{18}\text{O}$ measurements.

4.5.5 Influence of SST on derived salinity reconstructions

Salinity reconstructions (expressed as $\delta^{18}\text{O}_{\text{sw-ice}}$) that are based on combined $\delta^{18}\text{O}$ and SST reconstructions depend on solid SST estimations. To assess the effect of different changes in SST reconstructions at our coring site, $\delta^{18}\text{O}_{\text{sw-ice}}$ were calculated by the use of the different SST reconstructions obtained in this study (Figure 4.6).

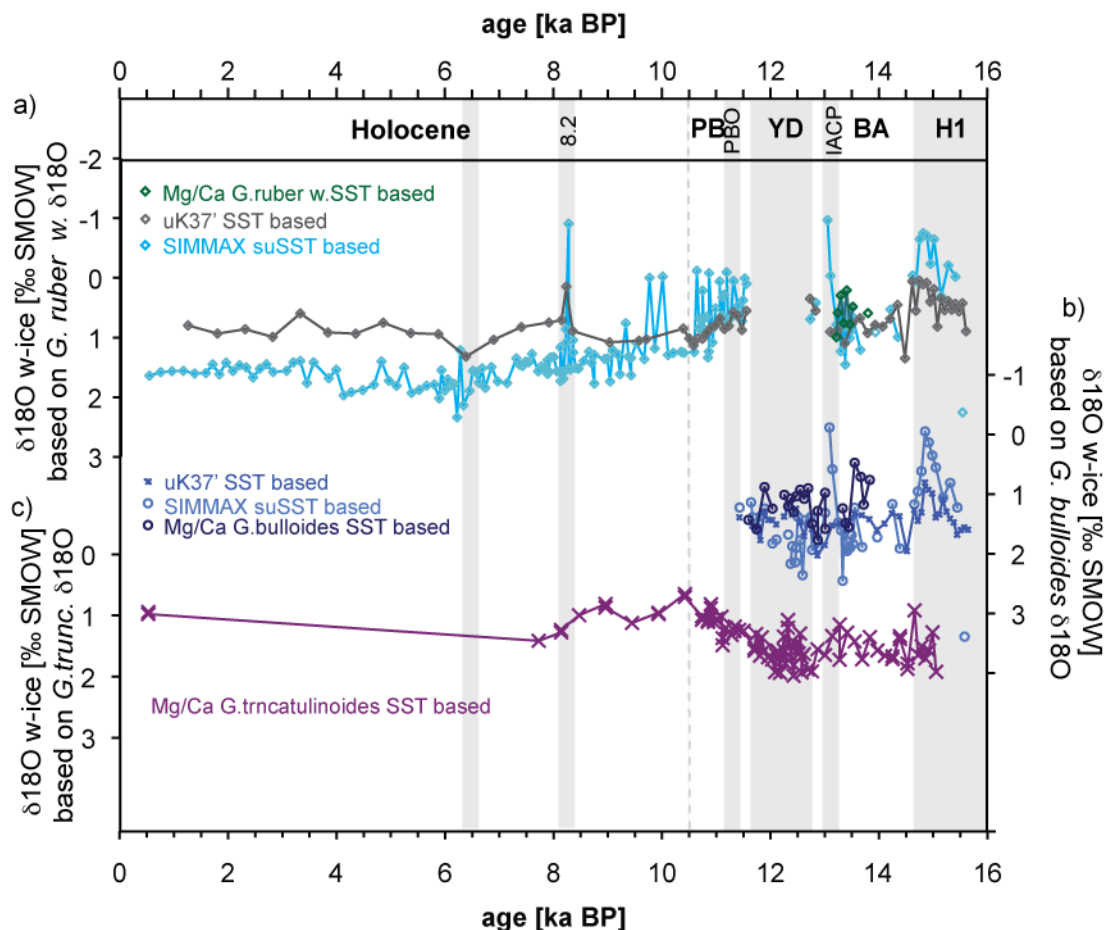


Figure 4.6 Comparison between different $\delta^{18}\text{O}_{\text{sw-ice}}$ reconstructions

a) comparison of reconstructions based on $\delta^{18}\text{O}$ of *G. ruber w.* combined with SIMMAX suSST (light blue) $U^{K'}_{37}$ SST (grey) and *G. ruber w.* Mg/Ca SST (green)

b) comparison of reconstructions based on $\delta^{18}\text{O}$ of *G. bulloides* combined with SIMMAX suSST (light blue) $U^{K'}_{37}$ SST (middle blue) and *G. ruber w.* Mg/Ca SST (dark blue)

c) reconstructions based on $\delta^{18}\text{O}$ of *G. truncatulinoides* combined *G. truncatulinoides* Mg/Ca temperatures (violet)

In general SIMMAX based $\delta^{18}\text{O}_{\text{sw-ice}}$ records are more variable than all other records and reflect the variability in the SIMMAX SST record. Mg/Ca *G. ruber w.* based $\delta^{18}\text{O}_{\text{sw-ice}}$ records show lower amplitudes than those based on *G. bulloides*. As *G. bulloides* is not bound to a specific living depth this is probably a result of vertical migration of this species during different climate conditions. The effect of seasonality changes on the $\delta^{18}\text{O}_{\text{sw-ice}}$ signal can be assessed by differences in the $\text{U}^{\text{K}'}_{37}$ and SIMMAX based Holocene reconstructions and amounts to 1 ‰ SMOW. The effect of an SIMMAX SST underestimation during extreme cold events can be estimated using $\delta^{18}\text{O}_{\text{sw-ice}}$ reconstructions for the major cold events H1 and 8.2. Results of SIMMAX based reconstructions indicate a strong freshening of 2 ‰ SMOW during both extreme cold events, whereas the freshening amounts to 1 ‰ SMOW in all other reconstructions: hence the underestimation of SIMMAX SST leads to an overestimation of the freshening by 0.5- 1 ‰ SMOW. These results show that differences in the living season of the organism carrying the SST or $\delta^{18}\text{O}$ signal can lead to changes in calculated $\delta^{18}\text{O}_{\text{sw-ice}}$ which is in the same order of magnitude as a signal of a freshening event itself. Thus it is important to assure that $\delta^{18}\text{O}$ signals and SST signals that are combined for $\delta^{18}\text{O}_{\text{sw-ice}}$ reconstructions are representative for the same season, which is ideally the combination of Mg/Ca temperature and $\delta^{18}\text{O}$ reconstructions from the same foraminifera species.

4.6 Summary and Conclusion

Within this study we disentangled deglacial multiproxy SST signals and assessed the reliability of the SST reconstructions from the Azores coring site that is situated the mid subtropical North Atlantic. The main conclusions are

- SIMMAX su/wi SST reconstructions are reliable recorders of summer and winter SST over the Holocene from 10.5 onwards and the Bølling-Allerød (14.6-13.2 ka BP) with exception of smaller cold interruptions during the Preboreal and the early Holocene and the three major cold events H1, IACP, 8.2 event.
- $\text{U}^{\text{K}'}_{37}$ SST reconstructions are reliable recorders of summer SST from H1 to early Holocene (10.5 ka BP), and match annual mean SST over the Holocene. Despite rather reliable long term reconstructions, $\text{U}^{\text{K}'}_{37}$ SST seem to underestimated the magnitude of short term cooling events (e.g H1, IACP, 8.2 event) that interrupt the long term deglacial and Holocene SST evolution.
- The SIMMAX SST amplitudes differ between the three major cold events and Preboreal oscillations. The amplitude of the cold events are not certain due to non analogue situations within SIMMAX SST, uncertain dampening of $\text{U}^{\text{K}'}_{37}$ record and overprinted Mg/Ca SST record.
- a strong cooling at the Azores coring site is reasonable as a southward shift of the STG and the occurrence of subpolar conditions are indicated by changes in the faunal assemblage at

the Azores coring site during major cold events. A maximal cooling of 5°C and a gyre displacement also is evident in model results from the KCM.

- During Younger Dryas, SIMMAX SST reflect subsurface conditions that indicate an thermocline warming due that may indicate a in the subsurface heat storage.
- Mg/Ca SST reconstruction from *G. ruber w.* reflect surface water SST over BA, Mg/Ca SST reconstruction from *G. bulloides* seem to be produced in the same season as alkenones but might be overprinted by changes in habitat depth. The only exception is during the IACP cold interval where high Fe/Ca values indicate a diagenetic overprint of the Mg/Ca signal.
- Mg/Ca reconstructions from *G. truncatulinoides* seem to reflect subsurface temperature.
- Seasonal differences in the chosen SST signals can have a strong overprint on $\delta^{18}\text{O}_{\text{sw-ice}}$ reconstructions, probably of the same amount as freshwater events.

4.7 References

- Adloff, F., U. Mikolajewicz, M. Kufçera, R. Grimm, E. Maier-Reimer, G. Schmiedl, and K. C. Emeis (2011), Upper ocean climate of the Eastern Mediterranean Sea during the Holocene Insolation Maximum, - a model study, *Clim. Past*, 7(4), 1103-1122.
- Alves, M., F. Gaillard, M. Sparrow, M. Knoll, and S. Giraud (2002), Circulation patterns and transport of the Azores Front-Current system, *Deep Sea Research Part II: Topical Studies in Oceanography*, 49(19), 3983-4002.
- Anand, P., H. Elderfield, and M. H. Conte (2003), Calibration of Mg/Ca thermometry in planktonic foraminifera from a sediment trap time series, *Paleoceanography*, 18(2), 1050.
- Arbuszewski, J., P. deMenocal, A. Kaplan, and E. C. Farmer (2010), On the fidelity of shell-derived $\delta^{18}\text{O}_{\text{seawater}}$ estimates, *Earth and Planetary Science Letters*, 300(3-4), 185-196.
- Bard, E. (2001), Paleooceanographic implications of the difference in deep-sea sediment mixing between large and fine particles, *Paleoceanography*, 16(3), 235-239.
- Barker, P. Diz, M. J. Vautravers, J. Pike, G. Knorr, I. R. Hall, and W. S. Broecker (2009), Interhemispheric Atlantic seesaw response during the last deglaciation, *Nature*, 457(7233), 1097-1102.
- Barker, S., M. Greaves, and H. Elderfield (2003), A study of cleaning procedures used for foraminiferal Mg/Ca paleothermometry, *Geochemistry, Geophysics, Geosystems*, 4(9), 8407.
- Bé, A. W. H., and D. S. Tolderlund (1971), Distribution and ecology of living planktonic foraminifera in surface waters of the Atlantic and Indian oceans, In: *Funnell, B.M., Riedel, W.R. (Eds.), Micropaleontology of the Oceans. Cambridge Univ. Press, London*, 105-149.
- Bemis, B. E., H. J. Spero, J. Bijma, and D. W. Lea (1998), Reevaluation of the Oxygen Isotopic Composition of Planktonic Foraminifera: Experimental Results and Revised Paleotemperature Equations, *Paleoceanography*, 13(2), 150-160.
- Benway, H. M., J. F. McManus, D. W. Oppo, and J. L. Cullen (2010), Hydrographic changes in the eastern subpolar North Atlantic during the last deglaciation, *Quaternary Science Reviews*, 29(23-24), 3336-3345.
- Bhatia, M. P., E. B. Kujawinski, S. B. Das, C. F. Breier, P. B. Henderson, and M. A. Charette (2013), Greenland meltwater as a significant and potentially bioavailable source of iron to the ocean, *Nature Geosci*, 6(4), 274-278.
- Bian, N., and P. A. Martin (2010), Investigating the fidelity of Mg/Ca and other elemental data from reductively cleaned planktonic foraminifera, *Paleoceanography*, 25(2), PA2215.
- Came, R. E., D. W. Oppo, and J. F. McManus (2007), Amplitude and timing of temperature and salinity variability in the subpolar North Atlantic over the past 10 k.y., *Geology*, 35(4), 315-318.
- Chapman, M., N. J. Shackleton, and J.-C. Duplessy (2000), Sea surface temperature variability during the last glacial-interglacial cycle: assessing the magnitude and pattern of climatic change in the North Atlantic, *Paleogeography, Paleoclimatology, Paleoecology*, 157, 1-25.
- Cléroux, C., E. Cortijo, J.-C. Duplessy, and R. Zahn (2007), Deep-dwelling foraminifera as thermocline temperature recorders, *G3*, 8(4), Q04N11.
- Cléroux, C., E. Cortijo, J.-C. Duplessy, and R. Zahn (2007), Deep-dwelling foraminifera as thermocline temperature recorders, *Geochemistry, Geophysics, Geosystems*, 8(4), Q04N11.
- Cléroux, C., E. Cortijo, P. Anand, L. Labeyrie, F. Bassinot, N. Caillon, and J.-C. Duplessy (2008), Mg/Ca and Sr/Ca ratios in planktonic foraminifera: Proxies for upper water column temperature reconstruction, *Paleoceanography*, 23(3), n/a-n/a.
- CLIMAP, and P. Members (1981), Seasonal reconstruction of the earths surface at the last glacial maximum, *Geological Society of America, Map and Chart Series*, 36, 18 pp.

- Darling, K. F., and C. M. Wade (2008), The genetic diversity of planktic foraminifera and the global distribution of ribosomal RNA genotypes, *Marine Micropaleontology*, 67(3,4), 216-238.
- Fraille, I., M. Schulz, S. Mulitza, U. Merkel, M. Prange, and A. Paul (2009), Modeling the seasonal distribution of planktonic foraminifera during the Last Glacial Maximum, *Paleoceanography*, 24(2), PA2216.
- Jansen, E., C. Andersson, M. Moros, K. H. Nisancioglu, B. F. Nyland, and R. J. Telford (2009), The Early to Mid-Holocene Thermal Optimum in the North Atlantic, in *Natural Climate Variability and Global Warming*, edited, pp. 123-137, Wiley Blackwell.
- Kageyama, M., A. Paul, D. M. Roche, and C. J. Van Meerbeek (2010), Modelling glacial climatic millennial-scale variability related to changes in the Atlantic meridional overturning circulation: a review, *Quaternary Science Reviews*, 29(21-22), 2931-2956.
- Kisakürek, B., A. Eisenhauer, F. Böhm, D. Garbe-Schönberg, and J. Erez (2008), Controls on shell Mg/Ca and Sr/Ca in cultured planktonic foraminifera, *Globigerinoides ruber* (white), *Earth and Planetary Science Letters*, 273(3/4), 260-269.
- Kozdon, R., A. Eisenhauer, M. Weinelt, M. Y. Meland, and D. Nürnberg (2009), Reassessing Mg/Ca temperature calibrations of *Neogloboquadrina pachyderma* (sinistral) using paired $\delta^{44}\text{Ca}$ and Mg/Ca measurements, *Geochemistry, Geophysics, Geosystems*, 10(3), Q03005.
- Kucera, M., A. Rosell-Melé, R. Schneider, C. Waelbroeck, and M. Weinelt (2005), Multiproxy approach for the reconstruction of the glacial ocean surface (MARGO), *Quaternary Science Reviews*, 24(7, 8), 813-819.
- Leduc, G., R. Schneider, J. H. Kim, and G. Lohmann (2010), Holocene and Eemian sea surface temperature trends as revealed by alkenone and Mg/Ca paleothermometry, *Quaternary Science Reviews*, 29(7-8), 989-1004.
- Liu, Z., et al. (2009), Transient Simulation of Last Deglaciation with a New Mechanism for Bolling-Allerod Warming, *Science*, 325(5938), 310-314.
- Lohmann, G., M. Pfeiffer, T. Laepple, G. Leduc, and J. H. Kim (2012), A model-data comparison of the Holocene global sea surface temperature evolution, *Clim. Past Discuss.*, 8(2), 1005-1056.
- Lombard, F., L. Labeyrie, E. Michel, L. Bopp, E. Cortijo, S. Retailliau, H. Howa, and F. Jorissen (2011), Modelling planktic foraminifer growth and distribution using an ecophysiological multi-species approach, *Biogeosciences*, 8, 853-873.
- Longhurst, A. R. (2007), Ecological geography of the sea, *Amsterdam: Academic Press*.
- MARGO (2009), Constraints on the magnitude and patterns of ocean cooling at the Last Glacial Maximum, *Nature Geosci.*, 2(2), 127-132.
- Maslin, M. A., N. J. Shackleton, and U. Pflaumann (1995), Surface Water Temperature, Salinity, and Density Changes in the Northeast Atlantic During the Last 45,000 Years: Heinrich Events, Deep Water Formation, and Climatic Rebounds, *Paleoceanography*, 10(3), 527-544.
- Meland, M. Y., E. Jansen, and H. Elderfield (2005), Constraints on SST estimates for the northern North Atlantic/ Nordic Seas during the LGM, *Quaternary Science Reviews*, 24, 835-852.
- Obbink, E. A., A. E. Carlson, and G. P. Klinkhammer (2010), Eastern North American freshwater discharge during the Bolling-Allerod warm periods, *Geology*, 38(2), 171-174.
- Ohkouchi, N., T. I. Eglinton, L. D. Keigwin, and J. M. Hayes (2002), Spatial and Temporal Offsets Between Proxy Records in a Sediment Drift, *Science*, 298(5596), 1224-1227.
- Ottens, J. J. (1991), Planktic foraminifera as North Atlantic water mass indicators, *Oceanologica Acta*, 14(2), 123-140.
- Peck, V. L., I. R. Hall, R. Zahn, and H. Elderfield (2008), Millennial-scale surface and subsurface paleothermometry from the northeast Atlantic, 55-8 ka BP, *Paleoceanography*, 23(3), PA3221.
- Pérez-Folgado, M., F. J. Sierro, J. A. Flores, I. Cacho, J. O. Grimalt, R. Zahn, and N. Shackleton (2003), Western Mediterranean planktonic foraminifera events and millennial climatic variability during the last 70 kyr, *Marine Micropaleontology*, 48(1, 2), 49-70.
- Pflaumann, U., J. Duprat, C. Pujol, and L. D. Labeyrie (1996), SIMMAX: A Modern Analog Technique to Deduce Atlantic Sea Surface Temperatures from Planktonic Foraminifera in Deep-Sea Sediments, *Paleoceanography*, 11(1), 15-35.
- Richter, T. (1998), Sedimentary fluxes at the mid-atlantic ridge - sediment sources, accumulation rates, and geochemical characterisation, *GEOMAR Report, GEOMAR Research Center for Marine Geosciences, Christian Albrechts University in Kiel(73)*, 173.
- Rogerson, M., E. J. Rohling, P. P. E. Weaver, and J. W. Murray (2004), The Azores Front since the Last Glacial Maximum, *Earth and Planetary Science Letters*, 222(3-4), 779-789.
- Sabbatini, A., F. Bassinot, S. Boussetta, A. Negri, H. Rebaubier, F. Dewilde, J. Nouet, N. Caillon, and C. Morigi (2011a), Further constraints on the diagenetic influences and salinity effect on *Globigerinoides ruber* (white) Mg/Ca thermometry: Implications in the Mediterranean Sea, *Geochem. Geophys. Geosyst.*, 12(10), Q10005.
- Sabbatini, A., F. Bassinot, S. Boussetta, A. Negri, H. Rebaubier, F. Dewilde, J. Nouet, N. Caillon, and C. Morigi (2011b), Further constraints on the diagenetic influences and salinity effect on *Globigerinoides ruber* (white) Mg/Ca thermometry: Implications in the Mediterranean Sea, *Geochemistry, Geophysics, Geosystems*, 12(10), Q10005.
- Schiebel, R., B. Schmuker, M. Alves, and C. Hemleben (2002), Tracking the Recent and late Pleistocene Azores front by the distribution of planktic foraminifers, *Journal of Marine Systems*, 37(1-3), 213-227.
- Schneider, B., G. Leduc, and W. Park (2010), Disentangling seasonal signals in Holocene climate trends by satellite-model-proxy integration, *Paleoceanography*, 25(4), PA4217.
- Schwab, C., H. Kinkel, M. Weinelt, and J. Repschläger (2012), Coccolithophore paleoproductivity and ecology response to deglacial and Holocene changes in the Azores Current System, *Paleoceanography*, 27(3), PA3210.
- Sicre, M. A., G. Siani, D. Genty, N. Kallel, and L. Essalami (2013), Seemingly divergent sea surface temperature proxy records in the central Mediterranean during the last deglacial, *Clim. Past Discuss.*, 9(1), 683-701.

- Simstich, J., M. Sarnthein, and H. Erlenkeuser (2003), Paired $\delta^{18}\text{O}$ signals of *Neogloboquadrina pachyderma* (s) and *Turborotalita quinqueloba* show thermal stratification structure in Nordic Seas, *Marine Micropaleontology*, 48, 107-125.
- Steinke, S., M. Kienast, J. Groeneveld, L.-C. Lin, M.-T. Chen, and R. Rendle-Bühning (2008), Proxy dependence of the temporal pattern of deglacial warming in the tropical South China Sea: toward resolving seasonality, *Quaternary Science Reviews*, 27(7-8), 688-700.
- Storz, D., H. Schulz, J. J. Waniek, D. E. Schulz-Bull, and M. Kufçera (2009), Seasonal and interannual variability of the planktic foraminiferal flux in the vicinity of the Azores Current, *Deep Sea Research Part I: Oceanographic Research Papers*, 56(1), 107-124.
- Stouffer, R. J., et al. (2006), Investigating the Causes of the Response of the Thermohaline Circulation to Past and Future Climate Changes, *Journal of Climate*, 19(8), 1365-1387.
- Telford, R. J., C. Li, and M. Kucera (2012), Mismatch between the depth habitat of planktonic foraminifera and the calibration depth of SST transfer functions may bias reconstructions, *Clim. Past Discuss.*, 8(4), 4075-4103.
- Teller, J. T., D. W. Leverington, and J. D. Mann (2002), Freshwater outbursts to the oceans from glacial Lake Agassiz and their role in climate change during the last deglaciation, *Quaternary Science Reviews*, 21(8, Åi9), 879-887.
- Thornalley, D. J. R., I. N. McCave, and H. Elderfield (2010), Freshwater input and abrupt deglacial climate change in the North Atlantic, *Paleoceanography*, 25(PA1201).
- Waelbroeck, C., L. Labeyrie, E. Michel, J. C. Duplessy, J. F. McManus, K. Lambeck, E. Balbon, and M. Labracherie (2002), Sea-level and deep water temperature changes derived from benthic foraminifera isotopic records, *Quaternary Science Reviews*, 21, 295-305.

Chapter 5

Response of the central subtropical North Atlantic surface hydrography on Deglacial and Holocene AMOC changes

This chapter corresponds to an article resubmitted to *Paleoceanography* with myself as leading author and the co-authors Mara Weinelt, Hanno Kinkel, Nils Andersen, Dieter Garbe-Schönberg and Christian Schwab.

5 Response of the subtropical North Atlantic surface hydrography on Deglacial and Holocene AMOC changes

Key points

- Azores Front position is coupled with AMOC strength over last deglaciation
- Magnitude of deglacial subtropical SST changes match subpolar SST changes
- Deglacial heat storage patterns in the subtropical North Atlantic

5.1 Abstract

The North Atlantic subtropical gyre (STG) circulates warm waters between 10 and 40°N and is a potential area of heat storage during periods of reduced North Atlantic Meridional Overturning Circulation (AMOC), when warm salt-rich waters are retained in the subtropics. In this study, we investigated multi-centennial to millennial scale changes in subtropical North Atlantic hydrography in response to AMOC changes during the last deglaciation and early Holocene, using sediment cores MD08-3180 and GEOFAR KF16. The coring site (38°N), which has exceptionally high sedimentation rates, is situated near the boundary between transitional eastern North Atlantic waters and STG waters that is formed by the Azores Front. Hydrographic changes are reconstructed using published stable isotope data of surface dwelling planktonic foraminifera and sea surface temperature estimates based upon alkenone analysis, supplemented with new stable isotope data of benthic and subsurface dwelling planktonic foraminifera, Mg/Ca measurements on planktonic foraminifera, and subtropical planktonic foraminifera abundances. These multiproxy data indicate a close coupling between the latitudinal position of the northern STG boundary and deglacial AMOC modes. During weak AMOC phases (Heinrich event 1, Younger Dryas (YD), 8.2 ka event), Northern Hemisphere subpolar water reached down to the northern STG boundary, displacing the boundary southward. During the Bølling-Allerød warm period, a strong warming trend of the subtropical region to 19°C is observed. A cooling of the SST by 6°C during the YD is accompanied by ongoing northward transport of warm subsurface water that might have contributed to the restart of AMOC.

5.2 Introduction

The North Atlantic Meridional Overturning Circulation (AMOC) transports subtropical water in its upper limb with the North Atlantic Current (NAC) (Figure 5.1) to the northern high latitudes and thereby warms the European continent. In the northern high latitudes the water cools and sinks down, returning southward as deepwater flow [e.g. Kanzow *et al.*, 2010]. Recent oceanographic data and modeling studies suggest a coupling between AMOC strength and the changing extension and strength of the North Atlantic Subtropical Gyre (STG) and Subpolar Gyre (SPG) on decadal

time scales [Born and Levermann, 2010; Häkkinen *et al.*, 2011; Hátún *et al.*, 2005; Lozier *et al.*, 2010]. Furthermore AMOC changes influence the heat content of the subtropical North Atlantic (NA) [e.g. Cunningham *et al.*, 2013], that result in wind speed changes. Increasing wind strength induces an eastward expansion of the SPG and a weakening of the STG that leads to enhanced transport of warm saline waters into the deepwater convection areas and results in increasing overturning in the SPG and increasing AMOC strength [e.g. Hátún *et al.*, 2005; Lozier *et al.*, 2010]. Knowledge of the subpolar and subtropical gyre dynamics in modern oceanographic and modeling studies scenarios, and intensive research on past changes of the SPG [Austin and Kroon, 2001; Benway *et al.*, 2010; Thornalley *et al.*, 2009] is increasing, but little is known regarding long-term changes of the STG and its coupling with AMOC. A reason for this lack of knowledge is low productivity within the STG, which results in notoriously low sedimentation rates [Longhurst *et al.*, 1995] and hence low resolution sediment core data, that hampers reconstructions on multi-decadal to millennial timescales.

During the last deglaciation, AMOC changed from the glacial shallow (2500-3000 m) but vigorous overturning mode during the Last Glacial Maximum (LGM) to the modern AMOC mode. Likewise for the Holocene, vigorous deepwater production in the North Atlantic (NA) that occupies the NA basin down to 4000 m water depth has been reconstructed using benthic $\delta^{13}\text{C}$ records, $^{231}\text{Pa}/^{230}\text{Th}$ and ϵ_{Nd} records [Benway *et al.*, 2010; Gherardi *et al.*, 2009; Lippold *et al.*, 2012; McManus *et al.*, 2004; Michel *et al.*, 1995; Oppo *et al.*, 2003; Roberts *et al.*, 2010; Sarnthein *et al.*, 1994].

The AMOC reorganization at the beginning of the last deglaciation started with the Heinrich 1 (H1) event (Greenland Stadial 2a (GS2a)) (~17.5-14.6 ka BP) (age boundaries according to the INTIMATE time scale [Lowe *et al.*, 2008], corrected for the difference between the b2K and BP time scale, the Greenland event stratigraphy was added to the commonly used land based terminology). The H1 event is characterized by a drastic reduction in deep water overturning and decreasing northern hemisphere sourced deepwater flow at all depths. A first strengthening in overturning circulation with moderate deepwater export at all deepwater levels induced the warm Bølling-Allerød (BA) (Greenland Interstadial 1 (GI 1e -1) (14.6-12.9 ka BP), [Gherardi *et al.*, 2009]. A second major AMOC slow down occurred during the cold Younger Dryas (YD) (Greenland Stadial 1 (GS1)) (12.9-11.7 ka BP). The YD circulation was intermediate between the circulation during the H1 and the BA, with a slight decrease in deepwater renewal rate below 3000 m water depth compared to the BA, while intermediate circulation at ~2000 m water depth was maintained [Gherardi *et al.*, 2009; Waelbroeck *et al.*, 2011]. During the onset of the Holocene, AMOC strengthened with increasing production of North Atlantic deepwater (NADW) in the Nordic seas. This strengthening of NADW production was disrupted by breakdowns associated with ice rafting events [Oppo *et al.*, 2003] and with cooling events of the Northern Hemisphere, of which the 8.2 ka Lake Agassiz flood event [Kleiven *et al.*, 2008] is the most prominent. The final Holocene AMOC mode was reached after 7 ka BP with the onset of modern Labrador Sea water

production [e.g. *Colin et al.*, 2010; *Hillaire-Marcel et al.*, 2001; *Hoogakker et al.*, 2011; *Born and Levermann*, 2010]

AMOC reductions were most likely caused by large amounts of meltwater that were released from the Northern Hemisphere ice sheets. These meltwater events led to surface water freshening and stratification in the NA deep-water convection areas, slowing down rates of overturning. The extension of freshwaters far into the subpolar NA is known from IRD layers in sediment cores [*Bond et al.*, 2001] and $\delta^{18}\text{O}_w$ reconstructions indicate that freshwater propagated along the Iberian Margin and even reached into the Gulf of Cadiz during H1 [*Eynaud et al.*, 2009; *Voelker et al.*, 2006; 2009]. The exact extension of freshwater into the central NA basin however remains uncertain. Freshwater hosing experiments with general ocean circulation models predict a 50% reduction of AMOC strength in response to a simulated freshwater disturbance of 0.1 Sv over 100 years. However, these models differ in estimates the amount of reduction AMOC reduction, the range of the freshwater plume extension into the open NA and the changes in the extension of the subtropical warm water pool [*Stouffer et al.*, 2006].

The AMOC reductions were concurrent with major northern hemisphere cooling during the H1 and the YD event and warming during the BA and the Holocene. *Barker et al.* [2009] suggest that cold events are associated with abrupt southward shifts of hydrographic and atmospheric frontal systems and climate zones in the Atlantic Ocean. Yet, it remains unclear whether these frontal displacements were associated with a displacement of its characteristic strong SST gradients [*Barker et al.*, 2009], or whether the most pronounced cooling during cold events that appeared in the northern high latitudes (6-8°C) gradually dispersed southwards due to mixing with warmer subtropical water [*Shakun and Carlson*, 2010]. With the result that during the last glacial SSTs in the STG were only moderately cooler than modern ($\sim 2.6 \pm 2$ °C) [*MARGO*, 2009] subtropical SST. Recent studies of sediment cores from the western tropical to subtropical NA, suggest that during shallow or weak AMOC phases heat and salt was stored in waters from these NA regions. Yet, it remains unclear whether this water was stored within the surface western subtropical NA [*Carlson*, 2008; *Schmidt et al.*, 2004], the surface tropical NA [*Carlson*, 2008; *Schmidt et al.*, 2004; *Weldeab et al.*, 2006] or the intermediate subtropical water mass [*Bakke et al.*, 2009; *Rühlemann et al.*, 2004]. The stored warm waters are assumed to have played a major role in the resumption of the AMOC. An abrupt release and export of warm saline waters into the subpolar deepwater convection areas, would lead to the resumption of a strong AMOC [*Carlson*, 2008; *Schmidt et al.*, 2004]. Some studies suggest that an initial subsurface warming preconditioned this advection of saline subtropical waters to the areas of deep convection [*Bakke et al.*, 2009; *Krebs and Timmermann*, 2007].

Furthermore, the extension and shape of the heat and salt pool in the eastern subtropical region is poorly constrained. Based on stable isotope and faunal abundance evidence of planktonic foraminifera in a sediment core from the Gulf of Cadiz, *Rogerson et al.* [2004] proposed that the

Azores Front (AF), marking the boundary between warm STG waters and cooler transitional waters, at its eastern limit, resided at the same position over the LGM and the last deglaciation. A southward displacement of the northern rim of the STG during glacial times, is qualitatively indicated by changes in the distribution patterns of foraminifera assemblages in a site south of the AF [Schiebel *et al.*, 2002b] and coccolithophore assemblages at the Azores coring site [Schwab *et al.*, 2012], as well as by a cooling of 5°C at a subtropical Gyre site (37 °N) [Calvo *et al.*, 2001]. Yet, SST changes may also be a result of changing transport within the Azores current (AC) that delineates the STG to the North, or SST changes in its source area in the West Atlantic warm pool. The aim of this study is to gain a more thorough insight into the dynamics of the STG over the last deglaciation, under conditions of changing AMOC strength. For this purpose we employ high-resolution records of the subtropical mixed layer from a coring site, which at present is situated at the northern boundary of the STG at the interface of warm subtropical and cooler temperate waters. This site is therefore considered to be highly sensitive to monitor changes in the frontal system and in the warm water advection in the AC. Our results are discussed with respect to the following aspects:

- 1) Changes in planktonic foraminiferal assemblages are used to reconstruct the position of the STG in order to unravel the response of the STG surface hydrography to different AMOC modes. The latter are reconstructed through comparison of the $\delta^{13}\text{C}$ composition of the North East Atlantic Deep Water (NEADW) at the coring site to known NA AMOC records.
- 2) We investigate the reaction of the STG on AMOC strengthening during the Bølling warming by investigating the magnitude of SST change within the STG. Additionally, changes in the water mass structure are reconstructed using paired surface and subsurface stable isotope and SST records and foraminiferal abundance data.
- 3) For AMOC weakening phases the potential storage of the retained tropical/subtropical warm waters within surface/subsurface waters of the STG, its coupling with the European climate, and its potential role in the resumption of AMOC is assessed.

5.3 Oceanographic setting and study location

Hydrographically, the coring location (38°N, 31.13°W) is situated at the northern boundary of the low productivity STG (Figure 5.1), which is formed by the AC system. This system is fed by warm tropical water that flows from the Caribbean through the Florida Strait along the American continental margin and is bordered by cold American Slope water towards the North. After leaving the American continental margin, the NAC turns northeastwards towards the eastern North Atlantic basin and the Nordic Seas [Dengg *et al.*, 1996]. Between 30 and 40°N the AC branches off the NAC and flows eastwards towards the Mediterranean Sea. At about 15°W a part of the water mass is mixed with Mediterranean surface outflow and contributes to the formation of the southward flowing Canary current (CC) [e.g. Fründt *et al.*, 2013, Peliz *et al.*, 2005]. A smaller branch of the

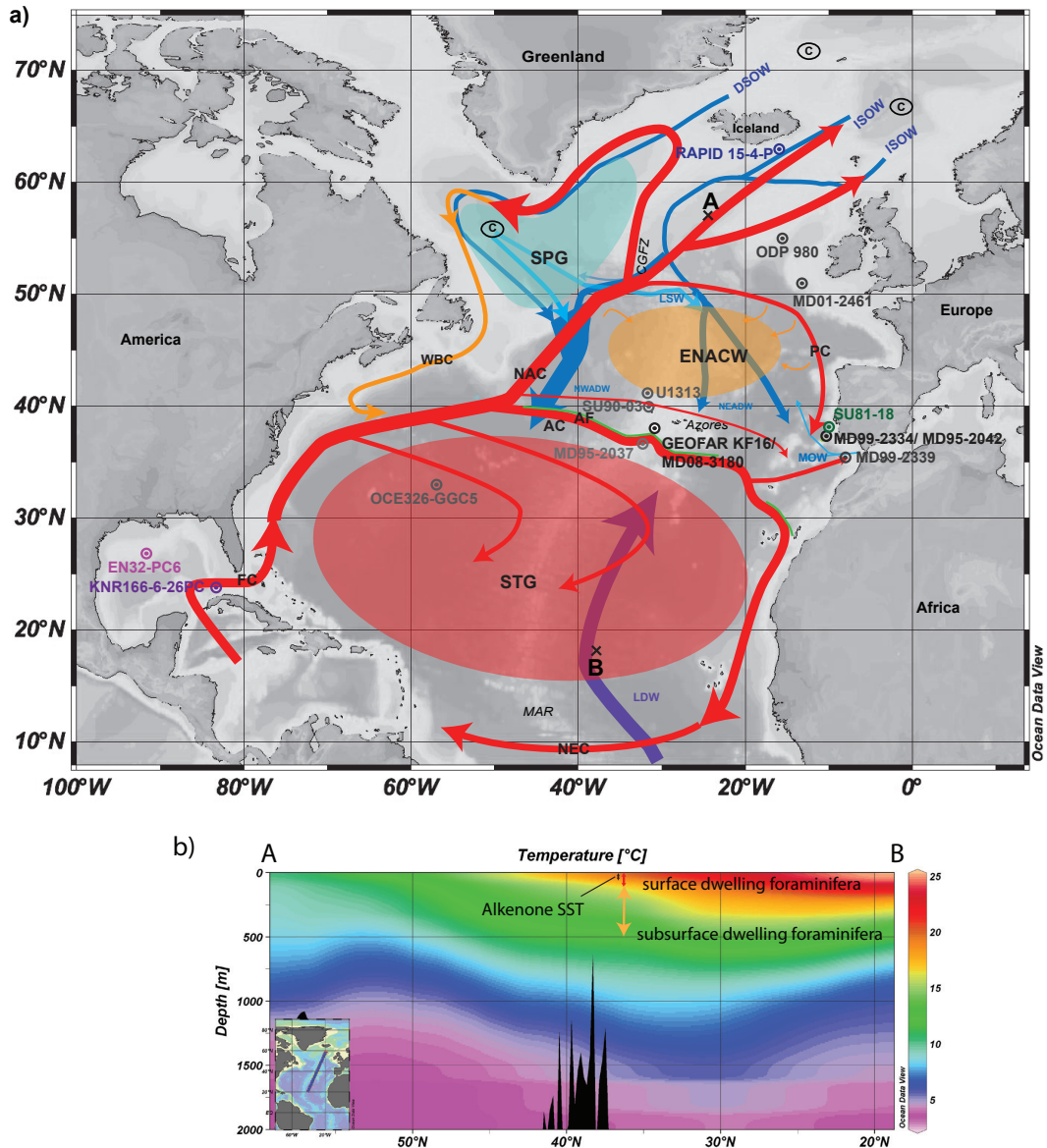


Figure 5.1 Modern surface water hydrography of the NA

Map and cross section obtained from Ocean Data View [Schlitzer *et al.*, 2004] and World Ocean Atlas [Locarnini, 2010]

a) Schematic overview of the modern NA hydrology, modified after Schott *et al.* [2004] and Lherminier *et al.* [2010]. Red arrows indicate warm surface currents (NAC North Atlantic current, FC Florida Current, AC Azores Current, PC Portugal current, ENAC East Atlantic Water, NEC North Equatorial Current), blue arrows indicate deep water currents (MOW Mediterranean Outflow water, LSW Labrador Sea water, ISOW Iceland Scotland Overflow water, DSO Denmark Strait Overflow water, NEADW North East Atlantic Deep Water, NWADW North West Atlantic Deep Water, LDW Lower Deep Water), C indicate deepwater convection sites also indicated are the Subtropical Gyre (STG) and the Supolar Gyre (SPG) and the transitional Eastern North Atlantic Water (ENATW)

Abbreviations: CGFZ Charlie Gibbs fracture Zone, MAR Mid Atlantic Ridge

b) North-South transect through the subpolar and subtropical NA from point A to point B as indicated in Figure 5.1a), the approximate depth horizons recorded by different surface water proxies are indicated

AC continues into the Gulf of Cadiz [Peliz *et al.*, 2005]. At 30°W the AC is situated between 32° and 36°N [e.g. Alves *et al.*, 2002; Volkov and Fu, 2011; Fründt *et al.*, 2013], is about 50 km wide and penetrates to at least 1000 m water depth. On its pathway it induces mesoscale eddies that can

reach the widths of 200 km and reach up to the Azores coring site [Barbosa Aguiar et al., 2011; Dickson et al., 1985; Gould, 1985; Käse and Siedler, 1982; Pingree, 1997]. The Azores counter current (ACC), that transports mixed Mediterranean water westwards, delineates the AC to the North, [e.g. Alves et al., 2002; Comas-Rodrigues et al., 2011]. Within this current system the AF separates oligotrophic subtropical 18 degree mode water, from nutrient rich transitional Eastern North Atlantic Central Water (ENACW). The AF is defined by the strongest dipping 15°C isotherm, situated above 200 m north of the front and dipping below 300 m south of the front [Gould, 1985; Fründt et al., 2013] (Figure 1b). Although it is not distinguishable by the surface SST distribution [Alves et al., 2002], the AF separates distinctly different fauna assemblages [Otters, 1991; Schiebel et al., 2002a,b] that can be used to track deglacial changes in the AF position.

The position of the AC is modulated by wind strength [Volkov and Fu, 2010, 2011]. Strengthening of the westerlies leads to a southward movement of the AC, while decreasing wind strength leads to a relaxation and northward expansion of the gyre. The strength of the Mediterranean Overflow Water (MOW) is assumed to drive the AC strength through the entrainment of surface waters into the MOW cascading from the Mediterranean Basin into the North East Atlantic basin at the Strait of Gibraltar [Kida et al., 2008; Lamas et al., 2010; Volkov and Fu, 2010].

To the northeast of the AC the Portugal Current (PC) is transporting a mixture of NAC waters and subpolar waters along the Iberian margin [e.g. Alves et al., 2000]. Below the thermocline depth the PC is underlain by the ENACW, which consists of a mixture of the Western North Atlantic Central Water (WNACW), subtropical ENACW (ENACW_T) that originates from the AF region and ENACW with subpolar origin (ENACW_P), also known as Subpolar Mode Water [Van Aken 2001; Brambilla et al., 2008 a,b; Pollard et al., 1996]. Mediterranean Overflow Water (MOW) underlies the ENACW [e.g. Van Aken 2001]. At depths below 3000 m the east Atlantic basin is filled with southern sourced Lower Deep Water (LDW) [van Aken, 2000] with typical $\delta^{13}\text{C}$ values of 0.5 ‰, which is overlain by North East Atlantic Deep Water (NEADW) with typical $\delta^{13}\text{C}$ values of 1.2 ‰ [Locarnini et al., 2010].

5.4 Material and methods

5.4.1 Coring site and cores

South of the Azores Islands along the Mid Atlantic Ridge (MAR) narrow basins were formed by transform faulting. These basins are characterized by steep flanks [Richter, 1998] and act as sediment trap for diffusive transported material. The resulting partly laminated sediments provide exceptionally high sedimentation rates up to 120 cm / ka. Calypso square core (CASQ) MD08-3180 (38°N, 31.1345°W, 3059 water depth) and piston core GEOFAR KF16 (37.999°N 31.1283°W, 3050 m water depth) [Richter, 1998] were retrieved in this region during GEOFAR

cruise onboard the research vessel Le Noroit [Richter, 1998] and IMAGES-AMOCINT MD168-cruise 2008 [Kissel *et al.*, 2008].

5.4.2 Sample preparation

Records used in this study are a stack of the two cores, GEOFAR KF16 [Richter, 1998] and MD08-3180. Core GEOFAR KF16 was sampled at 1 cm intervals over the Holocene section (0-200 cm core depth in core GEOFAR KF16), whilst core MD08-3180 was used for the older sections and sampled in 1-2 cm intervals over the Younger Dryas section, (150-250 cm core depth), and at 5 cm resolution over the Bølling-Allerød and termination 1A sections (250-395 cm core depth). The U^{K}_{37} record [Schwab *et al.*, 2012] was obtained from core MD08-3180 in 5 cm resolution. The sediment samples (~9 g) were freeze dried, washed over a 63 μm sieve and the residual oven dried at 40°C.

5.4.3 Stable isotope analyses

For stable isotope analyses monospecific samples of planktonic foraminifera from the size fraction 315-400 μm were handpicked, cracked, ethanol cleaned, decanted and dried at 40°C. These included parallel analyses of surface dwelling (0-10 m, [Lombard *et al.*, 2011]) *Globigerinoides ruber w.* (10-25 specimens) [Schwab *et al.*, 2012], *Globigerina bulloides* (15-25 specimens) (30-100 m, [Lombard *et al.*, 2011]) and of deep-dwelling (100-400 m, [Cleroux *et al.*, 2013; Loncaric *et al.*, 2006; Schiebel *et al.*, 2002a; Wilke *et al.*, 2009]) *Globorotalia truncatulinoides* (15 specimens). For the benthic stable isotope record one to three specimens of the epibenthic foraminifera *Cibicidoides wuellerstorfi* (315-400 μm) were used, following the same cleaning procedure as for planktonic foraminifera. All stable isotope analyses were carried out at the Leibniz Laboratory for Radiometric Dating and Stable Isotope Research in Kiel using a Finnigan MAT 253 mass spectrometer coupled with a Kiel IV carbonate preparation device and calibrated to the V-PDB scale. The analytic precision is better than 0.1‰ for $\delta^{18}\text{O}$ and better than 0.05‰ for $\delta^{13}\text{C}$. Duplicate sample preparation of at least 10 samples per species gave a $\delta^{18}\text{O}$ standard deviation of 0.11 ‰ for *G. ruber w.*, 0.14‰ for *G. bulloides* and 0.12 ‰ for *G. truncatulinoides*. The standard deviation for $\delta^{13}\text{C}$ in *C. wuellerstorfi* is 0.13 ‰.

For the surface water $\delta^{18}\text{O}$ record of the YD interval *G. bulloides* was spliced into the *G. ruber w.* record using a correction of -0.67‰ as observed by parallel measurements of both species, an offset also known from previous studies in the NA [Ganssen and Kroon, 2000]. However, this part of the record should be regarded with care as differences in the depth habitat and seasonality of *G. bulloides* and *G. ruber w.* might induce nonlinear offsets. *G. bulloides* lives slightly deeper than *G. ruber w.* and shows highest abundances during winter and spring whereas *G. ruber w.* occurs from July to January [Storz *et al.*, 2009].

The subsurface record obtained from *G. truncatulinoides* probably reflects winter conditions as the abundance maximum of *G. truncatulinoides* is observed during winter [Schiebel *et al.*, 2002a; Storz *et al.*, 2009].

To identify the well-known basin wide deglacial phases of weak AMOC in our record the $\delta^{13}\text{C}$ of *C. wuellerstorfi* is employed, a well-established proxy to trace water masses by their ventilation state [Duplessy *et al.*, 1984]. At our site, located at 3059 m water depth, changing proportions of low $\delta^{13}\text{C}$ LDW and high $\delta^{13}\text{C}$ NEADW can be related to data from transect studies in the NA, which are expected to respond to different AMOC modes.

5.4.4 Temperature reconstructions

The SST record published by Schwab *et al.* [2012] that was established using the U_{37}^K index as derived from alkenone undersaturation ratios were complemented by SST and subsurface T estimates using Mg/Ca measurements on the planktonic foraminifera species *G. bulloides* and *G. truncatulinoides*.

For Mg/Ca analyses 15 -30 individuals were gently cracked under a glass plate and cleaned following the standard procedure of Martin and Lea [2002], including reductive and oxidative cleaning steps. After oxidative cleaning, samples were transferred into leached vials. A final leaching step with 0.001N HNO_3 was applied before samples were dissolved and diluted in 0.1N HNO_3 and measured in a simultaneous ICPM-OES instrument with radial plasma observation. Analytical error for Mg/Ca analyses was 0.1% RSD. Possible shell contamination or coatings by heavy minerals were excluded by additional trace element measurements on the same samples. Duplicate down core sample preparation gave a standard deviation of 0.43 mmol/mol Mg/Ca for *G. bulloides* and 0.06 mmol/mol Mg/Ca for *G. truncatulinoides*.

Mg/Ca values of *G. bulloides* and *G. truncatulinoides* were converted into water temperatures using the species specific calibrations for surface dwelling species (Table 5.1), and the equation for mixed subsurface dwellers for *G. truncatulinoides* published by Cléroux *et al.* [2008] (Table 5.1). These calibrations are based on core top data from the subpolar and subtropical NA. Using this calibration, our core top data matches well with modern Azores coring site temperatures at the surface and 200 m water depth respectively. Using these calibrations a error of 0.45°C for the resulting *G. truncatulinoides* temperatures and 1.8 °C for *G. bulloides* temperatures has to be considered.

Table 5.1 Different Mg/Ca calibrations for planktonic foraminifera
General form of equation $\text{Mg/Ca} = b \exp(a \cdot T)$

species	source	b	a	reference
<i>G. bulloides</i>	Core tops North Atlantic	0.78±0.12	0.082±0.01	Cleroux <i>et al.</i> [2008]
<i>Subsurface dweller</i>	Core tops North Atlantic	0.78±0.04	0.052±0.003	Cleroux <i>et al.</i> [2008]

5.4.5 Foraminifera assemblages

The relative abundances of indicator species in planktonic foraminiferal assemblages can be used to qualitatively identify the alternating presence of temperate and subtropical water masses at the site and thus to trace shifts of the AF on seasonal to inter annual time scales [Ottens, 1991; Schiebel et al., 2002a; Schiebel et al., 2002b; Storz et al., 2009], as well as over the last glacial to interglacial transition [Eynaud et al., 2009; Rogerson et al., 2004; Schiebel et al., 2002a]. Accordingly, *G. ruber w.* and *G. truncatulinoides* are most abundant south of the AF, whereby *G. truncatulinoides* is assumed to be transported from the Sargasso Sea with the NAC/AC towards the coring site [Schmuker and Schiebel, 2002]. Despite this potential transport, the $\delta^{18}\text{O}$ signal of *G. truncatulinoides* is assumed to reflect the local conditions, as *G. truncatulinoides* builds a secondary calcite before its reproduction at thermocline depth that amounts to more than 50 to 70 % of the shell weight [Lohmann and Schweitzer, 1990; Lohmann, 1995; Masumoto and Lynch-Stieglitz, 2003]. *G. scitula* and *N. incompta* typically occur north of the AF within the ENACW. The species *T. quinqueloba* and *N. pachyderma s.* today are dominant in the Nordic seas and at the polar front and thus are valid indicators for subpolar to polar conditions. *G. inflata* is most abundant with the NAC water, with an abundance maximum east of the American continent [Ottens, 1991; Pflaumann et al., 1996].

For the relative abundance records, the samples from the size fraction $>150\ \mu\text{m}$ were spliced and 300-1000 individuals were counted following the taxonomy of Pflaumann et al. [1996], which is based on Bé and Tolderlund [1974]. For all abundance records an error of 5% is assumed.

Here, we use the relative abundances of *G. ruber w.* and of *N. incompta* to trace the varying influence of subtropical to transitional waters on the coring site and thus to reconstruct the position of the northern boundary of the AF relative to the coring site. Additionally, the relative abundance of *G. scitula* is used to trace the influence of transitional waters, whereas the abundance of *T. quinqueloba* is used as an indicator for subpolar to polar water masses on the coring site. The abundance of *G. inflata* is used to trace the abundance of NAC water and the abundance of *G. truncatulinoides* might be used as an indicator for the AC transport strength.

5.4.6 $\delta^{18}\text{O}_{\text{water}}$ reconstructions

Changes in salinity over time were reconstructed from the surface foraminiferal $\delta^{18}\text{O}_{\text{carbonate}}$ record by removing the temperature effect, estimated from the U^{K}_{37} SST and Mg/Ca SST. Calculated $\delta^{18}\text{O}_{\text{water}}$ values differ widely (1‰) dependent on the use of different equations. In order to use the equation that best matches the ecology of the foraminifera, we applied different species-specific $\delta^{18}\text{O}_{\text{water}}$ equations. For *G. bulloides* we applied the species specific equation for specimens with 13 chambers of Bemis et al. [1998], as only adult specimens of *G. bulloides* were used in this study. For *G. ruber w.* we used the LL calibration based on *O. universa* [Bemis et al., 1998] to account for

the anticipated light conditions in a natural environment and the symbionts *G. ruber* bears. For *G. truncatulinoides*, we applied the equation of *Shackleton et al.* [1974], following the arguments of *Cleroux et al.* [2008]. To correct the $\delta^{18}\text{O}_w$ records for ice volume, we used the relative sea level composite curve of *Waelbroeck et al.* [2002] obtained from benthic $\delta^{18}\text{O}$ measurements. The species-specific uncertainty for the $\delta^{18}\text{O}_w$ reconstructions is 0.28 ‰ for *G. ruber w.*, 0.4 ‰ for *G. bulloides* and 0.25 ‰ for *G. truncatulinoides*. The combination of $U^{K'}_{37}$ SST data and $\delta^{18}\text{O}$ data of planktonic foraminifera can produce bias in the estimates since the two proxies might record different seasons and water depth. Moreover the fine fraction containing alkenones might underlie different transport mechanisms than the coarse fraction containing foraminifera [*McCave*, 2002; *Ohkouchi et al.*, 2002]. However, the faunal composition records of foraminifera and coccolithophores [*Schwab et al.*, 2012] however closely match in their distribution patterns of subpolar and subtropical species. Thus we suggest that the $U^{K'}_{37}$ and foraminifer records are not affected by differential transport mechanisms. We additionally calculated $\delta^{18}\text{O}_w$ for the YD interval using paired foraminiferal $\delta^{18}\text{O}$ and Mg/Ca measurements, and compared our results to $\delta^{18}\text{O}_w$ values calculated from $U^{K'}_{37}$ data, to determine differences between the two methodologies. Both $\delta^{18}\text{O}_w$ reconstructions indicate a similar pattern for the YD (Figure 5.3d), thus we assume that the $\delta^{18}\text{O}_w$ data reconstructed using $U^{K'}_{37}$ SST are reliable within an uncertainty range of 0.6‰, which is lower than the detected change (0.7‰) during major freshening events.

5.5 Age model

The age model (Figure 5.2) [*Schwab et al.*, 2012] of the spliced cores MD08-3180/GEOFAR KF16 is based upon 15 ^{14}C AMS Accelerator Mass spectrometer measurements of mono-specific samples of planktonic foraminifera (*G. ruber w.* or *G. bulloides*). All ages were converted into calendar ages using the Calib 6.0 software [*Stuiver and Reimer*, 1986] using the Marine09 calibration curve [*Reimer et al.*, 2009] and a constant reservoir age correction of 400 years. The calculated ages reveal synchronicity of temperature variations in Greenland and the Azores region and thus justify fine tuning of the surface $\delta^{18}\text{O}$ record and the $U^{K'}_{37}$ SST record against the Greenland Ice core NGRIP [*Andersen et al.*, 2006]. Accordingly our proxy records cover the deglacial transition from 16 ka BP to 6 ka BP in 20 to 200 year resolution with particularly high resolution over the deglacial sequence. In contrast to other proxies, a high-resolution record of *G. ruber w.* abundance seems to indicate the beginning of the YD occurring deeper in the core than the $U^{K'}_{37}$ record suggests (Figure 5.3 a, b). The observed offset in timing between the different SST proxies [*Sicre et al.*, 2013] indicate that the tuning of SST records with the Greenland ice core record might induce systematic errors. The observed uncertainty of 300 yrs, is however, is within in the range of the ^{14}C dating accuracy. Furthermore, the benthic $\delta^{13}\text{C}$ record matches well-dated records from

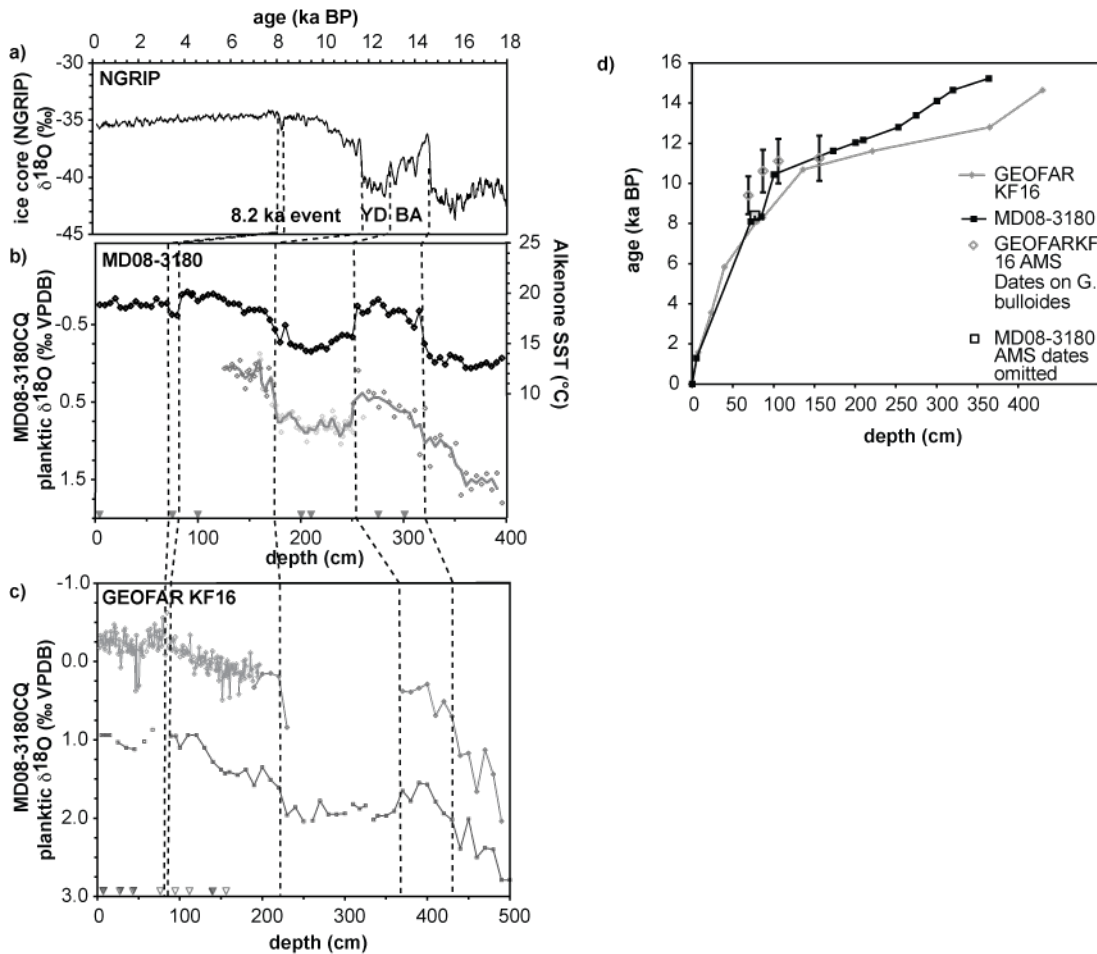


Figure 5.2 Age model for cores GEOFAR KF16 and MD08-3180

[Schwab et al., 2012]; The age models for both cores are based on AMS ^{14}C dates (indicated by triangles), both cores were additionally correlated with: a) NGRIP Greenland ice core data [Andersen et al., 2006], b) for this fine-tuning of core MD08-3180, planktonic $\delta^{18}\text{O}$ data of *G. ruber w.* (grey diamonds) were supplemented with *G. bulloides* (grey cycles) (corrected for -0.67%) (red line) as well as with UK'37 SST data (black diamonds, black line) [Schwab et al., 2012] were used, c) for GEOFAR KF16 planktonic $\delta^{18}\text{O}$ data of *G. ruber w.* (grey diamonds) and *G. scitula* (orange line) [Richter, 1998] were correlated with NGRIP. d) Age-depth plot for cores GEOFAR KF16 and MD08-3180. All ^{14}C AMS dating points are shown, omitted measurements are illustrated with open symbols

Iberian margin and subpolar NA [Skinner et al., 2003; Thornalley et al., 2010a]. Based upon these factors, we used the age model of Schwab et al. [2012] without additional modifications.

5.6 Results

The U^{K}_{37} SST record (Figure 5.3a), shows a succession of pronounced warming and cooling events, matching in timing and magnitude (2 to 6°C) the well-known patterns of the H1, the BA warming, the YD cold event and the Early Holocene warming (after 11.6 ka BP) that are recorded in high-resolution SST records from the subpolar NA and at the Iberian Margin [Bard et al., 2000; Benway et al., 2010; Eynaud et al., 2009].

At depth, these events generally coincide with marked changes in benthic foraminifera $\delta^{13}\text{C}$ (Figure 5.3f), reflecting the reorganization of deepwater masses during these times of different AMOC

modes [Austin and Kroon, 2001; Piotrowski et al., 2008; Sarnthein et al., 1994; Thornalley et al., 2010a; Waelbroeck et al., 2011]. Deepwater ventilation minima are indicated by depleted $\delta^{13}\text{C}$ values (Figure 5.3f) during the H1 event, the YD, the early Holocene and the 8.2 event. Abundances changes in benthic foraminifera during this time intervals corroborate the minima in ventilation. The high oxygen (3 to >6 ml/L) [Kaiho, 1994] environment recorder *C. wuellerstorfi*, that is typically found in NADW [Streeter and Shackleton, 1979] is replaced by *Melonis sp.* that is adapted to medium oxygen content (1.5-3 ml/L dissolved oxygen)[Kaiho, 1994]. Additional to the general $\delta^{13}\text{C}$ evolution, our high-resolution record indicates pronounced smaller scale variability. Initial ventilation recovery at the onset of BA, is followed by an abrupt $\delta^{13}\text{C}$ decrease of (0.4‰) at the IACP (GI 1-b), and a second decline of (0.3‰) at the onset of the YD. Generally low $\delta^{13}\text{C}$ values during the YD are interrupted by a 300 years lasting Mid YD (12.1-11.8 ka BP) $\delta^{13}\text{C}$ increase of (0.6‰). The benthic $\delta^{13}\text{C}$ record indicates a general rising trend from 0.1‰ to 1.2‰, between 11.6 and 7 ka BP and afterwards reach Holocene average values of 1‰. This trend is disrupted by a sequence of minor yet distinct multi-centennial $\delta^{13}\text{C}$ incursions at approximately 11 9.7, 9.1, and 8.4-8.2 ka BP.

These changes in the benthic $\delta^{13}\text{C}$ record coincide with major changes in the surface water hydrology at the Azores coring site as outlined in the following.

The $\delta^{13}\text{C}$ ventilation minima during the H1, the YD and the 8.2 event (Figure 5.3f), are accompanied by cold SST as indicated by $U^{K'}_{37}$ SST as cool as 12°C, 14°C and 18°C (Figure 5.3a). A pronounced $U^{K'}_{37}$ SST warming of 6°C to ~19°C, near modern values (~19°C) occurred at the onset of Bølling. The warm temperatures in this lower resolution record persist over the entire BA. At the beginning of the PBO, $U^{K'}_{37}$ SST rose in two abrupt steps to 18.5 °C at 11.57 ka BP and to 20.5°C at 10.6 ka BP. $U^{K'}_{37}$ SST stabilized at modern values after the 8.2 ka event. Although generally in agreement with the $\delta^{13}\text{C}$ record, the lower resolved $U^{K'}_{37}$ SST record remains warm over late Allerød and does not indicate any YD variability (Figure 5.3a,f).

Subsurface Mg/Ca temperatures range between 14°C and 12°C during H1 and increase in parallel with increasing $U^{K'}_{37}$ SST at the onset of the BA (GI-1e), and reach 16°C at 14.25 ka BP (GI-1e). Opposite to stable $U^{K'}_{37}$ SST, subsurface temperatures slightly decrease over the remaining BA (GI-1) and reach 14°C in the late Allerød (GS-1a,b) (Figure 5.3a). In contrast to extreme surface-water cooling at the onset of the YD (GS-1), subsurface Mg/Ca temperatures remain similar to those observed during the late Allerød oscillating between 13.5°C and 15°C (GI-1a,b) (Figure 5.3a). Within these oscillations a short term (less than 50 years) cooling by 2°C might be evident at the onset of the YD that is followed by a subsequent warming of 2°C. At onset of the Preboreal subsurface temperatures warm by 3°C to reach 17°C between 11.7 and 11.1 ka BP. The subsurface temperatures appear to decrease to 13°C between 11 and 8.5 ka BP and again rise at the 8.2 event, although an effect of lower resolution during the early Holocene cannot be excluded.

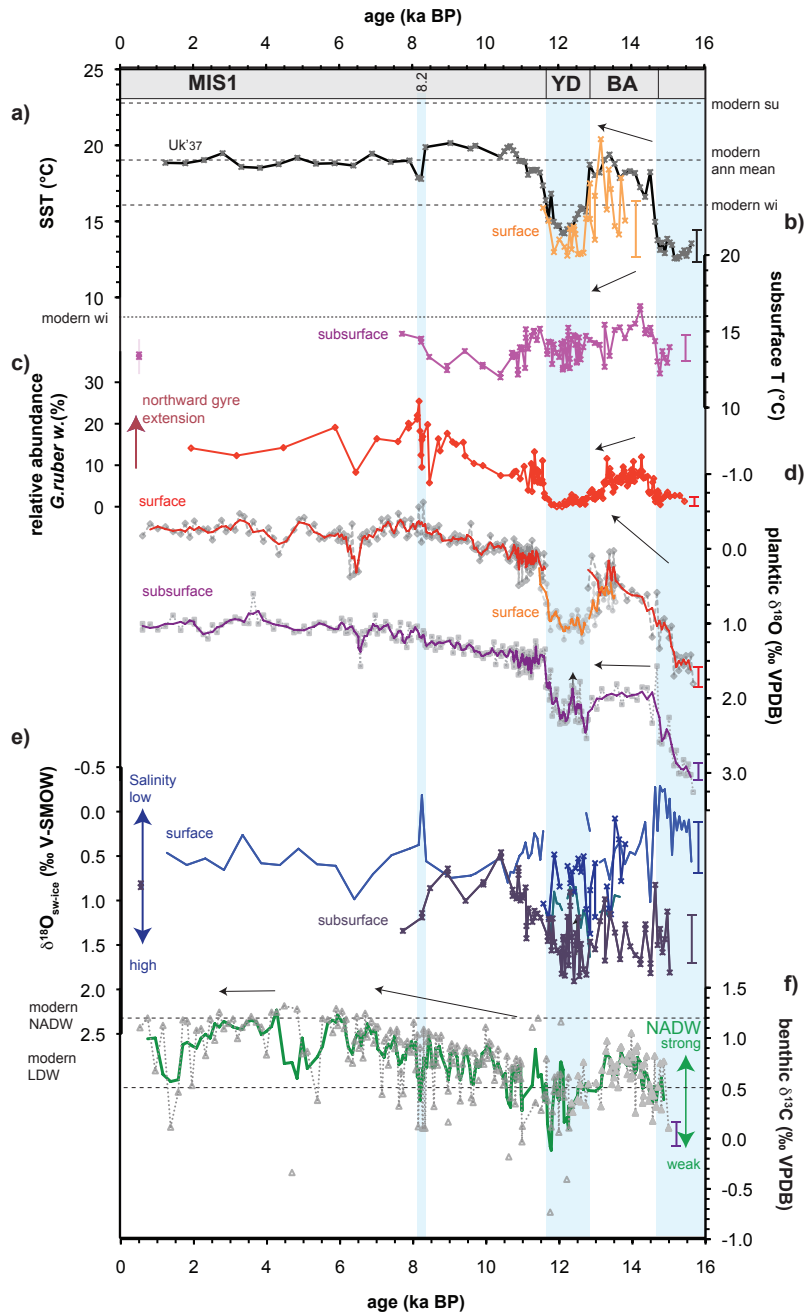


Figure 5.3 Overview over the results from stacked cores GEOFAR KF16 and MD08-3180,

a) $U^{K'37}$ SST (black line with crosses) [Schwab *et al.*, 2012] surface water SST obtained from Mg/Ca of *G. bulloides* (orange line with crosses)

b) Subsurface Mg/Ca temperatures (pink line with crosses) obtained from *G. truncatulinoides*

c) Abundance of subtropical species *G. ruber w.*, used as an indicator for the STG position

d) Planktonic $\delta^{18}O$ records. The red line shows a 3-point running mean of surface dweller records from *G. ruber w.* (grey diamonds) [Schwab *et al.*, 2012] and orange line 3-point running mean of *G. bulloides* (grey circles) [Schwab *et al.*, 2012] supplemented with additional data points over the BA-YD transition, deep violet line shows a 3-point running mean of subsurface dweller *G. truncatulinoides* (grey squares).

e) Surface water $\delta^{18}O_{w-ice}$ record (blue line), obtained from combined $U^{K'37}$ SST [Schwab *et al.*, 2012], and $\delta^{18}O$ planktonic surface water records. Additional $\delta^{18}O_{w-ice}$ from combined Mg/Ca SST reconstructions and $\delta^{18}O$ data from *G. bulloides* is shown in dark blue with crosses. Subsurface $\delta^{18}O_{w-ice}$ is reconstructed using paired Mg/Ca temperature $\delta^{18}O$ reconstructions of *G. truncatulinoides* (dark violet line with crosses). All records are corrected for ice volume changes by using the relative sea level composite curve of Waelbroeck *et al.* [2002].

f) Benthic $\delta^{13}C$ record obtained from *C. wuellerstorfi* (grey triangles), the green line shows the 3-point running mean. Values obtained from core MD08-3180 are indicated by filled symbols.

Error bars are shown at the right side of the figure. Blue bars mark the major deglacial cold events.

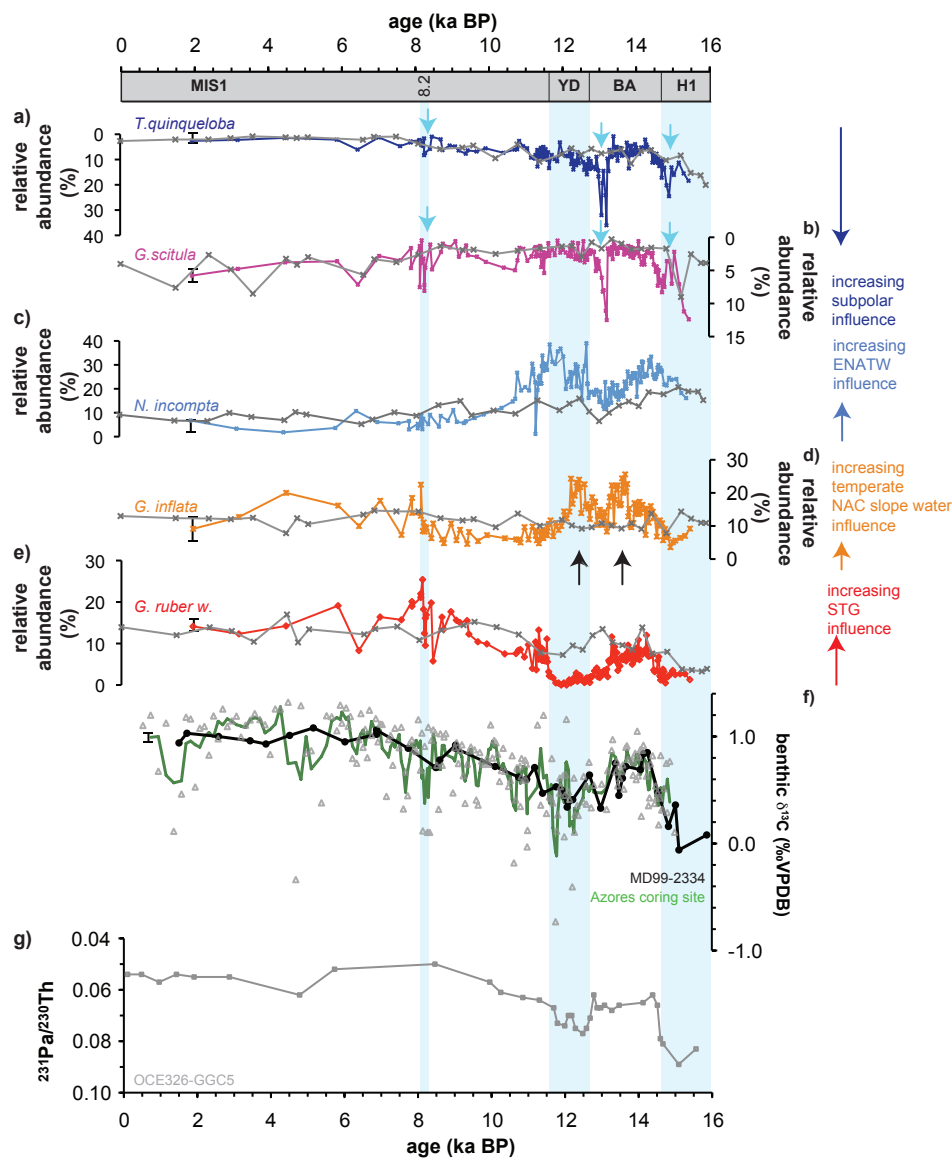


Figure 5.4 Deglacial and Holocene foraminiferal fauna abundances of selected foraminifera species from the Azores coring site and core SU90-03 [Chapman et al., 2000]

Azores coring site (colored), core SU90-03 (grey)

a) High abundance of subpolar species *T. quinqueloba* (dark blue) indicate the influence of subpolar water on the coring site coinciding with

b) Increasing abundance of *G. scitula* (pink) that indicate a southward movement of the STG.

c) Abundance of *N. pachyderma* (light blue) indicates an increasing contribution of ENAW at the coring site over YD.

d) High abundances of *G. inflata* (orange) indicate the increasing influence of NAC and WBC water at the coring site.

e) The abundance of subtropical species *G. ruber w.* (red) as indicator for the position of the AF.

f) Parallel changes in the fauna distribution and the $\delta^{13}\text{C}$ record of benthic foraminifera *C. wuellerstorfi* from the Azores Coring site (green line 3-point running mean) and Iberian Margin $\delta^{13}\text{C}$ record (MD95-2334) (black line) [Skinner and Shackleton, 2003] indicate a strong coupling between STG position and strength of AMOC.

g) Further comparison with the $^{231}\text{Pa}/^{230}\text{Th}$ record from core OCE326-GGC5 [McManus et al., 2004] indicates a close match of the YD variability within the limitations of the different age models.

Note that the scales for *T. quinqueloba* (a) and *G. scitula* (b) are plotted inverse. Light blue bars indicate last deglacial and early Holocene cold events.

In phase with increasing benthic $\delta^{13}\text{C}$ values (Figure 5.3f), surface and subsurface $\delta^{18}\text{O}$ values (Figure 5.3d) decrease from the end of the H1 event (GS-2a) into the BA (GI-1d) (16 to 14.6 ka BP) by 0.7 and 0.9‰, respectively. Over the BA the surface and subsurface water evolution shows signs of decoupling. The surface $\delta^{18}\text{O}$ signal is steadily decreasing from 1.0‰ at 14.9 ka BP to 0.2‰ at 13.2 ka BP and shows a slight increase over the late Allerød (GI-1a) (Figure 5.3c). The subsurface $\delta^{18}\text{O}$ signal remains stable over the BA (GI-1) (Figure 5.3d). At the onset of the YD (GS-1) (12.6 ka BP), the surface and subsurface $\delta^{18}\text{O}$ record both increase to 1‰ and 2.2‰, respectively. Superimposed upon these generally high $\delta^{18}\text{O}$ values, internal variability over the YD is observed. Between 12.65 and 12.1 ka BP the surface and subsurface $\delta^{18}\text{O}$ values decrease by 0.25‰ and 0.5‰, respectively (Figure 5.3c) and thereby are in phase with low benthic $\delta^{13}\text{C}$ values. Increases in the surface and subsurface $\delta^{18}\text{O}$ records between 12.1 and 11.6 ka BP parallel the increasing benthic $\delta^{13}\text{C}$ values. Relatively stable average $U^{K'}_{37}$ SST (14°C) and subsurface temperatures (13.5-15°C) during YD indicate, that the observed $\delta^{18}\text{O}$ variability is caused by salinity changes.

The surface $\delta^{18}\text{O}_{\text{water-ice}}$ values (Figure 5.3e) indicate a major and progressive freshening of 0.7‰ over the cold H1 event, with the maximum $\delta^{18}\text{O}$ depletion of 1.4‰ reached at the transition between the H1 and the Bølling-Allerød. A freshening of 0.7‰ during the 8.2 ka BP event, though only evidenced by one data point due to the low resolution $U^{K'}_{37}$ SST record, is supported by low surface $\delta^{18}\text{O}$ values prevailing over this interval and parallel changes in foraminifera abundances. Surface water $\delta^{18}\text{O}_w$ reconstructions based upon combined Mg/Ca SST and $U^{K'}_{37}$ SST and *G. bulloides* $\delta^{18}\text{O}$ might indicate additional freshening (0.6‰) over the YD (GS-1), although this feature is less well constrained since the spliced *G. bulloides* record may be subject to a large uncertainty. Generally high surface $\delta^{18}\text{O}_{\text{water-ice}}$ values during the Bølling (GI-1e) and the early Allerød (GI-1c) are similar to the late Holocene values.

The previously suggested salinity overprints on the subsurface $\delta^{18}\text{O}$ record become evident in $\delta^{18}\text{O}_{w\text{-ice}}$ calculations (Figure 5.3e), suggesting decreasing subsurface salinities of 1‰ at the end of the H1 event, of 0.9‰ during the early YD and a freshening of at least 1.2‰ at the onset of the PBO.

The observed changes in stable isotope and temperature data are accompanied by major shifts in foraminiferal abundances (Figure 5.4).

Generally low abundances of *T. quinqueloba* (5%) and *G. scitula* (4%) (Figure 5.4a,b) peak at the end of the H1 event (25%, 12%), the IACP (GI-1b) 13.1 ka BP (35%, 12%), and the 8.2 ka BP event (8%, 7%) and match well with observed freshening events with exception of the IACP event, that is less well constrained in the $\delta^{18}\text{O}_{w\text{-ice}}$ records (Figure 5.3e).

The subtropical species *G. ruber w.* is absent at the coring site during the cold H1 event and the YD. Its abundance increases from 1% to 7% (Figure 5.3c; 5.4e), in phase with the surface and

subsurface $\delta^{18}\text{O}$ decrease at the beginning of the Bølling (GI-1e). Abundances of *G. ruber w.* remain high over the Bølling (GI-1e), and decrease to 4.6% at 13.14 ka BP (GI-1b). The abundance of *G. ruber w.* is greatly reduced (2-4%), during the late Allerød (GI-1a) and nearly diminished (>2%) over YD (GS-1). The abundances increase again over the PBO and the Holocene and stabilize on modern values after 6 ka BP. This evolution is only disrupted by two minima at the 8.4 and 8.2 ka BP. Although the *G. ruber w.* abundance record is in general in phase with the benthic $\delta^{13}\text{C}$ record (Figure 5.3e) and match well with the abrupt late Allerød (GI-1a,b) $\delta^{13}\text{C}$ decrease, major fluctuations in the benthic $\delta^{13}\text{C}$ record over YD (GS-1) are not recorded in the *G. ruber w.* abundance record. In general, *G. ruber w.* abundance record also agrees with the $U^{K'}_{37}$ SST record (Figure 5.3a). However a major difference is observed in the late Allerød when *G. ruber w.* vanished from the coring site during IACP (GI-1b) (13.1 ka BP) and did not return until the end of the YD while $U^{K'}_{37}$ SST remained warm until the onset of the YD (GS-1a).

Between H1 and PBO when *G. ruber w.* abundances are below 10%, high abundances of the transitional species *N. incompta* (Figure 4c). and *G. inflata* (Figure 5.4d) are observed. After 11 ka BP *N. incompta* abundance is reduced to 5 % and *G. scitula* abundances vary between 7 and 15%. (Figure 5.4c,d).

The abundance of the subpolar species *N. incompta* (Figure 5.4c) increases at the onset of the BA to 30% decreases from 30% to 12% until 13.2 ka BP and then slightly increases over the late Allerød (GI-1a) to reach 20% (Figure 5.4c) at the end of BA (GI-1a). At the Mid of the YD (12.2ka BP), a second abundance increase is observed that reach maximum values of 35% at the onset of the PBO and then diminish over the early Holocene to reach less than 5% at 9 ka BP.

The abundance of *G. inflata* (Figure 5.4d) roughly parallels the subsurface $\delta^{18}\text{O}_{\text{water-ice}}$ record, increasing from 5% at the H1 event (GS-2a) to a maximum of 26% between 14 and 13.1 ka BP (GI-1c). This peak is followed by a decrease to 15 % lasting until the onset of the YD (GS-1). Between 12.1 and 12.6 ka BP maximum abundances of *G. inflata* parallel increased surface and subsurface $\delta^{18}\text{O}$ values and low benthic $\delta^{13}\text{C}$ values. The mid- YD change in the surface and subsurface and benthic stable isotope records coincides with a distinct shift in the abundance record of the subsurface dwelling foraminifera. The relative abundance of *G. inflata* (Figure 5.4c) decreases from 30 to 5% whilst the relative abundance of *N. incompta* increases from 10 to 35% (Figure 5.4c).

The changes in the abundance of the subtropical species *G. truncatulinoides* (Figure 5.5f) are below the limit of interpretation between H1 event and the onset of the PBO. Over the PBO and the Holocene the abundance of *G. truncatulinoides* fluctuated by 2% around values of 4%.

5.7 Discussion

5.7.1 Deglacial evolution of AMOC state and its coupling with subtropical gyre position

The benthic $\delta^{13}\text{C}$ record from the Azores is used to reconstruct AMOC strength from the same core as the surface water reconstructions in order to avoid age model related mismatches between the surface and deepwater records. We consider the $\delta^{13}\text{C}$ record to represent the distribution of the deepwater body in the NE Atlantic as it matches well the YD (GS-1) minima and BA (GI-1) maxima recorded in the cores from the Iberian Margin (core MD99-2334K, MD95-2042) [Shackleton *et al.*, 2000; Skinner *et al.*, 2003] (Figure 5.4f), and the $\delta^{13}\text{C}$ fluctuations in the nearby core MD95-2037 [Labeyrie *et al.*, 2005]. Arguably, the origin of the $\delta^{13}\text{C}$ decreases might result from changes in the NA deepwater mass distribution and sources, formation of brine waters within the Nordic seas [e.g. Thornalley *et al.*, 2010a; Waelbroeck *et al.*, 2011], or an overprint by local productivity. The latter, postulated to explain strongly depleted $\delta^{13}\text{C}$ values, can be neglected [Schwab *et al.*, 2012] and has never been observed in other studies within this area [Eberwein and Mackensen, 2006]. The distribution of deepwater formed by brine rejection in the Nordic seas mainly influenced water depths above 2200 m [Waelbroeck *et al.*, 2011]. Thus we assume that the Azores coring site at 3060 m water depth remained below the range of these brines. Atlantic transects including the cores MD95-2037, MD99-2334K, MD95-2042 [Gherardi *et al.*, 2009; Labeyrie *et al.*, 2005; Waelbroeck *et al.*, 2011] reveal that the deglacial $\delta^{13}\text{C}$ variability is related to different AMOC modes. Our record matches the record of cores MD99-2334K. Additionally, our data correlates with the $^{231}\text{Pa}/^{230}\text{Th}$ record of McManus *et al.* [2004], despite a mismatch at the end of the BA (GI-1a) that is within the uncertainties of the age models. Therefore we suggest that low $\delta^{13}\text{C}$ values reconstructed from our cores are related to shallow or weak overturning while increasing $\delta^{13}\text{C}$ values are related to a strengthening and/ or deepening of the NA overturning.

Our abundance record of the subtropical species *G. ruber w.* show agreement with benthic $\delta^{13}\text{C}$ variability (Figure 5.4e,f) with an increase at the beginning of the Bølling (GI-1e), decreases at the H1 event (GS-1) and the Allerød (GI-1d to a), nearly vanishing over the YD (GS-1), and stepwise increase during the early Holocene reaching modern levels subsequent to the 8.2 ka event. The distribution pattern of *G. ruber w.* generally opposes the distribution of the subpolar species *T. quinqueloba* and *N. incompta*, indicating the alternating influence of subtropical and subpolar waters at the coring site (Figure 5.4a,b,e). This is also evident in coccolithophore assemblages [Schwab *et al.*, 2012] and can be related to north-/southward shifts of the frontal system marking the northern STG rim. During weak AMOC phases (H1 (GS-2a), YD (GS-1), 8.2 ka event) the AF was displaced southwards (Figure 6b) whereas the AF shifted northward during times of increasing AMOC strength (Figure 6a). The AF reached its modern position after the 8.2 ka cold event. Peaks in the abundance of *G. scitula* and *T. quinqueloba* (Figure 5.4a,b) at 14.7, 13.1, 11.5, 8.3 and 8.1 ka

BP mark pronounced cold events and indicate the short term presence of transitional ENACW above the coring site that indicate a rapid shifts in the AF that are probably related to expansion and contraction of the STG. The general trends in *N. incompta*, *G. scitula* and *T. quinqueloba* abundance data agrees with abundance records from core SU 90-03 [Chapman *et al.*, 2000] (Figure 5.4) situated at 40°N, 32°W. Differences between the records might be related to age model differences and the different resolution of the records.

The shifts in the STG position generally agree with the findings of Schiebel *et al.* [2002b] who postulates variable a southward and northward displacement of the northern STG rim during glacial to interglacial transitions. Conflicting results from the Gulf of Cadiz [Rogerson *et al.*, 2004], showing no glacial interglacial variations of the AC position, may be a result from local hydrographic conditions. While the Azores open ocean site is governed by the changing position and strength of the westerlies [e.g. Volkov and Fu, 2010], the site within the Gulf of Cadiz is mainly influenced by the northern branch of the AC. Under modern conditions this inflow also persistent during winter times, when the AF in the central NA basin is supposed to be shifted southward [Peliz *et al.*, 2005]. Additional evidence for the prevailing transport of warm water within the AC system into the Gulf of Cadiz despite the southward shift of the AF is given by warm water coccolithophore species that are observed during the YD in core M39029-7 [Colmenero-Hidalgo *et al.*, 2004].

5.7.2 The influence of subpolar meltwater on the Azores coring site

It is postulated that several meltwater pulses of different origin caused widespread salinity anomalies in the subpolar NA and along the western boundary system and thus induced the deglacial AMOC disturbances [Benway *et al.*, 2010; Condrón and Winsor, 2011; Obbink *et al.*, 2010; Thornalley *et al.* 2010b]. At the Azores coring site the two most prominent freshening events of (0.5-0.8‰ SMOW) at the end of the H1 (GS-2a) and at the 8.2 ka event are evidenced in the surface $\delta^{18}\text{O}_{\text{w-ice}}$ record. Although the 8.2 ka freshening is only evident in one data point (Figure 3d), it is supported by prominent short term changes in the foraminifera abundance data (Figure 5.4b,d,e). Within the limits of accuracy, the reconstructed amplitudes match the records from the NA, where salinity anomalies of -0.8 to -1.4‰ SMOW at the end of H1 (GS-2a) [Benway *et al.*, 2010; Obbink *et al.*, 2010; Thornalley *et al.*, 2010b] and during the 8.2 ka event are observed. These are associated with well known slow downs of AMOC [Gherardi *et al.*, 2009]. Increased abundances of the subpolar species *T. quinqueloba* (Figure 4a) during the H1 and the 8.2 ka events and are also evident during H events in core MD99-2339 in the Gulf of Cadiz [Voelker *et al.*, 2009] and mark the Arctic front under modern conditions [Johannessen *et al.*, 2004]. Thus the high abundances of *T. quinqueloba* are either indicating a subpolar meltwater origin or are related to changes in the AF frontal system that is comparable with the modern Arctic front during the H1,

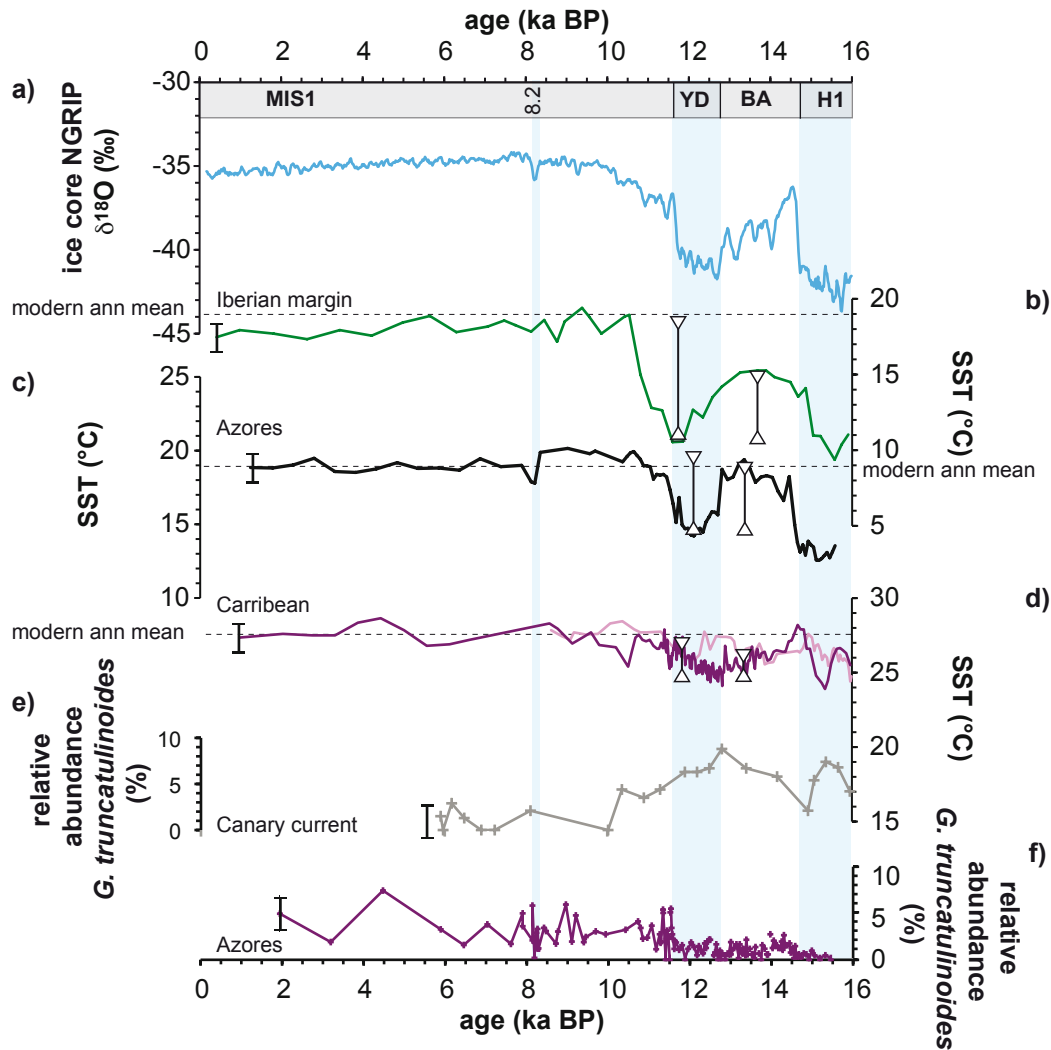


Figure 5.5 Comparison of SST records from the NA region

a) Greenland ice core $\delta^{18}\text{O}$ record NGRIP [Andersen *et al.*, 2006]

b) Core SU81-18 $\text{U}^{\text{K}37}$ SST data from the Iberian margin [Bard *et al.*, 2000] indicated by the dark green line.

c) Azores coring site $\text{U}^{\text{K}37}$ SST indicated by the black line [Schwab *et al.*, 2012]

d) Caribbean cores KNR166-6-26C Mg/Ca SST [Schmidt and Lynch-Stieglitz, 2011], 3-point running mean indicated by the dark violet line, EN32-PC6 Mg/Ca SST [Flower *et al.*, 2004] indicated by the pink line.

e) Abundance data of *G. truncatulioides* d. as indicator for AC strength from core GIK 15637-7 [Kiefer *et al.*, 1998] situated in the CC (27.01°N;18.99°W)

f) Abundance data of *G. truncatulioides* as an indicator for AC strength show no clear correlation between AC strength and SST changes for the deglacial and early Holocene.

Dashed lines indicate annual mean temperatures, black bars with triangles indicate maximum SST amplitudes between warm and cold periods, light blue bars indicate the major deglacial and early Holocene cold events. Error bars are given to the left of the records.

IACP and 8.2 event. The restricted extension of this frontal system or the difference in resolution might explain the lack of a clear peak in *T. quinqueloba* abundance in the nearby core SU90-03 [Chapman *et al.*, 2000].

The strong freshening signals at the northern STG boundary data show that the main deglacial freshwater pulses from the Laurentian ice sheet that caused the well known AMOC reductions, reached further south into the central NA than suggested by Shakun and Carlson, [2010]. Therefore

the expansion of a freshened (by -0.8 to -1.4‰ SMOW) and cool (18/14°C) water mass appears to have driven the STG displacement as postulated by Schwab et al. [2012].

During shallow/weak AMOC phases, the $U^{K'}_{37}$ SST data reveal magnitudes of cooling at the Azores coring site that reached 6°C during the H1, 4.5°C during the YD (GS-1), and 2.5°C at the 8.2 ka event (Figure 5.5c), which matches well with known 4°C amplitudes from the transitional NA (Figure 5.5b) [e.g. Bard et al., 2000] and the FA 20 SST reconstructions from core SU 90-03 [Chapman et al., 2000] situated at 40°N, 32°W. The observed cooling signal contradicts the $U^{K'}_{37}$ results from core U1313 at 41°N, 32.5°W [Naafs et al., 2013], which indicate a warming of the transitional NA during H events. Naafs et al., [2013] associate this warming to a northward shift in the AF. Such a shift in the AF position would be related to an increase of the abundance of *G. ruber w.* that is not observed in the abundance data from the Azores coring site (Figure 5.4). In core SU90-03 [Chapman et al., 2000] (Figure 5.4) the *G. ruber w.* abundances decreases during the YD and the H1 event. However the abundances are slightly higher than at the Azores coring site. Although we cannot fully explain this difference, we suggest that the YD cooling indicated in our *G. bulloides* Mg/Ca SST record, the foraminiferal and coccolithophore abundance records and the $U^{K'}_{37}$ record [Schwab et al., 2012] is robust and related to a southward movement of the AF.

This observed SST signal indicates that a postulated retention of warm waters in the subtropical NA during pronounced meltwater driven AMOC weakening was limited to the western subtropical and tropical Atlantic as observed in the Caribbean Sea and the eastern equatorial Atlantic [Carlson, 2008; Rühlemann et al., 2004; Schmidt et al., 2006; Weldeab et al., 2006]. Our site in the middle of the NA was instead strongly affected by freshening and cooling, suggesting a stronger impact of freshwater disturbances on the subtropical recirculation than proposed by Shakun and Carlson [2010].

5.7.3 Bølling/Allerød heat storage

An unexpected, pronounced warming of the Azores region is observed during the Bølling-Allerød (GI-1) warm period, with temperatures of 18-19°C resembling late Holocene values (19°C). Thereby the BA (GI-1) therefore exceeds the warming that is indicated in marine cores from the Caribbean source region [Flower, 2004; Schmidt and Lynch Stieglitz, 2011] and the transitional NA [Bard et al., 2000], which remained 2°C colder during the BA (GI-1) compared to the Holocene in both Mg/Ca and $U^{K'}_{37}$ SST records (Figure 5.5). This strong warming in the $U^{K'}_{37}$ record might be caused by a seasonal shift in the coccolithophore bloom from spring time as observed under modern conditions at the coring site, to summer time, as observed within the nutrient rich subpolar and transitional NA water masses [Longhurst, 2007]. Such a water mass influence of ENACW is evidenced by the increased abundance of *N. incompta* during the BA (GI-1) (10-33%) compared to the Holocene (2-15%) (Figure 5.4c).

Over the BA (GI-1) two distinct phases are observed within the benthic $\delta^{13}\text{C}$ records from the Azores coring site, the Iberian Margin and the subpolar NA, that are also evident in the mixed layer of the AC (Figure 3). Phase 1 (14.6-13.25 ka BP) (GI-1a to 1c) comprises the initial BA AMOC increase and a subsurface water warming. This increase was followed by a subsequent weakening of AMOC that was accompanied by a cooling of the subsurface water and heat storage within the STG surface water (Figure 6c). The initial BA (GI-1e) AMOC increase is indicated in abruptly rising benthic $\delta^{13}\text{C}$ values to 0.5‰ in paralleled with a SST warming of 5°C and a subsurface warming of 3°C (Figure 5.3a,e). The abrupt warming is accompanied by a distinct faunal shift, and salinity increase that suggests a rapid northward displacement of the STG. Subsequently, subsurface temperatures, subsurface salinities and the abundance of *G. ruber w.* decreased under a progressively weakening AMOC regime (Figure 5.3a,b,e). The AC strength, however seems to play a minor role in this warming as is indicated by the stable low (0-2%) abundances of *G. truncatulinoides* (Figure 5.5). On the contrary, high *G. truncatulinoides d.* abundances between 16 and 10 ka BP were observed in the CC coring site GIK15637 of Kiefer *et al.* [1998] (Figure 5e,f). This could be related to the increased eastward transport of warm waters within the AC on a more southern pathway.

The overall warm BA (GI-1) indicates a surface water warming that is also evident in the $\delta^{18}\text{O}$ record. The stepwise BA cooling in the NA under a gradually weakening AMOC regime has been explained by a return to the cold background circulation state after a brief BA (GI-1e) AMOC overshoot [Knorr and Lohmann, 2007; Liu *et al.*, 2009] or by enhanced freshwater inflow from the Laurentian Ice sheet (LIS) [Clark *et al.*, 2001; Obbink *et al.*, 2010; Thornalley *et al.*, 2010a,b; Thornalley *et al.* 2011]. Both mechanisms would result in a stepwise weakening of AMOC and lead to the subsequent cooling of the thermocline (Figure 5.6c). The STG generally remained at its interglacial position, though it was disrupted by a sequence of brief displacements which are evident in brief decreases in the *G. ruber w.* abundance record. These disruptions may also cause the noisy low resolution Mg/Ca SST record obtained from *G. bulloides* and might be related to several freshwater events observed in the subpolar NA [Thornalley *et al.*; 2010b]

Phase 2 (13.25 and 12.85 ka BP) (GI-1b and 1a) can be regarded as a transitional phase of heat storage between the warm BA (GI-1) and the cold YD (GS-1). Although the AMOC was already deceased and the subsurface water already cooled, the NAC still transported heat into the eastern NA basin (Figure 6d). This phase started during the IACP with peaks of the subpolar species *T. quinqueloba* and the transitional *G. scitula* indicating a short-term influence of subpolar and transitional waters at the coring site. During this disruption *G. ruber w.* vanished from the coring site for the next 1000 years, indicating a southward displacement of the STG that is accompanied by a weakened AMOC status as indicated by intermediate benthic $\delta^{13}\text{C}$ values (0.5‰). Nevertheless, for the remainder of the Allerød (GI-1a), the U^{K}_{37} record indicates warm SST, whilst

G. bulloides Mg/Ca SST are also well above the YD (GS-1) levels (Figure 5.3a). Given the southward retraction of the STG, the warm SST must be related to a warming of the surface transitional ENACW_T and/or by an increased inflow of NAC water that replaced the 18 degree mode water at the coring site. A decreasing abundance of the transitional species *N. incompta* over the BA (30 % to 15%) argues against an increasing contribution of ENACW_T (Figure 5.4c). The increasing abundance of *G. inflata* over the Bølling and early Allerød (GI-1c-e) and after 13.1 ka BP (GI-1b) instead indicates an increasing influence of NAC waters at the coring site (Figure 4d). Stable *G. inflata* abundances over the deglacial and Holocene in core SU90-03 [Chapman *et al.*, 2000] indicate a stable NAC transport and do not seem to be overprinted by short term changes in the AF system. An increasing NAC flow into the eastern NA basin during the late BA is further supported by the reconstruction of warm SST at core SU90-03 north of the Azores Island [Chapman *et al.*, 2000] and the BA (GI-1) evolution of $\delta^{18}\text{O}$ and U^{K}_{37} SST records from the transitional NA [e.g. Bard *et al.*, 2000] and several cores from the Iberian Margin [Voelker *et al.*, 2011]. Those SST reconstructions show a similar SST evolution, though with a differing amplitude to the records at the Azores coring site. These SST patterns could be explained by a hypothesis of Chapman and Maslin [1999], who suggested that warm NAC was deflected south of Iceland and flowed into the eastern NA basin during the LGM (Figure 5.6d).

The large deglacial temperature changes in the subtropical eastern NA must have had implications on regional climates. The AC surface $\delta^{18}\text{O}$ record closely matches the speleothem record from Pindal Cave (43.3833 °N, 4.54 °W) situated at the northern Iberian Peninsula [Moreno *et al.*, 2010]. A similar pattern as in the Azores U^{K}_{37} SST is observed in some more remote lake temperature records in Central Europe (e.g. Ammersee and Lake Lucern [Blaga *et al.*, 2013]). Those similarities indicate that long-term changes in the surface water temperatures at the Azores were connected with European climate. Assuming that the air temperature over Europe is driven by heat transport by the westerlies, changes within the westerlies wind belt can explain the close match between these signals. The southward STG displacement at the end of the Allerød is most probably associated with increasing westerly wind strength on a more southern path that was caused by the increasing temperature difference between polar regions and the subtropics.

5.7.4 Subtropical subsurface heat storage and AMOC resumption during YD

Our data show that the retention of warm subtropical water in the sub-/tropical Atlantic during weak AMOC phases as postulated by observations and model simulations for the H1 (GS-2a) and the YD (GS-1) [Carlson, 2008; Rühlemann *et al.*, 2004; Schmidt *et al.*, 2006; Weldeab *et al.*, 2006] did not immediately extend to the Azores. It may however have influenced the subsurface hydrography, as a subsurface heat reservoir has been postulated to have preconditioned the onset of

AMOC [Carlson, 2008; Krebs and Timmermann, 2007; Otto-Bliesner and Brady, 2010; Rühlemann et al., 2004; Schmidt et al., 2006; Weldeab et al., 2006].

The average subsurface temperature data show only a slight cooling (0.8°C) between the BA and the YD (GS-1) (Figure 5.3a). Compared to the strong cooling of the SST (4°C), this relatively small temperatures change indicates, that a subsurface warm water transport towards the north might still have been active during the YD (GS-1) (Figure 5.6e). Peck et al. [2008] and Benway et al. [2010] observe warm subsurface water temperatures in Mg/Ca temperature reconstructions from the subsurface dwelling species *N. pachyderma s.* during the early YD (GS-1) within cores MD01-2461 from the Porcupine Seabight and site ODP 980 from the Rockall Plateau. These warm temperatures might indicate that the relatively warm water continued on a northward path during an early YD (GS-1) (12.5 to 12.2 ka BP) weak AMOC phase as illustrated in Figure 6d. Within this scenario, stratification remained stable due to the prevailing temperature (1°C) and salinity gradient (at least 0.5‰) between surface and subsurface waters that is indicated in our data.

According to climate models [Bakke et al., 2009; Krebs and Timmermann, 2007; Otto-Bliesner and Brady, 2010; Rühlemann et al., 2004], the warm subtropical subsurface waters propagated into the subpolar NA and reached as far north as 62°N during the cold H1 (GS-2a) and YD (GS-1) event. There, a sea ice covered with a fresh water lens capped the deepwater convection areas and prevented the formation of deepwater. The warm subtropical sourced subsurface waters induced melting of the sea ice from underneath. Subsequently, shallow convection lead to the erosion of freshwater lenses and thus preconditioned the onset of AMOC that was amplified by the advection of saline subtropical waters. The dataset of Rashid et al. [2007] leads to the suggestion, that the surface water stratification already became unstable in the transitional NA. This mixed layer deepening might be associated with changes of the position of the subpolar front, which remains uncertain for the BA.

Despite the general YD trend, internal variability is observed. The Azores subsurface $\delta^{18}\text{O}$ record shows a strong $\delta^{18}\text{O}$ decrease (0.5‰) in the early YD (GS-1) lasting from 12.7 to 12.2 ka BP. Additional Mg/Ca measurements indicate a 2°C warming after an initial short term cooling of 2°C at the onset of the YD. This warming is not strong enough to explain the subsurface $\delta^{18}\text{O}$ decrease of 0.5‰ thus the decrease must be caused by a strong freshening of the subsurface waters that is also evident in the $\delta^{18}\text{O}_{\text{w-ice}}$ record, which freshens by about 0.5‰ (Figure 5.3a,c,d). The cause for such a freshening might either be a deepening of the mixed layer that leads to a homogenization of the surface and subsurface water of the AF as proposed by Rashid et al. [2007] for the subpolar NA, or the subsurface freshening signal may have occurred further upstream through the entrainment of freshwater into the subsurface waters, and was subsequently transported towards the Azores coring site.

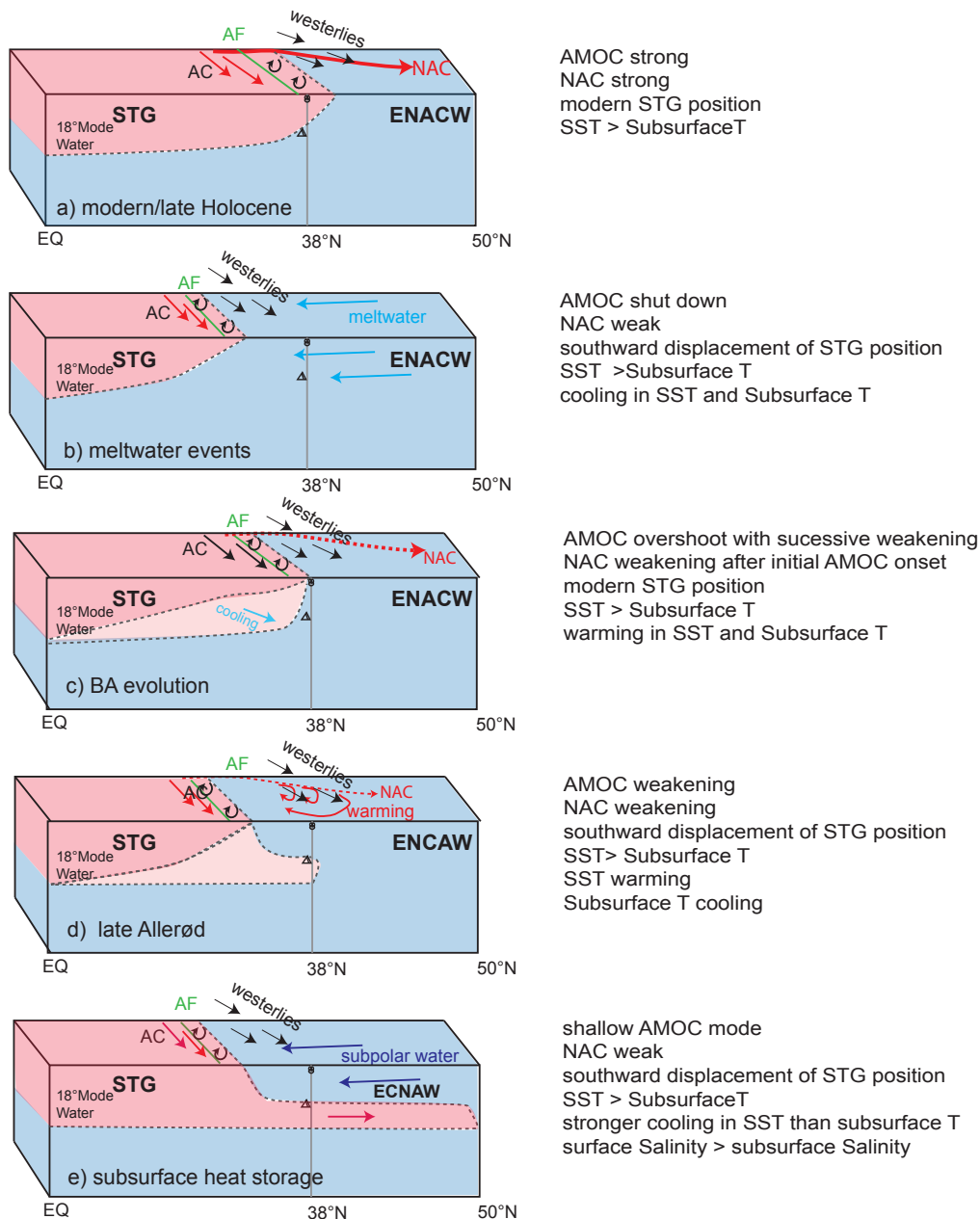


Figure 5.6 Conceptual model for the deglacial changes (from bottom to top) of the subtropical gyre position and heat storage patterns

Red colors indicate warm subtropical waters whereas blue colors indicate transitional water masses

a) Modern strong AMOC situation with modern position of the AF. The coring site is situated underneath the warm transition zone N of the AF where eddies lead to strong contribution of warm STG waters.

b) Meltwater events: during meltwater events (H1) the STG was completely displaced southward and the coring site was influenced by cold meltwater.

c) AMOC overshoot and subsequent shoaling/cooling of the thermocline: During the Bølling and early Allerød, stepwise AMOC reductions were accompanied by a the shoaling of the thermocline, as indicated by a cooling signal in the subsurface while surface waters remained warm.

d) Transitional state: the last 300 years of the Allerød were characterized by a southward displacement of the STG. Nevertheless SST still remained warm, most probably due to a warming of the ENAW caused by increasing entrainment of NDW into the southern part of the subpolar east Atlantic basin.

e) Subsurface warm water transport: during the YD weak AMOC phase, the STG was displaced southward. Nevertheless relatively warm subtropical waters were transported northward, while the surface was influenced by cold subpolar water.

Extensive mixing of the upper water mass would result in converging and/or similar $\delta^{18}\text{O}$ values of surface and subsurface waters as shown by *Rashid et al.* [2007]. However, the $\delta^{18}\text{O}$ values of *G. bulloides* and *G. truncatulinoides* differ by more than 1‰ over the early YD and both show a decreasing trend (Figure 5.3c,d). Thus it seems to be unlikely that a mixed layer deepening caused the subsurface water freshening at the Azores coring site and a different freshwater source must be found.

The subsurface water freshening at our coring site roughly corresponds in timing and duration with a freshening of the mixed layer at the outlet of the St. Lawrence River, that occurred between 13 and 12.1 ka BP [*Carlson et al.*, 2008], though this meltwater did not necessarily caused the YD (GS-1) AMOC weakening [*Condrón and Windsor*, 2011; *Murton et al.*, 2010; *Tarasov and Peltier* 2005, 2006]. *Condrón and Windsor* [2011] postulated from a high-resolution modeling study that meltwater from the St. Lawrence River is entrained into the American Slope waters and the STG. Such an entrainment of Slope waters into the STG could explain the freshening of the subsurface waters at the Azores coring site. Furthermore is an increased contribution of NAC water is indicated by high abundances of *G. inflata* (30%) (Figure 5.4d), which show maximum abundances in the modern ocean between 50 and 70 °W and 35-40°N within the NAC and slope current waters. At 12.2 ka BP the ~200 years long phase of subsurface freshening ended with an abrupt increase in salinities by ~ 1.4 PSU paralleling a cooling of the subsurface waters by ~2°C, as deduced from Mg/Ca subsurface temperature reconstructions. The temperature change and increase in subsurface $\delta^{18}\text{O}$ precisely coincides with the onset of a 500 years long mid YD (Figure 3f) AMOC resumption, which is also evident in the $^{231}\text{Pa}/^{230}\text{Th}$ record of *McManus et al.* [2004]. The observed sequence of AMOC shut down, subtropical subsurface heat storage, heat release and subsequent AMOC resumption support a mechanism for AMOC resumption proposed for the end of Heinrich events and the YD (GS-1)

[*Bakke et al.*, 2009; *Krebs and Timmermann*, 2007; *Otto-Bliesner and Brady*, 2010; *Rühlemann et al.*, 2004]. However the Mid YD (GS-1) AMOC onset was not related to any surface warming within the subtropical NA. The conceptual model of several authors [*Krebs and Timmermann*, 2007; *Otto-Bliesner and Brady*, 2010; *Rühlemann et al.*, 2004] included the export of subtropical warm saline waters, which induced the final onset of AMOC and led to a northward displacement of the ITCZ that was accompanied by a decrease in the salinity within the Caribbean region [*Schmidt and Lynch-Stieglitz*, 2011; *Schmidt et al.*, 2004]. Such a northward displacement of the ITCZ would push the track of the westerlies northward and thereby induce a northward displacement of the AC. Low abundances of *G. ruber w.* at the Azores coring site over the entire YD indicate no northward movement of the STG (Figure 5.4e). Therefore we assume that the brief YD AMOC onset was not related to a northward displacement of the westerly wind belt. This lack

of changes in atmospheric circulation might explain the short duration of the mid YD AMOC onset.

Nevertheless a replacement of the subtropical to transitional species *G. inflata* by the temperate *N.pachyderma d.* which is associated with ENACW_p waters occurred at 12.2 ka BP. This shift in the fauna abundance seems to be related to the end of the freshwater input from the St. Lawrence river system and an increasing contribution of ENACW_p water on the coring site. These changes in the surface water hydrography of the STG in the late YD might have preconditioned the final Holocene AMOC strengthening.

5.8 Summary and conclusion

High resolution records of mixed layer and deepwater changes at the Azores coring site indicate that the position of the STG was coupled with AMOC strength over the last deglaciation and the early to mid Holocene (16 -7 ka BP). Four different responses of the Azores mixed layer hydrology on AMOC weakening/strengthening phases are observed over the deglacial. Meltwater pulses that caused the AMOC weakening during the H1 event reached southward to the coring site and led to the short-term southward displacement of the STG (Figure 5.6b), thereby inducing temperature changes of 4-6°C that match the subpolar NA records.

The Bølling (GS-1e) AMOC onset (14.6-13.25 ka BP) and its subsequent weakening was accompanied by an initial surface water warming and a subsequent cooling of the thermocline. In parallel heat was stored within the STG surface water (Figure 5.6c).

During the late Allerød transitional period (GS-1b to 1a) (13.2-12.9 ka BP), an already weak AMOC state was accompanied by a southward displacement of the STG. Nevertheless a warm surface water mass is observed at the coring site that might be linked to the recirculation of warm NAC waters within the eastern NA basin (Figure 5.6d).

The AMOC shut down during the cold YD (GS-1) was accompanied by ongoing northward transport of warm subsurface water. Its release to the subpolar NA seems to have induced a mid-YD (GS-1) AMOC resumption and might have preconditioned the final onset of AMOC at the end of the YD (GS-1) (Figure 5.6e).

With this study we have shown that the subtropical NA hydrography is very sensitive to deglacial changes and influenced by both meltwater pulses from the NA as well as the retention of warm subtropical water.

5.9 Acknowledgements

We thank A. Voelker and the associated editor and two anonymous reviewers for their comments and suggestion that helped to improve this article for publishing in *Paleoceanography*. We thank M. Regenberg and K. Bremer for laboratory assistance and R. Schneider for final proof reading and financial support. The results represented here are obtained from cores taken on board the R.V.

Marion Dufresne (French Polar Institute, IPEV) during the IMAGES-AMOCINT MD168-cruise in the framework of the 06-EuroMARC-FP-006 Project. We thank the captain and the crew, as well as our colleagues onboard for their help. This manuscript has been made possible thanks to the support from the European Science Foundation (ESF) under the EUROCORES Program EuroMARC through contract No. ERAS-CT-2003-980409 of the European Commission, DG Research, FPG. Financial support is given by the German Science Foundation (DFG). Furthermore we would like to thank Mr. Bernard Dennielou and Ifremer for providing us with material from core GEOFAR KF16. All data are available within the database Pangaea (www.pangea.de).

5.10 References

- Alves, M., F. Gaillard, M. Sparrow, M. Knoll, and S. Giraud (2002), Circulation patterns and transport of the Azores Front-Current system, *Deep Sea Research Part II: Topical Studies in Oceanography*, 49(19), 3983-4002.
- Andersen, K. K., et al. (2006), The Greenland Ice Core Chronology 2005, 150 ka. Part 1: constructing the time scale, *Quaternary Science Reviews*, 25(23,24), 3246-3257.
- Austin, W. E. N., and D. Kroon (2001), Deep sea ventilation of the northeastern Atlantic during the last 15,000 years, *Global and Planetary Change*, 30(1,2), 13-31.
- Bakke, J., O. Lie, E. Heegaard, T. Dokken, G. H. Haug, H. H. Birks, P. Dulski, and T. Nilsen (2009), Rapid oceanic and atmospheric changes during the Younger Dryas cold period, *Nature Geosci*, 2(3), 202-205.
- Barbosa Aguiar, A. C., A. J. Peliz, A. Cordeiro Pires, and B. Le Cann (2011), Zonal structure of the mean flow and eddies in the Azores Current system, *J. Geophys. Res.*, 116(C2), C02012.
- Bard, E., F. Rostek, J.-L. Turon, and S. Gendreau (2000), Hydrological Impact of Heinrich Events in the Subtropical Northeast Atlantic, *Science*, 289(5483), 1321-1324.
- Barker, S., P. Diz, M. J. Vautravers, J. Pike, G. Knorr, I. R. Hall, and W. S. Broecker (2009), Interhemispheric Atlantic seesaw response during the last deglaciation, *Nature*, 457(7233), 1097-1102.
- Bemis, B. E., H. J. Spero, J. Bijma, and D. W. Lea (1998), Reevaluation of the Oxygen Isotopic Composition of Planktonic Foraminifera: Experimental Results and Revised Paleotemperature Equations, *Paleoceanography*, 13(2), 150-160.
- Benway, H. M., J. F. McManus, D. W. Oppo, and J. L. Cullen (2010), Hydrographic changes in the eastern subpolar North Atlantic during the last deglaciation, *Quaternary Science Reviews*, 29(23-24), 3336-3345.
- Blaga, C. I., G.-J. Reichert, A. F. Lotter, F. S. Anselmetti, and J. S. Sinninghe Damsté (2013), A TEX86 lake record suggests simultaneous shifts in temperature in Central Europe and Greenland during the last deglaciation, *Geophysical Research Letters*, 1-6.
- Bond, G., B. Kromer, J. Beer, R. Muscheler, M. N. Evans, W. Showers, S. Hoffmann, R. Lotti-Bond, I. Hajdas, and G. Bonani (2001), Persistent Solar Influence on North Atlantic Climate During the Holocene, *Science*, 294, 2130.
- Born, A., and A. Levermann (2010), The 8.2 ka event: Abrupt transition of the subpolar gyre toward a modern North Atlantic circulation, *Geochem. Geophys. Geosyst.*, 11(6), Q06011.
- Brambilla, E., and L. D. Talley (2008a), Subpolar Mode Water in the northeastern Atlantic: 1. Averaged properties and mean circulation, *Journal of Geophysical Research: Oceans*, 113(C4), C04025.
- Brambilla, E., L. D. Talley, and P. E. Robbins (2008b), Subpolar Mode Water in the northeastern Atlantic: 2. Origin and transformation, *Journal of Geophysical Research: Oceans*, 113(C4), C04026.
- Calvo, E., J. Villanueva, J. O. Grimalt, A. Boelaert, and L. Labeyrie (2001), New insights into the glacial latitudinal temperature gradients in the North Atlantic. Results from UK'37 sea surface temperatures and terrigenous inputs, *Earth and Planetary Science Letters*, 188(3-4), 509-519.
- Carlson, A. E. (2008), Why there was not a Younger Dryas-like event during the Penultimate Deglaciation, *Quaternary Science Reviews*, 27(9-10), 882-887.
- Chapman, M., N. J. Shackleton, and J.-C. Duplessy (2000), Sea surface temperature variability during the last glacial-interglacial cycle: assessing the magnitude and pattern of climatic change in the North Atlantic, *Paleoclimatology, Paleoecology*, 157, 1-25.
- Chapman, M. R., and M. A. Maslin (1999), Low-latitude forcing of meridional temperature and salinity gradients in the subpolar North Atlantic and the growth of glacial ice sheets, *Geology*, 27(10), 875-878.
- Clark, P. U., S. J. Marshall, G. K. C. Clarke, S. W. Hostetler, J. M. Licciardi, and J. T. Teller (2001), Freshwater Forcing of Abrupt Climate Change During the Last Glaciation, *Science*, 293, 283-287.
- Cléroux, C., E. Cortijo, P. Anand, L. Labeyrie, F. Bassinot, N. Caillon, and J.-C. Duplessy (2008), Mg/Ca and Sr/Ca ratios in planktonic foraminifera: Proxies for upper water column temperature reconstruction, *Paleoceanography*, 23(3), PA3214.
- Cléroux, C., P. deMenocal, J. Arbuszewski, and B. Linsley (2013), Reconstructing the upper water column thermal structure in the Atlantic Ocean, *Paleoceanography*, 28(3), 503-516.

- Colin, C., N. Frank, K. Copard, and E. Douville (2010), Neodymium isotopic composition of deep-sea corals from the NE Atlantic: implications for past hydrological changes during the Holocene, *Quaternary Science Reviews*, 29(19-20), 2509-2517.
- Comas-Rodríguez, I., A. Hernández-Guerra, E. Fraile-Nuez, A. Martínez-Marrero, V. M. Benítez-Barrios, M. D. Pérez-Hernández, and P. Vélez-Belchí (2011), The Azores Current System from a meridional section at 24.5°W, *J. Geophys. Res.*, 116(C9), C09021.
- Condron, A., and P. Winsor (2011), A subtropical fate awaited freshwater discharged from glacial Lake Agassiz, *Geophys. Res. Lett.*, 38(3), L03705.
- Dengg, J., A. Beckmann, and R. Gerdes, The Gulf Stream separation problem, in *The Warmwatersphere of the North Atlantic Ocean*, edited by W. Krauss, pp. 253–290, Gebrüder Borntraeger, Berlin, 1996
- Dickson, R. R., W. J. Gould, T. J. Müller, and C. Maillard (1985), Estimates of the mean circulation in the deep (>2,000m) layer of the Eastern North Atlantic, *Progress in Oceanography*, 14, 103-127.
- Duplessy, J.-C., N. J. Shackleton, R. K. Matthews, W. Prell, W. F. Ruddiman, M. I. Caralp, and C. H. Hendy (1984), 13C Record of benthic foraminifera in the last interglacial ocean: Implications for the carbon cycle and the global deep water circulation, *Quaternary Research*, 21(2), 225-243.
- Eberwein, A., and A. Mackensen (2006), Regional primary productivity differences off Morocco (NW-Africa) recorded by modern benthic foraminifera and their stable carbon isotopic composition, *Deep Sea Research Part I: Oceanographic Research Papers*, 53(8), 1379-1405.
- Eynaud, F., et al. (2009), Position of the Polar Front along the western Iberian margin during key cold episodes of the last 45 ka, *Geochim. Geophys. Geosyst.*, 10(7), Q07U05.
- Flower, B. P., D. W. Hastings, H. W. Hill, and T. M. Quinn (2004), Phasing of deglacial warming and Laurentide Ice Sheet meltwater in the Gulf of Mexico, *Geology*, 32(7), 597-600.
- Ganssen, G. M., and D. Kroon (2000), The isotopic signature of planktonic foraminifera from NE Atlantic surface sediments: implications for the reconstruction of past oceanic conditions, *Journal of The Geological Society*, 157(3), 693-699.
- Gherardi, J. M., L. Labeyrie, S. Nave, R. Francois, J. F. McManus, and E. Cortijo (2009), Glacial-interglacial circulation changes inferred from 231Pa/230Th sedimentary record in the North Atlantic region, *Paleoceanography*, 24(2), PA2204.
- Gould, W. J. (1985), Physical oceanography of the Azores front, *Progress in Oceanography*, 14, 167-190.
- Häkkinen, S., P. B. Rhines, and D. L. Worthen (2011), Warm and saline events embedded in the meridional circulation of the northern North Atlantic, *J. Geophys. Res.*, 116(C3), C03006.
- Hátún, H., A. B. Sandö, H. Drange, B. Hansen, and H. i. Valdimarsson (2005), Influence of the Atlantic Subpolar Gyre on the Thermohaline Circulation, *Science*, 309(5742), 1841-1844.
- Hillaire-Marcel, C., A. de Vernal, G. Bilodeau, and A. J. Weaver (2001), Absence of deep-water formation in the Labrador Sea during the last interglacial period, *Nature*, 410(6832), 1073-1077.
- Hoogakker, B. A. A., M. R. Chapman, I. N. McCave, C. Hillaire-Marcel, C. R. W. Ellison, I. R. Hall, and R. J. Telford (2011), Dynamics of North Atlantic Deep Water masses during the Holocene, *Paleoceanography*, 26(4), PA4214.
- Johannessen, T., E. Jansen, A. Flatøy, and A. C. Ravelo (1994), The relationship between surface water masses, oceanographic fronts and paleoclimatic proxies in surface sediments of the Greenland, Iceland, Norwegian seas, in *Carbon Cycling in the Glacial Ocean: Constraints on the Ocean's Role in Global Change*, edited by R. Zahn et al., pp. 61–85, Springer, Berlin.
- Kaiho, K. (1994), Benthic foraminiferal dissolved-oxygen index and dissolved-oxygen levels in the modern ocean, *Geology*, 22(8), 719-722.
- Kanzow, T., et al. (2010), Seasonal Variability of the Atlantic Meridional Overturning Circulation at 26.5°N, *Journal of Climate*, 23(21), 5678-5698.
- Käse, R. H., and G. Siedler (1982), Meandering of the subtropical front south-east of the Azores, *Nature*, 300(5889), 245-246.
- Kida, S., J. F. Price, and J. Yang (2008), The Upper-Oceanic Response to Overflows: A Mechanism for the Azores Current, *Journal of Physical Oceanography*, 38(4), 880-895.
- Kiefer, T. (1998), Produktivität und Temperaturen im subtropischen Nordatlantik: zyklische und abrupte Veränderungen im späten Quartär., *Berichte-Reports, Geol.-Paläontol. Inst. Univ. Kiel*, 90, 1-127.
- Kissel, C., H. Kleiven, X. Morin, and t. S. S. Party (2008), MD168-AMOCINT/1079 XVII IMAGES cruise report, *Les rapports de campagne à la mer, IPEV, 1080 OCE/2008/02*.
- Kleiven, H. K. F., C. Kissel, C. Laj, U. Ninnemann, T. O. Richter, and E. Cortijo (2008), Reduced North Atlantic deep water coeval with the glacial Lake Agassiz freshwater outburst, *Science*, 319, 60- 64.
- Knorr, G., and G. Lohmann (2007), Rapid transitions in the Atlantic thermohaline circulation triggered by global warming and meltwater during the last deglaciation, *Geochemistry, Geophysics, Geosystems (G3)*, 8, Q12006.
- Krebs, U., and A. Timmermann (2007), Fast advective recovery of the Atlantic meridional overturning circulation after a Heinrich event, *Paleoceanography*, 22, PA1220.
- Labeyrie, L., C. Waelbroeck, E. Cortijo, E. Michel, and J.-C. Duplessy (2005), Changes in deep water hydrology during the Last Deglaciation, *C. R. Geoscience*, 337, 919-927.
- Lamas, L., Á. Peliz, I. Ambar, A. Barbosa Aguiar, N. Maximenko, and A. Teles-Machado (2010), Evidence of time-mean cyclonic cell southwest of Iberian Peninsula: The Mediterranean Outflow-driven β -plume?, *Geophys. Res. Lett.*, 37(12), L12606.

- Lherminier, P., H. Mercier, T. Huck, C. Gourcuff, F. F. Perez, P. Morin, A. Sarafanov, and A. Falina (2010), The Atlantic Meridional Overturning Circulation and the subpolar gyre observed at the A25-OVIDE section in June 2002 and 2004, *Deep Sea Research Part I: Oceanographic Research Papers*, 57(11), 1374-1391.
- Lippold, J., Y. Luo, R. Francois, S. E. Allen, J. Gherardi, S. Pichat, B. Hickey, and H. Schulz (2012), Strength and geometry of the glacial Atlantic Meridional Overturning Circulation, *Nature Geosci, advance online publication*.
- Liu, Z., et al. (2009), Transient Simulation of Last Deglaciation with a New Mechanism for Bolling-Allerod Warming, *Science*, 325(5938), 310-314.
- Locarnini, R. A., A. V. Mishonov, J. I. Antonov, T. P. Boyer, and H. E. Garcia (2010), World Ocean Atlas 2009, Volume 1: Temperature, edited by S. Levitus, NOAA Atlas NESDIS 68, U.S. Government Printing Office, Washington, D.C.
- Lombard, F., L. Labeyrie, E. Michel, L. Bopp, E. Cortijo, S. Retailleau, H. Howa, and F. Jorissen (2011), Modelling planktic foraminifer growth and distribution using an ecophysiological multi-species approach, *Biogeosciences*, 8, 853-873.
- Longhurst, A., S. Sathyendranath, T. Platt, and C. Caverhill (1995), An estimate of global primary production in the ocean from satellite radiometer data, *Journal of Plankton Research*(17).
- Longhurst, A. R. (2007), Ecological geography of the sea, *Amsterdam: Academic Press*.
- Lozier, M. S., V. Roussenov, M. S. C. Reed, and R. G. Williams (2010), Opposing decadal changes for the North Atlantic meridional overturning circulation, *Nature Geosci*, 3(10), 728-734.
- MARGO (2009), Constraints on the magnitude and patterns of ocean cooling at the Last Glacial Maximum, *Nature Geosci*, 2(2), 127-132.
- Martin, P. A., and D. W. Lea (2002), A simple evaluation of cleaning procedures on fossil benthic foraminiferal Mg/Ca, *Geochemistry, Geophysics, Geosystems*, 3(10), 8401.
- McCave, I. N. (2002), A Poisoned Chalice?, *Science*, 298(5596), 1186-1187.
- McManus, J. F., R. Francois, J. M. Gherardi, L. D. Keigwin, and S. Brown-Leger (2004), Collapse and rapid resumption of Atlantic meridional circulation linked to deglacial climate changes, *Nature*, 428(6985), 834-837.
- Michel, E., L. D. Labeyrie, J.-C. Duplessy, N. Gorfti, M. Labracherie, and J.-L. Turon (1995), Could deep subantarctic convection feed the world deep basins during the Last Glacial Maximum?, *Paleoceanography*, 10(5), 927-941.
- Moreno, A., H. Stoll, M. Jiménez-Sánchez, I. Cacho, B. Valero-Garcés, E. Ito, and R. L. Edwards (2010), A speleothem record of glacial (25-11.6 kyr BP) rapid climatic changes from northern Iberian Peninsula, *Global and Planetary Change*, 71(3-4), 218-231.
- Murton, J. B., M. D. Bateman, S. R. Dallimore, J. T. Teller, and Z. Yang (2010), Identification of Younger Dryas outburst flood path from Lake Agassiz to the Arctic Ocean, *Nature*, 464(7289), 740-743.
- Obbink, E. A., A. E. Carlson, and G. P. Klinkhammer (2010), Eastern North American freshwater discharge during the Bolling-Allerod warm periods, *Geology*, 38(2), 171-174.
- Ohkouchi, N., T. I. Eglinton, L. D. Keigwin, and J. M. Hayes (2002), Spatial and Temporal Offsets Between Proxy Records in a Sediment Drift, *Science*, 298(5596), 1224-1227.
- Oppo, D. W., J. F. McManus, and J. L. Cullen (2003), Palaeo-oceanography: Deepwater variability in the Holocene epoch, *Nature*, 422(6929), 277-277.
- Ottens, J. J. (1991), Planktic foraminifera as North Atlantic water mass indicators, *Oceanologica Acta*, 14(2), 123-140.
- Otto-Bliesner, B. L., and E. C. Brady (2010), The sensitivity of the climate response to the magnitude and location of freshwater forcing: last glacial maximum experiments, *Quaternary Science Reviews*, 29(1-2), 56-73.
- Peck, V. L., I. R. Hall, R. Zahn, and H. Elderfield (2008), Millennial-scale surface and subsurface paleothermometry from the northeast Atlantic, 55-8 ka BP, *Paleoceanography*, 23(3), PA3221.
- Pingree, R. D. (1997), The eastern Subtropical gyre (North Atlantic): flow rings recirculations structure and subduction., *Journal of Marine Biological Association of the United Kingdom*, 77, 573-624.
- Piotrowski, A. M., S. L. Goldstein, H. S. R., R. G. Fairbanks, and D. R. Zylberberg (2008), Oscillating glacial northern and southern deep water formation from combined neodymium and carbon isotopes, *Earth and Planetary Science Letters*, 272(1-2), 394-405.
- Pollard, R. T., M. J. Griffiths, S. A. Cunningham, J. F. Read, F. F. Pérez, and A. F. Ríos (1996), Vivaldi 1991 - A study of the formation, circulation and ventilation of Eastern North Atlantic Central Water, *Progress in Oceanography*, 37(2), 167-172.
- Pflaumann, U., J. Duprat, C. Pujol, and L. D. Labeyrie (1996), SIMMAX: A Modern Analog Technique to Deduce Atlantic Sea Surface Temperatures from Planktonic Foraminifera in Deep-Sea Sediments, *Paleoceanography*, 11(1), 15-35.
- Reimer, P., et al. (2009), IntCal09 and Marine09 Radiocarbon Age Calibration Curves, 0-50,000 Years cal BP, *Radiocarbon*, 51(4), 1111-1150.
- Richter, T. (1998), Sedimentary fluxes at the mid-atlantic ridge - sediment sources, accumulation rates, and geochemical characterisation, *GEOMAR Report, GEOMAR Research Center for Marine Geosciences, Christian Albrechts University in Kiel*(73), 173.
- Roberts, N. L., A. M. Piotrowski, J. F. McManus, and L. D. Keigwin (2010), Synchronous Deglacial Overturning and Water Mass Source Changes, *Science*, 327(5961), 75-78.
- Rogerson, M., E. J. Rohling, P. P. E. Weaver, and J. W. Murray (2004), The Azores Front since the Last Glacial Maximum, *Earth and Planetary Science Letters*, 222(3-4), 779-789.
- Rühlemann, C., S. Mulitza, G. Lohmann, A. Paul, M. Prange, and G. Wefer (2004), Intermediate depth warming in the tropical Atlantic related to weakened thermohaline circulation: Combining paleoclimate data and modeling results for the last deglaciation, *Paleoceanography*, 19(1), PA1025.

- Sarnthein, M., K. Winn, S. J. A. Jung, J.-C. Duplessy, L. Labeyrie, H. Erlenkeuser, and G. Ganssen (1994), Changes in east Atlantic deepwater circulation over the last 30000 years: Eight time slice reconstructions, *Palaeoceanography*, 9(2), 209-267.
- Schiebel, R., J. Waniek, A. Zeltner, and M. Alves (2002a), Impact of the Azores Front on the distribution of planktic foraminifers, shelled gastropods, and coccolithophorids, *Deep Sea Research Part II: Topical Studies in Oceanography*, 49(19), 4035-4050.
- Schiebel, R., B. Schmuker, M. Alves, and C. Hemleben (2002b), Tracking the Recent and late Pleistocene Azores front by the distribution of planktic foraminifers, *Journal of Marine Systems*, 37(1-3), 213-227.
- Schlitzer, R. (2012), Ocean Data View, <http://odv.awi.de>.
- Schmidt, M. W., and J. Lynch-Stieglitz (2011), Florida Straits deglacial temperature and salinity change: Implications for tropical hydrologic cycle variability during the Younger Dryas, *Paleoceanography*, 26(4), PA4205.
- Schmidt, M. W., H. J. Spero, and D. W. Lea (2004), Links between salinity variation in the Caribbean and North Atlantic thermohaline circulation, *Nature*, 428(6979), 160-163.
- Schmidt, M. W., M. J. Vautravers, and H. J. Spero (2006), Rapid subtropical North Atlantic salinity oscillations across Dansgaard-Oeschger cycles, *Nature*, 443(7111), 561-564.
- Schmuker, B., and R. Schiebel (2002), Planktic foraminifers and hydrography of the eastern and northern Caribbean Sea, *Marine Micropaleontology*, 46(3-4), 387-403.
- Schott, F. A., R. Zantopp, L. Stramma, M. Dengler, J. r. Fischer, and M. Wibaux (2004), Circulation and Deep-Water Export at the Western Exit of the Subpolar North Atlantic, *Journal of Physical Oceanography*, 34(4), 817-843.
- Schwab, C., H. Kinkel, M. Weinelt, and J. Repschläger (2012), Coccolithophore paleoproductivity and ecology response to deglacial and Holocene changes in the Azores Current System, *Paleoceanography*, 27(3), PA3210.
- Shackleton, N. J. (1974), Attainment of isotopic equilibrium ocean water and the benthonic foraminifera genus *Uvigerina*: Isotopic changes in the ocean during the last glacial, *Cent. Natl.Rech. Sci. Colloq. Int.*, 219, 203-209.
- Shackleton, N. J., M. A. Hall, and E. Vincent (2000), Phase Relationships Between Millennial-Scale Events 64,000-24,000 Years Ago, *Paleoceanography*, 15(6), 565-569.
- Shakun, J. D., and A. E. Carlson (2010), A global perspective on Last Glacial Maximum to Holocene climate change, *Quaternary Science Reviews*, 29(15-16), 1801-1816.
- Sicre, M. A., G. Siani, D. Genty, N. Kallel, and L. Essallami (2013), Seemingly divergent sea surface temperature proxy records in the central Mediterranean during the last deglacial, *Clim. Past Discuss.*, 9(1), 683-701.
- Skinner, L. C., N. J. Shackleton, and H. Elderfield (2003), Millennial-scale variability of deep-water temperature and $\delta^{18}\text{O}_{\text{dw}}$ indicating deep-water source variations in the Northeast Atlantic, 0-34 cal. ka BP, *Geochem. Geophys. Geosyst.*, 4(12), 1098.
- Streeter, S. S., and N. J. Shackleton (1979), Paleocirculation of the Deep North Atlantic: 150,000-Year Record of Benthic Foraminifera and Oxygen-18, *Science*, 203(4376), 168-171.
- Storz, D., H. Schulz, J. J. Waniek, D. E. Schulz-Bull, and M. Kufgera (2009), Seasonal and interannual variability of the planktic foraminiferal flux in the vicinity of the Azores Current, *Deep Sea Research Part I: Oceanographic Research Papers*, 56(1), 107-124.
- Stouffer, R. J., et al. (2006), Investigating the Causes of the Response of the Thermohaline Circulation to Past and Future Climate Changes, *Journal of Climate*, 19(8), 1365-1387.
- Stuiver, M., and P. J. Reimer (1986), A computer program for radiocarbon age calibration, *Radiocarbon*, 28, 022-1030.
- Tarasov, L., and W. R. Peltier (2005), Arctic freshwater forcing of the Younger Dryas cold reversal, *Nature*, 435(7042), 662-665.
- Tarasov, L., and W. R. Peltier (2006), A calibrated deglacial drainage chronology for the North American continent: evidence of an Arctic trigger for the Younger Dryas, *Quaternary Science Reviews*, 25(7,8), 659-688.
- Thornalley, D. J. R., H. Elderfield, and I. N. McCave (2009), Holocene oscillations in temperature and salinity of the surface subpolar North Atlantic, *Nature*, 457(7230), 711-714.
- Thornalley, D. J. R., H. Elderfield, and I. N. McCave (2010a), Intermediate and deep water paleoceanography of the northern North Atlantic over the past 21,000 years, *Paleoceanography*, 25(1), (PA1211).
- Thornalley, D. J. R., I. N. McCave, and H. Elderfield (2010b), Freshwater input and abrupt deglacial climate change in the North Atlantic, *Paleoceanography*, 25(PA1201).
- Thornalley, D. J. R., H. Elderfield, and I. N. McCave (2011), Reconstructing North Atlantic deglacial surface hydrography and its link to the Atlantic overturning circulation, *Global and Planetary Change*, 79(3,4), 163-175.
- van Aken, H. M. (2000), The hydrography of the mid-latitude northeast Atlantic Ocean: I: The deep water masses, *Deep Sea Research Part I: Oceanographic Research Papers*, 47(5), 757-788.
- van Aken, H. M. (2001), The hydrography of the mid-latitude Northeast Atlantic Ocean -- Part III: the subducted thermocline water mass, *Deep Sea Research Part I: Oceanographic Research Papers*, 48(1), 237-267.
- Voelker, A. H. L., S. M. Lebreiro, J. Schönfeld, I. Cacho, H. Erlenkeuser, and F. Abrantes (2006), Mediterranean outflow strengthening during northern hemisphere coolings: A salt source for the glacial Atlantic?, *Earth and Planetary Science Letters*, 245(1-2), 39-55.
- Voelker, A. H. L., L. de Abreu, J. Schönfeld, H. Erlenkeuser, and F. Abrantes (2009), Hydrographic conditions along the western Iberian margin during marine isotope stage 2, *Geochemistry, Geophysics, Geosystems*, 10(12), Q12U08.
- Voelker, A. H. L., and L. de Abreu (2011), A Review of Abrupt Climate Change Events in the Northeastern Atlantic Ocean (Iberian Margin): Latitudinal, Longitudinal, and Vertical Gradients, in *Abrupt Climate Change: Mechanisms, Patterns, and Impacts*, edited, pp. 15-37, AGU, Washington, DC.
- Volkov, D. L., and L.-L. Fu (2010), On the Reasons for the Formation and Variability of the Azores Current, *Journal of Physical Oceanography*, 40(10), 2197-2220.

- Volkov, D. L., and L.-L. Fu (2011), Interannual variability of the Azores Current strength and eddy energy in relation to atmospheric forcing, *J. Geophys. Res.*, *116*(C11), C11011.
- Waelbroeck, C., L. Labeyrie, E. Michel, J. C. Duplessy, J. F. McManus, K. Lambeck, E. Balbon, and M. Labracherie (2002), Sea-level and deep water temperature changes derived from benthic foraminifera isotopic records, *Quaternary Science Reviews*, *21*, 295-305.
- Waelbroeck, C., L. C. Skinner, L. Labeyrie, J. C. Duplessy, E. Michel, N. Vazquez Riveiros, J. M. Gherardi, and F. Dewilde (2011), The timing of deglacial circulation changes in the Atlantic, *Paleoceanography*, *26*(3), PA3213.
- Weldeab, S., R. R. Schneider, and M. Kölling (2006), Deglacial sea surface temperature and salinity increase in the western tropical Atlantic in synchrony with high latitude climate instabilities, *Earth and Planetary Science Letters*, *241*(3-4), 699-706.
- Williams, C., B. P. Flower, D. W. Hastings, T. P. Guilderson, K. A. Quinn, and E. A. Goddard (2010), Deglacial abrupt climate change in the Atlantic Warm Pool: A Gulf of Mexico perspective, *Paleoceanography*, *25*(4), PA4221.

Chapter 6

Coccolithophore paleoproductivity and ecology response to deglacial and Holocene changes in the Azores Current System

(This chapter corresponds to the following manuscript published in *Paleoceanography*:
Schwab, C., Kinkel, H., Weinelt, M., Repschläger, J., 2012. Coccolithophore paleoproductivity and ecology response to deglacial and Holocene changes in the Azores Current

Coccolithophore paleoproductivity and ecology response to deglacial and Holocene changes in the Azores Current System

C. Schwab,¹ H. Kinkel,² M. Weinelt,² and J. Repschläger¹

Received 9 January 2012; revised 5 June 2012; accepted 9 June 2012; published 8 August 2012.

[1] In order to test the sensitivity of marine primary productivity in the midlatitude open ocean North Atlantic to changes in the Atlantic Meridional Overturning Circulation (AMOC), we investigated two spliced sediment cores from a site south of the Azores Islands at the northern rim of the North Atlantic subtropical gyre. For this purpose we analyzed coccolithophore assemblages, diatom abundances, alkenones and conducted X-ray fluorescence (XRF) core scanning. During times of reduced AMOC, especially during Heinrich event 1 (H1) and the Younger Dryas, we observe a strong increase in productivity as evidenced by high coccolith accumulation rates, high alkenone concentrations/accumulation rates, high Ba/Ti-ratios, high abundances of diatoms and low abundances of *F. profunda*. The increased productivity is partly caused by a more southern position of the Azores Front (AzF), and hence by a less northward extension of the subtropical gyre, as deduced from high abundances of the temperate coccolithophore species *G. muelleriae* and low abundances of subtropical species (*Oolithotus* spp., *Umbellosphaera* spp., *Umbilicosphaera* spp.). However, to explain the full range of the observed productivity increase, other factors like increased westerly winds and advection of nutrient-rich surface waters have also to be considered. Because this pattern can also be observed in other sediment cores from the midlatitude North Atlantic, we propose that during times of reduced AMOC there has been a band of strongly increased productivity across the North Atlantic at the northern rim of the contracted subtropical gyre, which partly counteracts the decreased organic carbon pump in the high northern latitudes.

Citation: Schwab, C., H. Kinkel, M. Weinelt, and J. Repschläger (2012), Coccolithophore paleoproductivity and ecology response to deglacial and Holocene changes in the Azores Current System, *Paleoceanography*, 27, PA3210, doi:10.1029/2012PA002281.

1. Introduction

[2] Primary productivity (PP) is an integral part of the climate system, because it affects the global carbon cycle due to the fixation of atmospheric carbon [e.g., *Falkowski*, 2000]. As half of the global net PP takes place in the oceans [*Field et al.*, 1998], changes in oceanic productivity are of high interest to the (paleo-)climate community. Therefore immense efforts have been undertaken to reconstruct past changes in productivity and to gain more insights into the sensitivity and relation of this process to climate changes [e.g., *Sarnthein et al.*, 1988;

Kohfeld et al., 2005; *Nave et al.*, 2007]. However, regarding the North Atlantic, most paleoproductivity estimates are conducted in the high northern latitudes and/or in coastal regions [e.g., *Sarnthein et al.*, 1988; *Nave et al.*, 2007], where thick piles of sediments allow a detailed reconstruction of past productivity changes. Reconstructions from the open ocean are scarce, because of the notoriously low sedimentation rates in this area. However, changes in this area are crucial due to the large area covered by the open ocean.

[3] In order to circumvent the patchy picture drawn from the sedimentary record and to gain more insights into the processes involved, this topic has also been a focus of many modeling studies [e.g., *Brovkin et al.*, 2002; *Schmittner*, 2005]. These studies suggest that during times of reduced AMOC, e.g., during Heinrich events, productivity drastically decreases in the global ocean and especially in the North Atlantic [*Schmittner*, 2005; *Menviel et al.*, 2008; *Mariotti et al.*, 2012]. Although this result is generally corroborated by the sedimentary record, there are still mismatches between the two approaches on a regional scale [e.g., *Salgueiro et al.*, 2010], pointing to the fact that the spatial resolution of coupled

¹Institute for Geosciences, Christian-Albrechts-Universität Kiel, Kiel, Germany.

²Graduate School Human Development in Landscapes, Christian-Albrechts-Universität Kiel, Kiel, Germany.

Corresponding author: C. Schwab, Institute for Geosciences, Christian-Albrechts-Universität Kiel, Ludewig-Meyn-Strasse 10, DE-24118 Kiel, Germany. (chs@gpi.uni-kiel.de)

biogeochemical models is still insufficient and/or that there are processes not considered by the models [Schmittner, 2005; Mariotti et al., 2012].

[4] Furthermore PP related to the subtropical gyres is of particular interest. Although PP in these oligotrophic ecosystems is low, their large size allows for a significant contribution on a global scale [Polovina et al., 2008]. They account for a quarter of global PP [Longhurst et al., 1995] and contribute up to 50% of global ocean carbon export [Emerson et al., 1997]. Because of this important role in the biogeochemical cycling of carbon, which controls atmospheric CO₂ levels over time [Sarmiento and Siegenthaler, 1992], changes in their spatial extension and/or nutrient inventory are crucial to the understanding of past and future climate changes.

[5] Because the northern boundary of the North Atlantic subtropical gyre is marked by the Azores Current System with its associated AzF [Maillard and Käse, 1989; Bashmachnikov et al., 2004], the northward extension of the gyre can be deduced from the latitudinal position of the AzF. However, results in the recent literature are contradictory concerning the past latitudinal position of the AzF and hence the past northward extension of the gyre. For example Rogerson et al. [2004] stated that in the Gulf of Cadiz the AzF did not change its position during the course of the last deglacial, whereas Schiebel et al. [2002a], based on low-resolution sediment cores from an open ocean site in the North Atlantic, reconstructed a more southern position of the front during glacials compared to interglacials. Therefore, based on two spliced and high-resolution sedimentary records drilled near the Azores Islands, we will test, if the AzF and hence the subtropical gyre changed their position/extension during the course of the last deglacial and Holocene. Furthermore we will discuss possible reasons for the observed variability and discuss a hypothetical connection between the front dynamics in the open ocean and near the coast. At last we will test the sensitivity of PP in the open ocean North Atlantic to changes in AMOC and within the AzF, and assess its potential impact on the carbon cycle.

[6] For this purpose we mainly analyzed coccolithophore assemblages, which are widely used to reconstruct paleoecological and paleoceanographic conditions [McIntyre and Bé, 1967; Beaufort et al., 1997; Kinkel et al., 2000; Flores et al., 2000; Giraudeau et al., 2010; Saavedra-Pellitero et al., 2011]. For example relative abundances of certain coccolithophore species within coccolithophore assemblages have been successfully used to reconstruct frontal movements [e.g., Findlay and Giraudeau, 2002]. Furthermore changes in the absolute abundances of coccolithophores have been successfully used to reconstruct past productivity changes [e.g., Stolz and Baumann, 2010]. At last coccolithophores are considered to be the most important primary producers in the open ocean of tropical to temperate regions [Brand, 1994] and therefore they are ideally suited to trace past productivity and AzF dynamics at our coring site.

2. Recent Hydrography and Productivity Regime

[7] Our study area is located southwest of the Azores Islands, slightly north of the Azores Current System (Figure 1a). Like the Portugal Current, the Azores Current System is a branch of the northeastward flowing North

Atlantic Current, the dominant surface water flow in the North Atlantic. Major components of the Azores Current System are the Azores Current and its associated AzF, which are situated between 32° and 35°N [Klein and Siedler, 1989; Maillard and Käse, 1989]. Recent modeling studies suggest that the water mass transformation within the Gulf of Cadiz is responsible for the formation of the Azores Current System [e.g., Jia, 2000; Volkov and Fu, 2010, 2011]. According to the β -plume theory the comparatively small outflow of Mediterranean Outflow Water (MOW) (1 Sv) forces the Azores Current (9–19 Sv), which partly replaces the waters lost due to the overflow. Thereby a stronger MOW results in a stronger Azores Current [Volkov and Fu, 2010]. The Azores Current and its associated front are persistent features of the subtropical North Atlantic throughout the year and mark the northern boundary of the North Atlantic subtropical gyre [Klein and Siedler, 1989; Maillard and Käse, 1989; Bashmachnikov et al., 2004]. The AzF corresponds to a region of strong dipping isotherms and is best defined as the position, where the 15°C isotherm is between 200 and 300 m water depth [Gould, 1985]. It separates southern subtropical water (Sargasso Sea mode water) with a shallow thermohaline mixed layer from colder and fresher North Atlantic Transitional Water (NATW) with a deep winter mixed layer [Käse and Siedler, 1982; Gould, 1985; Schiebel et al., 2011]. Southernmost NATW is the dominant surface water at our coring site. Furthermore mesoscale activity is an important feature of the Azores Current System [e.g., Kielmann and Käse, 1987]. Mature meanders pinch off the Azores Current, forming cyclonic eddies to the south and anticyclonic eddies to the north of the Azores Current [Alves et al., 2002]. It is important to note, that only the anticyclonic eddies, transporting a subtropical signal, can reach our coring site today [Alves et al., 2002; Pingree et al., 2002].

[8] The different conditions on each side of the AzF result in a high north-south PP gradient in our study area (Figure 1b). In the subtropical region PP is low, mainly due to the paucity of nutrients resulting from strong water column stratification and weak vertical mixing [Mouriño-Carballido and Neuer, 2008]. In the region north of the AzF PP is high, because of a deep winter mixed layer (200–300 m) and associated nutrient supply [Lévy et al., 2005]. Furthermore episodic nutrient input to the south can result from eddy pumping of the cyclonic eddies, whereas the anticyclonic eddies to the north, which occasionally reach our coring site, are normally associated with downwelling and low PP [Hernández-León et al., 2007; Mouriño-Carballido and Neuer, 2008]. Today peak PP takes place during early spring (March–April) (Figure 1c). However, it is known that peak coccolithophore productivity occurs slightly after the main PP peak [Margalef, 1978; Merico et al., 2004] and therefore maximum coccolithophore productivity should take place later in spring (April–June) at SSTs of approximately 18°C close to mean annual SST of 19.4°C (cf. Figures 1a and 1c).

[9] The different environmental/hydrographic conditions result in a transitional and a subtropical biogeographical province, separated by the AzF. These provinces are not only very distinct, e.g., in foraminiferal assemblages [Otten, 1991; Schiebel et al., 2002a, 2002b], but are also very well expressed in coccolithophore assemblages [McIntyre and Bé,

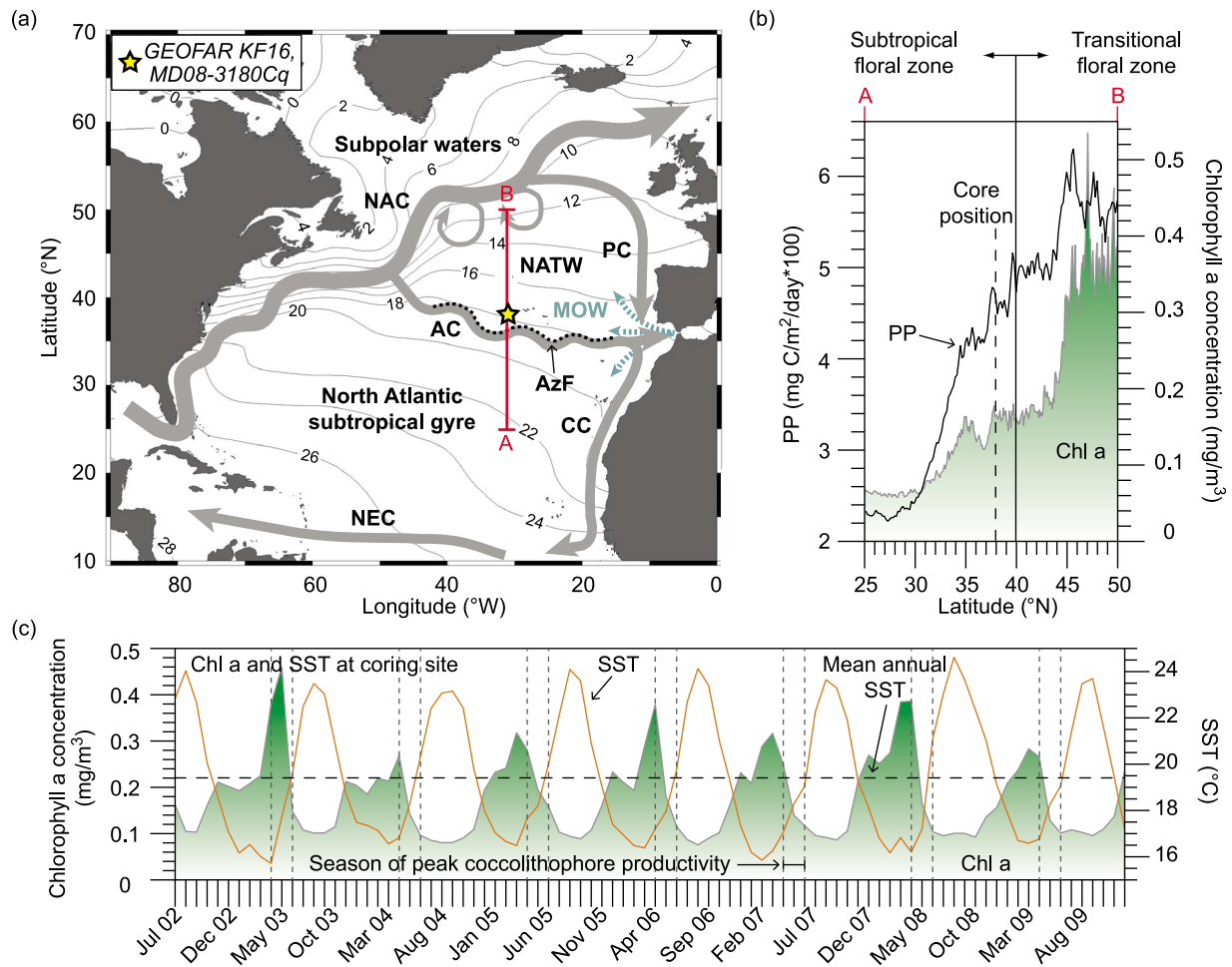


Figure 1. (a) Schematic surface ocean circulation of the North Atlantic overlaid on contour map of spring (April–June) sea surface temperatures (SSTs) [Locarnini *et al.*, 2010]. Major surface currents (gray arrows): North Atlantic Current (NAC), Portugal Current (PC), Azores Current (AC), North Equatorial Current (NEC). Blue dashed arrows mark Mediterranean Outflow Water (MOW). Black dashed lines indicate Azores Front (AzF). The position of North Atlantic Transitional Water (NATW) is bound by the NAC to the north and by the AC to the south. Yellow star marks location of studied sediment cores. Transect A-B (red line) is shown in Figure 1b. Map was generated using the ODV software by R. Schlitzer (Ocean Data View software, 2012, available at <http://odv.awi.de>). (b) Satellite-based annual mean PP estimates (solid black line) and chlorophyll a concentration (green shaded area) for year 2006 (derived from MODIS and SeaWiFS satellite data available at <http://www.science.oregonstate.edu/ocean.productivity> and <http://seadas.gsfc.nasa.gov>) along transect A-B shown in Figure 1a. Core position is marked by vertical dashed line. Boundary between subtropical and temperate coccolithophore biographical province after McIntyre and Bé [1967] is shown as vertical solid line. (c) Monthly chlorophyll a concentration (green shaded area) and SST (orange solid line) at the coring site derived from satellite data. Dashed horizontal line indicates mean SST. Dashed vertical lines delineate spring season (April–June), when peak coccolithophore productivity is expected.

1967; Schiebel *et al.*, 2011] (Figure 1b) and expansions/contractions of these provinces can be traced at our coring site.

3. Material and Methods

3.1. Sample Material and Age Control

[10] We analyzed sediment cores GEOFAR KF16 and MD08–3180Cq (Table 1), which consist of foraminifera bearing nannofossil ooze. GEOFAR KF16 was taken during GEOFAR cruise onboard the research vessel *Le Noroit* [Richter, 1998]. MD08–3180Cq was taken during cruise MD 168 onboard the research vessel *Marion Dufresne* in the

Table 1. Investigated Sediment Cores

Latitude	Longitude	Water Depth	Length	Coring Device	Reference
<i>GEOFAR KF16</i>					
37°59.59'N	31°7.698'W	3050 m	8 m	Piston corer	Richter [1998]
<i>MD08–3180Cq</i>					
37°59.99'N	31°8.07'W	3064 m	10.5 m	Calypso square-corer	Kissel <i>et al.</i> [2008]

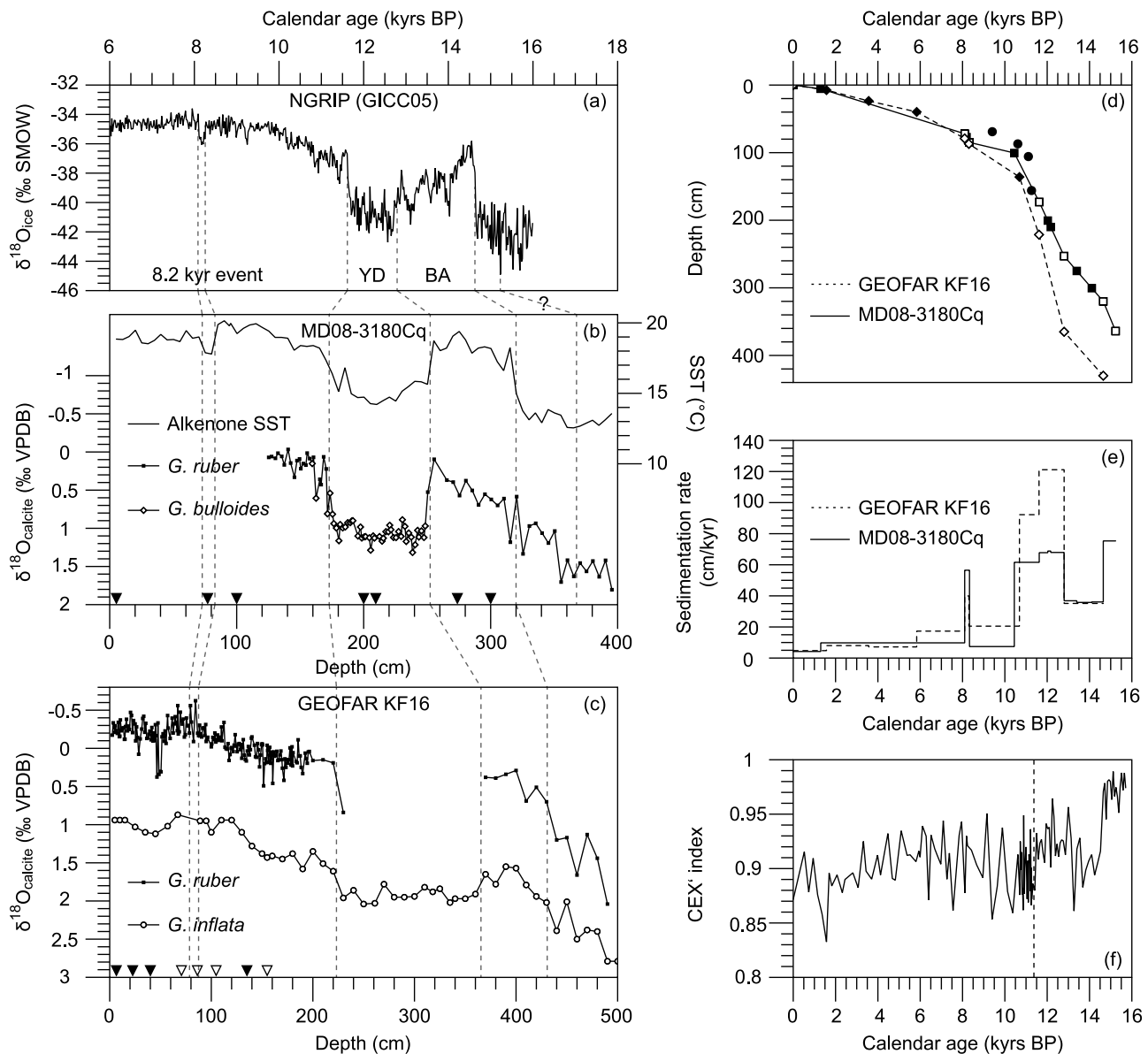


Figure 2. Age models and preservation index of coccolithophores of sediment cores GEOFAR KF16 and MD08-3180Cq. (a) NGRIP ice core oxygen isotope record (ice) on GICC05 timescale [Andersen *et al.*, 2007]. (b) Alkenone SST and planktonic oxygen isotope record of MD08-3180Cq. During the Younger Dryas *G. ruber* is absent at the coring site and therefore *G. bulloides* was measured and corrected for -0.6‰ to match *G. ruber* [Ganssen and Kroon, 2000]. (c) Oxygen isotope records of *G. ruber* and *G. inflata* in GEOFAR KF16 [Richter, 1998]. (d) Resulting age models based on AMS ^{14}C ages (filled symbols) and tuning to NGRIP (open symbols) of GEOFAR KF16 (dashed line with diamonds) and MD08-3180Cq (solid line with squares). Filled circles are omitted AMS ^{14}C ages of GEOFAR KF16. (e) Resulting sedimentation rates of GEOFAR KF16 (dashed line) and MD08-3180Cq (solid line). (f) CEX' index, indicating preservation of coccoliths. Grey dashed lines indicate correlation (tuning points) of both cores to the NGRIP record. Triangles indicate measured and used (filled triangles) and omitted (unfilled triangles) AMS ^{14}C ages. Black dashed vertical line indicates splicing of cores for coccolithophore analysis as described in the text.

framework of the AMOCINT IMAGES XVII campaign [Kissel *et al.*, 2008]. Both cores are from the same location in a small basin at the Mid-Atlantic Ridge, slightly southwest of the Azores Islands (Figure 1a). This basin accumulates sediments at higher rates compared to the surrounding slow accumulating open ocean sites due to sediment

focusing [Richter, 1998], enabling high-resolution analyses. In addition, a surface sample from companion boxcore GEOFAR KG14 was analyzed.

[11] The age models (Figures 2a–2d) of GEOFAR KF16 and MD08-3180Cq are based on 15 Accelerator Mass Spectrometer (AMS) radiocarbon ages of mono specific

Table 2. Age Control Points^a

Depth in Core (cm)	AMS ¹⁴ C Age (years BP)	Error (years)	Calibrated Age (years BP)	Additional Reservoir Age (years)	Tuned Age (years BP)
<i>GEOFAR KF16</i>					
7.5	2015	±30	1572	-	-
23.5	3660	±35	3567	-	-
39.75	5455	±35	5835	-	-
69	8715	±40	9406	-	-
79	-	-	-	-	8100
87	-	-	-	-	8300
87	9765	±45	10612	-	-
105.75	10075	±50	11111	-	-
136	9835	±55	10689	-	-
156	10290	±55	11260	-	-
221	-	-	-	-	11614
365	-	-	-	-	12800
430	-	-	-	-	14650
<i>MD08–3180</i>					
5.5	1755	±25	1300	-	-
72	-	-	-	-	8102
77	7935	±40	8391	201	8190
85	-	-	-	-	8329
100.5	9570	±45	10446	-	-
173	-	-	-	-	11624
200.5	11100	±60	12613	584	12029
210	11045	±55	12592	425	12167
253	-	-	-	-	12800
275	12560	±80	13997	600	13397
300.5	12780	±70	14360	250	14110
320	-	-	-	-	14650
364	-	-	-	-	15234

^aBold characters are ages used to construct the age models.

samples of planktonic foraminifera (*G. ruber* w. or *G. bulloides*) (Table 2), measured at Leibniz-Laboratory for Radiometric Dating and Isotope Research at Kiel University. All ages were converted into calendar ages using the Calib 6.0 software [Stuiver and Reimer, 1986] with Marine09 calibration curve [Reimer et al., 2009]. Furthermore the alkenone SST record in MD08–3180Cq and the planktonic oxygen isotope records of both cores were additionally tuned to the NGRIP oxygen isotope record [Andersen et al., 2007] (Figures 2a–2c). To match calibrated AMS ¹⁴C ages and tuned ages, additional reservoir ages were applied to the AMS ¹⁴C ages of the Bølling-Allerød, Younger Dryas and 8.2 kyr event. The applied reservoir corrections are consistent with reservoir corrections in the North Atlantic during these events based on the findings of Waelbroeck et al. [2001], Kleiven et al. [2008] and Thornalley et al. [2010]. Four calibrated AMS ¹⁴C ages in GEOFAR KF16 measured on *G. bulloides* yielded age reversals and/or unreasonable high sedimentation rates and therefore have been discarded. As *G. bulloides* can live deeper in the water column (down to 300 m) at the coring site [Schiebel et al., 2002a], these species can be influenced by deeper, ¹⁴C-depleted water masses. Furthermore the AMS ¹⁴C age at 69 cm in GEOFAR KF16 is dated within the transition from high to low abundances of this species, which can introduce a considerable error to AMS ¹⁴C ages due to bioturbational effects [e.g., Bard et al., 1987]. Based on the age models sedimentation rates range between 4 and 122 cm/kyr with maximum values during northern hemisphere cold periods (8.2 kyr event, Younger Dryas and H1) (Figure 2e). The constantly increasing offset between both cores in the age versus depth profiles and sedimentation rates can be related to the well-known stretching/compaction effect of different coring devices [e.g., Skinner and

McCave, 2003]. Because we partly started our analysis on GEOFAR KF16 before we retrieved MD08–3180Cq, which is from the same coring site (Figure 1a and Table 1), and because the core section of GEOFAR KF16 available to us only spanned the late deglacial and Holocene section, we partly had to combine both records (e.g., Figure 2f) to get continuous records over the last 16 kyr. However, a good correlation on the common time scale for both cores exists, taking into account e.g., the overlap in isotopes (cf. Figures 2b and 2c).

3.2. Quantification of Coccoliths

[12] For coccolithophore studies we analyzed GEOFAR KF16 from 0 to 11.4 kyr BP with a sampling interval of 1 to 5 cm (corresponding to an average resolution of 150 years) and MD08–3180Cq from 11.4 to 15.7 kyr BP with a sampling interval of 5 cm (corresponding to an average resolution of 90 years). Because both cores are from the same coring site (Figure 1a and Table 1), we combined them to get a continuous record with multicentennial-scale time resolution (e.g., Figure 2f).

[13] Samples for coccolithophore analyses were prepared with a combined dilution/filtration technique following Andruleit [1996]. For this purpose a small amount of freeze-dried sediment (0.07–0.08 g) was suspended in tap water and ultrasonicated for 15 to 30 s. The suspension was split by a factor of 100 using a rotary sample divider (™Fritsch Laborette 27) and filtered on a polycarbonate membrane filter with a pore size of 0.4 μm. After drying the filters for 24 h at 40°C a small piece of filter was cut out, mounted on a scanning electron microscope (SEM) stub and sputtered with gold/palladium. On average 375 coccoliths were counted in each sample using a CamScan 44 SEM. The coccoliths were

counted on measured transects at a magnification of 5000 and identified according to the taxonomy given in *Young et al.* [2003]. A taxonomic list of the identified species is given in the auxiliary material.¹ Furthermore extended counts were carried out to improve the accuracy for the rare species *C. pelagicus*. Therefore a whole transect across the filter was additionally scanned and only specimens of *C. pelagicus* were counted. Based on the counting relative proportions of each species to the total assemblage were calculated. Furthermore total and species coccolith concentration in a sediment sample were calculated, using the formula of *Andrulleit* [1996]: total/species coccolith concentration = (filtered area × number of counted coccoliths (total or per species) × split factor)/(investigated area × weight of sample). To estimate preservational effects on coccolithophore assemblages, we calculated the CEX' index following *Boeckel and Baumann* [2004]: $CEX' = (\%E. huxleyi + \% \text{small gephyrocapsids}) / (\%E. huxleyi + \% \text{small gephyrocapsids} + \%C. leptoporus)$. For paleoproductivity estimates we calculated coccolith accumulation rates, using the sedimentation rates shown in Figure 2e and dry bulk densities from GEOFAR KF16 [*Richter*, 1998] interpolated between two points of known densities: coccolith accumulation rate = total coccolith concentration × dry bulk density × sedimentation rate. During the Preboreal, where both cores were spliced, we used sedimentation rates from core MD08–3180Cq to calculate accumulation rates to avoid an artificial jump in accumulation rates due to the different compaction/stretching effect in both cores.

3.3. Alkenone Measurements

[14] Long-chain (C₃₇ - C₃₉) di-, tri- and tetra-unsaturated methyl and ethyl ketones (alkenones) were measured at the biomarker laboratory at the CAU Kiel. Alkenones were extracted from 2 g of freeze-dried and grounded sediment samples using dichloromethane (DCM) as a solvent and with an Accelerator Solvent Extraction system (Dionex ASE 200) set to 80 bar and 75°C. Samples were then analyzed using multidimensional, double-column gas chromatography using two Agilent 6890 gas chromatographs equipped with two independent ovens and two flame ionization detectors connected via a transfer line. A detailed description of the measuring procedure can be found in *Etourneau et al.* [2010]. SST was obtained using the U₃₇^K index which is defined after *Brassell et al.* [1986] as: $U_{37}^K = (C_{37:2}) / (C_{37:2} + C_{37:3})$. The U₃₇^K index was converted to SST using the global core top calibration of *Müller et al.* [1998]: $U_{37}^K = 0.033 \times SST + 0.044$. According to sample and standard replicates, the standard deviation of the SST estimate was approximately ±0.2°C.

3.4. XRF Core Scanning

[15] XRF measurements on core MD08–3180Cq were carried out using the AAVATECH XRF core scanner at the Institute of Geosciences at the CAU Kiel. The core was scanned every 0.5 cm with generator settings of 10 and 50 kV. Because Barium is used as a proxy for PP [e.g., *Dymond et al.*, 1992] we are using Ba measured by XRF scanning as a tracer for past productivity changes. Although

Ba in the sediment at the coring site is predominantly of biogenic origin [*Richter*, 1998], we normalized the Ba counts to Ti counts to roughly correct for Ba originating from the lithogenic fraction. However, using raw Ba counts does not alter the observed changes indicating that influence of terrigenous material is negligible. Ba measured by XRF core scanning was converted to Ba concentrations using Ba measured by XRF spectrometry [*Richter*, 1998]. Under the above postulated assumption that terrigenous input of Ba is negligible (see also following section and section 4.2), Ba concentrations were then converted to PP using the formula of *Dymond et al.* [1992] (see section 4.2).

[16] Because the coring site is far offshore the sediment is predominantly of biogenic origin. This is seen for example in the high CaCO₃ content which accounts for 73 wt% on average, reaching maximum values of 85 wt% during the late Holocene [*Richter*, 1998]. The purely pelagic character of the sediment becomes also evident by the visual examination of the samples by SEM, where only coccoliths, foraminifers, calcareous dinoflagellates, diatoms and silicoflagellates are observed. Because the sediments from this open ocean site are predominantly of biogenic origin we are using the Si/Ca ratio as an indicator for the relative contribution of siliceous plankton to the sediment. To confirm this we did some control counts of diatoms under the SEM. Therefore a transect of approximately 1 cm was scanned at a magnification of 500 on filters prepared for coccolith analyses. Only intact valves were counted without identification on the species level. A possible influence of detrital Si derived from terrigenous input will be discussed in the following section.

4. Results

4.1. Coccolith Counts

[17] The preservation of coccoliths in the studied cores is excellent, as indicated by the presence of complete delicate species like *G. ornata*, complete coccospheres or holococcoliths. Furthermore the good preservation of the coccoliths can be seen in the high CEX' values (Figure 2f), which are always above the critical value of 0.63. Both findings indicate that the coring location was always situated above the lysocline [*Boeckel and Baumann*, 2004] as also is postulated by *Crowley* [1983].

[18] As the relative abundances of coccoliths from individual coccolithophore species closely parallel their concentrations in the sediment (Figure 3), only abundances are furthermore considered. In general the coccolith assemblage is dominated by *E. huxleyi*, *G. muelleriae* and small gephyrocapsids, together comprising up to 84% of the total assemblage (Figures 3a–3c; see also the auxiliary material). All other species are minor contributors to the assemblage with relative abundances of each of these species never exceeding 12%.

[19] *E. huxleyi* tolerates a wide range of ecological conditions and therefore is abundant in nearly all oceanic environments [*Okada and Honjo*, 1973; *Okada and McIntyre*, 1979]. Therefore it may be difficult to reconstruct past ecological changes based on abundance variations of this species and no paleoecological interpretation of this species is given in this study (Table 3). However, at our coring site this species shows long-term (>500 years)

¹Auxiliary materials are available in the HTML. doi:10.1029/2012PA002281.

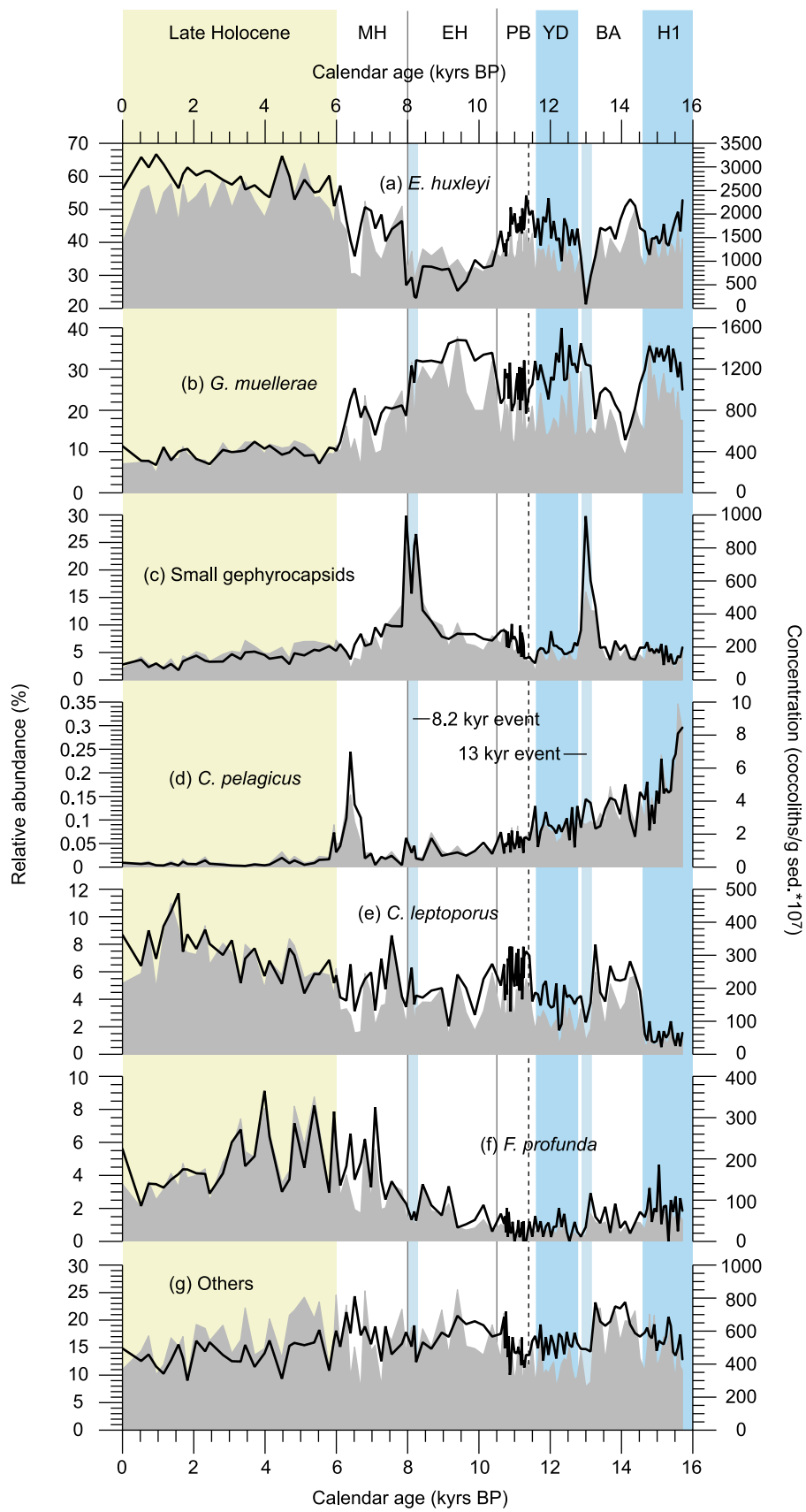


Figure 3

Table 3. Selected Coccolithophores and Inferred Ecological Changes

Species	Used as a Proxy for:
<i>E. huxleyi</i>	-
<i>G. muelleriae</i>	Influence of NATW
Small geophycocapsids	Nutrient-rich, less saline surface water conditions
<i>C. pelagicus</i>	Influence of subpolar water
<i>C. leptoporus</i>	-
<i>F. profunda</i>	Nutricline-depth
Grouped subtropical species	Influence of subtropical water

minima during H1, beginning Younger Dryas and during the early Holocene (Figure 3a). After 6 kyr BP *E. huxleyi* is the solely dominant species at our coring site with relative abundances of up to 67%. This overall evolution is interrupted by several pronounced short-term minima found at 13, 8.2 and 6.5 kyr BP. A nearly opposite trend is found in the abundance record of the cold/temperate water species *G. muelleriae*, which shows lowest abundances after 6 kyr BP (Figure 3b). Regarding the North Atlantic, and aside of its occurrence in the upwelling regions off northwest Africa [Sprengel et al., 2002] and in the subpolar realm of the North Atlantic due to drifting within waters of the North Atlantic Current [e.g., Samtleben and Schröder, 1992], this species has been reported to be restricted to the eastern North Atlantic occurring in waters with a temperature range of 12–18°C (optimum 14°C) [Giraudeau et al., 2010]. As this spatial distribution and temperature range of *G. muelleriae* corresponds to NATW [cf. Locarnini et al., 2010] it has been reported to occur only north of the AzF [Jordan, 1988; Schiebel et al., 2011] and can be used to reconstruct the influence of NATW at our coring site.

[20] In our samples small geophycocapsids ($\leq 2.7 \mu\text{m}$) mainly comprise *G. ericsonii* with an occasional low contribution of *G. ornata*. Like *E. huxleyi*, this species tolerates a wide range of ecological conditions [Haidar and Thierstein, 2001], although an affinity to high productivity [Baumann et al., 2008; and references therein] as well as a slight affinity to low salinities [Boeckel et al., 2006] have been reported. Assuming that the distribution of small geophycocapsids is governed by PP and salinity, we conclude that low saline and high productive conditions prevailed at the coring site at 13 and 8.2 kyr BP as deduced from pronounced peak abundances of up to 30% (Figure 3c).

[21] During the deglacial the abundance of *C. pelagicus* gradually decreases and it becomes nearly absent at the coring site since the mid-Holocene (Figure 3d). Although there are two well established morphotypes of *C. pelagicus*, a small (6–10 μm) morphotype (*C. pelagicus* ssp. *pelagicus*) associated with arctic conditions and a larger (9–15 μm) morphotype (*C. pelagicus* ssp. *braarudii*) associated with more temperate and nutrient-rich conditions [Ziveri et al., 2004, and references therein], we did not distinguish

between the two morphotypes due to their very low abundances in the cores (<0.35%). However, as the overall abundance of *C. pelagicus* in surface sediments closely parallels the abundance pattern of the small morphotype, with clear abundance maxima in the polar and subpolar North Atlantic [Baumann et al., 2005], we are using this species as an indicator for cool and nutrient-rich surface water masses of subpolar origin. Therefore the observed abundance variations indicate a gradual decrease in the influence of subpolar water masses during the course of the deglacial. Furthermore a distinct maximum in its abundance is evident at 6 kyr BP. However, distinct minima during this time, e.g., in less calcified coccolithophore species like *E. huxleyi* and exceptionally high oxygen isotope values of planktonic and benthic foraminifers (J. Repschläger et al., manuscript in preparation, 2012) (Figure 2c), indicate an “artificial” enrichment of *C. pelagicus*, which is one of the most heavy calcified coccolithophores, due to dissolution. As all coccolithophore species used to calculate the CEX’ index are affected by this dissolution (cf. section 3.2, Figure 3), this event cannot be detected in the CEX’ index (Figure 2f). As this core interval is associated with the transition from reddish, oxygenated sediments to greyish, unoxidized sediments [cf. Richter, 1998], the dissolution is probably caused by diagenetic processes associated with the oxygenation horizon.

[22] Although the cosmopolitan species *C. leptoporus* has an affinity to cold and nutrient-rich conditions in the equatorial Atlantic and in the Arabian Sea [Kinkel et al., 2000; Andrulleit and Rogalla, 2002], the distribution pattern of this species in the North Atlantic is patchy, with no clear ecological preferences [Ziveri et al., 2004]. At the Azores, this species clearly shows minimum abundances during H1 and the Younger Dryas and a slight increase in its abundance is obvious during the last 6 kyr with maximum abundances of up to 11% during the last 3 kyr (Figure 3e).

[23] The lower photic zone species *F. profunda* is widely used to monitor past changes in nutricline-depth and associated changes in productivity [Molfini and McIntyre, 1990a, 1990b; Beaufort et al., 1997; Kinkel et al., 2000]. Thereby high abundances of *F. profunda* indicate a deep nutricline and low productivity. During the deglacial and early Holocene *F. profunda* occasionally disappears from the coring site and shows low abundances never exceeding 5% (Figure 3f). However, a pronounced increase in its abundance can be observed during the mid-Holocene, resulting in maximum abundances of up to 9% during the late Holocene, indicating a deep nutricline and low productivity.

[24] The species *Umbellosphaera* spp., *Umbilicosphaera* spp. and *Oolithotus* spp. are associated with warm and oligotrophic water masses [Incarbona et al., 2011, and references therein]. Here we summarize these species as subtropical species, and use their abundance variations as an indicator for the influence of subtropical waters, which

Figure 3. Relative abundance of coccolith species (solid lines) and their concentration in the sediment (filled lines). (a) *E. huxleyi*, (b) *G. muelleriae*, (c) small geophycocapsids, (d) *C. pelagicus*, (e) *C. leptoporus*, (f) *F. profunda* and (g) others (see Figure S1 in the auxiliary material). Abbreviations: mid-Holocene (MH), early Holocene (EH), Preboreal (PB), Younger Dryas (YD), Bølling-Allerød (BA), Heinrich event 1 (H1). Vertical light blue bars mark the cold periods of H1 and the YD. Small vertical lighter blue bars mark the 13 and 8.2 kyr events. Vertical yellowish bar marks the stable late Holocene as discussed in the text. Vertical solid lines denote the boundaries between PB/EH and EH/MH. Dashed vertical line indicates splicing of cores for coccolithophore analysis as described in the text.

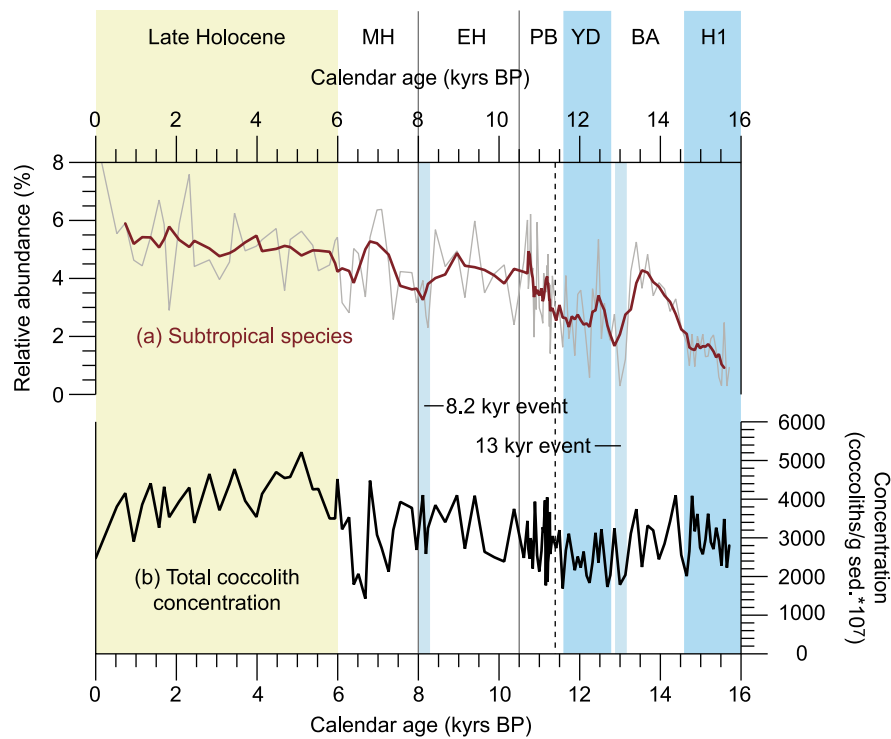


Figure 4. (a) Abundance of subtropical species (*Oolithotus* spp., *Umbellosphaera* spp., *Umbilicosphaera* spp.) (solid gray line) and 5 pt moving average (solid red line). (c) Total coccolith concentration in investigated sediment samples. Abbreviations and markers as in Figure 3.

are brought by the anticyclonic eddies to our coring site. Therefore the minimum abundances observed during H1 and the Younger Dryas indicate a decreased influence of subtropical waters (Figure 4a). During the late Holocene maximum abundances (up to 8%) indicate a maximum influence of this water mass at the coring site. Furthermore maximum coccolith concentrations of up to 5.2×10^{10} coccoliths/g sediment are observed during the late Holocene (Figure 4b).

4.2. SST and PP Reconstructions

[25] Alkenone derived SSTs were 7 and 5°C colder than today during H1 and the Younger Dryas respectively (Figure 5a). These changes are within the range of previously reported SST reconstructions from the midlatitude eastern North Atlantic [Bard *et al.*, 2000; Chapman *et al.*, 2000]. After rising during the Preboreal and early Holocene, SST stabilize between 18.5 and 19.5°C after 8 kyr BP, close to modern annual mean SST of 19.3°C at the coring site [Locarnini *et al.*, 2010]. This indicates that at least today alkenone SST reliably traces mean annual temperature. However, alkenone production probably shifted toward the summer season during extreme cold events like H1 and the Younger Dryas [Leduc *et al.*, 2010; Schneider *et al.*, 2010]. Therefore alkenone SST might be biased toward the warm season showing higher than average SSTs at the coring site during these events. This would mute the amplitude of change during H1 and Younger Dryas, but would not affect the general SST pattern. Aside of the observed general SST pattern several small-scale perturbations are evident in the SST record (Figure 5a). The most pronounced perturbation is at 8.2 kyr BP, where SST abruptly decrease down from 19.9 to 17.8°C.

[26] Based on our multiproxy approach a generally consistent pattern emerges with high productivity during the deglacial, especially during H1 and the Younger Dryas (Figures 5b–5g). For example a fourfold and twofold increase of the Ba/Ti ratio is observed during the cold H1 and Younger Dryas respectively (Figure 5b). Furthermore Ba/Ti ratios are decreased during the Bølling-Allerød and Preboreal but do not reach the very low values of the Holocene period. Although the use of Barium as a paleo-productivity proxy is still discussed controversially [e.g., McManus *et al.*, 1998], the most common limitation of this proxy, which are water depth and lateral advection of refractory organic matter and/or resuspended barite from the continental shelf [Dymond *et al.*, 1992], can be ruled out at our open ocean site at a water depth >1000 m. Furthermore Barium has been proposed to be a good indicator for productivity at the coring site due to its close correlation to TOC and PP estimates from the nearby Canary basin [Richter, 1998]. However, it has been recently supposed that a Ba peak in sediments off northwest Africa during H1 originates from Ba-enriched meltwater transported via the Azores and Canary Current [Plewa *et al.*, 2006], therefore the Ba/Ti peak observed during H1 might have been influenced by these meltwaters. But as increased productivity is also observed in all other proxies, we conclude that Ba/Ti mainly reflects productivity, although a minor influence of meltwater cannot be ruled out.

[27] An increased abundance of siliceous phytoplankton, mainly diatoms, during H1, Younger Dryas and the 8.2 kyr event can be deduced from the Si/Ca ratio (Figure 5c). However, although diatom abundances are increased during

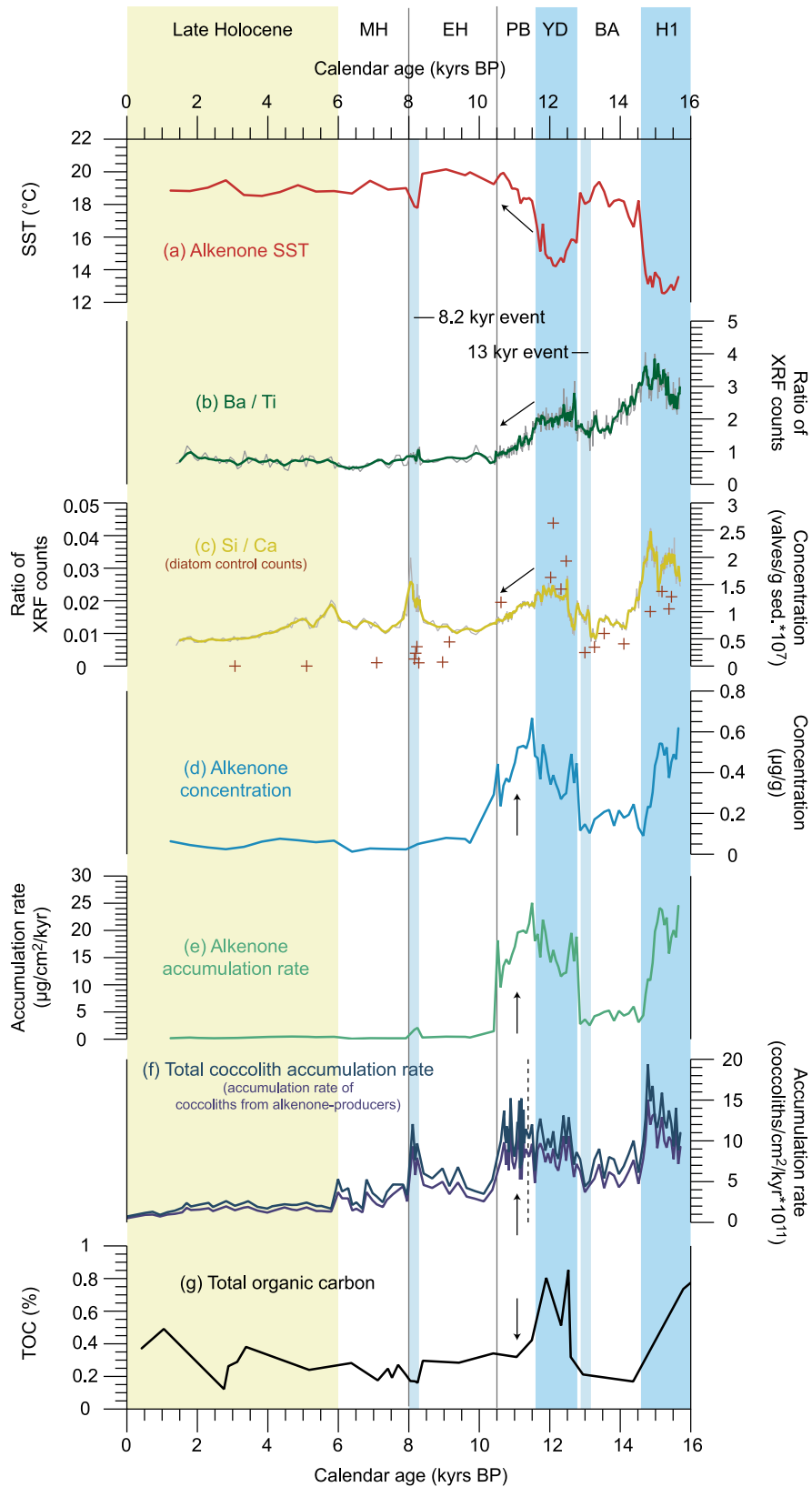


Figure 5

H1 the exceptional Si/Ca peak during this period partly stems from increased abundances of silicoflagellates, as observed by SEM. As diatoms are opportunistic species [e.g., *Abrantes et al.*, 2002], the increased abundances during the mentioned periods again indicate an increased productivity.

[28] Because westerly winds were increased during H1 and the Younger Dryas [*Nebout et al.*, 2002; *Rodrigo-Gámiz et al.*, 2011], an increased Si input via dust during these times would hamper our interpretation of the Si/Ca record. However, based on the visual examination of the samples under the SEM we found no evidences for any detrital input. A negligible aeolian input to the midlatitude open ocean North Atlantic during Heinrich events has also been proposed by *Villanueva et al.* [1997] and *Naafs et al.* [2010] based on the abundance of aeolian derived n-alkanes in nearby cores SU90/08 (43°20'N, 30°24'W) and U1313 (41°N, 32°34'W). Therefore fluctuations in aeolian dust input did not seem to exert a major control on Si/Ca ratio and therefore can also be ruled out to drive the observed productivity pattern.

[29] Increased PP during H1 and the Younger Dryas can also be deduced from coccolithophore specific PP proxies (Figures 5d–5f). Alkenone concentrations reach values up to 0.62 and 0.54 $\mu\text{g/g}$ during H1 and Younger Dryas respectively, whereas maximum values during the Holocene are as low as 0.08 $\mu\text{g/g}$ (Figure 5d). During the Bølling-Allerød PP is low, as deduced from alkenone concentrations, with maximum values of 0.25 $\mu\text{g/g}$, but not as low as during the Holocene. A similar PP pattern is observed in the accumulation rates of alkenones with maximum values of 25, 6 and 22 $\mu\text{g/cm}^2/\text{kyr}$ during H1, Bølling-Allerød and Younger Dryas respectively (Figure 5e). During the Holocene alkenone accumulation rates reach a maximum of 2 $\mu\text{g/cm}^2/\text{kyr}$ during the 8.2 kyr event. The changes in the accumulation rates of alkenones are paralleled by changes in the accumulation rates of coccoliths from alkenone-producing coccolithophores (*E. huxleyi* and *gephyrocapsids*) (Figure 5f). They show maximum values of 15, 8 and 11 $\cdot 10^{11}$ coccoliths/ cm^2/kyr during H1, Bølling-Allerød and Younger Dryas respectively. Lowest values are found throughout the entire late Holocene with increased values at 8.2 kyr BP. Total coccolith accumulation rates show values of 19, 10 and 13 $\cdot 10^{11}$ coccoliths/ cm^2/kyr during H1, Bølling-Allerød and Younger Dryas respectively (Figure 5f). Again, lowest values are found throughout the entire late Holocene with increased values at 8.2 kyr BP.

[30] All coccolithophore specific PP proxies show strongly increased PP during the Preboreal, with maximum alkenone concentrations up to 0.7 $\mu\text{g/g}$, maximum alkenone accumulation rates up to 25 $\mu\text{g/cm}^2/\text{kyr}$, maximum accumulation rates of coccoliths from alkenone-producing

coccolithophores up to 13 $\cdot 10^{11}$ coccoliths/ cm^2/kyr and maximum total coccolith accumulation rates up to 15 $\cdot 10^{11}$ coccoliths/ cm^2/kyr . This indicates that growth conditions for coccolithophores were optimal, just after the main PP peak during the Younger Dryas that favored the growth of diatoms. Furthermore slightly enhanced coccolithophore productivity seems to prevail until 6 kyr BP based on coccolith accumulation rates, which is not supported by alkenone concentrations and accumulations. This discrepancy might stem from the fact that the onset of modern NADW production sets in during early Holocene [*Alley and Clark*, 1999; *Chapman et al.*, 2000; *Piotrowski et al.*, 2004; *McManus et al.*, 2004], providing oxygen-rich bottom water to the coring site and therefore organic material (e.g., alkenones) might have been affected by preservation throughout the entire Holocene, resulting in their observed minimal concentrations. In summary, coccolithophores seem to sustain relative high productivity after the YD until 6 kyr BP, especially during the Preboreal. That coccolithophores can sustain high productivity after the main PP peak is also observed in the seasonal succession of phytoplankton species in which diatoms occur close to peak PP early in the year, whereas peak coccolithophore productivity can prevail into the more stratified, warmer season [*Margalef*, 1978; *Merico et al.*, 2004].

[31] Although we can observe a general pattern with increased PP during the deglacial, especially during H1 and the Younger Dryas, in all PP proxies, which therefore seems to be very robust, the amplitude of changes in the different PP proxies are different (Figures 5b–5g). The different amplitudes might be the result of the different sensitivities of the PP proxies to actual PP changes [cf. *Sarnthein et al.*, 1988; *Dymond et al.*, 1992; *Nelson et al.*, 1995; *Beaufort et al.*, 1997; *Haidar and Thierstein*, 2001] and/or of the different preservation potential of the different PP proxies [cf. *Gingele et al.*, 1999; *Rühlemann et al.*, 1999; *Tréguer et al.*, 1995; *Romero et al.*, 1999]. However, despite their different sensitivities and preservation potential, all shown PP proxies reveal the same pattern with increased PP at least during H1 and the Younger Dryas, although we want to note, that the observed changes have to be viewed from a qualitative rather than from a quantitative point of view.

[32] On the other hand, quantitative changes can be inferred from the conversion of Ba fluxes to PP (Figure 6). Because PP derived from Ba fluctuates close to the modern PP value of 461 $\text{mg C/m}^2/\text{day}$ during the mid and late Holocene, the conversion seems to yield reasonable results. Maximum values of 2457, 664 and 1460 $\text{mg C/m}^2/\text{day}$, indicating an increase of PP by a factor of 5.3, 1.4 and 3.2 compared to modern values, are observed during H1, Younger Dryas and Bølling-Allerød respectively. Furthermore, in accordance to coccolithophore specific PP proxies,

Figure 5. (a) Alkenone derived SSTs. (b) Ba/Ti ratio measured with XRF core scanner (gray solid line) and 5 pt moving average (green solid line). (c) Si/Ca ratio measured with XRF core scanner (gray solid line) and 5 pt moving average (yellow solid line), brown crosses show diatom control counts. (d) Total (C37:2 + C37:3) alkenone concentration of investigated sediment samples. (e) Total (C37:2 + C37:3) alkenone accumulation rate. (f) Accumulation rate of coccoliths (dark blue line) and from alkenone-producing coccolithophores (*E. huxleyi* and *gephyrocapsids*) (purple line). Dashed vertical line indicates splicing of cores for coccolithophore analysis as described in the text. (g) Percentage of total inorganic carbon in core GEOFAR KF16 [*Richter*, 1998]. Small arrows mark direction of observed changes during the Preboreal. Abbreviations and markers as in Figure 3.

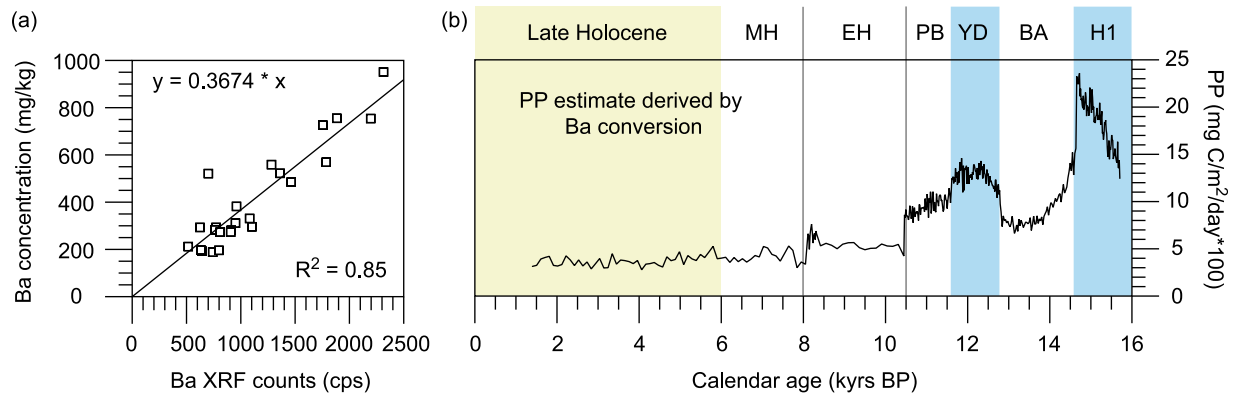


Figure 6. Conversion of Ba measured by XRF core scanning to PP. (a) Correlation of Ba counts measured by XRF to Ba concentrations measured by XRF spectrometry [Richter, 1998]. The relation $y = 0.3674x$ is used to convert Ba counts into concentrations. (b) Ba concentration converted to PP using the formula of Dymond *et al.* [1992]. Abbreviations and markers as in Figure 3.

especially to coccolith accumulation rates, increased PP can be observed during the Preboreal and early Holocene compared to late Holocene values.

5. Discussion

5.1. Frontal Movements and PP Changes During the Deglacial and Early Holocene

[33] During H1 and the Younger Dryas a higher influence of NATW and a decreased influence of subtropical water is indicated by maximum abundances of *G. muelleriae* (Figure 3b) and minimum abundances of subtropical species (Figure 4a) respectively. Thus we assume that during deglacial cold periods the AzF resided at a more southern position as compared to today. For warm Bølling-Allerød both proxies indicate a significant northward movement of the AzF and hence a northward extension of the subtropical gyre. This suggests that the AzF did not only migrate on glacial/interglacial timescales, as deduced by Schiebel *et al.* [2002a] from low-resolution records, but also on shorter, millennial-scale timescales, and in parallel to the reorganization of the North Atlantic during the course of the last deglacial [e.g., Sarnthein *et al.*, 2001]. This result seems to contradict the findings of Rogerson *et al.* [2004] from the Gulf of Cadiz, who concluded no latitudinal displacement of the AzF during cold periods of the last deglacial. However, recent modeling studies suggest that the water mass transformation in the Gulf of Cadiz is responsible for the formation of the Azores Current and that a stronger MOW would lead to a stronger Azores Current [e.g., Volkov and Fu, 2010]. As MOW existed and was even stronger than today during cold climatic intervals (e.g., Heinrich events, Younger Dryas) [e.g., Voelker *et al.*, 2006], the Azores Current would have still resided and a front could have developed in the Gulf of Cadiz as observed by Rogerson *et al.* [2004]. Therefore the connection between the Azores Current System and the MOW as suggested by models could be the reason for the observed decoupling of the AzF dynamics in the open ocean and near the coast, which is also seen in the modeling studies, where the Azores Current exhibits latitudinal variability only west of 20°W [Volkov and Fu, 2010]. Furthermore the modeling studies suggest that the latitudinal variability of the Azores

Current is driven by the strength of the westerly winds [Volkov and Fu, 2010, 2011]. Therefore, the increased westerly winds during the deglacial and early Holocene, especially during H1 and the Younger Dryas [Nebout *et al.*, 2002; Rodrigo-Gámiz *et al.*, 2011] could have been responsible for the observed shift of the Azores Current System in the open ocean North Atlantic.

[34] Aside of this general trend, a slight northward shift of the AzF seems to be obvious during the Preboreal, as evidenced by minimum abundances of *G. muelleriae* (Figure 3b). However, we argue that this minimum is caused by optimal growth conditions for coccolithophores (cf. section 4.2), in which the blooming of the opportunistic species *E. huxleyi* (Figure 3a), which is a much tougher competitor than *G. muelleriae* [e.g., Okada and Wells, 1997], lowered the relative abundance of temperate species like *G. muelleriae* (Figure 3b). A similar behavior of *E. huxleyi* during the Preboreal is reported by Hass *et al.* [2001] in a core from the northern North Atlantic (Voering Plateau), where due to a first intrusion of North Atlantic water masses the opportunistic species *E. huxleyi* recovered rapidly, whereas other species needed longer to adapt to the conditions following the Younger Dryas. Furthermore, contrary to *G. muelleriae*, the abundance of subtropical species indicates a significant northward shift of the AzF during the Preboreal and early Holocene comparable to the Bølling-Allerød (Figure 4a). But as the abundance record of subtropical species more closely parallels the temperature record than the abundance record of *G. muelleriae* (abundance subtropical species versus alkenone SST: $R^2 = 0.47$; abundance *G. muelleriae* versus alkenone SST: $R^2 = 0.28$), these species probably are additionally affected by temperature. However, slightly lower abundances of subtropical species during the Preboreal and early Holocene indicate a (slightly) more southern position of the AzF compared to the late Holocene in accordance to the *G. muelleriae* record.

[35] Because of the high PP gradient in our region (Figure 1b) even small movements of the AzF and the associated climatic and productivity regimes are likely to result in substantial changes of our paleoproductivity signals. Therefore the enhanced paleoproductivity during the

deglacial and early Holocene, and especially during H1 and the Younger Dryas (Figures 5b–5g), might be the result of the above postulated more southern position of the front. However, an increase of PP by a factors of up to 5.3 and 3.2 during H1 and the Younger Dryas respectively, as indicated by Ba derived PP changes (Figure 6), cannot be explained by a shift of the front solely, as such high values are nowhere found in the open North Atlantic today [e.g., *Behrenfeld et al.*, 2006] (cf. Figure 1b). Therefore additional factors, like increased westerly winds during H1 and the Younger Dryas [*Nebout et al.*, 2002; *Rodrigo-Gámiz et al.*, 2011], which would raise the nutricline due to deeper winter mixing, probably enhanced PP.

[36] Furthermore nutrients brought by subpolar water and/or by freshwater from melted icebergs might have affected PP at the coring site. Today nutrient-rich subpolar water is admixed to NATW via cold core rings pinching off the NAC [*Kupferman et al.*, 1986] and transporting a subpolar fauna and flora to lower latitudes [*The Ring Group*, 1981; *Beckmann et al.*, 1987]. An increased influence of subpolar water during the deglacial and early Holocene at the coring site can be deduced from the increased abundance of the subpolar species *C. pelagicus* (Figure 3d). During these periods a more southern position of the NAC and its associated Subpolar Front, as proposed by *Ruddiman and Glover* [1975], would have allowed the cold core rings to penetrate to the coring site and to fuel PP. However, a clear deglacial sequence with H1, Bølling-Allerød and Younger Dryas is missing in the abundance record of *C. pelagicus*. There might be at least two explanations for this: the NAC gradually moved northward during the deglacial and/or complex interplay and abundance changes between the two different morphotypes of *C. pelagicus* (cf. section 4.1).

[37] Although there are no evidences for icebergs at our coring site, an enhanced input of IRD to the North Atlantic just north of our coring site is recorded during H1 and the Younger Dryas [*Bond et al.*, 1997; *Chapman and Shackleton*, 1998], indicating at least the vicinity of icebergs at our coring site. As icebergs can act as nutrient sources [*Schwarz and Schodlok*, 2009], nutrients derived by melted icebergs have been described to increase PP in the midlatitude North Atlantic, especially during H1 [e.g., *Kiefer et al.*, 1995; *Gil et al.*, 2009]. Therefore nutrient-rich meltwaters from icebergs probably entered the coring site during H1 and the Younger Dryas and fueled productivity. This scenario is also supported by a freshening of the sea surface at the coring site during H1 and the Younger Dryas as recognized by *Repschläger et al.* (manuscript in preparation, 2012) (cf. Figure 2). In summary, the increased PP during the deglacial and early Holocene, especially during H1 and the Younger Dryas, are the result of a more southern position of the AzF, increased westerly winds, advection of subpolar waters and advection of nutrient-rich waters from melted icebergs.

[38] Recent modeling studies indicate that a reduction in AMOC, due to a freshwater input like during Heinrich events, would lead to a reduction in global export production, most notably in the North Atlantic [*Schmittner*, 2005; *Menviel et al.*, 2008]. In order to support this observation, the results have been compared to paleoproductivity records from south of Iceland, the Brazilian Margin and the north-west African upwelling areas. However, no comparison

between model and proxy-data has been shown for the open Atlantic, which would be crucial regarding the large area covered.

[39] Although we cannot test the global outcome of these models, our results from the Azores are in contrast to what the modeling studies suggest for this region. During all deglacial cold events associated with a reduction in AMOC we observe a strong increase in PP. This points to regional factors and/or processes, like AzF dynamics or advection of nutrient-rich surface waters, affecting PP in the Azores region, which are not considered and/or resolved by the models [*Schmittner*, 2005; *Mariotti et al.*, 2012]. However, enhanced surface water productivity during deglacial cold periods associated with advection of fertile subpolar waters and amplified by nutrients derived from icebergs, has also been reported from the Bermuda Rise, offshore southwestern Iberian Margin, Gulf of Cadiz and from the western Mediterranean Sea [*Lebreiro et al.*, 1997; *Rogerson et al.*, 2004; *Jimenez-Espejo et al.*, 2007; *Gil et al.*, 2009; *Penaud et al.*, 2011]. Therefore we propose that during the mentioned cold periods there has been a band of high productivity across the midlatitude North Atlantic at the northern boundary of the contracted subtropical gyre, which also seems to penetrate into the western Mediterranean and can be associated with the advection of fresh and nutrient-rich surface waters. As biogeochemical models potentially do not take into account the transport of nutrients at the surface into the subtropics [see, e.g., *Mariotti et al.*, 2012], we propose that the implications of freshwater forced AMOC perturbations on the biological activity in the midlatitude North Atlantic might have to be reconsidered.

[40] However, in accordance to the modeling studies, productivity was decreased in the higher latitudes of the North Atlantic [*Nave et al.*, 2007]. Decreased productivity during periods of reduced AMOC, in particular during Heinrich events, has been reported from core SU90-03 (40°3'N, 32°W) [*Nave et al.*, 2007], just north of our coring site. This decreased productivity has been related to a strong water column stratification induced by the freshwater input [*Nave et al.*, 2007]. Therefore the boundary between the low productive northern areas and the southern areas, where only a diluted component of the nutrient-rich freshwater arrives and promotes productivity, is somewhere between 38° and 40°N in the open ocean North Atlantic.

[41] Unfortunately no paleoproductivity reconstructions from more southern open ocean sites in the North Atlantic are available, and therefore the southern boundary of the high productivity band cannot be estimated. Nevertheless the band can be traced across the North Atlantic, at least from the Bermuda Rise to the Gulf of Cadiz, and within the western Mediterranean Sea, and therefore it probably occupied a large area. Furthermore, aside of an increase in PP due to a shift of the productivity regimes, the level of productivity within this band was strongly increased (Figure 6) due to additional processes like the advection of nutrient-rich surface waters. Because of the large areal coverage and the strongly increased level of PP, this high productivity band potentially could have counteracted the decreased productivity and resulting decreased organic carbon pump in the more northern latitudes of the North Atlantic during times of reduced AMOC.

5.2. Mid-Holocene Onset of Modern Hydrographic and Productivity Conditions

[42] Based on coccolith assemblages and PP reconstructions a reorganization of the hydrographic and productivity regime is evident during the mid-Holocene (Figures 3–6). Most proxies shift to full interglacial values during this period and stabilize on these values at the latest after 6 kyr BP. For example, lowest abundances of *G. muelleriae* (Figure 3b) are accompanied by highest abundances of subtropical species (Figure 4a). Based on the interpretation of these proxies given above, this indicates that the AzF reached its modern, northernmost position after 6 kyr BP and hence the contributions of NATW and subtropical water at the coring site were minimal and maximal respectively.

[43] Like during the deglacial, the reorganization of the hydrographic conditions is accompanied by changes in PP. Thereby most oligotrophic conditions during the last 16 kyr prevailed since the mid-Holocene as indicated, e.g., by lowest coccolith accumulation rates and lowest Ba derived PP (Figures 5f and 6). The shift toward oligotrophic conditions can also be deduced based on the abundance of *F. profunda* (Figure 3f), at which highest abundances since the mid-Holocene indicate a deep nutricline and associated lowest productivity. Furthermore the establishment of the oligotrophic conditions can also be deduced from the increased concentration of coccoliths in the sediment since the mid-Holocene (Figure 4b). As many coccolithophore species are K-selected they increase their relative contribution to the plankton assemblage under oligotrophic conditions [Baumann *et al.*, 2005]. Therefore, unlike coccolith accumulation rates (fluxes), which are high under nutrient-rich conditions, high coccolith concentrations in the sediment are found in nutrient-depleted environments (e.g., subtropical gyres) [Baumann *et al.*, 2004]. The oligotrophic conditions since the mid-Holocene are consequence of the maximum contribution of nutrient-depleted subtropical waters to the coring site (Figure 4a) and/or the absence of fertile water masses originating from the higher northern latitudes of the North Atlantic. The latter is indicated by the absence of *C. pelagicus* at the coring site since 6 kyr BP (Figure 3d).

[44] Beside this general shift during the mid-Holocene a decrease in the abundance of *F. profunda* occurs during the last 3 kyr (Figure 3f). This decrease is accompanied by maximum abundances of *C. leptoporus* (Figure 3e). The observed changes probably correspond to a slight shallowing of the nutricline, decreasing the abundance of the lower photic zone species and increasing the abundance of the nutrient affiliated *C. leptoporus* (see section 4.1). But the advection of nutrients associated with this process probably was insignificant resulting in low coccolithophore productivity (Figure 5f).

[45] In general, the observed changes indicate the most northern position of the AzF and hence the maximum northward extension of the subtropical gyre in the North Atlantic since the mid-Holocene. Furthermore, a general pattern emerges, with an expansion of the gyre during warm periods (Bølling-Allerød, (late) Holocene) and a contraction during cold periods (H1, Younger Dryas). Although it is hard to define a quantitative temperature/expansion relationship based on our proxy results, one could easily hypothesize that a further increase in temperatures, as expected for the following

decades [Intergovernmental Panel on Climate Change, 2007], would probably lead to a further expansion of the oligotrophic gyre. Indeed an expansion of the subtropical gyres, especially of the North Atlantic subtropical gyre, due to an increase of global temperatures between 1998 and 2006 has been reported [Polovina *et al.*, 2008]. Furthermore, this study indicates that the expansion of the oligotrophic gyres takes place at the expense of more productive areas. If this expansion is not compensated by increased productivity in the high latitudes due to an occupation of new habitats, such an expansion and resulting decreased overall marine productivity would provide a positive feedback to the temperature increase due to a decreased atmospheric carbon fixation by marine organisms.

5.3. Short-Term Reorganizations Caused by Freshwater Input

[46] One of the most pronounced short-term events is recorded at 8.2 kyr BP (Figures 3–6), coincident with the well-known 8.2 kyr event in the North Atlantic [Ellison *et al.*, 2006; Kleiven *et al.*, 2008]. This event was most probably triggered by a rapid drainage of glacial Lake Agassiz into the North Atlantic via Hudson Strait [Barber *et al.*, 1999; Teller and Leverington, 2004]. In the Azores region SSTs abruptly dropped by 2°C (Figure 5a) and PP slightly increased (Figures 5 and 6). Also the coccolith assemblage changed remarkably during this event, e.g., abundances of *E. huxleyi* show a distinct minimum (Figure 3a). The most profound change in the coccolith assemblage is recorded in the abundance of small geophyrocapsids (Figure 3c), which together with *G. muelleriae* dominate the assemblage. Furthermore low abundances of subtropical species are observed (Figure 4a). Altogether this points to a southward shift of the AzF during the 8.2 kyr event, due to an incursion of NATW. At 8.2 kyr BP a considerable freshening of the sea surface is recognized at the coring site (Repschläger *et al.*, manuscript in preparation, 2012) (cf. Figure 2). This is consistent with a routing of the discharged meltwater into the subtropical realm [Condrón and Winsor, 2011]. Furthermore recent modeling studies show exactly the observed SST drop in the Azores region during the 8.2 kyr event, if the model is forced by a freshwater discharge through Hudson Strait and with additional icebergs [Wiersma and Jongma, 2010]. As already stated, there are no evidence for icebergs in the Azores region, but ice-rafted detritus (IRD) just north of our coring site indicates at least the vicinity of icebergs, which can act as additional nutrient [Schwarz and Schodlok, 2009]. Therefore, in addition to a latitudinal shift of the productivity regime, nutrient-rich freshwaters, probably partly originating from melted icebergs, again fueled PP at the coring site. These fresh and nutrient-rich conditions under still relatively moderate temperatures (17.8°C) seem to be optimal for the growth of small geophyrocapsids at the coring site, resulting in their observed peak abundances.

[47] Another short-term reorganization of the hydrographic and productivity regime is recorded at 13 kyr BP (Figures 3–5), coincident with the well-known Inter-Allerød Cold Period [Benson *et al.*, 1997]. In our records this event bears striking similarities to the 8.2 kyr event. At this time SSTs dropped by 1.4°C (Figure 5a) and the coccolith assemblage changed in the same manner as during the 8.2 kyr event. The most striking similarity is seen in the abundance of small geophyrocapsids (Figure 3c), which at 13 kyr BP

together with *G. muelleriae* dominate the assemblage. The peak abundance of small geophyrocapsids might again be linked to additional nutrients and to a freshening of the sea surface as recognized Repschläger et al. (manuscript in preparation, 2012) (cf. Figure 2). This freshening event can be related to a meltwater discharge from St. Lawrence River [Clark et al., 2001] and/or to an export of less saline seawater from the Caribbean [Flower et al., 2004]. Evidences for additional nutrients, probably brought by melting icebergs, may come from an enhanced IRD input at the onset of the Inter-Allerød Cold Period [Bond et al., 1997]. However, based on the abundance of small geophyrocapsids, the 8.2 and 13 kyr events are the only two meltwater/freshwater events associated with iceberg discharge recognized in the Azores region. As there have been numerous of such events in the North Atlantic during the last 16 kyr [e.g., Bond et al., 1997; Clark et al., 2001], this probably points to unique conditions (SST, salinity, nutrients, etc.) found during these two events in the Azores region, which favored the growth of small geophyrocapsids.

6. Conclusions

[48] Our multiproxy reconstructions from sediment cores GEOFAR KF16 and MD08–3180Cq reveal significant changes in the hydrographic and productivity conditions near the Azores Islands during the last 16 kyr. Based on changes within coccolithophore assemblages, the temperate and subtropical biogeographical provinces, and hence the AzF, resided at a more southern latitude during the deglacial and early Holocene, especially during H1 and the Younger Dryas. Furthermore southward shifts of the AzF are recognized during the 8.2 kyr event and during the Inter-Allerød Cold Period. These results indicate, that the AzF in the open ocean North Atlantic did not only migrate on glacial/interglacial timescales, as deduced by Schiebel et al. [2002a] on low-resolution records, but also on millennial and even shorter timescales. Although, these results seem to contradict the findings of Rogerson et al. [2004] from the Gulf of Cadiz, recent modeling studies suggest that the connection between the Azores Current System and the MOW might be responsible for the decoupling of the AzF dynamics in the open ocean and near the coast.

[49] Furthermore, we observe an increased productivity during the deglacial and early Holocene, especially during H1 and the Younger Dryas. Although the observed productivity increase partly is caused by the more southern position of the AzF and the resulting shift of the productivity regimes, other factors like increased westerly winds and advection of nutrient-rich surface waters have to be considered to fully explain the observed productivity increase.

[50] Because we observe an increased productivity during times of reduced AMOC, e.g., H1 and the Younger Dryas, our results are in contrast to what modeling studies suggest for this region. This indicates that the observed PP changes were driven by regional factors and/or processes, like AzF dynamics and advection of nutrient-rich surface waters, which are not considered/resolved by the models. However, similar increases in productivity during times of reduced AMOC, related to the advection of nutrient-rich surface waters, have been reported from other midlatitude North Atlantic sites. Therefore we propose, that during times of

reduced AMOC, there has been a band of strongly increased productivity across the midlatitude North Atlantic, at the northern rim of the contracted subtropical gyre, which potentially could have counteracted the decreased organic carbon pump in the high northern latitudes.

[51] **Acknowledgments.** We thank the Editor, Rainer Zahn, and three anonymous reviewers for their suggestions, which improved the manuscript. K.-H. Baumann is thanked for useful suggestions on an earlier version of the manuscript. Thomas Blanz and Ralph Schneider are thanked for conducting alkenone measurements on core MD08–3180Cq. B. Danniellou and IFREMER are acknowledged for providing samples of core GEOFAR KF16. U. Schuld is thanked for assisting in the SEM laboratory in the Institute of Geosciences at the CAU in Kiel. We also thank the captain and the crew as well as the shipboard party on the research vessel *Marion Dufresne* for their help during the IMAGES XVII (AMOCINT) cruise. This research was conducted in the framework of the AMOCINT project, which is part of the EUROCORES program Euro-MARC of the European Science Foundation (ESF). Financial support came from the Deutsche Forschungsgemeinschaft (DFG).

References

- Abrantes, F., H. Meggers, S. Nave, J. Bollmann, S. Palma, C. Sprengel, J. Henderiks, A. Spies, E. Salgueiro, and T. Moita (2002), Fluxes of microorganisms along a productivity gradient in the Canary Islands region (29°N): Implications for paleoreconstructions, *Deep Sea Res., Part II*, 49(17), 3599–3629, doi:10.1016/S0967-0645(02)00100-5.
- Alley, R. B., and P. U. Clark (1999), The deglaciation of the northern hemisphere: A global perspective, *Annu. Rev. Earth Planet. Sci.*, 27(1), 149–182, doi:10.1146/annurev.earth.27.1.149.
- Alves, M., F. Gaillard, M. Sparrow, M. Knoll, and S. Giraud (2002), Circulation patterns and transport of the Azores Front-Current system, *Deep Sea Res., Part II*, 49(19), 3983–4002, doi:10.1016/S0967-0645(02)00138-8.
- Andersen, K. K., et al. (2007), Greenland Ice Core Chronology 2005 (GICC05) and 20 year means of oxygen isotope data from ice core NGRIP, <http://doi.pangaea.de/10.1594/PANGAEA.586838>, PANGAEA, Network for Geol. and Environ. Data, Bremerhaven, Germany.
- Andruleit, H. (1996), A filtration technique for quantitative studies of coccoliths, *Micropaleontology*, 42(4), 403–406, doi:10.2307/1485964.
- Andruleit, H., and U. Rogalla (2002), Coccolithophores in surface sediments of the Arabian Sea in relation to environmental gradients in surface waters, *Mar. Geol.*, 186(3–4), 505–526, doi:10.1016/S0025-3227(02)00312-2.
- Barber, D., et al. (1999), Forcing of the cold event of 8,200 years ago by catastrophic drainage of Laurentide lakes, *Nature*, 400(6742), 344–348, doi:10.1038/22504.
- Bard, E., M. Arnold, J. Duprat, and J. C. Duplessy (1987), Reconstruction of the last deglaciation: Deconvolved records of $\delta^{18}\text{O}$ profiles, micropaleontological variations and accelerator mass spectrometric ^{14}C dating, *Clim. Dyn.*, 1(2), 101–112, doi:10.1007/BF01054479.
- Bard, E., F. Rostek, J.-L. Turon, and S. Gendreau (2000), Hydrological impact of Heinrich Events in the subtropical Northeast Atlantic, *Science*, 289(5483), 1321–1324, doi:10.1126/science.289.5483.1321.
- Bashmachnikov, I., V. Lafon, and A. Martins (2004), Sea surface temperature distribution in the Azores region. Part II: Space time variability and underlying mechanisms, *Arquipelago Bol. Univ. Acores Cienc. Biol. Mar.*, 21A, 19–32.
- Baumann, K.-H., B. Boeckel, and M. Frenz (2004), Coccolith contribution to South Atlantic carbonate sedimentation, in *Coccolithophores: From Molecular Processes to Global Impact*, edited by H. R. Thierstein and J. R. Young, pp. 367–403, Springer, Berlin.
- Baumann, K.-H., H. Andruleit, B. Boeckel, M. Geisen, and H. Kinkel (2005), The significance of extant coccolithophores as indicators of ocean water masses, surface water temperature, and paleoproductivity: A review, *Palaontol. Z.*, 79(1), 93–112, doi:10.1007/BF03021756.
- Baumann, K.-H., B. Boeckel, and M. Čepček (2008), Spatial distribution of living coccolithophores along an east-west transect in the subtropical South Atlantic, *J. Nanoplankton Res.*, 30(1), 9–21.
- Beaufort, L., Y. Lancelot, P. Camberlin, O. Cayre, E. Vincent, F. Bassinot, and L. Labeyrie (1997), Insolation cycles as a major control of equatorial Indian Ocean primary production, *Science*, 278(5342), 1451–1454, doi:10.1126/science.278.5342.1451.
- Beckmann, W., A. Auras, and C. Hemleben (1987), Cyclonic cold-core eddy in the eastern North Atlantic. 3. Zooplankton, *Mar. Ecol. Prog. Ser.*, 39(2), 165–173, doi:10.3354/meps039165.
- Behrenfeld, M. J., R. T. O'Malley, D. A. Siegel, C. R. McClain, J. L. Sarmiento, G. C. Feldman, A. J. Milligan, P. G. Falkowski, R. M. Letelier, and E. S. Boss

- (2006), Climate-driven trends in contemporary ocean productivity, *Nature*, 444(7120), 752–755, doi:10.1038/nature05317.
- Benson, L., J. Burdett, S. Lund, M. Kashgarian, and S. Mensing (1997), Nearly synchronous climate change in the Northern Hemisphere during the last glacial termination, *Nature*, 388(6639), 263–265, doi:10.1038/40838.
- Boeckel, B., and K.-H. Baumann (2004), Distribution of coccoliths in surface sediments of the southeastern South Atlantic Ocean: Ecology, preservation and carbonate contribution, *Mar. Micropaleontol.*, 51(3–4), 301–320, doi:10.1016/j.marmicro.2004.01.001.
- Boeckel, B., K.-H. Baumann, R. Henrich, and H. Kinkel (2006), Coccolith distribution patterns in South Atlantic and Southern Ocean surface sediments in relation to environmental gradients, *Deep Sea Res., Part I*, 53(6), 1073–1099, doi:10.1016/j.dsr.2005.11.006.
- Bond, G., W. Showers, M. Cheseby, R. Lotti, P. Almasi, P. deMenocal, P. Priore, H. Cullen, I. Hajdas, and G. Bonani (1997), A pervasive millennial-scale cycle in North Atlantic Holocene and glacial climates, *Science*, 278(5341), 1257–1266, doi:10.1126/science.278.5341.1257.
- Brand, L. E. (1994), Physiological ecology of marine coccolithophores, in *Coccolithophores*, edited by A. Winter and W. Siesser, pp. 39–49, Cambridge Univ. Press, Cambridge, U. K.
- Brassell, S., G. Eglinton, I. T. Marlowe, U. Pflaumann, and M. Sarnthein (1986), Molecular stratigraphy: A new tool for climatic assessment, *Nature*, 320(6058), 129–133, doi:10.1038/320129a0.
- Brovkin, V., J. Bendtsen, M. Claussen, A. Ganopolski, C. Kubatzki, V. Petoukhov, and A. Andreev (2002), Carbon cycle, vegetation and climate dynamics in the Holocene: Experiments with the CLIMBER-2 model, *Global Biogeochem. Cycles*, 16(4), 1139, doi:10.1029/2001GB001662.
- Chapman, M., and N. Shackleton (1998), Millennial-scale fluctuations in North Atlantic heat flux during the last 150,000 years, *Earth Planet. Sci. Lett.*, 159(1–2), 57–70, doi:10.1016/S0012-821X(98)00068-5.
- Chapman, M., N. Shackleton, and J. Duplessy (2000), Sea surface temperature variability during the last glacial-interglacial cycle: Assessing the magnitude and pattern of climate change in the North Atlantic, *Palaeogeogr. Palaeoclimatol. Palaeoecol.*, 157(1–2), 1–25, doi:10.1016/S0031-0182(99)00168-6.
- Clark, P. U., S. J. Marshall, G. K. C. Clarke, S. W. Hostetler, J. M. Licciardi, and J. T. Teller (2001), Freshwater forcing of abrupt climate change during the last glaciation, *Science*, 293(5528), 283–287, doi:10.1126/science.1062517.
- Condron, A., and P. Winsor (2011), A subtropical fate awaited freshwater discharged from glacial Lake Agassiz, *Geophys. Res. Lett.*, 38, L03705, doi:10.1029/2010GL046011.
- Crowley, T. J. (1983), Calcium-carbonate preservation patterns in the central North Atlantic during the last 150,000 years, *Mar. Geol.*, 51(1–2), 1–14, doi:10.1016/0025-3227(83)90085-3.
- Dymond, J., E. Suess, and L. Lyle (1992), Barium in deep-sea sediment: A geochemical proxy for paleoproductivity, *Paleoceanography*, 7(2), 163–181, doi:10.1029/92PA00181.
- Ellison, C. R. W., M. R. Chapman, and I. R. Hall (2006), Surface and deep ocean interactions during the cold climate event 8200 years ago, *Science*, 312(5782), 1929–1932, doi:10.1126/science.1127213.
- Emerson, S., P. Quay, D. Karl, C. Winn, L. Tupas, and M. Landry (1997), Experimental determination of the organic carbon flux from open-ocean surface waters, *Nature*, 389(6654), 951–954, doi:10.1038/40111.
- Etourneau, J., R. Schneider, T. Blanz, and P. Martinez (2010), Intensification of the Walker and Hadley atmospheric circulations during the Pliocene–Pleistocene climate transition, *Earth Planet. Sci. Lett.*, 297(1–2), 103–110, doi:10.1016/j.epsl.2010.06.010.
- Falkowski, P. (2000), The global carbon cycle: A test of our knowledge of Earth as a system, *Science*, 290(5490), 291–296, doi:10.1126/science.290.5490.291.
- Field, C. B., M. Behrenfeld, J. T. Randerson, and P. Falkowski (1998), Primary production of the biosphere: Integrating terrestrial and oceanic components, *Science*, 281(5374), 237–240, doi:10.1126/science.281.5374.237.
- Findlay, C., and J. Giraudeau (2002), Movement of oceanic fronts south of Australia during the last 10 ka: Interpretation of calcareous nannoplankton in surface sediments from the Southern Ocean, *Mar. Micropaleontol.*, 46(3–4), 431–444, doi:10.1016/S0377-8398(02)00084-1.
- Flores, J., M. Bárcena, and F. Sierro (2000), Ocean-surface and wind dynamics in the Atlantic Ocean off Northwest Africa during the last 140 000 years, *Palaeogeogr. Palaeoclimatol. Palaeoecol.*, 161(3–4), 459–478, doi:10.1016/S0031-0182(00)00099-7.
- Flower, B. P., D. W. Hastings, H. W. Hill, and T. M. Quinn (2004), Phasing of deglacial warming and Laurentide Ice Sheet meltwater in the Gulf of Mexico, *Geology*, 32(7), 597, doi:10.1130/G20604.1.
- Ganssen, G. M., and D. Kroon (2000), The isotopic signature of planktonic foraminifera from NE Atlantic surface sediments: Implications for the reconstruction of past oceanic conditions, *J. Geol. Soc.*, 157(3), 693–699, doi:10.1144/jgs.157.3.693.
- Gil, I. M., L. D. Keigwin, and F. G. Abrantes (2009), Deglacial diatom productivity and surface ocean properties over the Bermuda Rise, northeast Sargasso Sea, *Paleoceanography*, 24(4), PA4101, doi:10.1029/2008PA001729.
- Gingele, F. X., M. Zabel, S. Kasten, W. J. Bonn, and C. C. Nürnberg (1999), Biogenic barium as a proxy for paleoproductivity: Methods and limitations of application, in *Use of Proxies in Paleoceanography*, edited by G. Fischer and G. Wefer, pp. 345–364, Springer, Berlin, doi:10.1007/978-3-642-58646-0_13.
- Giraudeau, J., M. Grélaud, S. Solignac, J. T. Andrews, M. Moros, and E. Jansen (2010), Millennial-scale variability in Atlantic water advection to the Nordic Seas derived from Holocene coccolith concentration records, *Quat. Sci. Rev.*, 29(9–10), 1276–1287, doi:10.1016/j.quascirev.2010.02.014.
- Gould, W. J. (1985), Physical oceanography of the Azores Front, *Prog. Oceanogr.*, 14, 167–190, doi:10.1016/0079-6611(85)90010-2.
- Haidar, A., and H. Thierstein (2001), Coccolithophore dynamics off Bermuda (N. Atlantic), *Deep Sea Res., Part II*, 48(8–9), 1925–1956, doi:10.1016/S0967-0645(00)00169-7.
- Hass, H. C., et al. (2001), The potential of synoptic plankton analyses for paleoclimatic investigations: Five plankton groups from the Holocene Nordic Seas, in *The Northern North Atlantic: A Changing Environment*, edited by P. Schaefer et al., pp. 291–318, Springer, Berlin, doi:10.1007/978-3-642-56876-3_18.
- Hernández-León, S., M. Gómez, and J. Aristegui (2007), Mesozooplankton in the Canary Current System: The coastal-ocean transition zone, *Prog. Oceanogr.*, 74(2–3), 397–421, doi:10.1016/j.pocean.2007.04.010.
- Incarbona, A., P. Ziveri, N. Sabatino, D. Salvaggio Manta, and M. Sprovieri (2011), Conflicting coccolithophore and geochemical evidence for productivity levels in the Eastern Mediterranean sapropel S1, *Mar. Micropaleontol.*, 81(3–4), 131–143, doi:10.1016/j.marmicro.2011.09.003.
- Intergovernmental Panel on Climate Change (2007), Summary for Policymakers, in *Climate Change 2007: The Physical Science Basis. Contribution of Working Group I to the Fourth Assessment Report of the Intergovernmental Panel on Climate Change*, edited by S. Solomon et al., pp. 1–18, Cambridge Univ. Press, New York.
- Jia, Y. (2000), Formation of an Azores Current due to Mediterranean overflow in a modeling study of the North Atlantic, *J. Phys. Oceanogr.*, 30(9), 2342–2358, doi:10.1175/1520-0485(2000)030<2342:FOAACD>2.0.CO;2.
- Jimenez-Espejo, F. J., F. Martinez-Ruiz, T. Sakamoto, K. Iijima, D. Gallego-Torres, and N. Harada (2007), Paleoenvironmental changes in the western Mediterranean since the last glacial maximum: High resolution multiproxy record from the Alegro-Balearic basin, *Palaeogeogr. Palaeoclimatol. Palaeoecol.*, 246(2–4), 292–306, doi:10.1016/j.palaeo.2006.10.005.
- Jordan, R. W. (1988), Coccolithophorid communities in the North East Atlantic, PhD thesis, Univ. of Surrey, Guildford, U. K.
- Käse, R., and G. Siedler (1982), Meandering of the subtropical front southeast of the Azores, *Nature*, 300(5889), 245–246, doi:10.1038/300245a0.
- Kiefer, T., F. Abrantes, M. Sarnthein, M. Weinelt, and L. Labeyrie (1995), Prominent productivity spikes in the subtropical North Atlantic parallel Heinrich meltwater events, paper presented at the 5th International Conference on Paleoceanography, PAGES, Halifax, N. S., Canada.
- Kielmann, J., and R. Käse (1987), Numerical modeling of meander and eddy formation in the Azores Current frontal zone, *J. Phys. Oceanogr.*, 17(4), 529–541, doi:10.1175/1520-0485(1987)017<0529:NMOMAE>2.0.CO;2.
- Kinkel, H., K.-H. Baumann, and M. Čepek (2000), Coccolithophores in the equatorial Atlantic Ocean: Response to seasonal and Late Quaternary surface water variability, *Mar. Micropaleontol.*, 39(1–4), 87–112, doi:10.1016/S0377-8398(00)00016-5.
- Kissel, C., H. Kleiven, and X. Morin, and the Scientific Shipboard Party (2008), MD168-AMOCINT/XVII IMAGES cruise report, *Rep. OCE/2008/02*, Inst. Polaire Fr., Plouzané, France.
- Klein, B., and G. Siedler (1989), On the origin of the Azores Current, *J. Geophys. Res.*, 94(C5), 6159–6168, doi:10.1029/JC094iC05p06159.
- Kleiven, H. F., C. Kissel, C. Laj, U. S. Ninnemann, T. O. Richter, and E. Cortijo (2008), Reduced North Atlantic Deep Water coeval with the Glacial Lake Agassiz freshwater outburst, *Science*, 319(5859), 60–64, doi:10.1126/science.1148924.
- Kohfeld, K. E., C. L. Quéré, S. P. Harrison, and R. F. Anderson (2005), Role of marine biology in glacial-interglacial CO₂ cycles, *Science*, 308(5718), 74–78, doi:10.1126/science.1105375.
- Kupferman, S., G. A. Becker, W. F. Simmons, U. Schauer, M. G. Marietta, and H. Nies (1986), An intense cold core eddy in the North-East Atlantic, *Nature*, 319(6053), 474–477, doi:10.1038/319474a0.
- Lebreiro, S. M., J. C. Moreno, F. F. Abrantes, and U. Pflaumann (1997), Productivity and paleoceanographic implications on Tore Seamount

- (Iberian Margin) during the last 225 kyr: Foraminiferal evidence, *Paleoceanography*, 12(5), 718–727, doi:10.1029/97PA01748.
- Leduc, G., R. Schneider, J.-H. Kim, and G. Lohmann (2010), Holocene and Eemian sea surface temperature trends as revealed by alkenone and Mg/Ca paleothermometry, *Quat. Sci. Rev.*, 29(7–8), 989–1004, doi:10.1016/j.quascirev.2010.01.004.
- Lévy, M., Y. Lehahn, J.-M. André, L. Mémerly, H. Loisel, and E. Heifetz (2005), Production regimes in the northeast Atlantic: A study based on Sea-viewing Wide Field-of-view Sensor (SeaWiFS) chlorophyll and ocean general circulation model mixed layer depth, *J. Geophys. Res.*, 110, C07S10, doi:10.1029/2004JC002771.
- Locarnini, R. A., A. V. Mishonov, J. I. Antonov, T. P. Boyer, and H. E. Garcia (2010), *World Ocean Atlas 2009*, vol. 1, *Temperature*, NOAA Atlas NESDIS, vol. 68, edited by S. Levitus, 184 pp., NOAA, Silver Spring, Md.
- Longhurst, A., S. Sathyendranath, T. Platt, and C. Caverhill (1995), An estimate of global primary production in the ocean from satellite radiometer data, *J. Plankton Res.*, 17(6), 1245–1271, doi:10.1093/plankt/17.6.1245.
- Maillard, C., and R. Käse (1989), The near-surface flow in the subtropical gyre south of the Azores, *J. Geophys. Res.*, 94(C11), 16,133–16,140, doi:10.1029/JC094iC11p16133.
- Margalef, R. (1978), Life-forms of phytoplankton as survival alternatives in an unstable environment, *Oceanol. Acta*, 1(4), 493–509.
- Mariotti, V., L. Bopp, A. Tagliabue, M. Kageyama, and D. Swingedouw (2012), Marine productivity response to Heinrich events: A model-data comparison, *Clim. Past Discuss.*, 8(1), 557–594, doi:10.5194/cpd-8-557-2012.
- McIntyre, A., and A. Bé (1967), Modern coccolithophoridae of the Atlantic ocean-I. Placoliths and cyrtoliths, *Deep Sea Res. Oceanogr. Abstr.*, 14(5), 561–597, doi:10.1016/0011-7471(67)90065-4.
- McManus, J., et al. (1998), Geochemistry of barium in marine sediments: Implications for its use as a paleoproxy, *Geochim. Cosmochim. Acta*, 62(21–22), 3453–3473, doi:10.1016/S0016-7037(98)00248-8.
- McManus, J. F., R. Francois, J.-M. Gherardi, L. D. Keigwin, and S. Brown-Leger (2004), Collapse and rapid resumption of Atlantic meridional circulation linked to deglacial climate changes, *Nature*, 428(6985), 834–837, doi:10.1038/nature02494.
- Menviel, L., A. Timmermann, A. Mouchet, and O. Timm (2008), Meridional reorganizations of marine and terrestrial productivity during Heinrich events, *Paleoceanography*, 23, PA1203, doi:10.1029/2007PA001445.
- Merico, A., T. Tyrell, E. J. Lessard, T. Oguz, P. J. Stabeno, S. I. Zeeman, and T. E. Whitledge (2004), Modelling phytoplankton succession on the Bering Sea shelf: Role of climate influences and tropic interactions in generating *Emiliania huxleyi* blooms 1997–2000, *Deep Sea Res., Part I*, 51(12), 1803–1826, doi:10.1016/j.dsr.2004.07.003.
- Molfino, B., and A. McIntyre (1990a), Nutricline variation in the equatorial Atlantic coincident with the Younger Dryas, *Paleoceanography*, 5(6), 997–1008, doi:10.1029/PA005i006p00997.
- Molfino, B., and A. McIntyre (1990b), Precessional forcing of nutricline dynamics in the equatorial Atlantic, *Science*, 249(4970), 766–769, doi:10.1126/science.249.4970.766.
- Mouriño-Carballido, B., and S. Neuer (2008), Eddy pumping in the North Atlantic subtropical gyre, *Oceanography*, 21(2), 52–61, doi:10.5670/oceanog.2008.53.
- Müller, P., G. Kirst, G. Ruhland, I. von Storch, and A. Rosell-Melé (1998), Calibration of the alkenone paleotemperature index UK'37 based on core-tops from the eastern South Atlantic and the global ocean (60°N–60°S), *Geochim. Cosmochim. Acta*, 62(10), 1757–1772, doi:10.1016/S0016-7037(98)00097-0.
- Naafs, B., J. Heftler, G. Acton, G. H. Haug, A. Martínez-García, R. Pancost, and R. Stein (2010), Strengthening of North American dust sources during the late Pliocene (2.7 Ma), *Earth Planet. Sci. Lett.*, 317–318(8–9), 1–12, doi:10.1016/j.epsl.2011.11.026.
- Nave, S., L. Labeyrie, J. Gheradi, N. Caillon, E. Cortijo, C. Kissel, and F. Abrantes (2007), Primary productivity response to Heinrich events in the North Atlantic Ocean and Norwegian Sea, *Paleoceanography*, 22, PA3216, doi:10.1029/2006PA001335.
- Nebout, N. C., J. L. Turon, R. Zahn, L. Capotondi, L. Londeix, and K. Pahnke (2002), Enhanced aridity and atmospheric high-pressure stability over the western Mediterranean during the North Atlantic cold events of the past 50 kyr, *Geology*, 30(10), 863–866, doi:10.1130/0091-7613(2002)030<0863:EAHP>2.0.CO;2.
- Nelson, D. M., P. Tréguer, M. A. Brzezinski, A. Leynaert, and B. Quéguiner (1995), Production and dissolution of biogenic silica in the ocean—revised global estimates, comparison with regional data and relationship to biogenic sedimentation, *Global Biogeochem. Cycles*, 9(3), 359–372, doi:10.1029/95GB01070.
- Okada, H., and S. Honjo (1973), The distribution of oceanic coccolithophorids in the Pacific, *Deep Sea Res.*, 20, 355–374, doi:10.1016/0011-7471(73)90059-4.
- Okada, H., and A. McIntyre (1979), Seasonal distribution of modern coccolithophores in the western North Atlantic Ocean, *Mar. Biol. Berlin*, 54(4), 319–328, doi:10.1007/BF00395438.
- Okada, H., and P. Wells (1997), Late Quaternary nannofossil indicators of climate change in two deep-sea cores associated with the Leeuwin Current off Western Australia, *Palaeogeogr. Palaeoclimatol. Palaeoecol.*, 131(3–4), 413–432, doi:10.1016/S0031-0182(97)00014-X.
- Ottens, J. J. (1991), Planktic foraminifera as North Atlantic water mass indicators, *Oceanol. Acta*, 14(2), 123–140.
- Penaud, A., F. Eynaud, A. Voelker, F. Marret, J. L. Turon, L. Rossignol, and T. Mulder (2011), Hydrological processes affecting the subtropical NE Atlantic (34–38°N) over the last 30 ka: evidence from phyto- and zooplankton assemblages, *Biogeosciences Discuss.*, 8(2), 2281–2327, doi:10.5194/bgd-8-2281-2011.
- Pingree, R., Y.-H. Kuo, and C. Garcia-Soto (2002), Can the Subtropical North Atlantic permanent thermocline be observed from space?, *J. Mar. Biol. Assoc. U. K.*, 82(5), 709–728, doi:10.1017/S0025315402006094.
- Piotrowski, A. M., S. L. Goldstein, S. R. Hemming, and R. G. Fairbanks (2004), Intensification and variability of ocean thermohaline circulation through the last deglaciation, *Earth Planet. Sci. Lett.*, 225, 205–220, doi:10.1016/j.epsl.2004.06.002.
- Plewa, K., H. Meggers, and S. Kasten (2006), Barium in sediments off northwest Africa: A tracer for paleoproductivity or meltwater events?, *Paleoceanography*, 21, PA2015, doi:10.1029/2005PA001136.
- Polovina, J. J., E. A. Howell, and M. Abecassis (2008), Ocean's least productive waters are expanding, *Geophys. Res. Lett.*, 35, L03618, doi:10.1029/2007GL031745.
- Reimer, P. J., et al. (2009), IntCal09 and Marine09 radiocarbon age calibration curves, 0–50,000 years cal BP, *Radiocarbon*, 51(4), 1111–1150.
- Richter, T. (1998), Sedimentary fluxes at the Mid-Atlantic Ridge: Sediment sources, accumulation rates, and geochemical characterization, *GEOMAR Rep. 73*, GEOMAR Res. Cent. for Mar. Geosci., Christian Albrechts Univ., Kiel, Germany.
- Rodrigo-Gámiz, M., F. Martínez-Ruiz, F. J. Jiménez-Espejo, D. Gallego-Torres, V. Nieto-Moreno, O. Romero, and D. Ariztegui (2011), Impact of climate variability in the western Mediterranean during the last 20,000 years: Oceanic and atmospheric responses, *Quat. Sci. Rev.*, 30, 2018–2034, doi:10.1016/j.quascirev.2011.05.011.
- Rogerson, M., E. J. Rohling, P. P. E. Weaver, and J. W. Murray (2004), The Azores Front since the Last Glacial Maximum, *Earth Planet. Sci. Lett.*, 223(3–4), 779–789, doi:10.1016/j.epsl.2004.03.039.
- Romero, O. E., C. B. Lange, G. Fischer, U. F. Treppke, and G. Wefer (1999), Variability in export production documented by downward fluxes and species composition or marine planktic diatoms: Observations from the tropical and equatorial Atlantic, in *Use of Proxies in Paleoceanography*, edited by G. Fischer and G. Wefer, pp. 365–392, Springer, Berlin, doi:10.1007/978-3-642-58646-0_14.
- Ruddiman, W., and L. Glover (1975), Subpolar North Atlantic circulation at 9300 yr BB: Faunal evidence, *Quat. Res.*, 5(3), 361–389, doi:10.1016/0033-5894(75)90038-1.
- Rühlemann, C., P. J. Müller, and R. R. Schneider (1999), Organic carbon and carbonate as paleoproductivity proxies: Examples from high and low productivity areas of the tropical Atlantic, in *Use of Proxies in Paleoceanography*, edited by G. Fischer and G. Wefer, pp. 315–344, Springer, Berlin, doi:10.1007/978-3-642-58646-0_12.
- Saavedra-Pellitero, M., J. A. Flores, F. Lamy, F. J. Sierro, and A. Cortina (2011), Coccolithophore estimates of paleotemperature and paleoproductivity changes in the southeast Pacific over the past ~27 kyr, *Paleoceanography*, 26, PA1201, doi:10.1029/2009PA001824.
- Salgueiro, E., A. H. L. Voelker, L. de Abreu, F. Abrantes, H. Meggers, and G. Wefer (2010), Temperature and productivity changes off the western Iberian margin during the last 150 kyr, *Quat. Sci. Rev.*, 29(5–6), 680–695, doi:10.1016/j.quascirev.2009.11.013.
- Samtleben, C., and A. Schröder (1992), Living coccolithophore communities in the Norwegian-Greenland Sea and their record in sediments, *Mar. Micropaleontol.*, 19(4), 333–354, doi:10.1016/0377-8398(92)90037-K.
- Sarmiento, J., and U. Siegenthaler (1992), New production and the global carbon cycle, in *Primary Productivity and Biogeochemical Cycles in the Sea*, edited by P. G. Falkowski and A. D. Woodhead, pp. 316–317, Plenum Press, New York.
- Sarnthein, M., K. Winn, J. C. Duplessy, and M. R. Fontugne (1988), Global variations of surface ocean productivity in low and mid latitudes: Influence on CO₂ reservoirs of the deep ocean and atmosphere during the last

- 21,000 years, *Paleoceanography*, 3(3), 361–399, doi:10.1029/PA003i003p00361.
- Sarnthein, M., et al. (2001), Fundamental Modes and Abrupt Changes in North Atlantic Circulation and Climate over the last 60 ky—Concepts, Reconstruction and Numerical Modeling, in *The Northern North Atlantic: A Changing Environment*, edited by P. Schaefer et al., pp. 365–410, Springer, Berlin, doi:10.1007/978-3-642-56876-3_21.
- Schiebel, R., B. Schmuker, M. Alves, and C. Hemleben (2002a), Tracking the Recent and late Pleistocene Azores front by the distribution of planktic foraminifers, *J. Mar. Syst.*, 37(1–3), 213–227, doi:10.1016/S0924-7963(02)00203-8.
- Schiebel, R., J. Wanick, A. Zeltner, and M. Alves (2002b), Impact of the Azores Front on the distribution of planktic foraminifers, shelled gastropods, and coccolithophorids, *Deep Sea Res., Part II*, 49(19), 4035–4050, doi:10.1016/S0967-0645(02)00141-8.
- Schiebel, R., U. Brupbacher, S. Schmidtke, G. Nausch, J. J. Wanick, and H.-R. Thierstein (2011), Spring coccolithophore production and dispersion in the temperate eastern North Atlantic Ocean, *J. Geophys. Res.*, 116, C08030, doi:10.1029/2010JC006841.
- Schmittner, A. (2005), Decline of the marine ecosystem caused by a reduction in the Atlantic Overturning Circulation, *Nature*, 434(7033), 628–633, doi:10.1038/nature03476.
- Schneider, B., G. Leduc, and W. Park (2010), Disentangling seasonal signals in Holocene climate trends by satellite-model-proxy integration, *Paleoceanography*, 25(4), PA4217, doi:10.1029/2009PA001893.
- Schwarz, J. N., and M. P. Schodlok (2009), Impact of drifting icebergs on surface phytoplankton biomass in the Southern Ocean: Ocean colour remote sensing and in situ iceberg tracking, *Deep Sea Res., Part I*, 56(10), 1727–1741, doi:10.1016/j.dsr.2009.05.003.
- Skinner, L. C., and I. N. McCave (2003), Analysis and modeling of gravity- and piston coring based on soil mechanics, *Mar. Geol.*, 199(1–2), 181–204, doi:10.1016/S0025-3227(03)00127-0.
- Sprengel, C., K.-H. Baumann, J. Henderiks, R. Henrich, and S. Neuer (2002), Modern coccolithophore and carbonate sedimentation along a productivity gradient in the Canary Islands region: Seasonal export production and surface accumulation rates, *Deep Sea Res., Part II*, 49(17), 3577–3598, doi:10.1016/S0967-0645(02)00099-1.
- Stolz, K., and K.-H. Baumann (2010), Changes in paleoceanography and paleoecology during Marine Isotope Stage (MIS) 5 in the eastern North Atlantic (ODP Site 980) deduced from calcareous nannoplankton observations, *Palaeogeogr. Palaeoclimatol. Palaeoecol.*, 292(1–2), 295–305, doi:10.1016/j.palaeo.2010.04.002.
- Stuiver, M., and P. J. Reimer (1986), A computer program for radiocarbon age calibration, *Radiocarbon*, 28(2B), 1022–1030.
- Teller, J. T., and D. W. Leverington (2004), Glacial Lake Agassiz: A 5000 yr history of change and its relationship to the $\delta^{18}\text{O}$ record of Greenland, *Geol. Soc. Am. Bull.*, 116(5), 729–742, doi:10.1130/B25316.1.
- The Ring Group (1981), Gulf Stream cold-core rings: Their physics, chemistry, and biology, *Science*, 212, 1091–1100, doi:10.1126/science.212.4499.1091.
- Thornalley, D. J. R., I. N. McCave, and H. Elderfield (2010), Freshwater input and abrupt deglacial climate change in the North Atlantic, *Paleoceanography*, 25, PA1201, doi:10.1029/2009PA001772.
- Tréguer, P., D. M. Nelson, A. J. Van Bennekom, D. J. DeMaster, A. Leynaert, and B. Quéguiner (1995), The silica balance in the world ocean: A reestimate, *Science*, 268(5209), 375–379, doi:10.1126/science.268.5209.375.
- Villanueva, J., J. O. Grimalt, E. Cortijo, L. Vidal, and L. Labeyrie (1997), A biomarker approach to the organic matter deposited in the North Atlantic during the last climatic cycle, *Geochim. Cosmochim. Acta*, 61(21), 4633–4646, doi:10.1016/S0016-7037(97)83123-7.
- Voelker, A. H. L., S. M. Lebreiro, J. Schoenfeld, I. Cacho, H. Erlenkeuser, and F. Abrantes (2006), Mediterranean outflow strengthening during northern hemisphere coolings: A salt source for the glacial Atlantic?, *Earth Planet. Sci. Lett.*, 245(1–2), 39–55, doi:10.1016/j.epsl.2006.03.014.
- Volkov, D. L., and L.-L. Fu (2010), On the reasons for the formation and variability of the Azores Current, *J. Phys. Oceanogr.*, 40(10), 2197–2220, doi:10.1175/2010JPO4326.1.
- Volkov, D. L., and L.-L. Fu (2011), Interannual variability of the Azores Current strength and eddy energy in relation to atmospheric forcing, *J. Geophys. Res.*, 116, C11011, doi:10.1029/2011JC007271.
- Waelbroeck, C., J. C. Duplessy, E. Michel, L. Labeyrie, D. Paillard, and J. Duprat (2001), The timing of the last deglaciation in North Atlantic climate records, *Nature*, 414, 724–727, doi:10.1038/35089060.
- Wiersma, A. P., and J. I. Jongma (2010), A role for icebergs in the 8.2 ka climate event, *Clim. Dyn.*, 35, 535–549, doi:10.1007/s00382-009-0645-1.
- Young, J., M. Geisen, L. Cros, A. Kleijne, C. Sprengel, I. Probert, and J. Østergaard (2003), A guide to extant coccolithophore taxonomy, *J. Nannoplankton Res., Spec. Issue*, 1, 125 pp.
- Ziveri, P., K.-H. Baumann, B. Boeckel, J. Bollmann, and J. Young (2004), Biogeography of selected Holocene coccoliths in the Atlantic Ocean, in *Coccolithophores: From Molecular Processes to Global Impact*, edited by H. R. Thierstein and J. R. Young, pp. 403–429, Springer, Berlin.

6 Coccolithophore paleoproductivity and ecology response to deglacial and Holocene changes in the Azores Current System

6.1 Comment on Chapter 6

The approach of C. Schwab study to use changes in the abundance of marine species to reconstruct changes in the Azores hydrography is the same approach as used in my study, with the difference of the used species. With this study C. Schwab showed that the STG boundary was displaced southward during the last deglacial cold events. These results corroborate my own results.

The close match between distribution patterns of the subtropical and transitional coccolithophore and foraminifera species indicates that offsets between both species due to bioturbation and lateral transport that affect the different grain size fraction of the core in different ways can be neglected.

Furthermore explains C. Schwab detailed the interaction between the wind patterns and the position of the AC current. This reconstruction is only very briefly repeated in my own study.

Furthermore coincides the stabilization of the records after 6 ka BP well with the stabilization of a modern surface and deepwater circulation as obtained in my results. This strengthens the argument that the onset of modern LSW production in the Mid- Holocene led to the establishment of the modern circulation pattern.

Chapter 7

Deglacial and early Holocene evolution of deepwater composition in the Eastern North Atlantic Basin

This chapter corresponds to an article to be submitted to EPSL with me as leading author and the co-authors Mara Weinelt, Nils Andersen, Dieter Garbe-Schönberg and Ralph Schneider

7 Deglacial and early Holocene evolution of deepwater composition in the Eastern North Atlantic Basin

7.1 Key points

- Deglacial deepwater temperature reconstructions from eastern NA basin
- Eastern NA basin deepwater evolution governed by a Northern source
- Deglacial changes in NA deepwater source composition
- Deglacial deepwater stratification changes probably triggered in NH

7.2 Abstract

Over the last decades extensive research has been carried out on changes in the Atlantic Meridional Overturning Circulation (AMOC) and its role for the last deglaciation. At present, only a few high-resolution data sets from the deep eastern North Atlantic (NA) exist for this period. It therefore remains uncertain whether deepwater changes in the Eastern North Atlantic Basin (ENAB) were governed by alternating contributions of northern and southern deepwater or whether the ENAB reflects changes in the initial composition and source of the NA deepwater. Furthermore, it is still debated whether such changes are triggered by northern or Southern Hemisphere climatic changes. In this centennial to decadal scale resolution study we investigate deepwater composition changes in the eastern NA basin over the last 15 ka BP. We used sediment cores GEOFAR KF16 and MD08-3180 (37.984°N; 31.118°W, wd. 3050 m/37.999°N; 31.134°W, wd 3064 m) obtained from a small basin at the eastern flank of the Mid Atlantic Ridge (MAR) south of the Azores Islands. Under modern conditions the coring site is situated at the boundary between southern Lower Deep Water (LDW) and northern North East Atlantic Deep Water (NEADW) consisting of Iceland Scotland Overflow Water (ISOW) and Labrador Sea Water (LSW). Distinct differences between the three water masses in terms of ventilation state, temperature and salinity signatures are ideal to track changes in the deglacial NA deepwater distribution using paired benthic foraminifera stable isotope ($\delta^{13}\text{C}$, $\delta^{18}\text{O}$) and Mg/Ca bottom water temperature (BWT) reconstructions.

The results show a close coupling of low BWT (1.5°C) and $\delta^{13}\text{C}$ (0-0.5‰) values during cold Heinrich event 1 (H1), the Younger Dryas (YD) and the Preboreal (PB), that went along with major freshening of the deepwater. The strong similarity between subtropical eastern NA deepwater and subpolar NA surface and deepwater changes indicate that the deglacial changes in the eastern NA deepwater distribution were triggered in the NA. In consequence this would imply that the NA changes contributed even to deglacial changes in the Antarctic bottom water composition. During early Holocene stepwise increasing $\delta^{13}\text{C}$ values suggest increasing NEADW production with minor but distinct interruptions (at 10.8, 10.6, 9.1, 8.4, 8.1 and 7.2 ka BP), that are most probably also triggered in the subpolar NA.

7.3 Introduction

The Atlantic Meridional Overturning Circulation (AMOC) governs the North Atlantic (NA) climate system by transporting warm and saline surface water toward the NA deepwater convection sites, where it cools, descends, and returns as deepwater flow. Changes in the AMOC strength are not only related to changes in the northward heat transport but also with severe changes in the Atlantic deepwater distribution. As the deep ocean is supposed to act as a trap for Greenhouse gases during glacial periods, the reconstruction of the deglacial changes in this system are of major interest in order to understand the feedback mechanisms of our climate system at glacial terminations [Adkins, 2013; and citations therein].

The evolution of AMOC and the Atlantic deepwater distribution have been extensively investigated during the last decades using different approaches. The classical approach using stable carbon and oxygen isotope data from benthic foraminifera [e.g. Michel *et al.*, 1995; Oppo *et al.*, 2003; Sarnthein *et al.*, 1994] with $\delta^{13}\text{C}$ as ventilation proxy, is still controversially discussed, as local productivity changes potentially cause a depletion in the $\delta^{13}\text{C}$ values incorporated in benthic foraminifera due to organic matter remineralization at depth. More recently, transects of combined $\delta^{13}\text{C}$ and $\delta^{18}\text{O}$ were used to reconstruct the deepwater sources and geometry in the Atlantic basin, including the influence of Northern Hemisphere (NH) brine water [Labeyrie *et al.*, 2005; Oppo *et al.*, 2003; Sarnthein *et al.*, 1994; Thornalley *et al.*, 2010; Waelbroeck *et al.*, 2011]. Combined benthic foraminifera Mg/Ca and stable isotope analyses were used to reconstruct bottom water temperature (BWT) changes [e.g. Marcott *et al.*, 2011; Skinner *et al.*, 2003] and to identify changes in the distribution of deepwater masses. Piotrowski *et al.* [2008], [2012] and Roberts *et al.* [2010] used the $^{143}\text{Nd}/^{144}\text{Nd}$ ratio (ϵNd) as tracer for water mass sources whereas overturning rates were reconstructed by the $^{231}\text{Pa}/^{230}\text{Th}_0$ ratios [Gherardi *et al.*, 2005; Gherardi *et al.*, 2009; Lippold *et al.*, 2012; McManus *et al.*, 2004; Roberts *et al.*, 2010]. These reconstructions suggest a dramatic reorganization of the AMOC system over the last Deglacial (19-10.5 ka BP).

Before, during the Last Glacial Maximum (LGM) (23-17.9 ka BP), the deepwater circulation was characterized by a vigorous overturning at intermediate depths (1000 to 2000 m wd), whereas deepwater renewal rates were more sluggish deeper than 2000 m [Adkins, 2013; Boyle and Keigwin, 1987; Duplessy *et al.*, 1988; Gherardi *et al.*, 2009; Lippold *et al.*, 2012; Oppo and Fairbanks, 1987; Sarnthein *et al.*, 1994]. During the Deglacial, the most drastic reduction in deepwater overturning occurred during Heinrich event 1 (H1) (17.9-14.9 ka BP), with a general decrease in overturning affecting all depth levels as inferred from $^{231}\text{Pa}/^{230}\text{Th}$ [e.g. Gherardi *et al.*, 2005; Gherardi *et al.*, 2009; McManus *et al.*, 2004]. A first strengthening in AMOC after this breakdown occurred during the Bølling-Allerød (BA) (14.9-12.9 ka BP), associated with a moderate southward water transport at all levels below 1000 m. Thereby the circulation mode was intermediate between more active LGM circulation and nearly collapsed H1 overturning [Gherardi

et al., 2009]. During the Younger Dryas (YD), the deepwater circulation decreased again including a decrease in deepwater renewal rate below 3000 m wd compared to the BA, whereas the intermediate circulation at ~2000 m wd was maintained [Gherardi *et al.*, 2009]. At the onset of the Holocene, a strengthening of AMOC probably is related to the increasing deepwater formation in the Nordic Seas [Colin *et al.*, 2010] and its southward propagation as Denmark Strait Overflow Water (DSOW) and Iceland–Scotland- Overflow Water (ISOW) that formed the major part of the North Atlantic Deep Water (NADW). This strengthening of AMOC was interrupted by several decadal to centennial scale events [Hoogakker *et al.*, 2011a; Oppo *et al.*, 2003] of which the 8.2 event with a meltwater induced AMOC reduction of about 50% was the most outstanding [Kleiven *et al.*, 2008]. The modern NA circulation started between 8 and 6 ka BP with the onset of modern Labrador Sea Water (LSW) production [Colin *et al.*, 2010; Hoogakker *et al.*, 2011a; Kissel *et al.*, 2013; Solignac *et al.*, 2004; Thornalley *et al.*, 2013] and was associated with decreases in the Overflow and NADW strength and an increase in southern Lower Deep Water (LDW) (Figure 7.1) [Hoogakker *et al.*, 2011a].

Previously it was proposed that the Deglacial cold periods H1 event and YD, considered as shallow overturning phases, were coupled with an increasing influence of southern sourced deepwater that flushed the NA basin [e.g. Gherardi *et al.*, 2005; McManus *et al.*, 2004; Meckler *et al.*, 2013; Oppo *et al.*, 2003; Sarnthein *et al.*, 1994]. In this way, a simple, two end member see-saw like pattern between the southern and northern deepwater sources was suggested [e.g. Skinner *et al.*, 2003]. More recent studies, however, indicate a more complex deepwater distribution pattern. During the H1 and the YD, the north south seesaw pattern might partially be overprinted by brine waters of NA origin [Labeyrie *et al.*, 2005; Meland *et al.*, 2008; Thornalley *et al.*, 2010; Waelbroeck *et al.*, 2011]. The latter, traced by its depleted $\delta^{13}\text{C}$ and $\delta^{18}\text{O}$ signatures within the subpolar NA, were identified in a NA N-S transect between 900 m and 2200 m water depth [Waelbroeck *et al.*, 2011]. Additionally, the comparison of ϵNd data from the eastern and western NA basins [Piotrowski *et al.*, 2012] indicates that during the YD, the deepwater composition changed in the Eastern North Atlantic Basin (ENAB) to a lesser extent than in the western basin. This pattern might be explained by a restricted southern deepwater intrusion into the ENAB. This untested hypothesis would imply that the deepwater composition in the ENAB is governed by long-term changes in NA deepwater source composition rather than by changes between the volume of northern and southern deepwater.

Changes in the deepwater source composition could be tested using BWT and salinity reconstructions using combined Mg/Ca and $\delta^{18}\text{O}$ data from benthic foraminifera, but the data coverage for the deep NA is sparse. This deficiency is due to a possible bias in the temperature signal by carbonate ion saturation changes affecting Mg/Ca in benthic foraminifera [e.g. Yu and Elderfield, 2008]. The existing reconstructions from the Iberian Margin [Skinner *et al.*, 2003]

indicate BWT of about -1.5 C during the LGM and -1°C during H1 in the deep NA and deepwater warming of $3 - 4^{\circ}\text{C}$ into the Holocene with a cold reversal to about 0°C during the YD that is associated with a freshening of the deepwater and supposed to be related to changing contributions of NADW and Antarctic Deep Water (AABW).

The reconstruction of the deglacial deepwater changes is however complicated by composition changes of the AABW. For the LGM, a colder and more saline AABW is reconstructed by increasing Southern Ocean (SO) $\delta^{18}\text{O}$ values [e.g. *Ninnemann and Charles, 2002; Waelbroeck et al., 2011*] that are corroborated by chlorinity porewater data [Adkins et al., 2002]. Adkins [2013] propose that the high glacial AABW salinity led to a strong stratification of the deep ocean and decreased mixing rates between southern and northern sourced deepwater. Over the Deglacial, the stratification changed into a thermal driven stratification with increased deepwater mixing.

Despite the concept that the deglacial NH ice sheet instability triggered the deglacial changes in the NADW composition and distribution [e.g. *Matsumoto and Yokoyama, 2013; Rahmstorf et al., 2005; Renssen et al., 2010; Van Meerbeek et al., 2011*], the detailed interaction between NADW and AABW formation remains unsolved for the Deglacial and might be a main driver of the deglacial climate change.

Within these studies uncertainties remain in the following points. The exact deglacial deepwater evolution in the ENAB remains vague. It is uncertain whether the eastern NA deepwater composition is governed by a N-S Atlantic seesaw pattern or driven mainly by changes in the NH deepwater source area. So far BWT and salinity changes within the ENAB are only reconstructed at one coring site. The impact of short term NADW weakening in the ENAB is untested. Furthermore there is an ongoing controversial discussion about N versus S forcing of deglacial climate change and the role of deepwater production in coupling of both hemispheres.

7.4 Approach

In this study we established a new decadal to centennial scale Mg/Ca BWT record using benthic epifaunal and shallow infaunal species from a deepwater site (3060 m wd) in the midlatitude ENAB (38°N ; 31.1°W) not directly influenced by boundary currents and continental meltwater runoff. The coring site is situated at the modern interface between LDW and NADW and therefore is a key site to track changes between those water masses. We used the combination of BWT estimates with benthic stable oxygen and carbon isotopes to reconstruct the deglacial evolution of BWT, ventilation and salinity, and thereby distinguish between northern versus southern deepwater sources in the ENAB. This approach is based on modern deepwater mass properties revealing temperature difference of 1.5°C between LDW and North East Atlantic Deep Water (NEADW) and 3°C between LSW and Iceland Scotland Overflow Water (ISOW) and $\delta^{13}\text{C}$ differences of 0.5‰ between LDW and NEADW (see table 1 for details) as well as salinity reconstructions using ($\delta^{18}\text{O}_{\text{sw-ice}}$). Additionally the possible influence of brine waters during cold events is assessed.

Furthermore, we discuss a mechanism that could have led to the change from salinity to temperature-governed stratification in the NA. Finally, we discuss NADW composition changes (LSW versus ISOW) for the Holocene period.

7.5 Hydrographic Setting

Hydrographically, the coring site of cores GEOFAR KF16/ MD08-3180 (37.984°N; 31.118°W, wd. 3050 m/ 37.999°N; 31.134°W, wd 3064 m) is situated at the boundary between LDW and NEADW (Figure 7.1), all water mass properties are given in Table 7.1. The modern LDW originates from AABW that enters the ENAB through the Vema Fracture Zone at 11°N [Van Aken, 2000; Van Aken and De Boer, 1995], extending northward along the eastern flank of Mid Atlantic Ridge (MAR) up to 30°N than continuing northward in an eastern intensified flow intruding into subpolar latitudes [Frew *et al.*, 2000 and citations therein]. The LDW is overlain by NEADW, which typically occupies water depths between 2.0 and 3.5 km [Van Aken, 2000; Van Aken and De Boer, 1995]. The NEADW is formed of ISOW that originates from the Greenland-Iceland-Norwegian (GIN) Seas [Hansen and Østerhus, 2000; Van Aken and De Boer, 1995]. The ISOW flows over the Iceland-Farøer-Channel into the ENAB. Thereby it entrains Subpolar Mode Water (SPMW) and a small proportion of LSW that enters the ENAB via Charlie Gibbs Fracture Zone (CGFZ) [Talley and McCartney, 1982; Curry *et al.*, 2003]. After crossing the CGFZ, a small northward branch circulates within the ENAB whereas the major part of LSW propagates southward along the MAR. Due to its relatively high temperatures and low salinities, the LSW has a lower density as NEADW and the southward branch occupies the water depth between 200 and 2200 m [Frew *et al.*, 2000; Van Sebille *et al.*, 2011]. Towards the east the Upper NADW is mixed with Mediterranean Overflow Water (MOW) that enters the ENAB via the Strait

Table 7.1: modern Atlantic water mass properties

Water mass	T [°C]	S [PSU]	$\delta^{18}\text{O}$ [‰ V-PDB]	$\delta^{13}\text{C}$ [‰ V-PDB]	citation
ISOW (modern)	0.5	34.9-35.03		1.2	ODV WOCE Atlas 2009] [Frew <i>et al.</i> , 2000] [Olsen and Ninnemann, 2010];
NEADW (modern)	2.4	34.8-34.9	0.17- 0.22	1.25	[Frew <i>et al.</i> , 2000] [Olsen and Ninnemann, 2010]
LSW (modern)	3.3-3.4	34.8-34.9	0.08- 0.12	1.25	[Curry and Oppo, 2005] [Talley and McCartney, 1981; Curry <i>et al.</i> 2003] [Frew <i>et al.</i> , 2000] [Olsen and Ninnemann, 2010]
LDW (modern)	2-3	34.9	0.1	0.8	[Frew <i>et al.</i> , 2000] [Olsen and Ninnemann, 2010]
Antarctic bottom water (AABW) (modern)	-1.5	34.63	-0.4	0.5	[Wepping <i>et al.</i> , 1996 [Frew <i>et al.</i> , 2000]] [Olsen and Ninnemann, 2010]

of Gibraltar and is found in depth between 800 and 2000 m [Curry *et al.*, 2003]. Its high salinities increase the salinity of the NADW.

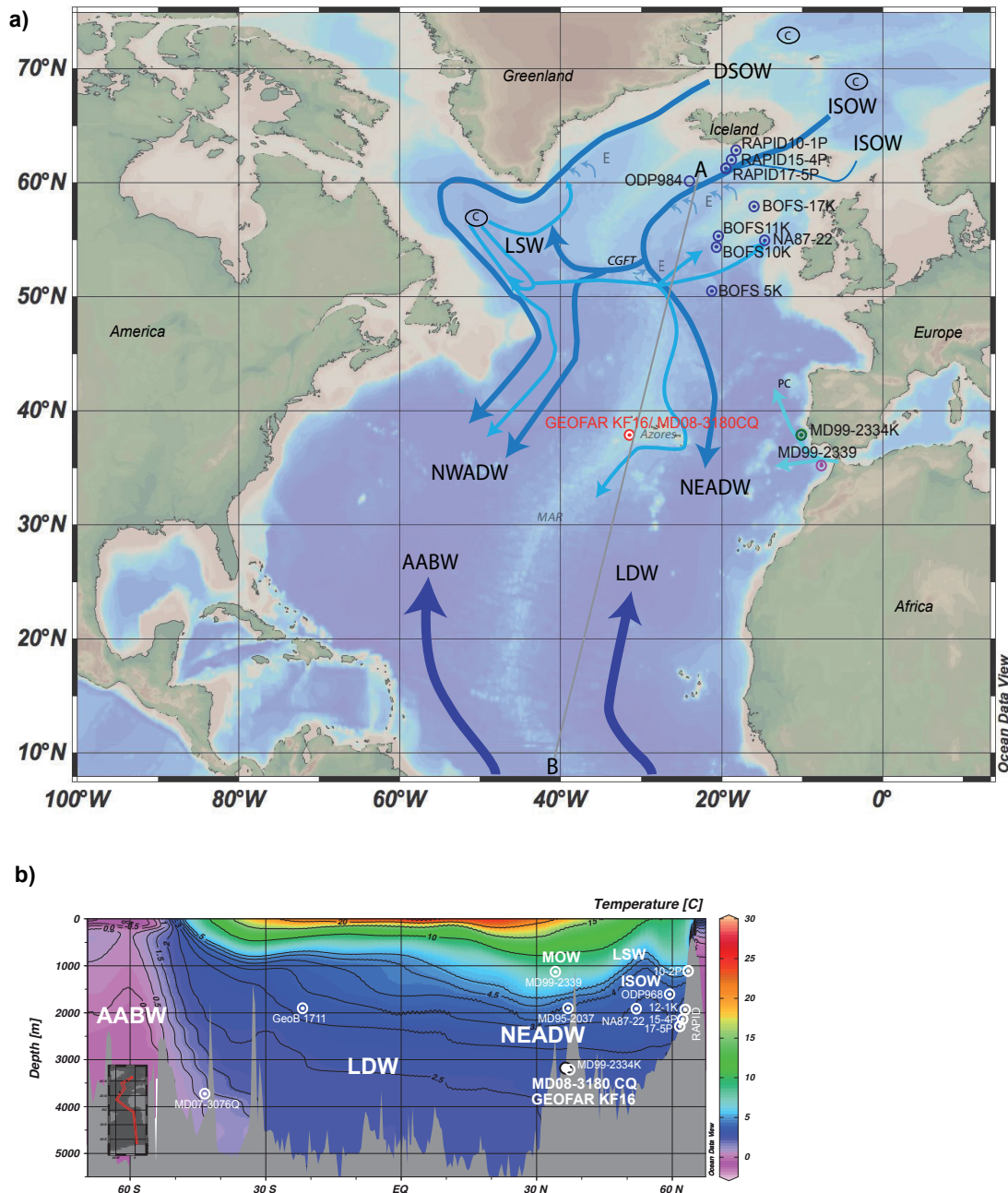


Figure 7.1 Overview of the modern deepwater hydrography at the Azores coring site (GEOFAR16/ MD08-3180) (red dot), additional cores [Skinner *et al.*, 2003; Thornalley *et al.*, 2010; Waelbroeck *et al.*, 2011; Yu *et al.*, 2008] used in this study are indicated in blue dots

a) Map with the main deepwater currents of the NA modified after Schott *et al.* [2004] supplemented with data of Van Sebille *et al.* [2011], Van Aken and deBoer [1995]

b) S-N Temperature cross section of the eastern North Atlantic basin with cores used in this study; both figures are based on Ocean Data View [Schlitzer, 2012]

Abbreviations: NAC North Atlantic Current; ISOW Iceland-Scotland Overflow Water; DSOW Denmark Strait-Overflow-Water; LSW Labrador-Sea Water; MOW Mediterranean Overflow Water; NEADW North East Atlantic Deep Water; NWADW North-West Atlantic Deep Water; LDW Lower Deep Water; AABW Antarctic Bottom Water, CGFT Charlie- Gibbs-Fracture-Zone, E Entrainment, C Deepwater convection areas

7.6 Material and Methods

7.6.1 Material

For this study spliced records from the parallel cores GEOFAR KF16 and MD08-3180CQ [Kissel *et al.*, 2008; Richter, 1998] from the mid-latitude ENAB were used. The coring site is located within a 3060 m deep small basin with steep flanks at the eastern flank of the MAR. At the site high sedimentation rates of 10 to 70 cm/ka result from sediment focusing. The cores were sampled in 1 cm intervals over the Mid to Late Holocene (50-200 cm core depth in core GEOFAR KF16), 2 cm intervals at the Younger Dryas (YD) section, (150-250 cm core depth in core MD08-3180CQ), and at 5 cm intervals over the BA and termination 1A sections (250-395 cm core depth in core MD08-3180CQ) All sediment samples were freeze dried, washed over a 63 μm sieve and the residual oven-dried at 40°C and subsequently processed as described below.

The age model of Schwab *et al.* [2012] is used, that is based on 14 $\Delta^{14}\text{C}$ AMS dates and further refined by fine tuning with NGRIP [Andersen *et al.*, 2006] using stable isotope records of planktonic foraminifera and U^{K}_{37} based SST. According to this age model, the stacked record provides a decadal resolution over the YD and the early Holocene, and multi-decadal resolution over the BA.

7.6.2 Methods

7.6.3 Stable isotopes

For stable isotope analyses monospecific samples of benthic foraminifera were handpicked, cracked, ethanol cleaned, decanted and dried at 40°C. For the stable isotope records spliced benthic species *M. affinis* and *C. wuellerstorfi* in the size fraction $>250 \mu\text{m}$ were used. All stable isotope analyses were carried out at the Leibniz Laboratory for Radiometric Dating and Stable Isotope Research in Kiel using a Finnigan MAT 253 mass spectrometer coupled with a Kiel IV carbonate preparation device and calibrated to the V-PDB scale. This V-PDB scale is applied to all $\delta^{18}\text{O}_{\text{CaCO}_3}$ analyses whereas $\delta^{18}\text{O}_{\text{sw}}$ reconstructions are referenced to Standard Mean Ocean Water (SMOW). The analytic precision is better than 0.1‰ for $\delta^{18}\text{O}$ and better than 0.05‰ for $\delta^{13}\text{C}$, replicate measurements of 10 samples gave a 2σ standard deviation of 0.18‰ for $\delta^{18}\text{O}$ and 0.15‰ for $\delta^{13}\text{C}$ analyses. The $\delta^{18}\text{O}$ record *C. wuellerstorfi* was corrected for +0.64‰ to match the offset to *Uvigerina sp.*, the species considered to calcify in equilibrium with the ambient seawater [Duplessy *et al.*, 1984; Shackleton and Opdyke, 1973]. The $\delta^{18}\text{O}$ record of *M. affinis* was corrected for +0.48‰. This correction has been calculated using 7 paired measurements of *C. wuellerstorfi* and *M. affinis* and lies within the range of offsets (0.4‰) observed for *Melonis barleanum* vs *Uvigerina sp.* [Curry and Oppo, 2005; Hoogakker *et al.*, 2011b; Jansen *et al.*, 1988]. For the YD interval the

$\delta^{13}\text{C}$ signal of *M. affinis* was corrected for a constant offset of +1.39‰ (with error of stddev 0.26‰) to match *C. wuellerstorfi* as obtained from 7 double measurements assuming that *M. affinis* did not migrate within the sediment and is not affected by pore water chemistry over the YD interval.

7.6.4 Mg/Ca BWT reconstructions

Monospecific samples of 11-52 *M. affinis*, *M. barleanum* (size fraction 250-400 μm) and 7-40 specimens of *C. wuellerstorfi* (size fraction 150-400 μm) have been used for Mg/Ca analyses. The samples were gently cracked between two glass plates, transferred into pre-leached safe-lock minivials, and cleaned using the protocol of *Martin and Lea* [2002] including a reductive and an oxidative cleaning step and a final leaching step with 0.001N HNO_3 . The samples were dissolved and diluted in 0.1N HNO_3 and measured in a simultaneous ICPM-OES instrument with radial plasma observation at the IfG Kiel. Analytical error for Mg/Ca analyses was 0.1% RSD, and accuracy was monitored with ECRM-752 (Greaves et al., 2008). Errors from possible shell contamination or coatings were identified and excluded after monitoring additional trace elements. Duplicate sample preparation of 26 samples gave the standard deviation of 0.1 mmol/mol Mg/Ca for *C. wuellerstorfi*, 0.05 mmol/mol Mg/Ca for *M. barleanum* and 0.04 mmol/mol Mg/Ca for *M. affinis*.

7.6.5 Calibration and error assessment

To identify the most reliable calibration for our multispecies dataset different calibrations were tested (supplementary information). The monospecies calibration for *C. wuellerstorfi* of *Healey et al.* [2008] resulted in the best agreement between late Holocene BWT and modern BWT. Furthermore, we applied this monospecific calibration on our multispecies record after the potential interspecies offsets between Mg/Ca values were investigated by parallel measurements and did not exceed the error of the calibration. This calculation may induce a systematical error in the estimated temperatures that leads to a potential overestimation of the BWT by 1°C that might be considered for the interpretation of the parts of the record where *Melonis sp.* were used (15-10 ka BP).

7.6.6 Possible overprint by carbonate ion concentration

The Mg/Ca signal in benthic foraminifera might be overprinted by the carbonate ion effect that leads to an underestimation of the temperatures with decreasing $[\text{CO}_3]^{2-}$ concentrations [*Healey et al.*, 2008; *Tisserand et al.*, 2013; *Yu and Elderfield*, 2008]. Decreased glacial $[\text{CO}_3]^{2-}$ concentrations could account for a BWT underestimation of 1°C, thus a potential overprint has to

be excluded. In this purpose, we compared our Mg/Ca data with $[\text{CO}_3]^{2-}$ reconstructions based on B/Ca ratios from the eastern NA at water depth between 2800 and 3500 m wd [Yu and Elderfield [2008]. The B/Ca data does not match our Mg/Ca record, thus an overprint by $[\text{CO}_3]^{2-}$ seems to be neglect able (see supplementary information for details).

7.6.7 $\delta^{18}\text{O}_w$ reconstructions

Changes in salinity over time were reconstructed from the benthic foraminiferal $\delta^{18}\text{O}_{\text{carbonate}}$ record by removing the temperature effect, known from the Mg/Ca BWT reconstructions and by using the formula of Shackleton [1974]. To correct our $\delta^{18}\text{O}_w$ record for ice volume, we used the composite relative sea level curve of Waelbroeck *et al.* [2002] obtained from benthic $\delta^{18}\text{O}$.

7.7 Results

In our record (Figure 7.2) the deglacial evolution of BWT coincides in general with the benthic $\delta^{13}\text{C}$ evolution. Both records show high values during BA and Holocene and lower values during H1 and YD and thus are in phase with Greenland ice core $\delta^{18}\text{O}$ record. The BWT (Figure 7.2c) is warming from to 2.75°C at the BA onset, cooling by 1°C at the onset of the YD, with coldest temperatures between 12.5 and 12 ka BP. A post YD warming in two steps finally reaches 3.5°C at 10.8 ka BP. Between 10.8 and 6.5 ka BP BWT oscillate around ~3.3°C with 1°C cooling at 10.2, 9.6, 9.3, 8.5-8.3, 7.6 and 7.1 ka BP.

The $\delta^{13}\text{C}$ record (Figure 7.2d) is characterized by high frequent oscillations of about 0.2‰ around mean values of 0.5‰ during H1, 0.9‰ during the BA, and again 0.5‰ at the start of the YD. During the YD well into the Preboreal, decadal scale $\delta^{13}\text{C}$ oscillations between -0.2 and 0.7‰ are observed. During the Preboreal Oscillation (PO) (~11 ka BP), the $\delta^{13}\text{C}$ oscillations match well the cold reversal in BWT (Figure 7.2b). The $\delta^{13}\text{C}$ continuous to oscillate over the Early to Mid Holocene with major incursions at about 11.3, 10.9, 10.6-10.2, 9.6, 9.3, 8.4-8.2, 7.6 and 7.1 ka BP down to 0‰ that interrupt the general increasing Early Holocene trend to mean $\delta^{13}\text{C}$ values of about 1.1‰ reached at 7 ka BP. This $\delta^{13}\text{C}$ variability seems to coincide with BWT cooling events of 1°C in amplitude although the BWT record is less well resolved. Modern $\delta^{13}\text{C}$ values were reached after 7 ka BP. The $\delta^{18}\text{O}$ values decrease from 4.5‰ at 14.8 ka BP to 3.35‰ at 14.75 ka BP and a plateau of 3.9‰ to 3.5‰ between over BA (14.5 ka BP and 13.2 ka BP) (Figure 7.2a). $\delta^{18}\text{O}$ values stepwise decrease over the YD from 3.5‰ at 13.3 ka BP to reach Holocene values of ~3‰ at 10.8 ka BP. Over the Holocene the $\delta^{18}\text{O}$ record varies little (+/-0.2‰). The $\delta^{18}\text{O}$ record shows less variability compared to the BWT and $\delta^{13}\text{C}$ records suggesting that the overall $\delta^{18}\text{O}$ evolution is mainly governed by ice volume as is evident in the comparison with the composite relative sea level $\delta^{18}\text{O}$ data [Waelbroeck *et al.*, 2002], indicative for ice volume changes (Figure 7.2b).

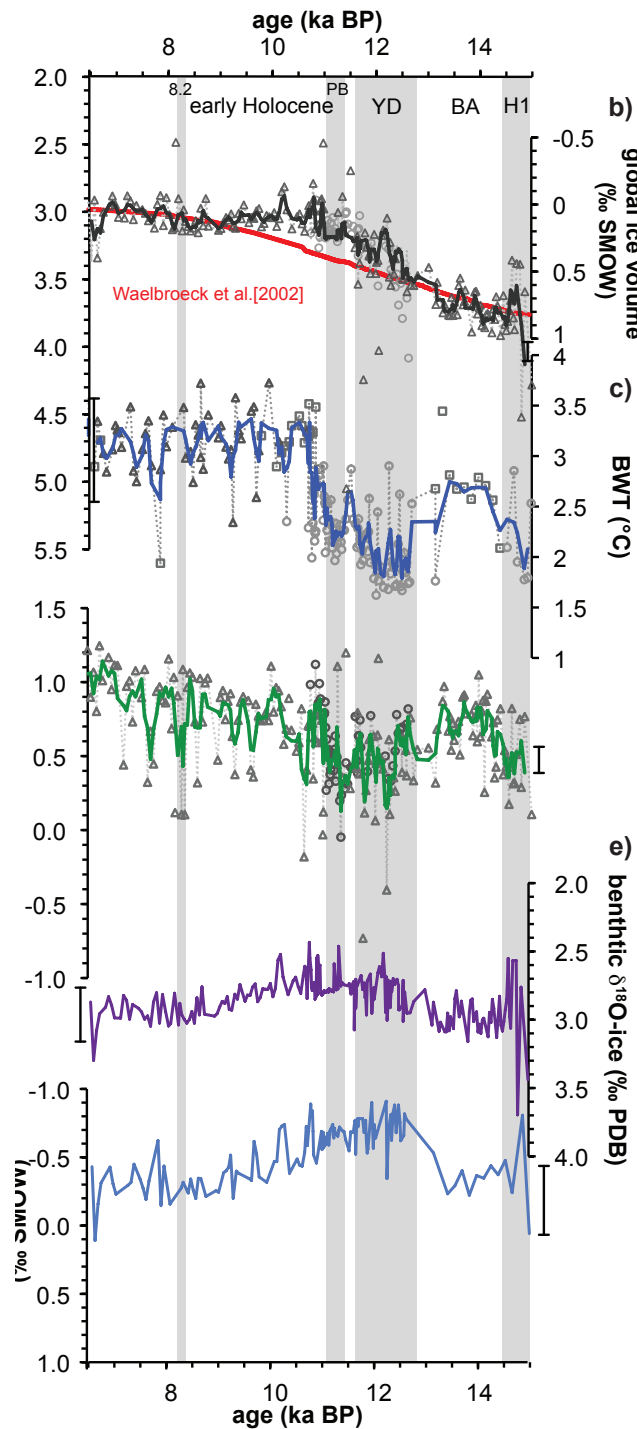


Figure 7.2 Results

- a) mixed benthic $\delta^{18}\text{O}$ record using corrected for species specific offsets, black line indicates 3 point mean
 - b) mixed composite curve of $\delta^{18}\text{O}$ change relative sea level [Waelbroeck et al. 2002](red line)
 - c) mixed benthic $\delta^{13}\text{C}$ record corrected by species specific offsets, green line indicates 3-point mean
 - d) mixed benthic Mg/Ca BWT record calculated applying the formula of Healey et al. [2008], blue line indicates 3-point running mean
 - e) ice volume corrected [Waelbroeck et al., 2002] benthic $\delta^{18}\text{O}$ record
 - f) temperature [Shackleton, 1974] and ice volume [Waelbroeck et al., 2002] corrected mixed benthic $\delta^{18}\text{O}_{w-ice}$ record
- For the stacked records *C. wuellerstorfi* data is indicated by triangles, *M. affinis* by circles and *M. barleanum* by squares.

Nevertheless, the $\delta^{18}\text{O}$ -ice data (Figure 7.2e) showing an abrupt decrease by 0.5‰ during H1, and a longer lasting decrease of the same magnitude (0.5‰) between 12.6 and 9 ka BP. These changes are related to a freshening of the deepwater as it becomes evident in the $^{18}\text{O}_{\text{w-ice}}$ record (Figure 7.2f), that fluctuates around 0.25‰ SMOW and shows a short decrease of 0.7‰ SMOW during H1. A decrease of the same amount, at the beginning of the YD, and again rising values over PB indicates a deepwater freshening. Even an overestimation of BWT as discussed above would increase the freshening signal. Taking an uncertainty of 1°C in BWT estimates into account, a freshening of 0.5‰ [SMOW] would still be evident. This record indicates that the deepwater at the central ENAB was strongly influenced by $\delta^{18}\text{O}_{\text{w-ice}}$ changes that are also detectable at the Iberian Margin [Skinner *et al.*, 2003].

7.8 Discussion

7.8.1 Deglacial deepwater composition and distribution changes

Our data suggest that the YD and H1 deepwater cooling and freshening and the BA warming are in phase with the Greenland ice core record (Figure 7.3). Thus the question arises whether the BWT cooling at 38°N is governed by the increasing influence of southern deepwater in the NA basins during the YD and the H1 event as assumed in the classical interpretation of deglacial $\delta^{13}\text{C}$ and Pa/Th data sets [Gherardi *et al.*, 2009; McManus, 2004; Piotrowski *et al.*, 2012; Roberts *et al.*, 2010; Sarnthein *et al.*, 1994], or by a cooling and freshening and/or brine water formation within the NH waters as suggested from modeling results [Renssen *et al.*, 2010] and from benthic Mg/Ca, $\delta^{18}\text{O}$ and $\delta^{13}\text{C}$ reconstructions [Skinner *et al.*, 2003; Thornalley *et al.*, 2010; Waelbroeck *et al.*, 2011]. The problem with the classical interpretation is the missing consideration of changes in the AABW composition, from less saline but cold during LGM, to modern cold but less saline AABW [Adkins, 2013], that is also apparent from Figure 7.4 $\delta^{13}\text{C}/\delta^{18}\text{O}$ cross plots.

The AABW $\delta^{18}\text{O}$ signature was more positive during the LGM and the H1 than the NH end-member (Figure 7.4). Therefore the more negative $\delta^{18}\text{O}_{\text{sw-ice}}$ excursions during the H1 and the YD indicated in the data from the Azores coring site and the Iberian margin (MD99-2334K) (37.8°N; 10.2°W) [Skinner *et al.*, 2003] (Figure 7.6) and interpreted as a strong freshening signal can not be explained by an increase in southern deepwater influence the strong freshening signal. Furthermore, a lead of NH $\delta^{18}\text{O}$ changes over the SH changes for the H1 event and the YD argues against a southern origin of the light $\delta^{18}\text{O}_{\text{sw-ice}}$ signal [Waelbroeck *et al.*, 2011](Figure 7.6). Thus we assume a northern origin of the cold, less saline, low $\delta^{13}\text{C}$ deepwater that is observed at the Azores coring site during the H1 event and the YD. This assumption is in agreement with Skinner *et al.* [2003] but contradicts the classical $\delta^{13}\text{C}$ interpretation and requires to find a process

explaining a more negative $\delta^{13}\text{C}$ NH water mass. The origin of the $\delta^{13}\text{C}$ decreases might be the

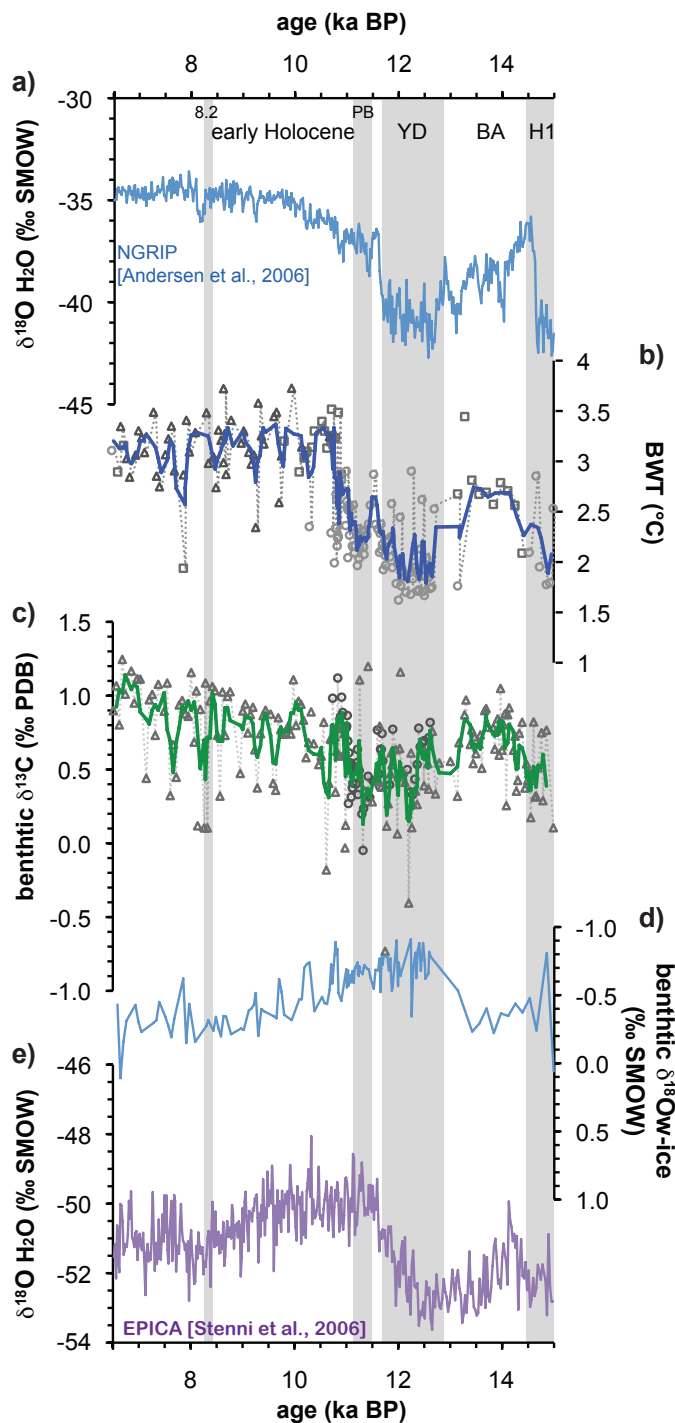


Figure 7.3 Comparison between the benthic marine records and ice core records

The Comparison between the a) Greenland $\delta^{18}\text{O}$ Ice core record [Andersen et al., 2006] and the b) benthic Mg Ca BWT record (blue line indicates 3 point running mean) c) $\delta^{13}\text{C}$ record (green line indicating 3 point running mean) d) benthic $\delta^{18}\text{O}_{\text{sw-ice}}$ record (light blue line indicating 3 point running mean) from the Azores coring site and the Antarctic $\delta^{18}\text{O}$ Ice core record [Stenni et al., 2006] indicate that cold temperatures in Greenland during H1 and YD were in phase with a deepwater cooling, freshening and decrease of deepwater ventilation. at the Azores coring site.

For the stacked records C. wuellerstorfi data is indicated by triangles, M. affinis by circles and M. barleanum by squares.

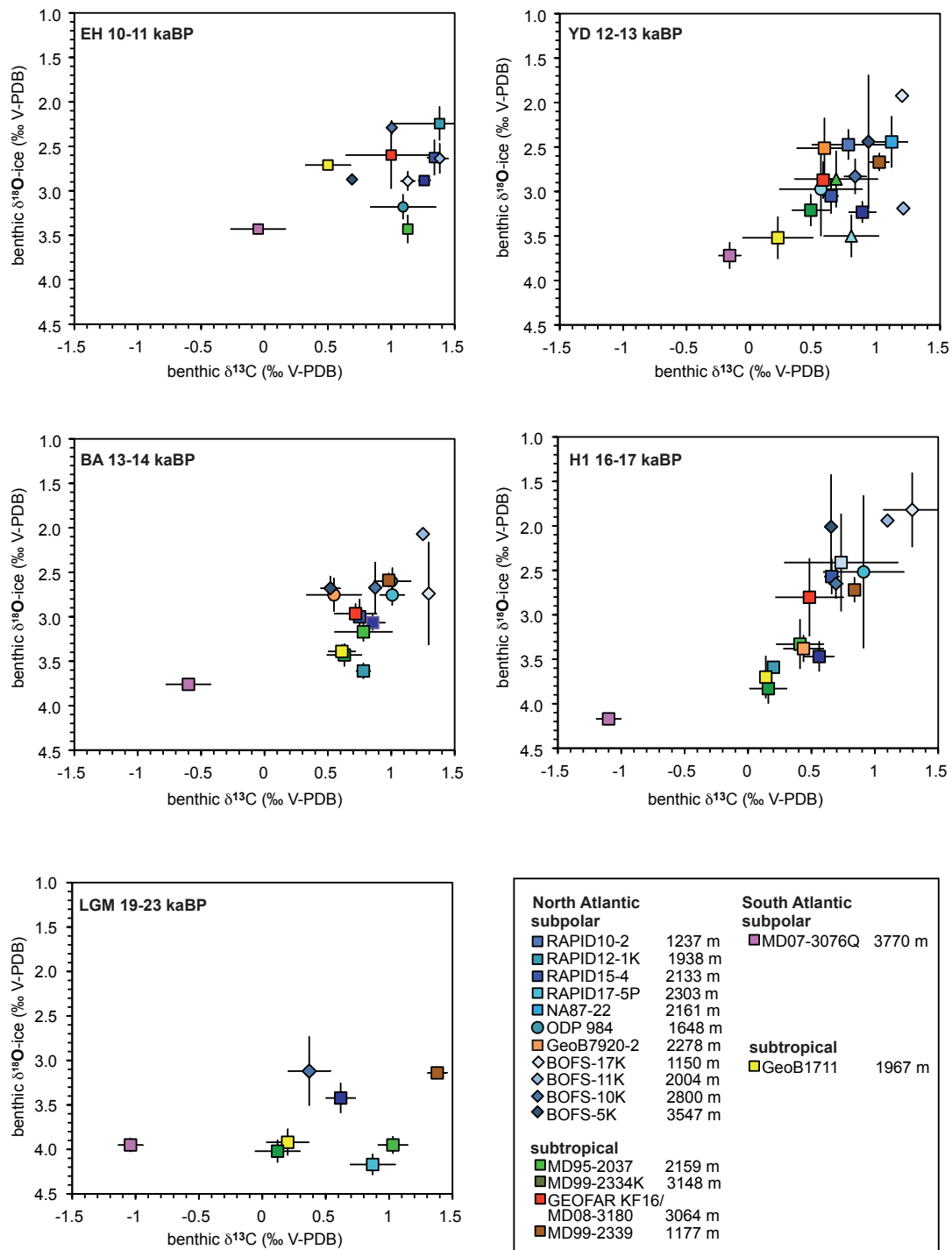


Figure 7.4 five deglacial time slices showing $\delta^{18}\text{O}/\delta^{13}\text{C}$ cross plots comparing cores GEOFAR KF16/MD08-3180 from the Azores coring site with cores obtained from the eastern Atlantic basin published by Waelbroeck et al. [2011] and supplemented with four RADIP cores from the South Iceland Rise [Thornalley et al., 2010], BOFS cores from the subpolar ENAB [Yu and Elderfield, 2008 and citations therein] cores core ODP 986 from the Reykjanes Ridge [Praetorius et al., 2008] and one core MD99-2339 from the Mediterranean Outflow [Voelker et al., 2006]. These dataset indicates that changing contributions and compositions of northern and southern sourced deepwater can explain the deglacial deepwater changes

result from an overprint by local productivity, the formation of brine waters within the Nordic seas [e.g. *Meland et al.*, 2008; *Thornalley et al.*, 2010; *Waelbroeck et al.*, 2011], and/ or the influence of a third deglacial water mass with NH origin [*Yu and Elderfield*, 2008].

Local productivity changes are often postulated to explain depleted $\delta^{13}\text{C}$ patterns, but can be neglected at the Azores coring site as changes in $\delta^{13}\text{C}$ of 1‰ are generally too high to be caused by surface productivity changes alone [*Waelbroeck et al.*, 2011] and the expected dependency between $\delta^{13}\text{C}$ and DIC could not be confirmed for the Canary Island region and for the Iberian Margin [*Eberwein and Mackensen*, 2006; *Fontanier et al.*, 2006]. Additionally, productivity reconstructions from the Azores coring site using Ba/Ti ratios [*Schwab et al.*, 2012] (Figure 7.S4) show no correlation with the $\delta^{13}\text{C}$ record, thus we assume that the negative $\delta^{13}\text{C}$ signatures during the H1 event and the YD are not caused by productivity changes.

Another source of a depleted $\delta^{13}\text{C}$ signal could be NH brine water that would be characterized by low $\delta^{18}\text{O}$ and low $\delta^{13}\text{C}$ and has been observed in shallower NA coring sites at depth between 1000 m and 2160 m wd [*Meland et al.*, 2008; *Thornalley et al.*, 2010; *Waelbroeck et al.*, 2011]. such an overprint seems to be unlikely at 3060 m wd as for our coring site, a influence of brine water seems to be evident in the cross plot $\delta^{18}\text{O}/\delta^{13}\text{C}$ for the YD and the early Holocene (Figure 7.5) with all data points lying closer to brine water than to glacial NADW (GNADW). *Yu and Elderfield* [2008] suggest that during the LGM, brine water driven deepwater convection remained active in the nearly entirely ice covered Nordic Seas. The resulting water mass was $\delta^{18}\text{O}$ and $\delta^{13}\text{C}$ depleted and is called lower Glacial North Atlantic Deep Water (IGNADW).

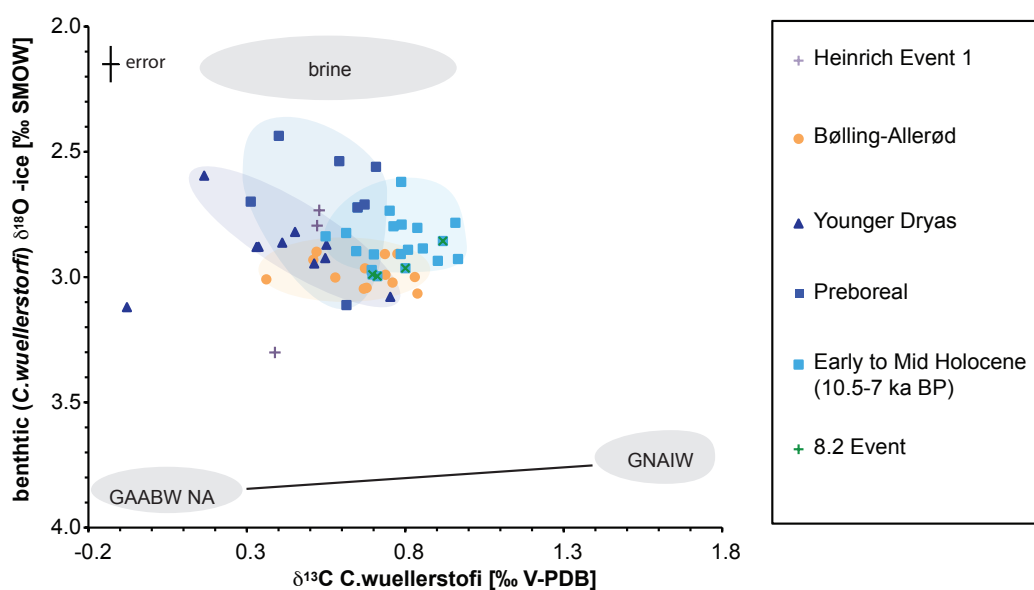


Figure 7.5 Influence of brine water on deglacial deepwater evolution

The benthic $\delta^{18}\text{O}$ (C. wuellerstorfi) versus $\delta^{13}\text{C}$ (C. wuellerstorfi) plot (3 point average) indicate the influence of brine water during the YD and the early Holocene on the coring site, the offset from the GAABW GNAIW mixing line indicates that the deepwater at the Azores coring site was not directly influenced by those water masses. Data for brine water, GAABW and GNAIW stems from *Thornalley et al.* [2010] and *Curry and Oppo*, [2005].

IGNADW entered the subpolar east Atlantic at water depth between 2000 and 3000 m and underlied the upper Glacial NADW (uGNADW) that occupied the NA between 500 and 2000 m water depth. The southward propagation of this weakly ventilated IGNADW during the H1 event and the YD could explain the freshening signature and the low $\delta^{13}\text{C}$ signatures observed at the Azores coring site. As supposed previously [Skinner *et al.*, 2003; Waelbroeck *et al.*, 2011], the observed deepwater freshening signal must originate from the NADW source area and agrees with surface water freshening that is reconstructed for the subpolar NA during cold events and most probably related to the release of deglacial meltwater [e.g. Benway *et al.*, 2010; Rahmstorf *et al.*, 2005; Thornalley *et al.*, 2011; Van Meerbeeck *et al.*, 2011]. However ^{14}C age reconstructions from the Iberian margin [Skinner *et al.*, 2014] indicate that extremely old deepwater reached the ENAB during the H1 event and the YD. Assuming a NH origin of this water masses a mechanism must be found that forms extremely old deepwater in the Nordic seas and how meltwater would trigger the southward propagation of these old deepwater.

Our results however strengthen the arguments that deepwater convection remained active in the Nordic Seas over the Deglacial [e.g. Dokken and Jansen, 1999; Meland *et al.*, 2008], and indicate that deglacial deepwater changes are governed by changes in the NADW composition instead of changing contributions of AABW and NADW. This is in agreement with a modeling study of Gebbie *et al.* [2014] that shows little variability in the NADW/AABW distribution in the ENAB between the LGM and the late Holocene.

Our assumption contradicts previous studies that suggested a complete shut down of AMOC [Gherardi *et al.*, 2005; Gherardi *et al.*, 2009; McManus *et al.*, 2004; Rahmsdorf, 2002] and only minor contributions of NADW below 2000 m wd during the H1 event and the YD [e.g. Gherardi *et al.*, 2009, Roberts *et al.*, 2010]. As most of the deglacial deepwater reconstructions are based on cores from the western NA basin a different evolution of both basins might partially account for this differences. Nevertheless, alterations of the AABW and NADW compositions instead of deepwater volume changes have to be considered in the reconstruction of the Deglacial deepwater circulation.

In the following we investigate the potential mixing between strongly altered glacial and deglacial AABW and NADW. For this purpose we compare cross plots of our $\delta^{13}\text{C}$ and $\delta^{18}\text{O}$ data of five deglacial time slices with ENAB data partially published by Waelbroeck *et al.* [2011] and supplemented with data from cores from the subpolar ENAB that are suggested to reflect the ISOW overflow composition [Thornalley *et al.*, 2010, Yu and Elderfield, 2008]. The cross plots indicate the distinct evolution from a glacial low $\delta^{18}\text{O}$ gradient between AABW and NADW with relatively high $\delta^{18}\text{O}$ values in the AABW, toward the modern state with lower $\delta^{18}\text{O}$ AABW than $\delta^{18}\text{O}$ NADW. The distinctly different $\delta^{18}\text{O}$ and $\delta^{13}\text{C}$ signatures of the AABW and the northern cores during LGM, H1 and BA indicate that the SO was isolated from the GNADW, as already

suggested by *Adkins* [2013]. A decreased difference between the $\delta^{18}\text{O}$ and $\delta^{13}\text{C}$ signatures of the NH cores and the deep SO site during the YD and the Holocene indicates an increasing mixing of NADW and AABW, that might be related to a change from a salinity driven to a thermal driven deepwater stratification.

7.9 NADW freshening as a driver for deglacial AABW composition changes

The mechanism that inverts the glacial salinity driven stratification deepwater stratification with low vertical mixing rates, into the interglacial thermal driven mode with strong vertical mixing over the deglacial is still unknown [*Adkins*, 2013].

The suggested freshening of the ENADW during the H1 event and the YD might provide a mechanism to explain the change from glacial to the modern deep ocean stratification. To propose a mechanism our new BWT and $\delta^{18}\text{O}_{\text{sw-ice}}$ reconstructions in addition to the published $\delta^{18}\text{O}$ data of core RAPID 14-5 from the subpolar NA deepwater source area [*Thornalley et al.*, 2010], BWT and $\delta^{18}\text{O}$ data from core MD99-2334K at the Iberian Margin [*Skinner et al.*, 2003] and the deglacial timing between southern and northern deepwater cores using the $\delta^{18}\text{O}$ values of MD99-2334K and MD07-3076Q from the SO [*Waelbroeck et al.*, 2011] (Figure 7.6) may provide supporting evidence for NADW freshening as a driver for deglacial AABW composition changes.

The data from the Iberian Margin and our new BWT and $\delta^{18}\text{O}_{\text{sw-ice}}$ reconstructions (Figure 7.6e) as well as light $\delta^{18}\text{O}$ values in core RAPID 14-5 indicate that a cold fresh water mass entered the deep NA ocean during mid H1 (16.1-15 kaBP) as already shown by *Waelbroeck et al.* [2011]. This deepwater freshening precedes the $\delta^{18}\text{O}$ increase of the AABW (MD07-3076Q) by about 1 ka. The latter starts at about 15 ka in phase with the onset of BA BWT warming in the NA cores. AABW is formed through brine water formation [*Adkins*, 2013 and citations therein], its $\delta^{18}\text{O}$ signal bears the signature of the preconditioned surface waters, which circulate around Antarctica in the Antarctic Circumpolar Current (ACC). Thus the decrease in AABW $\delta^{18}\text{O}$ at 15 ka BP is closely related to changes in the ACC and should response to a warming or a freshening of the surface and subsurface water masses.

At the onset of BA, a warming of the AABW cannot completely be ruled out without BWT reconstructions. But SST warming at site MD07-2076 [*Skinner et al.*, 2010 supp. Information] preceded the AABW $\delta^{18}\text{O}$ decrease by 1-2 ka, thus a AABW warming seems to be unlikely as cause for the observed $\delta^{18}\text{O}$ changes. The timing also seems to exclude the possibility that increased basal melting of the Antarctic shelf ice caused a freshening of the ACC that was transferred into the deep SO by brine water formation [*Adkins*, 2013]. Thus we suppose that $\delta^{18}\text{O}$ decrease must originate from mixing with a low saline water mass different from SO surface waters.

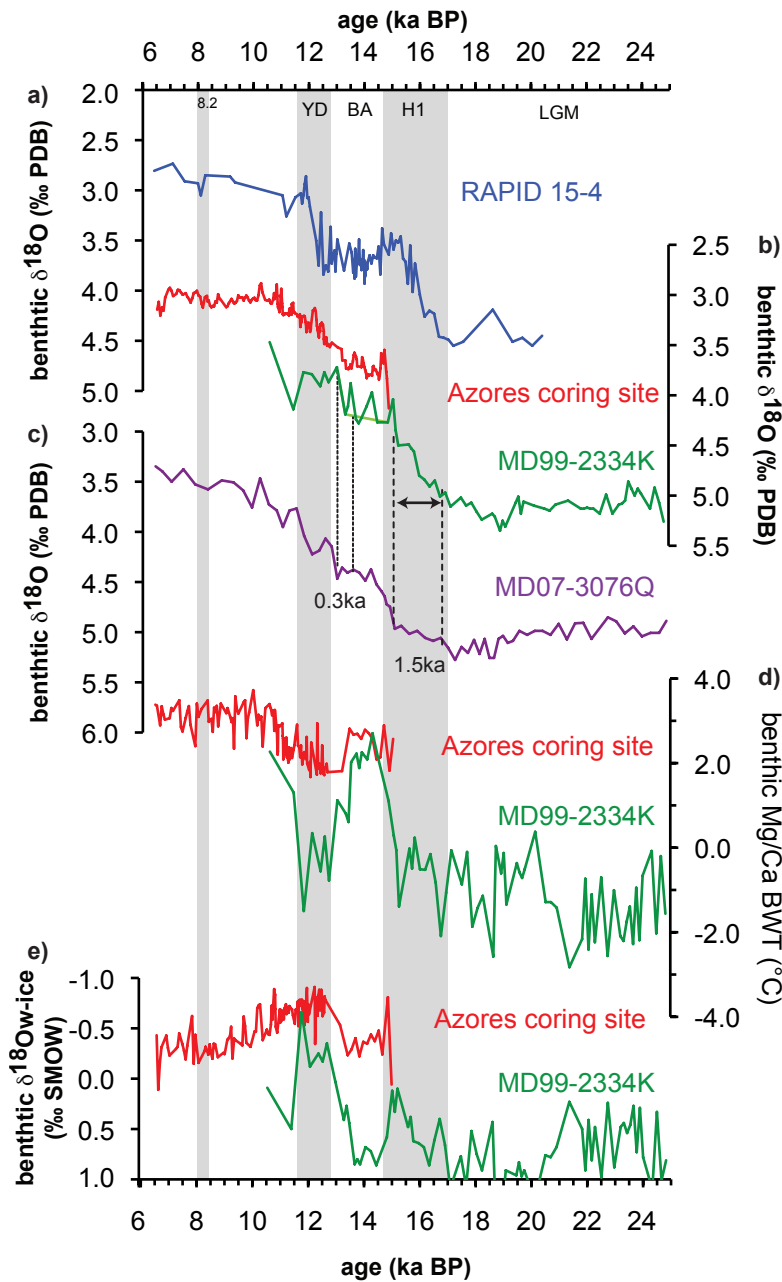


Figure 7.6 Comparison between the deglacial benthic $\delta^{18}\text{O}$ records

of a) core RAPID 15-4 [Thornalley et al., 2010], b) subtropical cores GEOFAR KF16/MD08-3180 (3-point running mean), core MD99-2334K from the Iberian Margin [Skinner and Shackleton, 2003] and c) the southern ocean core MD07-3076 [Waelbroeck] with the d) BWT records from the subtropical NA, and e) deepwater $\delta^{18}\text{O}_{\text{sw-ice}}$ reconstructions from the subtropical eastern NA basin might indicate that the delayed deglacial $\delta^{18}\text{O}$ increases in the southern ocean were caused by a freshening of the NADW during cold events

We suppose that the southward transport of the relatively fresh IGNADW water during H1 could act as such a source. From the limited data, and within the accuracy of dating we suppose that freshened IGNADW that entered the deep NA during H1 reached the SO during BA with a time delay of at least 1000 years. In the end of H1, the freshened waters could have reached the SO, were it was entrained into the circumpolar current and transferred into the deep SO via brine water

formation. Such an entrainment of northern sourced less saline deepwater could provide the mechanism to freshen the AABW and to decrease the SO deepwater stratification at the onset of BA. Such an enhanced mixing is corroborated by a prominent reduction in radiocarbon reservoir ages of SO deepwater exactly at 15 ka BP [e.g. *Skinner et al.*, 2010; *Burke and Robinson*, 2012]. Already half way into the interglacial mode, the second deglacial NADW freshening event during the YD differs from the H1 event. The $\delta^{18}\text{O}/\delta^{13}\text{C}$ cross plot (Figure 7.4) indicates increasing mixing of AABW and NADW with AABW approaching the values typical for NADW. The freshening signal of 0.5 to 1.5 ‰ SMOW and BWT cooling of 1-3°C at the Azores coring site and the Iberian Margin leads the decreasing $\delta^{18}\text{O}$ values of core MD07-3076 by less than 400 years (Figure 7.6). This decrease in AABW $\delta^{18}\text{O}$ values probably was related to the entrainment of freshened NADW produced in the beginning of the YD and was transported southward within 400 years due to an increase in AMOC [e.g. *Mc Manus et al.*, 2004]. However we cannot rule out that the $\delta^{18}\text{O}$ decrease was caused by a warming of the ACC, either driven by the upwelling of warm NADW that was formed in the BA or by surface water warming due to a warming of Antarctica. The warming would cause an increased basal melting of the Antarctic shelf ice that results in freshening of the ACC and AABW as suggested by *Adkins* [2013]. This hypothesis did not fit in timing for the H1 event but during the YD a combination of our new proposed mechanism and a basal melting might have occurred. The proposed changes in the AABW composition probably caused an increasing deepwater mixing that finally led into the Holocene deepwater stratification mode.

7.10 Holocene instabilities in the deepwater composition

Following the previous arguments, the question arises whether the Early to Mid Holocene (EH) (11.6 to 7 ka BP) changes in the deepwater properties of the ENAB are a result of varying contributions of AABW and NADW as suggested by the classical interpretation [e.g. *Oppo et al.*, 2003; *Kleiven et al.*, 2008] or also are mainly governed by changes in NH water mass properties.

At the Azores coring site (EH) is characterized by relatively warm BWT (3.0-3.5 °C), increasing $\delta^{13}\text{C}$ values and increasing deepwater salinities (Figure 7.2) that indicate an AMOC strengthening. This evolution was punctuated by centennial scale decreases in the $\delta^{13}\text{C}$ and BWT signature that probably indicate short-term interruptions in the AMOC recovery over the PB and early to mid Holocene at 11.3, 10.9, 9.6, 9.3, 8.4-8.2, 7.6 and 7.1 ka BP. Our data match well with the abrupt warming in the subpolar NA at the beginning of the Holocene [*Moros et al.*, 2004] and with AMOC instabilities that are reported from the western and subpolar NA Basin [*Hoogakker et al.*, 2011a; *Oppo et al.*, 2003]. The latter are probably related to the last phase of the deglacial melting that caused several short-term freshening events in the subpolar NA [e.g. *Benway et al.*, 2010; *Thornalley et al.*, 2011]. The tendency of more negative $\delta^{18}\text{O}$ values corresponds with the negative

$\delta^{13}\text{C}$ excursions apparent in our record (Figure 7.3) and indicates a freshening of the NH deepwater during the EH events. The EH $\delta^{13}\text{C}/\delta^{18}\text{O}$ signature of our cores (Figure 7.4) match well with the data from the subpolar NA and are distinctly different from the SO waters. Thus we assume that the EH instabilities are related to a freshening and a decreased ventilation of the NADW. It remains uncertain whether this ventilation changes were associated with the occurrence of old water masses in the ENAB or were simply associated with a change in the NH deepwater convection. Our results however argue against previous studies [e.g. *Oppo et al.*, 2003] that suppose the influence of AABW behind the EH $\delta^{13}\text{C}$ excursions.

7.11 Conclusion

In this study combined Mg/Ca and stable isotope data obtained from benthic foraminifera were used to reconstruct deglacial changes in the deepwater temperature, ventilation and salinity in the eastern subtropical NA. The comparison of this dataset with previous published ones, indicates that over the Deglacial and early Holocene ENAB was mainly influenced by changes of the initial composition of the NA deepwater source.

The ventilation of ENADW in the subtropical ENAB stepwise increased over the last 15 ka BP. This general evolution was disrupted by several drawbacks that occurred during the H1 event, the YD and the early Holocene. During these intervals a $\delta^{13}\text{C}$ depletion by 0.5‰, cooling by at least 1.5°C and freshening at a level of at least 0.5‰ SMOW decrease of the deepwater mass is observed. The freshening of the deepwater can be associated with a strong freshening of the NH deepwater source and the decrease in $\delta^{13}\text{C}$ values probably originates poorly ventilated IGNADW that reached down to the Azores coring site, during the H1 event, the YD and the early Holocene. Although the mixing between southern and northern deepwater seem to increase over the Deglacial, the Azores coring site is mainly influenced by the NADW composition changes instead of changing contributions of northern versus southern hemisphere deepwater. These findings oppose previous studies that suppose a complete shutdown of AMOC in H1 and a strong reduction and shoaling of NADW during the YD reconstructed mainly in the western NA basin. These discrepancies might be caused by different evolutions of both the eastern and western NA basin.

The southward transport of the freshened ENADW, its upwelling and final inclusion into the AABW through brine water formation might lead to a decrease of the AABW salinities from glacial high to interglacial low values and thereby also would decrease the deepwater stratification. This untested mechanism could explain the deglacial change from a saline to a thermal governed deepwater stratification mode. Our data set corroborates the concept that the deglacial NH ice sheet instability triggered the deglacial changes in the NA deepwater composition and distribution.

The early Holocene oscillations are in phase with those of the Western Atlantic Basin, indicating that both were sensitive to early Holocene AMOC disturbances and are most probably caused by several meltwater peaks that had a severe impact on the early Holocene NH deepwater convection.

Although more high resolution BWT, $\delta^{13}\text{C}$ and $\delta^{18}\text{O}$ datasets would be needed to fully understand the geometry of the deglacial deepwater changes and its driving mechanisms, our study indicates that the deglacial and early Holocene deepwater circulation and composition changes are triggered by changes in the NH.

7.12 Acknowledgements

We like to thank M. Regenberg, K. Bremer, U. Westernstroer, for laboratory assistance and Mg/Ca data discussions. The results represented here are obtained from cores taken onboard R.V. Marion Dufresne (French Polar Institute, IPEV) during the IMAGES-AMOCINT MD168-cruise in the framework of the 06-EuroMARC-FP-006 Project. We thank the captain and the crew, as well as our colleagues onboard for their help. This manuscript has been made possible thanks to the support from the European Science Foundation (ESF) under the EUROCORES Program EuroMARC through contract No. ERAS-CT-2003-980409 of the European Commission, DG Research, FPG. Financial support is given by the German Science Foundation (DFG). Furthermore we would like to thank Mr. Bernard Dennielou and Ifremer for providing us with material from core GEOFAR KF16.

7.13 References

- Adkins, J. F. (2013), The role of deep ocean circulation in setting glacial climates, *Paleoceanography*, 28(3), 539-561.
- Adkins, J. F., K. McIntyre, and D. P. Schrag (2002), The Salinity, Temperature, and $\delta^{18}\text{O}$ of the Glacial Deep Ocean, *Science*, 298, 1769-1773.
- Andersen, K. K., et al. (2006), The Greenland Ice Core Chronology 2005, 150-0 ka. Part 1: constructing the time scale, *Quaternary Science Reviews*, 25(23-24), 3246-3257.
- Antonov, J. I., D. Seidov, T. P. Boyer, R. A. Locarnini, A. V. Mishonov, H. E. Garcia, O. K. Baranova, M. M. Zweng, and D. R. Johnson (2010), *World Ocean Atlas 2009: Volume 2: Salinity*, 184 pp.
- Benway, H. M., J. F. McManus, D. W. Oppo, and J. L. Cullen (2010), Hydrographic changes in the eastern subpolar North Atlantic during the last deglaciation, *Quaternary Science Reviews*, 29(23-24), 3336-3345.
- Boyle, E. A., and L. Keigwin (1987), North Atlantic thermohaline circulation during the past 20,000 years linked to high-latitude surface temperature, *Nature*, 330(6143), 35-40.
- Burke, A., and L. F. Robinson (2012), The Southern Ocean's Role in Carbon Exchange During the Last Deglaciation, *Science*, 335(6068), 557-561.
- Colin, C., N. Frank, K. Copard, and E. Douville (2010), Neodymium isotopic composition of deep-sea corals from the NE Atlantic: implications for past hydrological changes during the Holocene, *Quaternary Science Reviews*, 29(19-20), 2509-2517.
- Curry, R., B. Dickson, and I. Yashayaev (2003), A change in the freshwater balance of the Atlantic Ocean over the past four decades, *Nature*, 426(6968), 826-829.
- Curry, W. B., and D. W. Oppo (2005), Glacial water mass geometry and the distribution of $\delta^{13}\text{C}$ of ΣCO_2 in the western Atlantic Ocean, *Paleoceanography*, 20(1), PA1017, doi:10.1029/2004PA001021
- Dokken, T., and E. Jansen (1999), Rapid changes in the mechanism of ocean convection during the last glacial period, *Nature*, 401, 458-461.
- Duplessy, J.-C., N. J. Shackleton, R. K. Matthews, W. Prell, W. F. Ruddiman, M. I. Caralp, and C. H. Hendy (1984), ^{13}C Record of benthic foraminifera in the last interglacial ocean: Implications for the carbon cycle and the global deep water circulation, *Quaternary Research*, 21(2), 225-243.
- Duplessy, J. C., N. J. Shackleton, R. G. Fairbanks, L. Labeyrie, D. Oppo, and N. Kallel (1988), Deepwater source variations during the last climatic cycle and their impact on the global deepwater circulation, *Paleoceanography*, 3(3), 343-360.
- Eberwein, A., and A. Mackensen (2006), Regional primary productivity differences off Morocco (NW-Africa) recorded by modern benthic foraminifera and their stable carbon isotopic composition, *Deep Sea Research Part I: Oceanographic Research Papers*, 53(8), 1379-1405.
- Fontanier, C., A. Mackensen, F. Jorissen, P. Anschutz, L. Licari, and C. Griveaud (2006), Stable oxygen and carbon isotopes of live benthic foraminifera from the Bay of Biscay: Microhabitat impact and seasonal variability, *Marine Micropaleontology*, 58(3), 159-183.

- Frew, R. D., P. F. Dennis, K. J. Heywood, M. P. Meredith, and S. M. Boswell (2000), The oxygen isotope composition of water masses in the northern North Atlantic, *Deep Sea Research Part I: Oceanographic Research Papers*, 47(12), 2265-2286.
- Gebbie, G. (2014), How much did Glacial North Atlantic Water shoal?, *Paleoceanography*, 29(3), 190-209.
- Gherardi, J.-M., L. Labeyrie, J. F. McManus, R. Francois, L. C. Skinner, and E. Cortijo (2005), Evidence from the Northeastern Atlantic basin for variability in the rate of the meridional overturning circulation through the last deglaciation, *Earth and Planetary Science Letters*, 240, 710-723.
- Gherardi, J. M., L. Labeyrie, S. Nave, R. Francois, J. F. McManus, and E. Cortijo (2009), Glacial-interglacial circulation changes inferred from 231Pa/230Th sedimentary record in the North Atlantic region, *Paleoceanography*, 24(2), PA2204.
- Hansen, B., and S. Østerhus (2000), North Atlantic - Nordic Seas exchanges, *Prog. Oceanogr*, 45, 109-208.
- Healey, S. L., R. C. Thunell, and B. H. Corliss (2008), The Mg/Ca-temperature relationship of benthic foraminiferal calcite: New core-top calibrations in the <4°C temperature range, *Earth and Planetary Science Letters*, 272(3-4), 523-530.
- Hoogakker, B. A. A., M. R. Chapman, I. N. McCave, C. Hillaire-Marcel, C. R. W. Ellison, I. R. Hall, and R. J. Telford (2011a), Dynamics of North Atlantic Deep Water masses during the Holocene, *Paleoceanography*, 26(4), PA4214.
- Hoogakker, B., H. Elderfield, K. Oliver, and S. Crowhurst (2011b), Benthic foraminiferal oxygen isotope offsets over the last glacial-interglacial cycle, *Paleoceanography*, 25(4), PA4229.
- Jansen, E., U. Bleil, R. Heinrich, L. Kringstad, and B. Slettemark (1988), Paleoenvironmental Changes in the Norwegian Sea and the Northeast Atlantic During the Last 2.8 m.y.: Deep Sea Drilling Project/Ocean Drilling Program Sites 610, 642, 643 and 644, *Paleoceanography*, 3(5), 563-581.
- Kissel, C., H. Kleiven, X. Morin, and t. S. S. Party (2008), MD168-AMOCINT/1079 XVII IMAGES cruise report, *Les rapports de campagne à la mer, IPEV, 1080 OCE/2008/02*.
- Kissel, C., A. Van Toer, C. Laj, E. Cortijo, and E. Michel (2013), Variations in the strength of the North Atlantic bottom water during Holocene, *Earth and Planetary Science Letters*, 369-370(0), 248-259.
- Kleiven, H. K. F., C. Kissel, C. Laj, U. Ninnemann, T. O. Richter, and E. cortijo (2008), Reduced North Atlantic deep water coeval with the glacial Lake Agassiz freshwater outburst, *Science*, 319, 60- 64.
- Labeyrie, L., C. Waelbroeck, E. Cortijo, E. Michel, and J.-C. Duplessy (2005), Changes in deep water hydrology during the Last Deglaciation, *C. R. Geoscience*, 337, 919-927.
- Lippold, J., Y. Luo, R. Francois, S. E. Allen, J. Gherardi, S. Pichat, B. Hickey, and H. Schulz (2012), Strength and geometry of the glacial Atlantic Meridional Overturning Circulation, *Nature Geosci, advance online publication*.
- Locarnini, R. A., A. V. Mishonov, J. I. Antonov, T. P. Boyer, and H. E. Garcia (2010), World Ocean Atlas 2009, Volume 1: Temperature, edited by S. Levitus, NOAA Atlas NESDIS 68, U.S. Government Printing Office, Washington, D.C.
- Marcott, S. A., et al. (2011), Ice-shelf collapse from subsurface warming as a trigger for Heinrich events, *Proceedings of the National Academy of Sciences*, 108(33), 13415-13419.
- Martin, P. A., and D. W. Lea (2002), A simple evaluation of cleaning procedures on fossil benthic foraminiferal Mg/Ca, *Geochemistry, Geophysics, Geosystems*, 3(10), 8401.
- Matsumoto, K., and Y. Yokoyama (2013), Atmospheric $\Delta^{14}C$ reduction in simulations of Atlantic overturning circulation shutdown, *Global Biogeochemical Cycles*, 27, 1-9.
- McManus, J. F., R. Francois, J. M. Gherardi, L. D. Keigwin, and S. Brown-Leger (2004), Collapse and rapid resumption of Atlantic meridional circulation linked to deglacial climate changes, *Nature*, 428(6985), 834-837.
- Meckler, A. N., D. M. Sigman, K. A. Gibson, R. Francois, A. Martinez-Garcia, S. L. Jaccard, U. Rohl, L. C. Peterson, R. Tiedemann, and G. H. Haug (2013), Deglacial pulses of deep-ocean silicate into the subtropical North Atlantic Ocean, *Nature*, 495(7442), 495-498.
- Meland, M. Y., T. M. Dokken, E. Jansen, and K. Hevroy (2008), Water mass properties and exchange between the Nordic seas and the northern North Atlantic during the period 23-6 ka: Benthic oxygen isotopic evidence, *Paleoceanography*, 23(1), 19.
- Michel, E., L. D. Labeyrie, J.-C. Duplessy, N. Gorfti, M. Labracherie, and J.-L. Turon (1995), Could deep subantarctic convection feed the world deep basins during the Last Glacial Maximum?, *Paleoceanography*, 10(5), 927-941.
- Moros, M., K. Emeis, B. Risebrobakken, I. Snowball, A. Kuijpers, J. McManus, and E. Jansen (2004), Sea surface temperatures and ice rafting in the Holocene North Atlantic: climate influences on northern Europe and Greenland, *Quaternary Science Reviews*, 23(20-22), 2113-2126.
- Ninnemann, U. S., and C. D. Charles (2002), Changes in the mode of Southern Ocean circulation over the last glacial cycle revealed by foraminiferal stable isotopic variability, *Earth and Planetary Science Letters*, 201(2), 383-396.
- Olsen, A., and U. Ninnemann (2010), Large $d^{13}C$ Gradients in the Preindustrial North Atlantic Revealed, *Science*, 330(6004), 658-659.
- Oppo, D. W., and R. G. Fairbanks (1987), Variability in the deep and intermediate water circulation of the Atlantic Ocean during the past 25,000 years: Northern Hemisphere modulation of the Southern Ocean, *Earth and Planetary Science Letters*, 86(1), 1-15.
- Oppo, D. W., J. F. McManus, and J. L. Cullen (2003), Palaeo-oceanography: Deepwater variability in the Holocene epoch, *Nature*, 422(6929), 277-277.
- Piotrowski, A. M., S. L. Goldstein, H. S. R., R. G. Fairbanks, and D. R. Zylberberg (2008), Oscillating glacial northern and southern deep water formation from combined neodymium and carbon isotopes, *Earth and Planetary Science Letters*, 272(1-2), 394-405.

- Piotrowski, A. M., A. Galy, J. A. L. Nicholl, N. Roberts, D. J. Wilson, J. A. Clegg, and J. Yu (2012), Reconstructing deglacial North and South Atlantic deep water sourcing using foraminiferal Nd isotopes, *Earth and Planetary Science Letters*, 357-358(0), 289-297.
- Rahmstorf, S., et al. (2005), Thermohaline circulation hysteresis: A model intercomparison, *Geophysical Research Letters*, 32(23), L23605.
- Renssen, H., H. Goosse, X. Crosta, and D. M. Roche (2010), Early Holocene Laurentide Ice Sheet deglaciation causes cooling in the high-latitude Southern Hemisphere through oceanic teleconnection, *Paleoceanography*, 25(3), PA3204
- Richter, T. (1998), Sedimentary fluxes at the mid-atlantic ridge - sediment sources, accumulation rates, and geochemical characterisation, *GEOMAR Report, GEOMAR Research Center for Marine Geosciences, Christian Albrechts University in Kiel*(73), 173.
- Roberts, N. L., A. M. Piotrowski, J. F. McManus, and L. D. Keigwin (2010), Synchronous Deglacial Overturning and Water Mass Source Changes, *Science*, 327(5961), 75-78.
- Sarnthein, M., K. Winn, S. J. A. Jung, J.-C. Duplessy, L. Labeyrie, H. Erlenkeuser, and G. Ganssen (1994), Changes in east Atlantic deepwater circulation over the last 30000 years: Eight time slice reconstructions, *Paleoceanography*, 9(2), 209-267.
- Schlitzer, R. (2012), Ocean Data View, <http://odv.awi.de>.
- Schott, F. A., R. Zantopp, L. Stramma, M. Dengler, J. r. Fischer, and M. Wibaux (2004), Circulation and Deep-Water Export at the Western Exit of the Subpolar North Atlantic, *Journal of Physical Oceanography*, 34(4), 817-843.
- Schwab, C., H. Kinkel, M. Weinelt, and J. Repschläger (2012), Coccolithophore paleoproductivity and ecology response to deglacial and Holocene changes in the Azores Current System, *Paleoceanography*, 27(3), PA3210.
- Shackleton, N. J., and N. D. Opdyke (1973), Oxygen isotope and palaeomagnetic stratigraphy of Equatorial Pacific core V28-238: Oxygen isotope temperatures and ice volumes on a 105 year and 106 year scale, *Quaternary Research*, 3(1), 39-55.
- Shackleton, N. J. (1974), Attainment of isotopic equilibrium ocean water and the benthonic foraminifera genus *Uvigerina*: Isotopic changes in the ocean during the last glacial, *Cent. Natl.Rech. Sci. Colloq. Int.*, 219, 203-209.
- Skinner, L. C., C. Waelbroeck, A. E. Scrivner, and S. J. Fallon (2014), Radiocarbon evidence for alternating northern and southern sources of ventilation of the deep Atlantic carbon pool during the last deglaciation, *Proceedings of the National Academy of Sciences*, 111(15), 5480-5484.
- Skinner, L. C., S. Fallon, C. Waelbroeck, E. Michel, and S. Barker (2010), Ventilation of the Deep Southern Ocean and Deglacial CO₂ Rise, *Science*, 328(5982), 1147-1151.
- Skinner, L. C., N. J. Shackleton, and H. Elderfield (2003), Millennial-scale variability of deep-water temperature and $\delta^{18}O_{dw}$ indicating deep-water source variations in the Northeast Atlantic, 0-34 cal. ka BP, *Geochemistry, Geophysics, Geosystems*, 4(12), 1098.
- Solignac, S., A. de Vernal, and C. Hillaire-Marcel (2004), Holocene sea-surface conditions in the North Atlantic--contrasted trends and regimes in the western and eastern sectors (Labrador Sea vs. Iceland Basin), *Quaternary Science Reviews*, 23(3-4), 319-334.
- Stenni, B., and et al. (2006), EPICA Dome C Stable Isotope Data to 44.8 KYrBP, IGBP PAGES/World Data Center for Paleoclimatology NOAA/NCDC Paleoclimatology Program, Boulder CO, USA.
- Talley, L. D., and M. S. McCartney (1982), Distribution and circulation of Labrador Sea Water, *Journal of Physical Oceanography*, 12., 1189-1205.
- Thornalley, D., H. Elderfield, and I. N. McCave (2010), Intermediate and deep water paleoceanography of the northern North Atlantic over the past 21,000 years, *Paleoceanography*, 25(1), PA1211.
- Thornalley, D., S. Barker, W. S. Broecker, H. Elderfield, and I. N. McCave (2011), The Deglacial Evolution of North Atlantic Deep Convection, *Science*, 331(6014), 202-205.
- Thornalley, D. J. R., M. Blaschek, F. J. Davies, S. Praetorius, D. W. Oppo, J. F. McManus, I. R. Hall, H. Kleiven, H. Renssen, and I. N. McCave (2013), Long-term variations in Iceland-Scotland overflow strength during the Holocene, *Clim. Past*, 9(5), 2073-2084.
- Van Aken, H. M. (2000), The hydrography of the mid-latitude northeast Atlantic Ocean: I: The deep water masses, *Deep Sea Research Part I: Oceanographic Research Papers*, 47(5), 757-788.
- Van Aken, H. M., and C. J. De Boer (1995), On the synoptic hydrography of intermediate and deep water masses in the Iceland Basin, *Deep Sea Research Part I: Oceanographic Research Papers*, 42(2), 165-189.
- Van Meerbeek, C., D. Roche, and H. Renssen (2011), Assessing the sensitivity of the North Atlantic Ocean circulation to freshwater perturbation in various glacial climate states, *Climate Dynamics*, 1-19.
- Van Sebille, E., M. O. Baringer, W. E. Johns, C. S. Meinen, L. M. Beal, M. F. de Jong, and H. M. van Aken (2011), Propagation pathways of classical Labrador Sea water from its source region to 26°N, *J. Geophys. Res.*, 116(C12), C12027.
- Waelbroeck, C., L. Labeyrie, E. Michel, J. C. Duplessy, J. F. McManus, K. Lambeck, E. Balbon, and M. Labracherie (2002), Sea-level and deep water temperature changes derived from benthic foraminifera isotopic records, *Quaternary Science Reviews*, 21, 295-305.
- Waelbroeck, C., L. C. Skinner, L. Labeyrie, J. C. Duplessy, E. Michel, N. Vazquez Riveiros, J. M. Gherardi, and F. Dewilde (2011), The timing of deglacial circulation changes in the Atlantic, *Paleoceanography*, 26(3), PA3213.
- Weppernig, R., P. Schlosser, S. Khatriwala, and R. Fairbanks (1996), Isotope data from Ice Station Weddell: implications for deep water formation in the Weddell Sea, *Journal of Geophysical Research* 101(C10), 25723-25739.
- Yu, J., and H. Elderfield (2008), Mg/Ca in the benthic foraminifera *Cibicoides wuellerstorfi* and *Cibicoides mundulus*: Temperature versus carbonate ion saturation, *Earth and Planetary Science Letters*, 276(1-2), 129-139.

7.14 Supplementary information

7.14.1 Calibration of benthic Mg/Ca data

An array of different monospecific and multispecies Mg/Ca temperature calibrations exists for benthic foraminifera. In order to identify the most reliable calibration for our dataset different calibrations were tested. The Mg/Ca temperature calibration of *Kristjánsdóttir et al.* [2007] for *M. barleanum* and that of *Lear et al.* [2002] for *C. wuellerstorfi* and *M. barleanum* result in temperature estimates with differences of less than 0.5°C as observed in our own parallel measurements of both species. Despite these similarities both calibrations appear to overestimate BWT during the Holocene by 3°C when compared to modern values (Figure S1b,c). This overestimation of the temperature might be the result of an overprint by varying $[\text{CO}_3]^{2-}$ concentration levels on the calibration data set as suggested by *Tisserand et al.* [2013]. The calibration data sets of *Kristjánsdóttir et al.* [2007] and *Lear et al.* [2002] were obtained from subpolar North Atlantic sites that are most probably influenced by strong gradients in $[\text{CO}_3]^{2-}$ concentration, that however were not considered in the calibrations.

In contrast, the possible impact of $[\text{CO}_3]^{2-}$ is accounted for in the calibration of *Healey et al.* [2008], which results in reasonable estimates for *C. wuellerstorfi* Mg/Ca-based BWT (Figure 1b) and is therefore considered to be more reliable. Parallel measurements on *C. wuellerstorfi*, *M. barleanum* and *M. affinis* show no systematic offset in Mg/Ca ratios between *C. wuellerstorfi* and *M. barleanum*. An offset of 0.3 mmol/mol Mg/Ca between *C. wuellerstorfi* and *M. affinis* affects the calculated BWT by 0.05°C and thus can be regarded as insignificant. Assuming that *C. wuellerstorfi*, *M. barleanum* and *M. affinis* follow similar slopes in their individual empirical calibration equations [*Lear et al.*, 2002], we applied the calibration of *Healey et al.*, [2008] on all samples. Thereby late Holocene BWT results are in good agreement with modern BWT. Nevertheless applying a monospecific calibration on a multispecies record may induce systematic errors in the estimated temperatures. Indeed the BWT amplitude between YD and Holocene increases when using the calibrations of *Kristjánsdóttir et al.* [2007] or *Lear et al.* [2002]. This mismatch in amplitudes also becomes evident when comparing the amplitude of BWT rise from the YD into the Holocene from the Azores coring site (2°C) with data from the Iberian Margin (3°C). The by 1°C larger difference [*Skinner et al.*, 2003], is probably caused by the application of different species and calibrations rather than showing a true temperature gradient between the two locations. Therefore a potential overestimation of the BWT by 1°C has to be considered for the interpretation of the part of the record where *Melonis sp.* was used (15-10 ka BP).

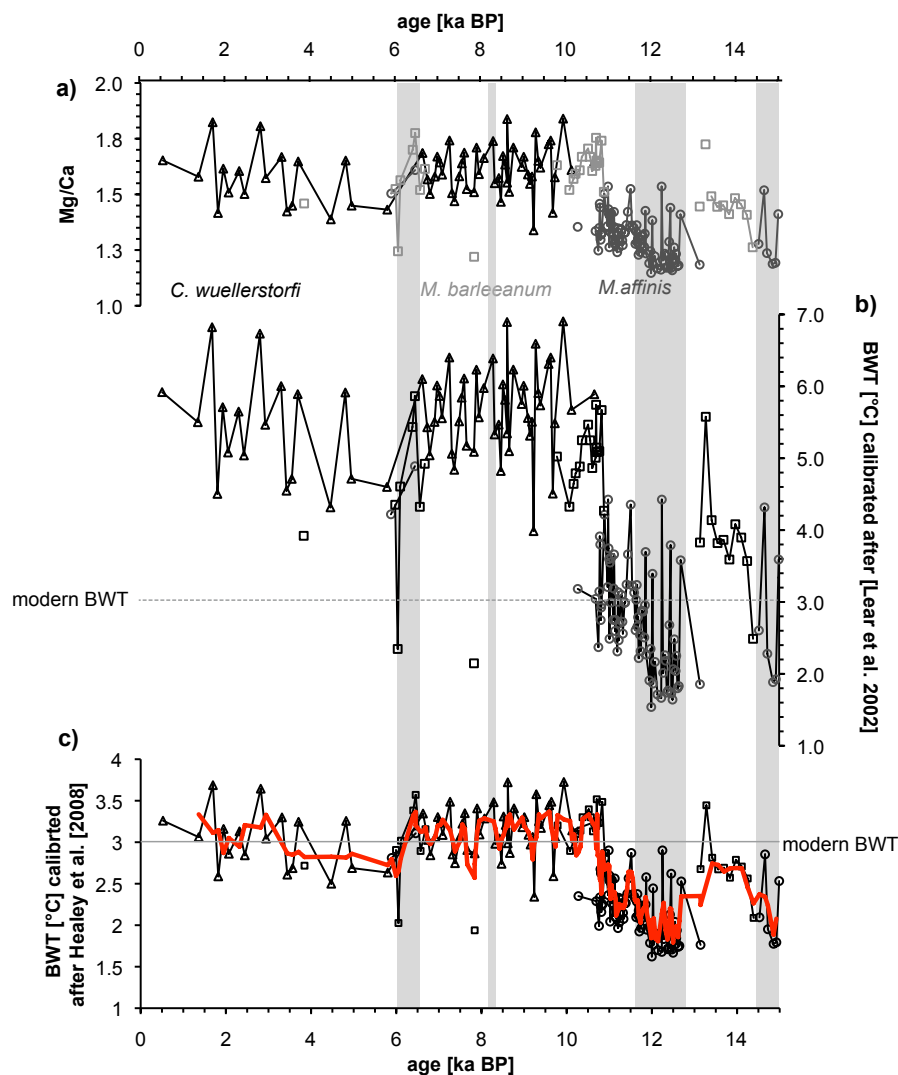


Figure 7.S1 multispecies benthic Mg/Ca BWT records using different calibrations

- Mg/Ca ratios analyzed for 3 different benthic species *C. wuellerstorfi* (triangles), *M. affinis* (circles) and *M. barleanum* (rectangles) with Mg/Ca ratios of *M. affinis* corrected for the offset of 0.3 to match *M. barleanum*
- BWT calculated from the Mg/Ca records of the three different species with *M. affinis*, *M. barleanum* (symbols as in a)) using the calibration equation of Lear et al., [2002] (light grey lines) and Healey et al. [2008] (dark grey lines) Note that calculation of BWT by the Lear et al. [2002] calibration results in BWT values on average 3° above modern BWT and suggests a 4°C difference between the Younger Dryas and the Early Holocene
- BWT record calibrated applying the Healey et al. [2008] calibration for all species with Mg/Ca *M. affinis* corrected for the internal factor of 0.3 to match *M. barleanum*. The red line presents the 3-point average mean of this record.

7.14.2 Potential overprint by carbon ion saturation

Yu and Elderfield [2008] reconstructed changes in $[\text{CO}_3]^{2-}$ concentration in the NA over the last deglacial using B/Ca ratios with a estimated maximal increase of $30 \mu\text{mol/kg } [\text{CO}_3]^{2-}$ during the last 15 ka BP. Using the calibration of Healey et al. [2008] the maximum change of $30 \mu\text{mol/kg } [\text{CO}_3]^{2-}$ would lead to a change of $0.3 \text{ mmol/mol Mg/Ca}$, which is equivalent to an underestimation of glacial temperatures by 1°C . Regarding the BWT difference of 2°C between YD and early Holocene, this would amount half of the signal. Nevertheless the strongly fluctuating B/Ca records of Yu and Elderfield [2008] from 2800 and 3500 m wd in the NA do not match the pattern of our Mg/Ca record (Figure S2), thus an overprint by $[\text{CO}_3]^{2-}$ seems to be neglectable.

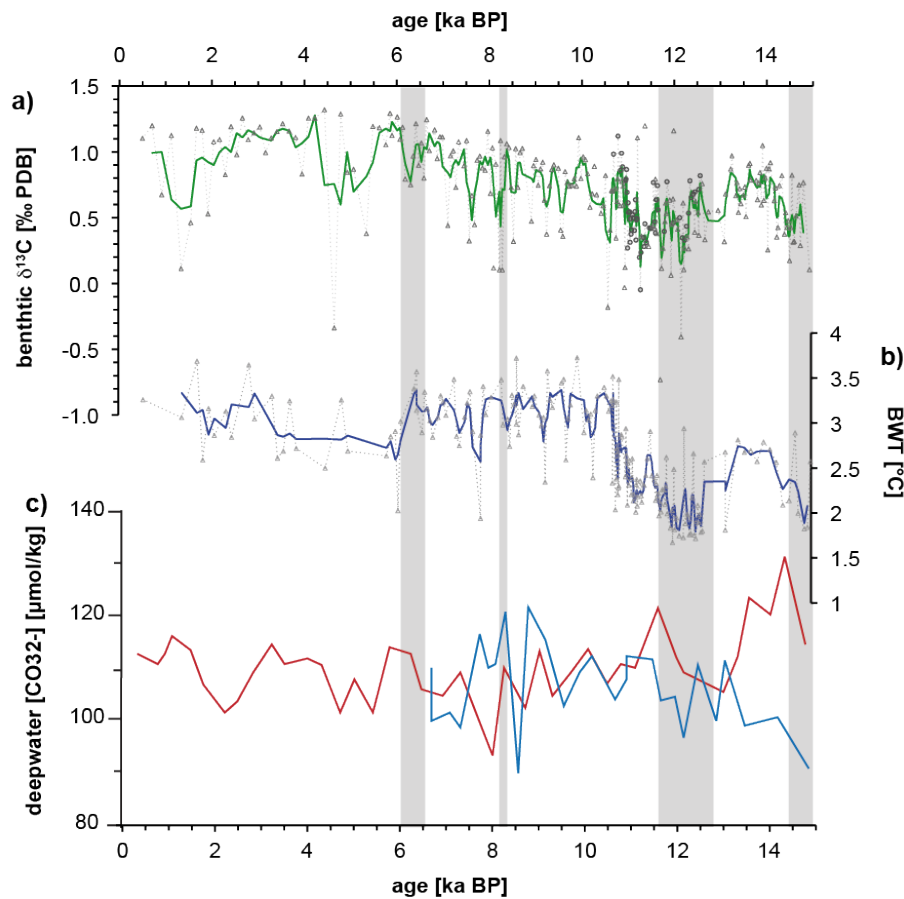


Figure 7.S2 Comparison of benthic BWT and $\delta^{13}\text{C}$ records from our coring site with NA $[\text{CO}_3]^{2-}$ records [Yu et al., 2008] from site BOFS10K at 2777 m water depth (red line) and BOFS 8K at 4045 m water depth.

- stacked $\delta^{13}\text{C}$ record of *C. wuellerstorfi* and *M. affinis*, the latter corrected by a factor of 1.36‰ (internal factor observed by double measurements)
- calculation of BWT based on species specific Mg/Ca ratios using the equation by Healey et al. [2008] with Mg/Ca *M. affinis* corrected for the internal factor of 0.3 to match *M. barleanum*
- $[\text{CO}_3]^{2-}$ records from Yu et al. [2008] from site BOFS10K at 2777 m water depth (red line) and BOFS 5K at 3547 m water depth (blue line). The dissimilarity between records in a, b and c indicates that neither the $\delta^{13}\text{C}$ record nor the BWT is overprinted by changes in the carbonate ion concentration

7.14.3 Potential overprint of $\delta^{13}\text{C}$ signals by productivity changes

Usually the nearly parallel evolution of the BWT and $\delta^{13}\text{C}$ (Figure S2 a,b) would be explained by a change in the deepwater composition, however an overprint by biological productivity and variable organic matter fluxes to the bottom waters on the BWT and $\delta^{13}\text{C}$ signals [Waelbroeck *et al.*, 2011] needs to be ruled out.

The overprint by productivity would be induced by the decay of increased flux of organic matter that would decrease the $\delta^{13}\text{C}$ values and decrease in the CO_3^{2-} concentration of the bottom water leading to an underestimation of BWT. This overprint can be tested by the use of the

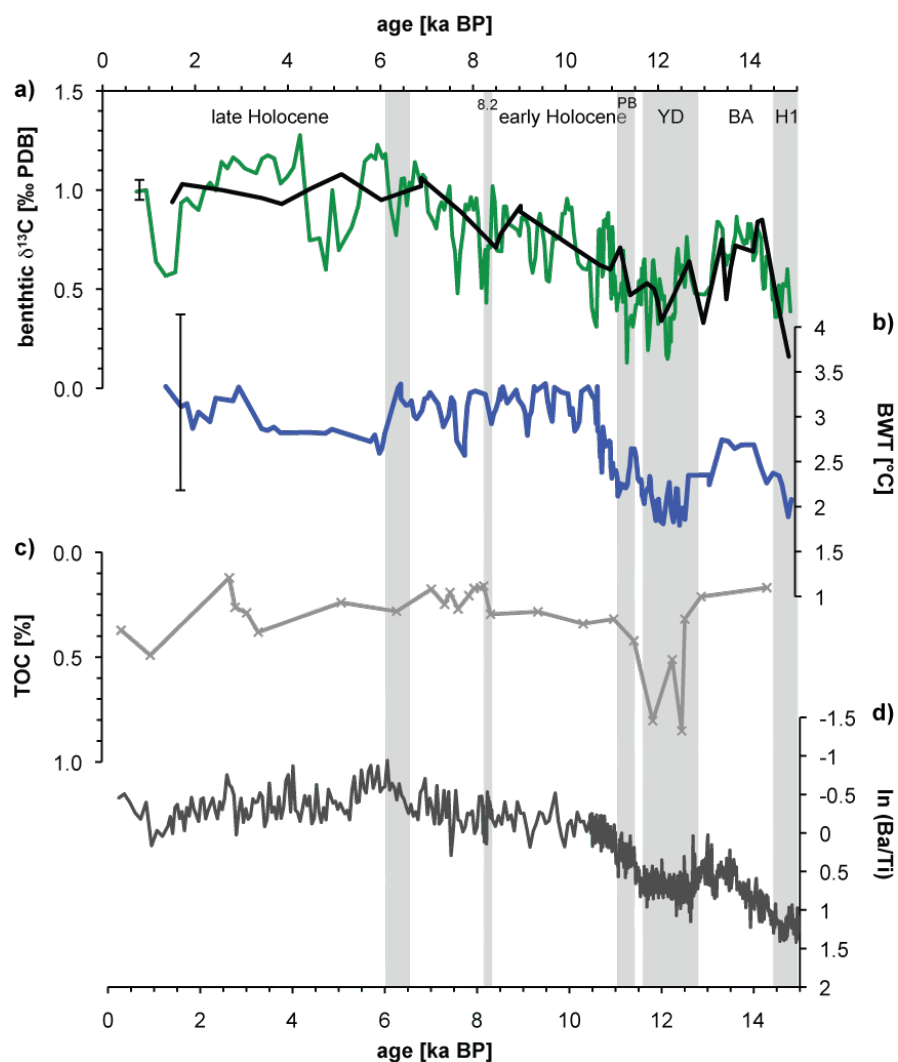


Figure 7.S3 Possible overprint Comparison of the benthic foraminifera $\delta^{13}\text{C}$ record with by productivity changes

- Three point running mean of a stacked $\delta^{13}\text{C}$ record for *C. wuellerstorfi* and corrected *M. affinis* (1.46‰) (green line) and the $\delta^{13}\text{C}$ record of core MD95-2042 from the Iberian Margin [Skinner and Shackleton, 2003] (black line)
- 3- point running mean of mixed benthic (*C. wuellerstorfi*, *M. affinis*, *M. barleanum*) Mg/Ca based BWT record (blue line),
- TOC % from core GEOFAR KF16 [Richter *et al.*, 1998] close to our study site.
- XRF scanner derived ln Ba/Ti record for core MD08-3180 [Schwab *et al.*, 2012].

paleoproductivity (PP) reconstruction based on Ba/Ti ratios [Schwab *et al.*, 2012b] and TOC [Richter, 1998] for our study site. The $\ln(\text{Ba}/\text{Ti})$ record shows a similar pattern as BWT and $\delta^{13}\text{C}$ and thus indicates a decreased PP over BA, an increase in PP during YD, a successive decrease over early Holocene and a mid Holocene stabilization (Figure S3 a,b). Thus a potential overprint by varying organic matter fluxes has to be considered. The pattern of the TOC record, however, shows a decrease during the YD with an abrupt increase at the end, and thereby differs from what would be expected for the $\delta^{13}\text{C}$ record, that is increasing $\delta^{13}\text{C}$ values with decreasing TOC fluxes reaching the deeper waters and the seafloor. Despite the general assumption that the benthic $\delta^{13}\text{C}$ signal might be affected by productivity changes [Eberwein and Mackensen, 2006; Fontanier *et al.*, 2006] the expected dependency between $\delta^{13}\text{C}$ and resulting changes in DIC could not be confirmed for the Canary Island region and for the Iberian Margin as well. Additionally, Waelbroeck *et al.* [2011] argue that changes in $\delta^{13}\text{C}$ of 1‰ are generally too high to be caused by surface productivity changes alone.

Furthermore, no correlation between the $\delta^{13}\text{C}$ and (Ba/Ti) ratios [Schwab *et al.*, 2012] (figure S4) is observed ($R^2=0.16$) in cores GEOFAR KF16/MD08-3180, thus an overprint of $\delta^{13}\text{C}$ by productivity changes can be ruled out.

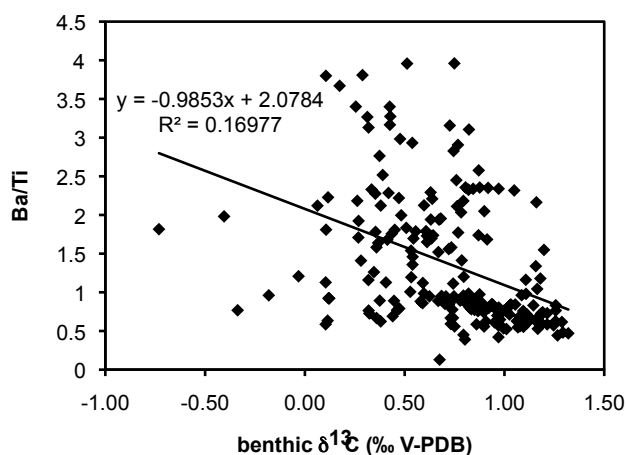


Figure 7.S4 versus $\delta^{13}\text{C}$ (Ba/Ti) cross plot
indicates no overprint of $\delta^{13}\text{C}$ by productivity changes Ba /Ti data from Schwab *et al.*[2012]

7.14.4 References

Eberwein, A., and A. Mackensen (2006), Regional primary productivity differences off Morocco (NW-Africa) recorded by modern benthic foraminifera and their stable carbon isotopic composition, *Deep Sea Research Part I: Oceanographic Research Papers*, 53(8), 1379-1405.

- Fontanier, C., A. Mackensen, F. Jorissen, P. Anschutz, L. Licari, and C. Griveaud (2006), Stable oxygen and carbon isotopes of live benthic foraminifera from the Bay of Biscay: Microhabitat impact and seasonal variability, *Marine Micropaleontology*, 58(3), 159-183.
- Healey, S. L., R. C. Thunell, and B. H. Corliss (2008), The Mg/Ca-temperature relationship of benthic foraminiferal calcite: New core-top calibrations in the <math><4^{\circ}\text{C}</math> temperature range, *Earth and Planetary Science Letters*, 272(3-4), 523-530.
- Kristjánisdóttir, G. B., D. W. Lea, A. E. Jennings, D. K. Pak, and C. Belanger (2007), New spatial Mg/Ca-temperature calibrations for three Arctic, benthic foraminifera and reconstruction of north Iceland shelf temperature for the past 4000 years, *Geochem. Geophys. Geosyst.*, 8.
- Lear, C. H., Y. Rosenthal, and N. Slowey (2002), Benthic foraminiferal Mg/Ca-paleothermometry: A revised core-top calibration, *Geochimica et Cosmochimica Acta*, 66(19), 3375-3387.
- Richter, T. (1998), Sedimentary fluxes at the mid-atlantic ridge - sediment sources, accumulation rates, and geochemical characterisation, *GEOMAR Report, GEOMAR Research Center for Marine Geosciences, Christian Albrechts University in Kiel*(73), 173.
- Schwab, C., H. Kinkel, M. Weinelt, and J. Repschläger (2012), Coccolithophore paleoproductivity and ecology response to deglacial and Holocene changes in the Azores Current System, *Paleoceanography*, 27(3), PA3210.
- Skinner, L. C., N. J. Shackleton, and H. Elderfield (2003), Millennial-scale variability of deep-water temperature and $\delta^{18}\text{O}_{\text{dw}}$ indicating deep-water source variations in the Northeast Atlantic, 0-34 cal. ka BP, *Geochem. Geophys. Geosyst.*, 4(12), 1098.
- Thornalley, D., H. Elderfield, and I. N. McCave (2010), Intermediate and deep water paleoceanography of the northern North Atlantic over the past 21,000 years, *Paleoceanography*, 25(1), PA1211.
- Waelbroeck, C., L. C. Skinner, L. Labeyrie, J. C. Duplessy, E. Michel, N. Vazquez Riveiros, J. M. Gherardi, and F. Dewilde (2011), The timing of deglacial circulation changes in the Atlantic, *Paleoceanography*, 26(3), PA3213.
- Yu, J., and H. Elderfield (2008), Mg/Ca in the benthic foraminifera *Cibicides wuellerstorfi* and *Cibicides mundulus*: Temperature versus carbonate ion saturation, *Earth and Planetary Science Letters*, 276(1-2), 129-139.

Chapter 8

Summary and Conclusion

8 Summary and conclusion

In this study the impact of AMOC changes on the subtropical North Atlantic (NA) surface and deepwater hydrography was investigated. The study was conducted on the deglacial and Holocene sections of high-resolution sediment cores (MD08-3180/GEOFAR KF16) from the Azores (37.999°N; 31.134°W/ 37.984°N/31.118°W). These open ocean site is situated south of the Azores Island in the eastern NA basin at the northern boundary of the subtropical gyre (STG).

In this study multiproxy SST ($U^{K'}_{37}$, SIMMAX and Mg/Ca of surface and subsurface dwelling foraminifera) reconstructions were used to gain a reliable deglacial SST record from the subtropical NA. Furthermore, the differences between the applied SST proxies indicate that different hydrological and climatic changes influence the used SST proxies. The impact of meltwater on the coring site was identified by the combination of the SST data with stable isotope analyses of surface and subsurface dwelling foraminifera (expressed as $\delta^{18}O_{sw-ice}$). The changing influence of subpolar, subtropical and temperate water masses on the coring site was reconstructed by changes in the relative abundances of selected indicator foraminifera species. Thereby it was shown that the Azores coring site is more sensitive to deglacial SST changes and NH freshwater pulses than previously thought [Shakun and Carlson, 2010]. The reconstruction of the STG position indicates a southward displacement of the STG during cold periods over the last deglacial and Holocene. Different heat storage patterns of the STG during the deglacial weak AMOC phases were deciphered and their potential impact on the European climate was shown.

For the first time eastern NA basin deepwater temperatures were obtained from benthic Mg/Ca reconstructions in a high-resolution deglacial and early Holocene record. These temperatures were combined with deepwater ventilation ($\delta^{13}C$) and salinity ($\delta^{18}O_{sw-ice}$) reconstructions to investigate changes in the deepwater mass geometry.

8.1 Multiproxy temperature reconstructions

Within this study deglacial multiproxy SST signals were disentangled and the reliability of SST reconstructions from the Azores coring site was assessed. SIMMAX SST is recording summer and winter SST during the Holocene (SST_{su} 22-24°C) (10.5 –modern) and over most parts of the BA (14.6-13.2 ka BP) (SST_{su} 18.5-21.5°C). During the YD, SIMMAX SST seems to reflect subsurface conditions that indicate a thermocline warming and hence a subsurface heat storage. $U^{K'}_{37}$ SST reconstructions are reliable recorders of summer SST from the H1 event to the early Holocene (10.5 ka BP), but seem to underestimate the magnitude of short-term cooling events (e.g. H1, IACP, 8.2 event) interrupting the long-term deglacial and Holocene SST evolution. Mg/Ca SST reconstructions of *G. bulloides* are effected by changes in growth season and depth habitat, whereas *G. ruber w.* and *G. truncatulinoides* are faithful recorders of the surface and thermocline temperature, respectively. SIMMAX SST amplitudes differ between three major cold events with

occurring at the H1 event, the IACP, during the 8.2 event (up to 12°C) and the Preboreal oscillations (up to 6°C). The amplitude of cold events are not certain due to non-analogue situations within SIMMAX SST, uncertain dampening of $U^{K'}_{37}$ record and overprinted Mg/Ca SST record. However, a strong cooling at the Azores coring site is reasonable as a southward shift of the STG and the occurrence of subpolar conditions are indicated by changes in faunal assemblage at the Azores coring site during major cold events. A maximal cooling of 5°C and a gyre displacement is also evident in model results from the KCM. Furthermore, observed seasonal differences in the chosen SST signals have a strong overprint on the $\delta^{18}O_{sw-ice}$ reconstructions, probably of the same amount as freshwater events.

8.2 Coupled AMOC and surface water hydrography evolution over Holocene and deglacial

Over the deglacial and Holocene the position of the STG is coupled to the strength of AMOC. The STG moved southwards during weak AMOC phases and northwards during AMOC strengthening. During the major cold events IACP, YD and 8.2 event the STG displacement was caused by meltwater pulses (inducing changes of 1‰ SMOW) that reached down to the Azores coring site and led to a strong decrease in SST of 6°C in minimum.

Two different deglacial heat storage scenarios are evident at the Azores coring site. During BA a weakening of AMOC and is accompanied by a warming of the surface water. These warm waters even prevailed at the Azores coring site during late Allerød, when the STG already retracted southward and possibly had an influence on the European climate. Furthermore, subsurface heat storage is observed during the YD as deduced from SIMMAX SST, Mg/Ca SST, $U^{K'}_{37}$ SST and Mg/Ca thermocline temperature reconstructions.

8.3 Deglacial deepwater composition changes

A new high-resolution BWT, ventilation and $\delta^{18}O_w$ record from the subtropical eastern NA indicates that the deepwater composition in the eastern North Atlantic basin changed over the last 15 ka BP. A general evolution toward a warmer better ventilated deepwater was disrupted during the H1 event, the YD and the early Holocene by a less ventilated, cool (1.5°C cooling during YD) and freshened water. The parallel evolution of BWT, $\delta^{13}C$ and $\delta^{18}O_w$ with changes in the deep- and surface water compositions in the subpolar NA and with the Greenland ice core records indicate that variations in deepwater composition over the last 15 ka BP were triggered in the subpolar North Atlantic. In consequence these deepwater composition changes might also have affected the deglacial AABW composition changes and deglacial deepwater stratification changes.

This study showed that the Azores coring site is very sensitive for changes in the AMOC system and thus is suitable for further high resolutions studies on climate change.

Chapter 9

Outlook

9 Outlook

9.1 The 6.5 ka BP event – a “new” Holocene cold event?

In the paleoclimatic records from the Azores coring site a distinct event occurs between 6.9 and 6.3 ka BP that is evident in nearly all paleoclimatic reconstructions from this site. As the mid point of this event is at 6.5 ka it is henceforward referred to as 6.5 ka BP event.

The 6.5 ka BP event starts with a distinct increase in the relative abundance of subpolar and transitional species and a decrease in the relative abundance of the subtropical species *G. ruber w.*. *G. ruber w* reaches its abundance minimum between 6.6 and 6.3 ka BP (Figure 9.1d). This change in the species abundance is accompanied by SIMMAX SST cooling of 1.5°C (Figure 9.1a). The start of this event coincides with a coarsening of the sediment (Figure 9.1e) that is caused by a distinct ash layer that reaches its maximum at 6.5 ka BP and thereafter ends abruptly. From 6.5 to 6.4 ka subsurface and surface $\delta^{18}\text{O}$ values successively increase by 0.5 and 0.6‰ V-PBD respectively. This increase in the planktonic $\delta^{18}\text{O}$ is followed by a benthic $\delta^{18}\text{O}$ increase of 0.5‰ V-PBD and $\delta^{13}\text{C}$ decrease of 0.4‰ V-PBD that started at 6.45 ka BP. At 6.2 ka all records recovered abruptly.

The most characteristic feature in the 6.5 ka BP event is the $\delta^{18}\text{O}$ increase by 0.6-0.5‰ that occurs time-delayed in the subsurface, surface and deepwater records. These low $\delta^{18}\text{O}$ values either might have been caused by dissolution or by a cooling of all water masses by 2°C. The causes for the cooling either might be a freshwater pulse or a volcanic eruption as indicated by the ash layer. The 6.5 ka BP event distinctly differs from the earlier Holocene meltwater events (e.g 8.2, 9.6 10.2 ka BP) that are nearly indistinguishable in its isotope signatures from the residual of the record. At the beginning of the event increasing salinities are observed by the $\delta^{18}\text{O}_{\text{w-ice}}$ record obtained from coupled SIMMAX SST and stable isotope data of *G. ruber w.* (Figure 9.1e). A single point freshwater peak is evident in this record at 6.3 ka BP that coincides with the maximum deepwater stable isotope values in the end of 6.5 ka BP event. This freshening occurs far to late to have caused the 6.5 ka BP event.

The propagation of the signal from the surface to the deepwater and the distinct changes in the fauna composition indicate that this event was not caused by dissolution.

The synchronous start of the ash layer and the changes in the foraminifera fauna however indicate that a volcanic eruption might have caused the 6.5 ka BP event. But such has neither been reported from North Atlantic high-resolution marine sediment cores nor from the Greenland ice cores so far. The reason for this lack of data might be a shorter duration of the event than indicated within our record, as the ash layer causes an increase in sedimentation rates. Thus the 6.5 event might only be evident in a single point in other records. To further investigate the source of the ash layer and its possible distribution in the NA basin, and the exact dating of this event is needed.

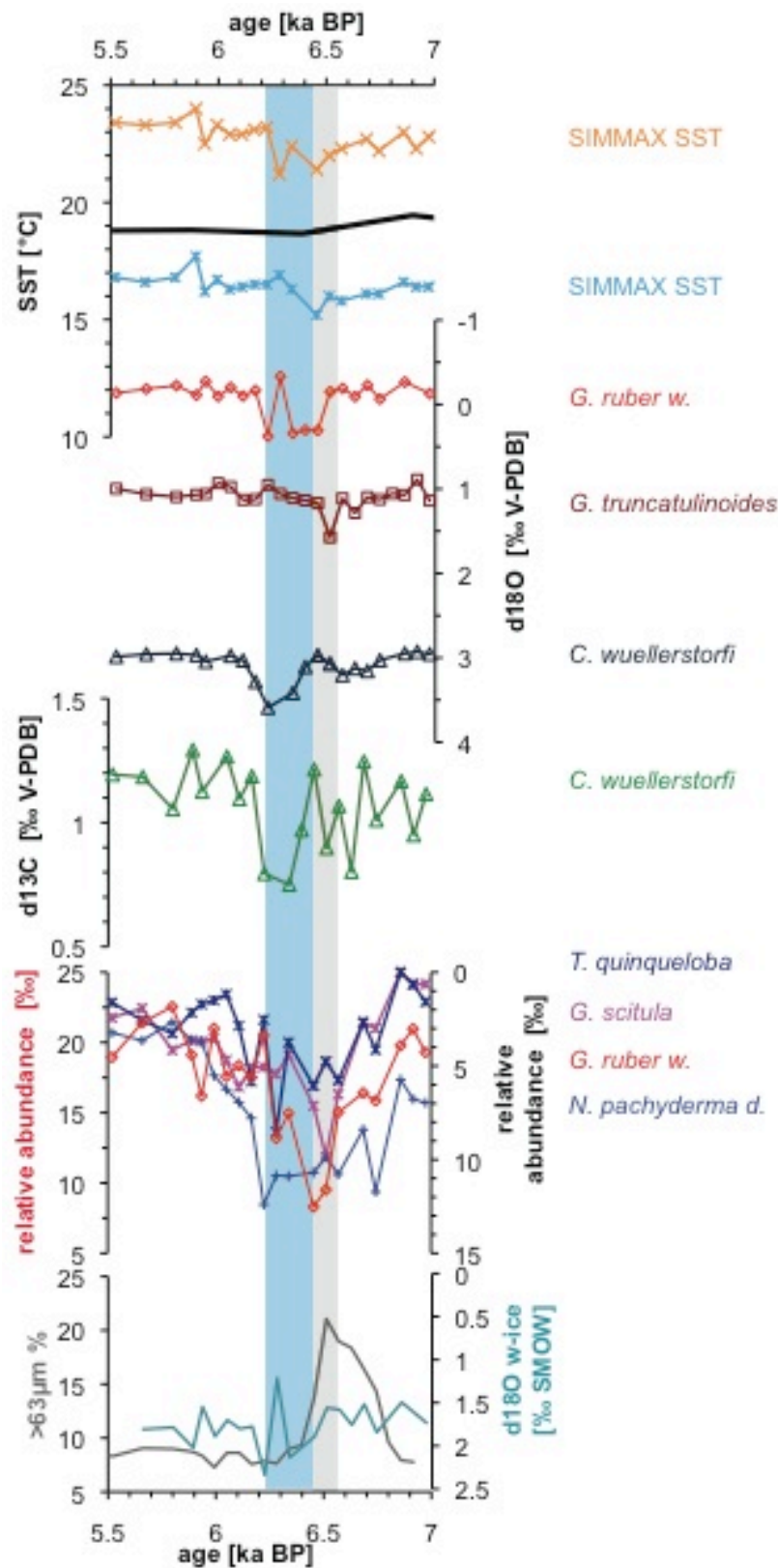


Figure 9.1 Various surface and deepwater records indicating the 6.5 ka BP event

Though of uncertain origin, the 6.5 ka BP event seems to have induced a major change in the surface and subsurface water circulation that was followed by a delayed deepwater signal. This

distinct time-delay in the signal propagation might give us further insight into the dynamics of AMOC and short-term climate variability during the Holocene.

9.2 Core MD08-3181- a midocean sediment core with decadal resolution?

Calypso piston core MD08-3181 was taken in addition to Casq core MD08-3180 at the same coring location. Core MD08-3181 is 2336 cm long and consists of silty clay with foraminifera that is laminated nearly throughout the core [Kissel *et al.*, 2008], with a lamina width of 0.1-0.5 cm. A preliminary stack of core MD08-3181 with parallel core MD08-3180 using the Ca/Ti data from XRF core scanning and additional planktonic stable isotope data of core MD08-3181 (this study) and MD08-3180 (Balmer unpublished data) indicates that the top of core MD08-3181 approximately begins at the end of Heinrich stadium 1 (15 ka BP). Additional ^{14}C dating at 2324-2325 cm of core MD08-3181 has the age of 33740 ka BP when converted into calendar ages using the Calib 6.0 software [Stuiver and Reimer, 1986] with marine09 calibration curve [Reimer *et al.*, 2009] assuming a constant reservoir age of 400 years. This very preliminary age model suggests sedimentation rates of 0.8 cm/ 10 years in core MD08-3181 over Marine Isotope Stage 2 (MIS2). Thus the resolution of our core has a decadal resolution and the laminae might even reach annual resolution. This high-resolution sediment core provides an opportunity to compare changes in the last glacial surface and deepwater hydrography of the subtropical North Atlantic with changes in the Greenland ice core record. A high-resolution dataset was obtained from the lowest 136 cm (1200-2336 cm) of the core including Mg/Ca and isotope measurements on benthic foraminifera as well as stable isotopes of planktonic foraminifera. Based on the preliminary age model, the data covers the glacial Heinrich events H3 and H4. This data indicates that severe changes in deepwater and surface hydrology also occurred during last glacial Heinrich events and the LGM.

The high resolution LGM obtained in core MD08-3181 by far exceeds the expectations of the AMOCINT coring survey. The coring site of MD08-3180/81 is a possible target for IODP coring, as the high sedimentation rates would allow to analyze older interglacials with a high resolution. However, for this purpose, extensive site survey is needed.

This study shows that the Azores coring site is a suitable site for further research on climate change, as the Azores hydrographic system reacts highly sensitive to different AMOC forcing.

Appendix

Table A1: Deglacial stages and their age boundaries

stage	Abbreviation	Greenland stadium	Age boundaries [kaBP]	reference
Last Glacial Maximum	LGM	GS2a	26.5-19.0	[Cutler et al., 2003; Lambeck and Chappell, 2001; Peltier, 2002]
Heinrich event 1	H1	GS2a	19-14.6	[Stanford et al., 2011]
Bølling	B	GI1b	14.642- 13.904	[Lowe et al., 2008; Yu and Eicher, 2001]
Inter Bølling Cold Period	IBCP	GI1d	14025-13904	Lowe et al., 2008; Yu and Eicher, 2001]
Older Dryas	OD	GI1c	? not dated in NGRIP	Lowe et al., 2008; Yu and Eicher, 2001]
Allerød	A	GI1a-c	13904-12.850	Lowe et al., 2008; Yu and Eicher, 2001]
Inter Allerød cold period	IACP	GI1b	13.35-13.1	Lowe et al., 2008; Yu and Eicher, 2001]
Younger Dryas	YD	GS1	12850-11650	Lowe et al., 2008; Yu and Eicher, 2001]
Preboreal oscillation	PBO		11.3 11.4-11.27	[Björck et al., 1998; Björck et al., 1996; Fisher et al., 2002]
Preboreal	PB		11.6-10.8	[Andresen et al., 2004; Björck et al., 1998; Bos et al., 2007]
8.2 event	8.2		8190 mid volc event 8186	Lowe et al., 2008; Yu and Eicher, 2001]
Holocene			11650-0	Lowe et al., 2008; Yu and Eicher, 2001]

Andresen, C. S., S. Björck, O. Bennike, and G. Bond (2004), Holocene climate changes in southern Greenland: evidence from lake sediments, *Journal of Quaternary Science*, 19(8), 783-795.

Björck, S., M. J. C. Walker, L. C. Cwynar, S. Johnsen, K.-L. Knudsen, J. J. Lowe, and B. Wohlfarth (1998), An event stratigraphy for the Last Termination in the North Atlantic region based on the Greenland ice-core record: a proposal by the INTIMATE group, *Journal of Quaternary Science*, 13(4), 283-292.

Björck, S., et al. (1996), Synchronized Terrestrial/Atmospheric Deglacial Records Around the North Atlantic, *Science*, 274(5290), 1155-1160.

Bos, J. A. A., B. van Geel, J. van der Plicht, and S. J. P. Bohncke (2007), Preboreal climate oscillations in Europe: Wiggle-match dating and synthesis of Dutch high-resolution multi-proxy records, *Quaternary Science Reviews*, 26(15-16), 1927-1950.

Cutler, K. B., R. L. Edwards, F. W. Taylor, H. Cheng, J. Adkins, C. D. Gallup, P. M. Cutler, G. S. Burr, and A. L. Bloom (2003), Rapid sea-level fall and deep-ocean temperature change since the last interglacial period, *Earth and Planetary Science Letters*, 206, 253-271.

Fisher, T. G., D. G. Smith, and J. T. Andrews (2002), Preboreal oscillation caused by a glacial Lake Agassiz flood, *Quaternary Science Reviews*, 21(8-9), 873-878.

Lambeck, K., and J. Chappell (2001), Sea Level Change Through the Last Glacial Cycle, *Science*, 292(5517), 679-686.

Lowe, J. J., S. O. Rasmussen, S. Björck, W. Z. Hoek, J. P. Steffensen, M. J. C. Walker, and Z. C. Yu (2008), Synchronisation of palaeoenvironmental events in the North Atlantic region during the Last Termination: a revised protocol recommended by the INTIMATE group, *Quaternary Science Reviews*, 27(1, Äi2), 6-17.

Peltier, W. R. (2002), On eustatic sea level history: Last Glacial Maximum to Holocene, *Quaternary Science Reviews*, 21(1-3), 377-396.

Stanford, J. D., E. J. Rohling, S. Bacon, A. P. Roberts, F. E. Grousset, and M. Bolshaw (2011), A new concept for the paleoceanographic evolution of Heinrich event 1 in the North Atlantic, *Quaternary Science Reviews*, 9-10, 1047-1066.

Yu, Z., and U. Eicher (2001), Three amphi-Atlantic century-scale cold events during the Bølling-Allerød warm period, *Géographie physique et Quaternaire*, 55(2), 171-179.

Table A 2 sampling intervals

Abbreviations: JR: Janne Repschläger; CS: Christian Schwab

Core	Core interval [cm]	Sample size	Sampling interval	comments	Analyse d by
GEOFAR KF16 working half	0-200	1 cm slices	1cm	Residuals of presampled working half completely sampled; Bulk sediment for Nannoplankton analyses and Alkenone analyses taken	J.R. C.S.
MD08- 3180CQ Series B	60-150	0.5cm slices	0.5 cm	Completely sampled	J.R.
	150-400	1 cm slices	1cm	Completely sampled	J.R.
MD08- 3180CQ Series A	0-400	1 cm slices	1 cm	Completely sampled	J.R.
MD08- 3181 working half	1909-2336	Syringe sample 1 cm diamete r	Every 10 th cm		J.R. C.S.
	0-1890.5	1 cm slices	Every 10 th cm	Bulk sediment for Nannoplankton analyses and Alkenone analyses taken	J.R. C.S.
	1900-1902; 1907-1908; 1943-1944; 1967-1987; 2013-2020	0.5 cm slices	0.5 cm	Completely sampled Bulk sediment for Nannoplankton analyses and Alkenone analyses taken	J.R. C.S.
	1902- 1907; 1908-1943; 1944-1967; 1987-2013; 2020-2336	1 cm slices	1 cm	Completely sampled Bulk sediment for Nannoplankton analyses and Alkenone analyses taken	J.R. C.S.

Table A3 stable isotope data GEOFAR KF16

GEOFAR KF16								
core depth [cm]	sample intervall [cm]	age [years BP]	comment	$\delta^{18}\text{O}$ <i>G. ruber w.</i> >315 μm [‰ VPDB]	$\delta^{18}\text{O}$ <i>G. truncatulinoides</i> >315 μm [‰ VPDB]	$\delta^{13}\text{C}$ <i>C. wuellerstorfi</i> >315 μm [‰ VPDB]	$\delta^{18}\text{O}$ <i>C. wuellerstorfi</i> >315 μm [‰ VPDB]	$\delta^{18}\text{O}$ <i>C. wuellerstorfi</i> >315 μm corrected [‰ VPDB]
2.5	2-3	524		-0.17	1.00	1.10	2.30	2.94
3.5	3-4	734		-0.33	1.01	1.20	2.22	2.86
4.5	4-5	943		-0.27	1.09	0.68	2.29	2.93
5.5	5-6	1153		-0.30	1.04	1.13	2.32	2.96
6.5	6-7	1362		-0.23	0.89	0.11	2.35	2.99
7.5	7-8	1572		-0.20	1.09	0.46	2.33	2.97
8.5	8-9	1697		-0.34	0.95	1.18	2.32	2.96
9.5	9-10	1821		-0.15	0.98	1.16	2.36	3.00
10.5	10-11	1946		-0.37	0.95	0.53	2.36	3.00
11.5	11-12	2071		-0.23	1.08	1.08	2.32	2.96
12.5	12-13	2195		-0.27	1.15	1.09	2.39	3.03
13.5	13-14	2320		-0.27	1.21	0.83	2.31	2.95
14.5	14-15	2445		-0.12	1.02	1.19	2.36	3.00
15.5	15-16	2569		-0.29	1.12	0.98	2.37	3.01
16.5	16-17	2694		-0.38	1.02	1.26	2.24	2.88
17.5	17-18	2819		-0.23	0.97	1.09	2.34	2.98
18.5	18-19	2943		-0.29	0.97	1.15	2.28	2.92
19.5	19-20	3068		-0.25	0.92	1.19	2.36	3.00
20.5	20-21	3193		-0.47	0.94	1.00	2.31	2.95
21.5	21-22	3317		-0.43	1.00	1.11	2.30	2.94
22.5	22-23	3442		-0.21	1.00	1.15	2.38	3.02
23.5	23-24	3567		-0.36	0.60	1.21	2.29	2.93
24.5	24-25	3706			1.01	1.16	2.32	2.96
25.5	25-26	3846		-0.10	0.89	1.11	2.29	2.93
26.5	26-27	3985		-0.28	0.98	0.83	2.23	2.87
27.5	27-28	4125		-0.14	1.07	1.26	2.41	3.05
28.5	28-29	4264		0.08	0.97	1.26	2.36	3.00
30	29-31	4474	!2samples	-0.12	1.03	1.32	2.38	3.02
31.5	31-32	4683		-0.25		-0.34	2.28	2.92
32.5	32-33	4823		-0.39	1.11	1.29	2.41	3.05
33.5	33-34	4962		-0.42	1.04	0.84	2.35	2.99
34.5	34-35	5102		-0.21	1.13	0.87	2.31	2.95
35.5	35-36	5241		-0.33	1.01			
36.5	36-37	5381		-0.13	0.99	0.38	2.31	2.95
37.5	37-38	5520		-0.14	1.00	1.19	2.45	3.09
38.5	38-39	5660		-0.18	1.06	1.18	2.28	2.92
39.5	39-40,5	5800		-0.22	1.09	1.05	2.22	2.86
40.75	40,5-41	5892		-0.11	1.07	1.29	2.42	3.06
41.5	41-42	5936		-0.27	1.06	1.13	2.34	2.98
42.5	42-43	5993		-0.10	0.93			
43.5	43-44	6051		-0.20	0.97	1.27	2.46	3.10
44.5	44-45	6109		-0.10	1.13	1.10	2.21	2.85
45.5	45-46	6166		-0.17	1.12	1.19	2.51	3.15
46.5	46-47	6224		0.38	0.95	0.68	3.51	4.15
47.5	47-48	6282		-0.33	1.06			
48.5	48-49	6340		0.34	1.11	0.75	3.13	3.77

APPENDIX

GEOFAR KF16								
core depth [cm]	sample intervall [cm]	age [years BP]	comment	$\delta^{18}\text{O}$	$\delta^{18}\text{O}$	$\delta^{13}\text{C}$	$\delta^{18}\text{O}$	$\delta^{18}\text{O}$
				<i>G. ruber w.</i> >315 μm [‰ VPDB]	<i>G. truncatulinoides</i> >315 μm [‰ VPDB]	<i>C. wuellers-torfi</i> >315 μm [‰ VPDB]	<i>C. wuellers-torfi</i> >315 μm [‰ VPDB]	<i>C. wuellers-torfi</i> >315 μm corrected [‰ VPDB]
49.5	49-50	6397		0.30	1.14			
50.5	50-51	6455		0.31	1.17	1.21	2.29	2.93
51.5	51-52	6513	Ash layer	-0.15	1.57	0.90	2.72	3.36
52.5	52-53	6570	Ash layer	-0.19	1.11	1.07	2.27	2.91
53.5	53-54	6628	Ash layer	-0.09	1.29	0.80	2.70	3.34
54.5	54-55	6686	Ash layer	-0.23	1.10	1.25	2.48	3.12
55.5	55-56	6744	Ash layer	-0.07	1.12	1.01	2.36	3.00
56.5	56-57	6801	Ash layer		1.06			
57.5	57-58	6859		-0.27	1.07	1.17	2.32	2.96
58.5	58-59	6917			0.89	0.95	2.24	2.88
59.5	59-60	6974	color change from red-yellow to grey	-0.13	1.14	1.12	2.31	2.95
60.5	60-61	7032			1.07	1.11	2.40	3.04
61.5	61-62	7090		-0.40	1.04			
62.5	62-63	7148		-0.20	1.10	0.44	2.41	3.05
63.5	63-64	7205		-0.32	0.98	0.97	2.24	2.88
64.5	64-65	7263		-0.42	1.02	1.01	2.28	2.92
65.5	65-66	7321		-0.34	1.04	0.73	2.42	3.06
66.5	66-67	7379		-0.23	1.20	1.08	2.31	2.95
67.5	67-68	7436		-0.19	1.16			
68.5	68-69	7494		-0.22	1.23	0.90	2.34	2.98
69.5	69-70	7552		-0.47	1.10	1.09	2.37	3.01
70.5	70-71	7609	color change from grey to red-yellow	-0.36	0.99	0.32	2.43	3.07
71.5	71-72	7667		-0.32	1.21	0.67	2.40	3.04
72.5	72-73	7725	Haires /Serpentinite	-0.38	1.23	0.45	2.48	3.12
73.5	73-74	7783		-0.15	1.32	0.94	2.30	2.94
74.5	74-75	7840		-0.18	1.01	0.97	2.24	2.88
75.5	75-76	7898		-0.40	1.23	0.88	2.46	3.10
76.5	76-77	7956		-0.30	1.07	0.86	2.25	2.89
77.5	77-78	8013		-0.30	1.05	1.16	2.38	3.02
78.5	78-79	8071		-0.20	1.04	0.68	2.49	3.13
79.5	79-80	8113		-0.56	1.19	1.03	2.48	3.12
80.5	80-81	8138		-0.35	1.18	0.12	1.85	2.49
81.5	81-82	8163			1.18			
82.5	82-83	8188		-0.09	1.18	1.00	2.29	2.93
83.5	83-84	8213			1.22			
84.5	84-85	8238		-0.62	1.10			
85.5	85-86	8263			1.14	0.10	2.50	3.14
86.5	86-87	8288		-0.20	1.29	1.09	2.35	2.99
87.5	87-88	8324		-0.17	1.32	0.10	2.43	3.07
88.5	88-89	8373	color change from red-yellow to greyish green	-0.30		0.96	2.47	3.11
89.5	89-90	8422		-0.16	1.29	1.06	2.50	3.14
90.5	90-91	8471		-0.15	1.18	1.03	2.48	3.12
91.5	91-92	8519		-0.26	1.26	0.73	2.43	3.07
92.5	92-93	8568		-0.27	1.36	0.32	2.51	3.15
93.5	93-94	8617		-0.17	1.25	1.03	2.33	2.97

GEOFAR KF16								
core depth [cm]	sample intervall [cm]	age [years BP]	comment	$\delta^{18}\text{O}$	$\delta^{18}\text{O}$	$\delta^{13}\text{C}$	$\delta^{18}\text{O}$	$\delta^{18}\text{O}$
				<i>G. ruber w.</i> >315 μm [‰ VPDB]	<i>G. truncatulinoides</i> >315 μm [‰ VPDB]	<i>C. wuellers-torfi</i> >315 μm [‰ VPDB]	<i>C. wuellers-torfi</i> >315 μm [‰ VPDB]	<i>C. wuellers-torfi</i> >315 μm corrected [‰ VPDB]
94.5	94-95	8666		-0.31	1.19	0.73	2.46	3.10
95.5	95-96	8714		-0.12	1.32	1.00	2.26	2.90
96.5	96-97	8763		-0.15	1.26	1.03	2.47	3.11
97.5	97-98	8812						
98.5	98-99	8861	not existent					
99.5	99-100	8909						
100.5	100-101	8958		-0.06	1.21	0.47	2.50	3.14
101.5	101-102	9007		-0.14	1.22	0.90	2.48	3.12
102.5	102-103	9056		-0.11	1.39	0.94	2.44	3.08
103.5	103-104	9104		-0.20	1.29	0.75	2.40	3.04
104.5	104-105	9153		-0.08	1.29	0.87	2.42	3.06
105.5	105-106	9202		-0.11	1.19	0.92	2.38	3.02
106.25	106-106,5	9239		-0.18	1.32	0.63	2.47	3.11
107.25	106,5-108	9287		-0.10	1.33	0.38	2.48	3.12
108.5	108-109	9348		-0.15	1.41	0.74	2.37	3.01
109.5	109-110	9397		-0.12	1.31	0.87	2.41	3.05
110.5	110-111	9446		-0.10	1.31	0.90	2.31	2.95
111.5	111-112	9495			1.29			
112.5	112-113	9543		-0.34	1.25	0.88	2.44	3.08
113.5	113-114	9592		-0.02	1.36	0.41	2.40	3.04
114.5	114-115	9641		0.00	1.35	0.36	2.41	3.05
115.5	115-116	9690		0.01	1.42	0.85	2.35	2.99
116.5	116-117	9738		-0.06	1.33	0.77	2.34	2.98
117.5	117-118	9787		0.16	1.40	0.74	2.47	3.11
118.5	118-119	9836		0.08	1.43	0.75	2.45	3.09
119.5	119-120	9885		-0.00	1.47	0.80	2.39	3.03
120.5	120-121	9933			1.40	0.74	2.40	3.04
121.5	121-122	9982		0.04	1.39	1.11	2.40	3.04
122.5	122-123	10031		-0.04	1.41	0.80	2.37	3.01
123.5	123-124	10080		-0.18	1.40	0.96	2.47	3.11
124.5	124-125	10128		-0.03	1.35	0.94	2.41	3.05
125.5	125-126	10177		0.04	1.25	0.83	2.21	2.85
126.5	126-127	10226		-0.05	1.55	0.58	2.17	2.81
127.5	127-128	10275		-0.06	1.39	0.68	2.35	2.99
128.5	128-129	10323		0.02	1.37			
129.5	129-130	10372		-0.05	1.44	0.68	2.49	3.13
130.5	130-131	10421		-0.01	1.30			
131.5	131-132	10470		-0.11	1.39	0.53	2.40	3.04
132.5	132-133	10518		0.09	1.57	0.59	2.37	3.01
133.5	133-134	10567		0.15	1.38	0.82	2.45	3.09
134.5	134-135	10616		0.17	1.34	-0.18	2.50	3.14
135.5	135-136	10665		0.04	1.33	0.41	2.38	3.02
136.5	136-137	10694		-0.02	1.47	0.71	2.31	2.95
137.5	137-138	10705		0.09	1.36			
138.5	138-139	10716		0.02	1.52	0.70	2.33	2.97
139.5	139-140	10727		-0.13	1.58			
140.5	140-141	10738			1.43			
141.5	141-142	10749			1.47			
142.5	142-143	10759		-0.04	1.45			
143.5	143-144	10770		0.11	1.37			

APPENDIX

GEOFAR KF16								
core depth [cm]	sample intervall [cm]	age [years BP]	comment	$\delta^{18}\text{O}$	$\delta^{18}\text{O}$	$\delta^{13}\text{C}$	$\delta^{18}\text{O}$	$\delta^{18}\text{O}$
				<i>G. ruber w.</i> >315 μm [‰ VPDB]	<i>G. truncatulinoides</i> >315 μm [‰ VPDB]	<i>C. wuellers-torfi</i> >315 μm [‰ VPDB]	<i>C. wuellers-torfi</i> >315 μm [‰ VPDB]	<i>C. wuellers-torfi</i> >315 μm corrected [‰ VPDB]
142.5	142-143	10759		-0.04	1.45			
143.5	143-144	10770		0.11	1.37			
144.5	144-145	10781		0.12	1.47	0.72	2.15	2.79
145.5	145-146	10792		-0.06	1.28	0.35	2.27	2.91
146.5	146-147	10803		0.02	1.37			
147.5	147-148	10814		0.24	1.47	0.62	2.35	2.99
148.5	148-149	10825		0.09	1.51	0.79	2.49	3.13
149.5	149-150	10835		-0.05	1.46			
150.5	150-151	10846		-0.05	1.49			
151.5	151-152	10857		0.49	1.50			
152.5	152-153	10868		0.20	1.57			
153.5	153-154	10879		0.14	1.53	0.59	2.45	3.09
154.5	154-155	10890		0.19	1.67			
155.5	155-156	10900		0.03	1.49			
156.5	156-157	10911		0.18	1.53			
157.5	157-158	10922		-0.01	1.52	0.78	2.28	2.92
158.5	158-159	10933		0.20	1.47			
159.5	159-160	10944		0.05	1.48	0.60	2.26	2.90
160.5	160-161	10955		0.46	1.41	0.74	2.33	2.97
161.5	161-162	10965		0.05	1.34			
162.5	162-163	10976		0.10	1.40	-0.03	1.85	2.49
163.5	163-164	10987		0.09	1.56	0.12	2.34	2.98
164.5	164-165	10998		0.04	1.48			
165.5	165-166	11009		0.16	1.39			
166.5	166-167	11020		0.15	1.49			
167.5	167-168	11031		0.09	1.50			
168.5	168-169	11041		0.04	1.56			
169.5	169-170	11052		0.15	1.53			
170.5	170-171	11063			1.51			
171.5	171-172	11074		0.42	1.42			
172.5	172-173	11085		0.14	1.44			
173.5	173-174	11096		0.25	1.51			
174.5	174-175	11106		0.15	1.51			
175.5	175-176	11117		0.20	1.56			
176.5	176-177	11128		0.15	1.66			
177.5	177-178	11139		-0.01	1.41			
178.5	178-179	11150		0.22	1.38			
179.5	179-180	11161		-0.02	1.59			
180.5	180-181	11172		0.06	1.43			
181.5	181-182	11182			1.48			
182.5	182-183	11193			1.72			
183.5	183-184	11204		0.17	1.68			
184.5	184-185	11215		0.19	1.53			
185.5	185-186	11226		-0.11	1.58			
186.5	186-187	11237		0.10	1.52			
187.5	187-188	11247		0.10	1.54			
188.5	188-189	11258		0.25	1.48	1.11	2.36	3.00
189.5	189-190	11269			1.53			
190.5	190-191	11280			1.51			
191.5	191-192	11291			1.54			

GEOFAR KF16								
core depth [cm]	sample intervall [cm]	age [years BP]	comment	$\delta^{18}\text{O}$	$\delta^{18}\text{O}$	$\delta^{13}\text{C}$	$\delta^{18}\text{O}$	$\delta^{18}\text{O}$
				<i>G. ruber w.</i> >315 μm [‰ VPDB]	<i>G. truncatulinoides</i> >315 μm [‰ VPDB]	<i>C. wuellerstorfi</i> >315 μm [‰ VPDB]	<i>C. wuellerstorfi</i> >315 μm [‰ VPDB]	<i>C. wuellerstorfi</i> >315 μm corrected [‰ VPDB]
192.5	192-193	11302		0.06	1.56			
193.5	193-194	11312		0.14	1.47			
194.5	194-195	11323		0.20	1.24			
195.5	195-196	11334		0.05	1.39			
196.5	196-197	11345		0.04	1.41	0.36	2.25	2.89
197.5	197-198	11356						
198.5	198-199	11367	not existent					
199.5	199-200	11378						

Table A4 benthic stable isotope data GEOFAR KF16

GEOFAR KF16							
depth [cm]	sample intervall [cm]	age [years BP]	$\delta^{13}\text{C}$	$\delta^{18}\text{O}$	$\delta^{13}\text{C}$	$\delta^{18}\text{O}$	$\delta^{18}\text{O}$
			<i>Melonis barleanus</i> 250-315 μm [‰ VPDB]	<i>Melonis barleanus</i> 250-315 μm [‰ VPDB]	<i>Melonis affinis</i> 250-315 μm [‰ VPDB]	<i>Melonis affinis</i> 250-315 μm [‰ VPDB]	<i>Melonis affinis</i> 250-315 μm corrected [‰ VPDB]
137.5	137-138	10705	-1.24	2.67			
139.5	139-140	10727	-1.30	2.64			
140.5	140-141	10738			-0.57	2.68	3.08
149.5	149-150	10835			-0.43	2.43	2.84
154.5	154-155	10890			-0.69	2.79	3.20
156.5	156-157	10911			-0.56	2.71	3.12
158.5	158-159	10933			-0.66	2.66	3.07
164.5	164-165	10998			-0.77	2.64	3.05
165.5	165-166	11009			-0.76	2.63	3.04
166.5	166-167	11020			-0.68	2.71	3.12
167.5	167-168	11031			-0.86	2.71	3.12
168.5	168-169	11041			-1.28	2.70	3.11
169.5	169-170	11052			-0.94	2.63	3.04
170.5	170-171	11063			-1.01	2.58	2.99
172.5	172-173	11085			-1.01	2.66	3.07
173.5	173-174	11096			-1.24	2.65	3.06
174.5	174-175	11106			-1.06	2.66	3.07
175.5	175-176	11117			-1.18	2.60	3.01
176.5	176-177	11128			-1.14	2.60	3.01
178.5	178-179	11150			-1.03	2.69	3.20
179.5	179-180	11161			-1.05	2.56	2.97
182.5	182-183	11193			-1.15	2.67	3.08
183.5	183-184	11204			-1.00	2.64	3.05
184.5	184-185	11215			-0.91	2.68	3.0
185.5	185-186	11226			-1.22	2.70	3.11
186.5	186-187	11237			-1.07	2.71	3.12
187.5	187-188	11247			-1.06	2.74	3.15
192.5	192-193	11302			-1.35	2.70	3.11
194.5	194-195	11323			-1.60	2.68	3.09
195.5	195-196	11334			-1.31	2.68	3.09

Table A5 stable isotope data MD08-3180

MD08-3180								
core depth [cm]	sampled intervall [cm]	age [years BP]	$\delta^{18}\text{O}$ <i>G. ruber w.</i> >315 μm [‰ VPDB]	$\delta^{18}\text{O}$ <i>G. bulloides</i> >315 μm [‰ VPDB]	$\delta^{18}\text{O}$ <i>G. truncatulinoides</i> >315 μm [‰ VPDB]	$\delta^{13}\text{C}$ <i>C. wuellerstorfi</i> >315 μm [‰ VPDB]	$\delta^{18}\text{O}$ <i>C. wuellerstorfi</i> >315 μm [‰ VPDB]	$\delta^{18}\text{O}$ <i>C. wuellerstorfi</i> corr. >315 μm [‰ VPDB]
125.25	125.5-126	10848	0.07		1.69			
127.5	127-128	10885	0.06		1.53			
130.5	130-131	10933	0.08		1.41			
132.5	132-133	10966	0.02		1.53			
135.5	134-135	11015	0.06		1.65			
137.5	137-138	11047	0.17		1.56			
140.5	140-141	11096	-0.03		1.62			
142.5	142-143	11128	0.15		1.64			
145.5	145-146	11177	0.33		1.55			
147.5	147-148	11210	0.11		1.59			
149.5	149-150	11242	0.09		1.44			
150.5	150-151	11258	0.22		1.40			
155.5	155-156	11340	0.02		1.31			
157.5	157-158	11372	0.09		1.58			
159.5	159-160	11405		0.75	1.54			
160.5	160-161	11421	0.07	0.83	1.50	1.20	4.41	5.05
162.5	162-163	11453		1.21	1.41			
165.5	165-166	11502	0.36		1.37	0.28	2.05	2.69
166.5	166-167	11518	0.43		1.49			
168.5	168-169	11551	0.06		1.47			
170.5	170-171	11583	0.22		1.34	0.44	2.63	3.27
171.5	171-172	11600		1.41	1.85			
173.5	173-174	11631		1.14	1.82	0.42	2.54	
174.5	174-175	11646				0.79	2.90	
175.5	175-176	11661		1.42	1.86			
176.5	176-177	11676		1.54	1.72	0.38	2.74	
178.5	178-179	11705		1.60	2.02			
180.5	180-181	11734		1.76	1.63			
181.5	181-182	11749		1.55	1.96	-0.73	3.60	4.24
183.5	183-184	11779		1.60	2.24	0.12	2.52	3.16
185.5	185-186	11808		1.58	2.00	0.27	2.62	3.26
187.5	187-188	11838		1.53	2.00			
188.5	188-189	11852				0.47	2.68	3.32
189.5	189-190	11867		1.53	2.16	0.61	2.69	3.33
190.5	190-191	11882		1.51	1.95	0.53	2.82	3.46
191.5	191-192	11896		1.50	1.88			
195.5	195-196	11955		1.70	2.19	0.63	2.53	3.17
197.5	197-198	11985		1.58	2.35	0.06	2.82	3.46
198.5	198-199	12000		1.73	2.19	0.45	2.73	3.37
200.5	200-201	12029		1.71	2.29	0.64	2.72	3.36
201.5	201-202	12044		1.71	2.19	1.16	3.39	4.03
204.5	204-205	12087		1.72	2.31			
205.5	205-206	12102		1.89	2.04	0.48	2.54	3.18
207.5	207-208	12131		1.70	2.33	0.41	2.50	3.14
208.5	208-209	12145		1.73	2.28			
210.5	210-211	12174			2.31			
212.5	212-213	12204		1.71	2.29	-0.41	2.41	3.05
214.5	214-215	12233		1.77	2.19			
215.5	215-216	12248		1.73	2.07	0.61	2.84	3.48
216.5	216-217	12263				0.11	2.59	
217.5	217-218	12277		1.64	1.99	0.27	2.91	3.55
219.5	219-220	12307		1.65	2.16			
220.5	220-221	12322		1.56	1.83			
221.5	221-222	12336		1.62	1.91	0.35	2.82	
223.5	223-224	12366		1.72	1.87	0.26	2.71	3.35
225.5	225-226	12395		1.72	2.16			

MD08-3180								
core depth [cm]	sampled intervall [cm]	age [years BP]	$\delta^{18}\text{O}$ <i>G. ruber w.</i> >315 μm [‰ VPDB]	$\delta^{18}\text{O}$ <i>G. bulloides</i> >315 μm [‰ VPDB]	$\delta^{18}\text{O}$ <i>G. truncatulinoides</i> >315 μm [‰ VPDB]	$\delta^{13}\text{C}$ <i>C. wuellerstorfi</i> >315 μm [‰ VPDB]	$\delta^{18}\text{O}$ <i>C. wuellerstorfi</i> >315 μm [‰ VPDB]	$\delta^{18}\text{O}$ <i>C. wuellerstorfi</i> corr. >315 μm [‰ VPDB]
227.5	227-228	12425		1.64	2.31			
229.5	229-230	12454		1.71	2.17			
230.5	230-231	12469		1.49	1.93			
232.5	232-233	12498		1.58	2.15	0.39	2.86	
233.5	233-234	12513		1.77	2.32	0.63	2.86	
235.5	235-236	12542		1.66	1.78			
237.5	237-238	12572		1.72	2.30	0.54	2.83	3.47
238.5	238-239	12587		1.92	2.18	0.37	2.95	3.59
240.5	240-241	12616		1.82	2.31			
242.5	242-243	12645		1.63	2.29			
243.5	243-244	12660		1.72	2.44	0.76	2.90	
245.5	245-246	12690		1.63	2.40			
247.5	247-248	12719		1.72	2.54	0.33	2.91	
248.5	248-249	12734		1.57	2.30			
250.5	250-251	12763	0.53	1.77	2.29			
252.5	252-253	12793		1.48		0.54	2.83	
254.5	254-255	12841		1.40				
255.5	255-256	12868	0.10	1.57	1.99			
256.5	256-257	12895		1.38				
257.5	257-258	12922		1.14				
258.5	258-259	12949		1.70				
260.5	260-261	13004		1.57	2.15	0.56	2.77	3.41
261.5	261-262	13031	0.36	1.27				
262.5	262-263	13058	0.84	1.27				
263.5	263-264	13085	0.43	1.28				
264.5	264-265	13112		1.14				
265.5	265-266	13139	0.37	1.21	1.88	0.32	3.05	3.69
266.5	266-267	13166		1.19		0.68	2.88	
267.5	267-268	13193		1.35				
268.5	268-269	13221		1.24				
269.5	269-270	13248	0.59	1.28				
270.5	270-271	13275	0.40	1.02	2.01	0.87	3.11	3.75
271.5	271-272	13302	0.20	1.23		0.97	3.05	
272.5	272-273	13329	0.24	1.46				
273.5	273-274	13356	0.04	1.13				
274.5	274-275	13383	0.48	1.16		0.67	3.13	
275.5	275-276	13411	0.57	1.07	2.00	0.77	3.13	3.77
276.5	276-277	13439	0.22	1.50		0.54	3.00	
277.5	277-278	13467	0.03	1.34		0.72	3.13	
278.5	278-279	13495	0.49	1.17		0.61	3.03	
279.5	279-280	13523	0.43	1.38				
280.5	280-281	13551	0.38	0.95	1.81	0.67	3.12	3.76
281.5	281-282	13579				0.73	2.91	
282.5	282-283	13607				0.51	2.85	
284.5	284-285	13663				0.90	3.05	
285.5	285-286	13691	0.50	1.18	2.08	0.91	3.02	3.66
286.5	286-287	13719				0.79	2.94	
290.5	290-291	13830	0.69	1.19	1.88	0.78	3.25	3.89
291.5	291-292	13858				0.64	3.04	
292.5	292-293	13886				0.76	2.95	
293.5	293-294	13914				0.84	2.95	
294.5	294-295	13942				0.60	3.12	
295.5	295-296	13970	0.55	1.37	1.97	1.05	3.07	3.71
296.5	296-297	13998				0.63	3.05	
297.5	297-298	14026				0.81	3.20	
298.5	298-299	14054				0.88	3.15	
299.5	299-300	14082				0.26	3.22	
300.5	300-301	14110	0.62	1.30	2.02	0.87	3.12	3.76
301.5	301-302	14138				0.92	3.11	

APPENDIX

MD08-3180								
core depth [cm]	sampled intervall [cm]	age [years BP]	$\delta^{18}\text{O}$ <i>G. ruber w.</i> >315 μm [‰ VPDB]	$\delta^{18}\text{O}$ <i>G. bulloides</i> >315 μm [‰ VPDB]	$\delta^{18}\text{O}$ <i>G. truncatulinoides</i> >315 μm [‰ VPDB]	$\delta^{13}\text{C}$ <i>C. wuellerstorfi</i> >315 μm [‰ VPDB]	$\delta^{18}\text{O}$ <i>C. wuellerstorfi</i> >315 μm [‰ VPDB]	$\delta^{18}\text{O}$ <i>C. wuellerstorfi</i> corr. >315 μm [‰ VPDB]
304.5	304-305	14221				0.63	3.26	
305.5	305-306	14248	0.70	1.34	1.85	0.73	3.08	3.72
306.5	306-307	14276				0.35	3.16	
307.5	307-308	14304				0.43	2.99	
308.5	308-309	14332				0.75	3.06	
310.5	310-311	14387	0.61		1.86	0.82	3.28	3.92
312.5	312-313	14442				0.37	2.98	
313.5	313-314	14470				0.54	3.20	
314.5	314-315	14498				0.43	3.24	
315.5	315-316	14525	1.18		2.33	0.48	3.17	3.81
316.5	316-317	14553			1.96	0.17	3.09	
317.5	317-318	14581			1.95	0.43	3.02	
318.5	318-319	14608			1.84	0.82	2.72	
319.5	319-320	14636			1.77	0.31	3.15	
320.5	320-321	14657	0.59		1.57	0.32	3.23	3.87
323.5	323-324	14696				0.51	2.74	
325.5	325-326	14723	1.34		2.59			
326.5	326-327	14736			2.34			
327.5	327-328	14750			2.26			
328.5	328-329	14763				0.75	2.75	
329.5	329-330	14776			1.54			
330.5	330-331	14789	0.97		2.61	0.29	3.88	4.52
335.5	335-336	14856	0.94		2.51	0.77	2.95	3.59
340.5	340-341	14922	1.06		2.48			
345.5	345-346	14988	1.19		2.26	0.11	3.64	4.28
350.5	350-351	15055	1.04		2.69			
355.5	355-356	15121	1.70		2.90			
360.5	360-361	15188	1.42		2.70			
365.5	365-366	15254	1.63		3.01			
370.5	370-371	15320	1.46		3.01			
375.5	375-376	15387	1.56		2.82			
380.5	380-381	15453	1.43		3.03			
385.5	385-386	15519	1.64		2.88			
390.5	390-391	15586	1.42		3.02			
395.5	395-396	15652	1.81		3.26			
grey letters			samples prepared and measured by S.Balmer					

Table A6 benthic stable isotope data MD08-3180

MD08-3180						
depth [cm]	sampled intervall [cm]	age [years BP]	$\delta^{13}\text{C}$ <i>Melonis affinis</i> 250-315 μm [‰ VPDB]	$\delta^{18}\text{O}$ <i>Melonis affinis</i> 250-315 μm [‰ VPDB]	$\delta^{18}\text{O}$ <i>Melonis affinis</i> corr. 250-315 μm [‰ VPDB]	
158.5	158-159	11388	-1.20	2.62	3.135	
159.5	159-160	11405	-1.27	2.53	3.053	
160.5	160-161	11421	-1.10	2.52	3.040	
162.5	162-163	11453	-1.24	2.61	3.131	
166.5	166-167	11518	-1.13	2.69	3.205	
168.5	168-169	11551	-1.13	2.63	3.146	
171.5	171-172	11600	-0.78	2.73	3.251	
173.5	173-174	11631	-1.08	2.65	3.172	
174.5	174-175	11646	-1.17	2.85	3.366	
175.5	175-176	11661	-0.91	2.64	3.164	
176.5	176-177	11676	-0.91	2.55	3.068	

MD08-3180						
depth [cm]	sampled intervall [cm]	age [years BP]	$\delta^{13}\text{C}$ <i>Melonis affinis</i>	$\delta^{18}\text{O}$ <i>Melonis affinis</i>	$\delta^{18}\text{O}$ <i>Melonis affinis</i> corr.	
			250-315 μm [‰ VPDB]	250-315 μm [‰ VPDB]	250-315 μm [‰ VPDB]	
177.5	177-178	11690	-0.81	2.77	3.287	
178.5	178-179	11705	-0.99	2.80	3.317	
187.5	187-188	11838	-1.15	2.79	3.305	
191.5	191-192	11896	-0.78	2.75	3.271	
200.5	200-2001	12029	-1.09	3.07	3.589	
210.5	210-211	12174	-1.05	2.77	3.294	
214.5	214-215	12233	-1.20	2.80	3.315	
219.5	219-220	12307	-1.22	2.95	3.467	
221.5	221-222	12336	-1.12	3.02	3.542	
225.5	225-226	12395	-1.02	3.08	3.597	
227.5	227-228	12425	-0.77	2.98	3.501	
229.5	229-230	12454	-0.90	3.21	3.731	
232.5	232-233	12498	-0.87	3.05	3.570	
233.5	233-234	12513	-0.86	3.31	3.830	
240.5	240-241	12616	-0.83	3.16	3.679	
242.5	242-243	12645	-0.73	3.60	4.123	

Table A7 relative abundance of planktonic foraminifera core GEOFAR KF16

GEOFAR KF16									
age [years BP]	depth [cm]	counted by	<i>G. bull-oides</i> [%]	<i>N. pachyderma</i> s. [%]	<i>N. pachyderma</i> d. [%]	<i>T. quinqueloba</i> [%]	<i>G. ruber</i> w. [%]	<i>G. scitula</i> [%]	<i>G. truncatulinoides</i> [%]
524	2.5	M.W.	36.0	1.0	6.2	1.6	11.5	8.3	7.4
734	3.5	M.W.	28.3	0.0	9.7	1.9	13.5	9.1	9.7
943	4.5	M.W.	34.4	0.0	6.1	2.2	17.8	5.6	6.1
1153	5.5	M.W.	38.1	0.0	6.4	0.5	11.0	6.4	12.8
1362	6.5	M.W.	33.8	0.2	7.9	2.6	14.3	6.0	8.4
1572	7.5	M.W.	32.9	0.0	6.7	2.9	13.7	3.5	8.0
1697	8.5	M.W.	37.3	0.4	6.2	0.8	17.4	6.8	6.9
1821	9.5	M.W.	37.1	0.8	6.1	1.1	17.4	3.8	8.7
1946	10.5	J.R.	22.8	1.3	6.7	2.6	14.1	5.8	4.9
2071	11.5	M.W.	40.6	0.3	3.9	1.6	16.2	9.4	3.9
2195	12.5	M.W.	43.7	0.0	3.8	1.4	13.3	6.8	5.5
2320	13.5	M.W.	37.1	0.5	7.7	1.8	13.3	4.3	5.6
2445	14.5	M.W.	37.9	0.0	5.0	1.9	14.9	6.9	4.2
2569	15.5	M.W.	39.2	0.3	6.6	0.6	12.3	7.3	7.6
2694	16.5	M.W.	35.5	0.0	5.4	0.0	14.8	7.5	4.2
2819	17.5	M.W.	39.5	0.6	3.9	4.1	15.8	6.2	3.3
3068	19.5	M.W.	39.0	0.0	4.8	0.0	17.3	3.9	4.8
3193	20.5	J.R.	24.2	1.3	3.3	2.2	12.3	4.8	1.7
3317	21.5	M.W.	36.0	0.9	4.0	1.3	15.6	8.0	3.6
3442	22.5	M.W.	28.2	0.0	4.9	1.4	16.4	3.8	7.5
3567	23.5	M.W.	37.3	0.0	4.7	1.2	15.5	5.6	3.7
3706	24.5	M.W.	38.7	0.3	2.8	1.5	15.1	3.3	3.8
3846	25.5	M.W.	40.4	1.4	2.7	0.0	11.6	4.8	2.7
3985	26.5	M.W.	40.9	0.0	3.4	0.9	13.4	6.0	5.2
4125	27.5	M.W.	28.4	0.3	2.1	0.6	25.7	1.5	6.3
4264	28.5	M.W.	41.3	0.4	5.2	0.4	23.4	3.2	3.6
4404	29.5	M.W.	31.4	0.0	5.1	1.9	20.6	7.0	4.1

APPENDIX

GEOFAR KF16									
age [years BP]	depth [cm]	counted by	<i>G. bull-oides</i> [%]	<i>N. pachy-derma</i> s. [%]	<i>N. pachy-derma</i> d. [%]	<i>T. quinque-loba</i> [%]	<i>G. ruber</i> w. [%]	<i>G. scitula</i> [%]	<i>G. trunca-tulinoides</i> [%]
4474	30.0	J.R.	18.0	0.9	1.8	1.4	14.2	3.8	7.4
4683	31.5	M.W.	30.5	0.4	4.0	0.7	22.9	1.1	4.0
4823	32.5	M.W.	37.9	0.7	3.3	0.0	18.3	6.5	2.0
4962	33.5	M.W.	30.4	0.0	2.3	2.3	27.5	1.2	4.1
5102	34.5	M.W.	28.7	0.4	2.9	1.1	18.9	3.3	7.3
5241	35.5	M.W.	37.8	0.0	1.3	2.6	20.0	1.3	6.1
5381	36.5	M.W.	30.3	0.0	2.9	1.1	22.3	2.9	5.7
5520	37.5	M.W.	28.2	0.0	3.2	1.6	19.0	2.4	6.5
5660	38.5	M.W.	31.9	0.0	3.6	2.6	21.4	1.9	6.4
5800	39.5	M.W.	25.2	0.0	2.7	3.3	22.6	4.2	3.9
5889	40.8	J.R.	13.5	1.4	3.6	2.2	19.1	3.6	3.1
5936	41.5	M.W.	33.5	0.9	3.7	1.7	16.2	3.7	3.7
5993	42.5	M.W.	24.5	0.5	5.5	1.5	21.0	3.5	5.5
6051	43.5	M.W.	32.8	0.4	6.3	1.2	17.6	4.7	2.3
6109	44.5	M.W.	33.1	0.0	6.9	2.9	18.4	6.1	2.4
6166	45.5	M.W.	29.2	0.2	7.8	5.8	17.5	5.1	2.9
6224	46.5	M.W.	24.1	1.0	12.4	2.5	20.5	5.1	1.8
6282	47.5	M.W.	41.9	0.8	10.9	8.5	13.2	5.4	0.0
6340	48.5	M.W.	34.4	0.0	10.9	3.7	15.0	4.4	1.0
6455	50.5	J.R.	18.4	3.0	10.7	6.1	8.3	7.1	1.4
6513	51.5	M.W.	32.7	0.0	9.9	4.8	9.5	9.9	3.4
6570	52.5	M.W.	27.6	0.8	10.8	5.8	15.0	6.5	2.5
6686	54.5	M.W.	31.7	0.8	8.4	2.7	16.4	2.7	2.3
6744	55.5	M.W.	32.9	0.5	11.7	4.1	15.9	3.0	2.1
6859	57.5	M.W.	35.9	0.0	5.7	0.0	19.8	0.0	4.2
6917	58.5	M.W.	37.4	0.0	6.8	0.6	21.0	0.6	1.9
6974	59.5	M.W.	33.9	0.3	7.0	1.6	19.3	0.6	1.9
7032	60.5	J.R.	21.2	0.7	6.1	1.3	16.4	2.8	3.7
7148	62.5	M.W.	42.2	0.0	6.0	3.0	18.7	0.9	1.5
7321	65.5	M.W.	42.1	0.2	4.1	5.0	18.3	2.1	2.2
7379	66.5	M.W.	42.7	0.0	6.7	1.8	19.6	1.5	3.5
7436	67.5	M.W.	43.9	0.0	6.8	1.8	19.9	2.7	1.8
7494	68.5	M.W.	37.0	0.0	5.7	3.3	23.7	1.5	4.4
7552	69.5	M.W.	45.5	0.3	5.1	3.2	23.4	1.9	1.9
7609	70.5	J.R.	22.9	2.4	5.6	4.7	15.7	3.5	1.5
7725	72.5	M.W.	39.9	0.8	5.7	9.3	15.8	2.3	1.9
7783	73.5	M.W.	42.1	0.4	5.7	1.5	23.0	1.5	1.5
7840	74.5	M.W.	37.4	0.0	6.0	1.8	20.8	1.0	2.3
7898	75.5	J.R.	25.5	0.0	6.5	3.3	20.1	1.6	4.9
7898	75.5	M.W.	25.8	0.5	3.0	2.8	19.0	4.7	3.5
7898	75.5	M.W.	25.5	0.0	6.5	3.3	20.1	1.6	4.9
8013	77.5	M.W.	42.2	0.0	4.4	1.0	18.1	0.0	1.5
8071	78.5	M.W.	36.5	0.0	4.1	1.5	20.3	0.4	2.6
8138	80.5	J.R.	33.7	0.0	5.3	2.4	21.1	1.3	1.9
8138	80.5	M.W.	8.7	1.3	3.5	2.3	22.0	7.5	5.7
8138	80.5	M.W.	33.7	0.0	5.3	2.4	21.1	1.3	1.9
8163	81.5	M.W.	43.6	0.0	4.0	4.0	20.2	1.2	1.7
8188	82.5	M.W.	43.9	0.0	4.9	4.3	25.4	0.5	0.2
8213	83.5	M.W.	36.5	0.7	9.1	3.3	18.2	3.9	1.6
8238	84.5	M.W.	42.4	0.0	8.8	4.6	12.4	3.2	2.8

GEOFAR KF16									
age [years BP]	depth [cm]	counted by	<i>G. bull-oides</i> [%]	<i>N. pachyderma</i> s. [%]	<i>N. pachyderma</i> d. [%]	<i>T. quinqueloba</i> [%]	<i>G. ruber</i> w. [%]	<i>G. scitula</i> [%]	<i>G. truncatulinoides</i> [%]
8263	85.5	J.R.	32.6	0.8	3.1	1.6	16.1	7.2	0.8
8238	84.5	M.W.	42.4	0.0	8.8	4.6	12.4	3.2	2.8
8263	85.5	J.R.	32.6	0.8	3.1	1.6	16.1	7.2	0.8
8263	85.5	M.W.	18.2	2.6	5.2	8.3	9.5	8.1	3.2
8263	85.5	M.W.	32.6	0.8	1.8	2.9	16.1	7.2	0.8
8288	86.5	M.W.	34.2	0.4	7.4	7.4	16.9	4.6	1.1
8288	86.5	M.W.	34.2	0.4	7.4	7.4	16.9	4.6	1.1
8324	87.5	M.W.	44.2	1.1	8.6	5.8	16.4	1.7	3.1
8373	88.5	M.W.	39.8	0.0	3.8	3.5	18.3	2.3	3.5
8422	89.5	M.W.	39.0	0.3	5.2	5.8	19.8	1.1	3.3
8422	89.5	M.W.	39.0	0.3	5.2	5.8	19.8	1.1	3.3
8471	90.5	J.R.	4.2	1.6	9.1	0.9	5.8	4.8	3.0
8568	92.5	M.W.	48.2	0.0	8.4	4.3	19.7	1.2	2.9
8666	94.5	M.W.	46.2	0.0	6.0	6.0	16.9	2.7	4.4
8666	94.5	M.W.	46.2	0.0	6.0	6.0	16.9	2.7	4.4
8714	95.5	J.R.	15.7	0.2	4.2	2.0	16.4	2.2	1.6
8763	96.5	M.W.	42.3	1.4	8.7	6.3	13.5	1.0	2.9
8763	96.5	M.W.	42.3	1.4	8.7	6.3	13.5	1.0	2.9
8958	100.5	J.R.	24.1	1.2	6.7	4.4	17.7	1.5	5.9
9056	102.5	M.W.	48.0	0.3	7.4	6.1	13.5	2.7	2.0
9104	103.5	M.W.	45.3	1.2	11.1	4.8	15.6	0.6	1.8
9104	103.5	M.W.	45.3	1.2	11.1	4.8	15.6	0.6	1.8
9202	105.5	J.R.	24.3	0.2	6.2	6.4	15.1	2.9	4.7
9251	106.5	M.W.	41.5	0.5	4.8	7.7	11.6	4.8	1.9
9348	108.5	M.W.	44.7	0.3	6.1	5.9	13.0	3.2	4.0
9397	109.5	J.R.	22.0	0.4	5.7	7.7	15.5	1.2	1.7
9446	110.5	M.W.	41.4	0.0	6.4	6.4	12.3	2.7	2.3
9446	110.5	M.W.	41.4	0.0	6.4	6.4	12.3	2.7	2.3
9543	112.5	M.W.	40.3	0.5	11.7	8.7	10.7	2.9	4.4
9690	115.5	J.R.	21.6	2.9	7.8	6.8	10.4	2.9	2.9
9787	117.5	M.W.	48.1	0.0	7.3	6.1	8.0	1.9	4.2
9885	119.5	M.W.	46.3	0.0	10.2	6.5	9.8	1.2	4.5
9933	120.5	J.R.	23.4	2.2	9.3	5.6	9.9	3.7	2.6
10031	122.5	M.W.	45.9	0.3	7.6	7.6	14.2	2.7	2.4
10128	124.5	M.W.	42.8	0.6	8.1	6.0	11.7	2.7	3.3
10226	126.5	M.W.	42.1	0.2	13.4	7.4	10.8	4.1	1.4
10421	130.5	J.R.	20.4	0.1	12.0	7.3	7.5	4.6	3.1
10665	135.5	M.W.	42.7	0.0	18.3	8.8	9.5	0.0	1.0
10705	137.5	M.W.	47.9	0.0	21.5	3.5	7.6	2.5	4.4
10727	139.5	J.R.	18.6	0.7	14.7	6.1	7.6	5.0	4.0
10738	140.5	M.W.	42.9	0.5	23.1	5.5	7.1	2.5	4.4
10749	141.5	M.W.	39.7	0.3	24.7	4.2	9.9	1.9	5.1
10770	143.5	M.W.	38.1	0.5	25.1	4.6	10.4	1.4	2.5
10792	145.5	J.R.	30.3	0.4	15.8	5.9	8.4	3.5	3.3
10792	145.5	M.W.	44.9	0.0	20.9	4.7	9.1	1.6	2.6
10846	150.5	J.R.	20.9	1.6	26.7	2.6	8.5	1.6	2.1
10890	154.5	M.W.	41.3	0.0	22.6	4.4	7.5	2.4	2.4
10955	160.5	M.W.	26.2	0.7	19.3	4.7	6.7	1.7	2.2
11063	170.5	M.W.	23.2	0.8	20.7	5.5	9.7	3.5	3.5
11085	172.5	M.W.	38.2	0.4	20.7	7.5	9.6	1.8	1.4

GEOFAR KF16									
age [years BP]	depth [cm]	counted by	<i>G. bull-oides</i> [%]	<i>N. pachy-derma s.</i> [%]	<i>N. pachy-derma d.</i> [%]	<i>T. quinque-loba</i> [%]	<i>G. ruber w.</i> [%]	<i>G. scitula</i> [%]	<i>G. trunca-tulinoides</i> [%]
11106	174.5	M.W.	41.0	0.0	22.6	4.3	6.6	2.5	1.0
11128	176.5	M.W.	38.8	0.0	23.3	9.8	6.5	1.2	2.0
11172	180.5	J.R.	25.9	1.9	19.3	9.3	4.0	2.9	1.0
11215	184.5	M.W.	36.6	0.7	31.5	5.5	7.0	2.6	1.5
11280	190.5	J.R.	18.2	1.0	28.3	9.7	3.7	1.5	1.7
11345	196.5	J.R.	18.8	1.0	23.0	10.3	10.3	1.4	4.3

Table A8 relative abundance of planktonic foraminifera core MD08-3180

MD08-3180									
age [years BP]	depth cm	counted by	<i>G. bull-oides</i> [%]	<i>N. pachy-derma s.</i> [%]	<i>N. pachy-derma d.</i> [%]	<i>T. quinque-loba</i> [%]	<i>G. ruber w.</i> [%]	<i>G. scitula</i> [%]	<i>G. trunca-tulinoides</i> [%]
7923	70.3	M.W.	44.6	0.0	5.8	3.6	18.7	2.2	2.9
8159	75.3	M.W.	47.1	1.3	8.1	4.9	16.1	2.2	0.4
8176	76.3	M.W.	36.4	0.8	6.1	6.5	21.9	4.5	2.4
8194	77.3	M.W.	35.9	1.0	4.6	8.7	22.6	3.1	2.1
8211	78.3	M.W.	35.0	1.2	3.1	9.8	22.1	3.7	0.6
8246	80.3	M.W.	26.6	1.3	8.9	22.8	8.2	7.6	0.6
8264	81.3	M.W.	20.6	1.1	13.9	16.9	4.2	8.1	1.4
8272	81.8	M.W.	18.6	3.3	11.4	29.0	6.7	9.5	1.9
8363	85.3	M.W.	40.6	1.2	6.0	14.7	12.6	3.9	1.7
9046	90.3	M.W.	47.9	0.0	7.4	3.5	16.5	2.1	2.5
10412	100.3	M.W.	48.3	0.5	7.6	5.2	14.7	2.8	3.3
10608	110.5	M.W.	41.2	0.6	13.5	9.4	11.5	3.5	1.8
10771	120.5	M.W.	38.6	0.5	21.4	14.0	9.3	0.9	1.9
10864	126.3	M.W.	38.0	0.2	19.1	4.4	10.6	1.5	3.1
10881	127.3	M.W.	41.7	0.0	19.3	2.1	12.8	0.3	4.1
10954	131.8	M.W.	35.2	1.0	23.8	3.1	11.4	0.7	3.8
11003	134.8	M.W.	34.9	0.4	19.7	7.9	8.7	4.4	2.6
11108	141.3	M.W.	39.7	0.3	20.7	6.6	9.7	2.8	2.1
11141	143.3	M.W.	30.7	0.6	22.6	10.4	9.8	1.2	1.5
11157	144.3	M.W.	43.9	1.0	22.0	8.8	7.8	2.0	2.4
11189	146.3	M.W.	36.0	0.0	25.8	6.2	9.0	0.6	1.7
11238	149.3	M.W.	37.9	1.0	27.2	5.8	9.2	1.9	4.4
11258	150.5	M.W.	26.6	0.4	30.5	9.1	10.4	1.7	2.6
11291	152.5	M.W.	37.3	0.7	26.2	8.2	10.0	2.9	1.8
11340	155.5	M.W.	36.9	1.8	22.7	6.2	6.2	2.7	5.3
11404	159.5	M.W.	38.9	0.2	19.5	7.1	7.6	1.3	0.0
11421	160.5	M.W.	38.4	0.0	22.1	8.9	8.9	2.8	2.1
11437	161.5	M.W.	39.6	0.0	24.8	5.4	5.9	4.5	3.0
11470	163.5	M.W.	34.6	0.0	25.5	8.7	8.3	4.2	2.3
11502	165.5	J.R.	40.3	0.0	22.2	5.1	6.0	2.3	0.0
11502	165.5	M.W.	40.3	0.0	22.3	5.1	6.0	2.3	
11518	166.5	M.W.	27.0	0.7	29.5	9.4	5.8	5.4	5.0
11535	167.5	M.W.	25.5	0.0	33.9	6.9	6.0	3.0	5.4
11551	168.5	M.W.	26.8	0.3	30.7	9.8	6.5	2.4	3.3
11567	169.5	M.W.	27.5	0.3	27.5	5.9	11.1	2.6	2.6
11583	170.5	M.W.	28.6	0.7	29.6	9.1	5.6	2.8	2.1

MD08-3180									
age [years BP]	depth cm	counted by	<i>G. bull-oides</i> [%]	<i>N. pachyderma</i> s. [%]	<i>N. pachyderma</i> d. [%]	<i>T. quinqueloba</i> [%]	<i>G. ruber</i> w. [%]	<i>G. scitula</i> [%]	<i>G. truncatulinoides</i> [%]
11616	172.5	M.W.	30.9	0.5	30.4	10.1	3.2	2.5	1.0
11631	173.5	M.W.	33.8	0.9	28.6	7.1	2.2	0.9	1.8
11661	175.5	M.W.	27.9	1.7	27.9	13.4	2.2	2.8	1.7
11734	180.5	M.W.	30.7	1.7	38.5	8.2	1.7	1.7	0.9
11808	185.5	M.W.	29.7	0.3	31.3	9.8	0.5	2.7	1.4
11882	190.5	M.W.	33.3	0.5	30.4	10.7	0.5	0.5	0.0
11955	195.5	M.W.	32.4	1.0	35.6	3.2	0.0	2.3	1.0
12029	200.5	M.W.	27.6	0.2	36.8	7.7	0.5	1.9	1.7
12102	205.5	M.W.	25.4	1.9	33.5	8.5	0.0	2.3	1.2
12174	210.5	J.R.	15.3	1.6	19.9	8.7	1.2	2.8	0.3
12219	213.5	M.W.	32.5	1.1	23.0	6.0	0.5	1.4	1.3
12263	216.5	M.W.	25.9	1.7	24.1	11.8	0.9	2.9	0.9
12292	218.5	M.W.	31.1	0.4	27.0	7.8	1.0	0.8	
12322	220.5	J.R.	15.5	2.4	20.7	14.0	1.9	1.7	0.5
12366	223.5	M.W.	16.6	1.6	26.4	10.4	2.9	3.3	1.6
12395	225.5	M.W.	16.3	1.4	26.6	12.3	0.9	2.9	1.1
12439	228.5	M.W.	18.7	2.2	30.2	7.1	1.3	0.9	1.8
12469	230.5	J.R.	13.0	1.0	21.0	11.5	2.3	3.3	2.0
12498	232.5	M.W.	25.2	0.7	29.3	8.5	1.3	3.5	2.0
12587	238.5	M.W.	30.5	2.4	20.4	11.0	0.6	0.6	0.3
12616	240.5	J.R.	14.6	3.2	15.3	14.1	0.9	3.8	0.6
12645	242.5	M.W.	22.3	1.5	27.3	11.8	1.7	2.1	1.5
12690	245.5	M.W.	23.9	0.6	29.5	15.9	1.7	3.4	0.0
12734	248.5	M.W.	24.4	0.6	39.0	9.6	0.6	2.0	0.8
12763	250.5	J.R.	27.2	0.7	22.1	13.7	2.0	2.5	0.0
12763	250.5	M.W.	27.2	0.7	22.1	13.7	2.0	2.5	
12793	252.5	M.W.	27.8	0.5	16.2	10.6	2.0	2.0	0.5
12868	255.5	J.R.	31.6	0.3	18.7	13.1	3.4	2.2	0.0
12868	255.5	M.W.	31.6	0.3	18.7	13.1	3.4	2.2	
12922	257.5	M.W.	35.4	1.0	18.5	13.8	4.1	5.1	0.5
12949	258.5	M.W.	34.6	1.6	17.5	8.9	2.0	3.3	0.4
13004	260.5	J.R.	5.1	1.3	19.2	14.4	3.0	4.8	1.7
13004	260.5	M.W.	28.3	0.0	19.6	16.7	1.8	3.6	0.4
13085	263.5	M.W.	14.7	2.6	14.5	32.0	2.6	6.1	1.1
13112	264.5	J.R.	18.3	2.8	18.8	19.3	3.4	8.2	
13139	265.5	M.W.	18.2	0.7	14.5	14.5	3.3	8.0	1.5
13193	267.5	M.W.	19.0	1.2	12.8	24.1	3.8	11.1	0.2
13221	268.5	M.W.	12.5	2.0	11.5	36.0	2.0	12.5	1.5
13248	269.5	J.R.	30.6	0.6	22.8	9.6	5.9	1.7	0.8
13275	270.5	J.R.	18.9	1.8	12.0	14.6	5.4	2.2	0.5
13302	271.5	M.W.	34.6	0.5	15.2	6.2	5.7	2.6	1.0
13329	272.5	M.W.	28.8	0.0	13.4	7.7	11.6	2.4	0.9
13356	273.5	M.W.	34.0	0.3	20.1	9.0	6.8	1.5	0.3
13383	274.5	M.W.	40.7	0.4	19.1	7.3	7.7	3.3	2.0
13411	275.5	M.W.	48.8	0.0	14.2	0.8	9.2	0.8	0.4
13439	276.5	M.W.	30.5	0.4	22.6	8.4	5.8	1.3	
13467	277.5	M.W.	31.5	0.3	21.4	5.4	7.8	1.7	1.0
13495	278.5	M.W.	37.4	0.0	18.3	5.0	3.5	2.5	
13523	279.5	M.W.	36.7	0.0	17.7	10.5	4.8	2.4	0.4
13551	280.5	J.R.	24.5	2.6	16.8	7.2	4.6	1.6	0.4

APPENDIX

MD08-3180									
age [years BP]	depth cm	counted by	<i>G. bull-oides</i> [%]	<i>N. pachyderma</i> s. [%]	<i>N. pachyderma</i> d. [%]	<i>T. quinqueloba</i> [%]	<i>G. ruber</i> w. [%]	<i>G. scitula</i> [%]	<i>G. truncatulinoides</i> [%]
13579	281.5	M.W.	38.1	0.0	21.5	5.5	6.4	1.5	0.2
13607	282.5	M.W.	31.0	0.4	15.5	5.5	6.9	1.6	1.2
13635	283.5	M.W.	31.5	0.0	18.8	8.5	6.1	1.2	
13691	285.5	M.W.	31.3	0.9	16.9	7.1	7.1	2.6	0.5
13719	286.5	M.W.	31.8	0.4	19.3	8.2	5.8	1.8	
13747	287.5	M.W.	30.5	0.6	16.9	8.1	7.8	1.7	0.0
13774	288.5	M.W.	34.2	0.2	23.0	3.3	9.6	2.4	1.4
13802	289.5	M.W.	35.9	0.0	21.6	8.4	8.7	1.3	
13830	290.5	J.R.	18.4	1.4	20.1	13.5	6.5	1.7	1.0
13858	291.5	M.W.	31.8	0.8	27.2	4.6	7.5	2.9	
13886	292.5	M.W.	41.6	1.1	25.2	4.6	5.0	1.5	0.4
13914	293.5	M.W.	34.1	0.4	25.0	8.3	6.9	2.2	0.4
13942	294.5	M.W.	32.5	0.6	22.2	6.3	5.9	3.1	
13970	295.5	M.W.	27.9	1.1	24.2	7.9	7.9	2.6	2.6
13998	296.5	M.W.	32.5	0.0	26.5	3.9	8.9	1.7	
14026	297.5	M.W.	29.5	1.1	24.6	5.3	6.4	2.3	1.1
14054	298.5	M.W.	32.9	0.8	24.8	7.4	10.9	2.3	1.9
14082	299.5	M.W.	27.5	0.6	26.5	6.4	6.1	0.6	1.6
14110	300.5	J.R.	18.8	3.1	16.7	7.8	8.4	2.9	1.4
14165	302.5	M.W.	29.0	0.7	29.0	5.2	7.4	4.1	1.1
14221	304.5	M.W.	28.9	5.4	22.7	5.4	7.9	2.9	1.1
14248	305.5	M.W.	29.2	0.2	31.4	5.7	8.6	4.1	1.8
14273	306.4	M.W.	30.4	0.0	31.1	2.1	12.0	2.8	0.9
14304	307.5	M.W.	34.3	0.8	25.0	4.0	8.5	2.3	2.5
14332	308.5	M.W.	37.6	2.8	26.1	5.0	6.9	1.8	1.4
14387	310.5	M.W.	28.2	1.4	25.5	6.8	7.1	2.4	1.4
14442	312.5	M.W.	26.7	0.7	31.9	6.1	7.3	3.0	1.6
14470	313.5	M.W.	24.9	0.3	29.2	11.2	3.6	2.4	0.6
14498	314.5	M.W.	23.3	1.0	33.4	7.6	3.2	4.1	1.0
14553	316.5	M.W.	29.0	1.4	25.9	11.2	3.5	5.2	0.2
14581	317.5	M.W.	29.1	0.7	24.7	7.7	5.9	4.4	1.3
14608	318.5	M.W.	29.0	1.2	24.1	11.0	6.8	7.3	0.2
14636	319.5	M.W.	31.5	0.9	24.9	9.5	2.2	5.0	0.3
14657	320.5	M.W.	27.6	0.6	26.2	12.6	1.2	6.8	0.3
14670	321.5	M.W.	25.1	2.5	28.8	11.2	1.9	6.4	0.4
14696	323.5	M.W.	22.9	3.4	30.0	10.4	3.4	6.7	
14723	325.5	M.W.	23.0	4.2	27.2	17.2	3.8	8.3	0.2
14750	327.5	M.W.	20.8	4.2	28.8	10.4	3.2	6.6	
14776	329.5	M.W.	22.5	6.2	27.9	14.1	1.8	5.8	
14789	330.5	M.W.	27.3	5.5	27.3	13.2	0.5	7.5	0.5
14856	335.5	M.W.	28.2	4.8	21.8	20.2	2.0	3.6	0.4
14922	340.5	M.W.	28.1	5.2	21.4	24.5	2.6	3.6	0.0
14988	345.5	M.W.	28.6	4.3	24.6	13.1	3.5	7.0	0.8
15055	350.5	M.W.	29.4	5.6	23.8	16.1	2.5	2.2	0.3
15188	360.5	M.W.	30.2	3.4	24.1	11.2	2.7	7.1	0.0
15320	370.5	M.W.	28.5	2.4	18.2	15.5	2.7	11.2	0.3
15453	380.5	M.W.	22.6	3.2	16.1	18.4	1.3	12.4	0.0

Table A 9 SIMMAX reconstructions and $\delta^{18}\text{O}_w$ and $\delta^{18}\text{O}_{w\text{-ice}}$ calculations GEOFAR KF16
 Abbreviations J.R.: Janne Repschläger; M.W. Mara Weinelt

GEOFAR KF16								
depth [cm]	age [years BP]	SST _{wi} ndw [°C]	SST _{su} ndw [°C]	similarity	$\delta^{18}\text{O}_{\text{ice}}$ <i>Waelbroeck (2002)</i> [‰ SMOW]	$\delta^{18}\text{O}$ <i>G.ruber w.</i> [‰ V-PDB]	$\delta^{18}\text{O}_w$ <i>G.ruber w.</i> [‰ SMOW]	$\delta^{18}\text{O}_{w\text{-ice}}$ <i>G.ruber w.</i> [‰ SMOW]
2.5	524	16.5	22.3	>0.9	0.00	-0.17	1.64	1.64
3.5	734	16.3	22.8	>0.9	0.00	-0.33	1.58	1.58
4.5	943	16.3	22.4	>0.9	0.00	-0.27	1.56	1.56
5.5	1153	16.6	22.5	>0.9	0.00	-0.30	1.56	1.56
6.5	1362	16.4	22.4	>0.9	0.00	-0.23	1.60	1.60
7.5	1572	16.5	22.2	>0.9	0.00	-0.20	1.59	1.59
8.5	1697	16.5	22.2	>0.9	0.00	-0.34	1.45	1.45
9.5	1821	16.7	22.1	>0.9	0.00	-0.15	1.62	1.62
10.5	1946	16.8	22.2	0.78	0.00	-0.37	1.42	1.42
11.5	2071	16.5	22.2	>0.9	0.00	-0.23	1.56	1.56
12.5	2195	17.1	21.9	>0.9	0.00	-0.27	1.46	1.46
13.5	2320	16.7	22.1	>0.9	0.00	-0.27	1.50	1.50
14.5	2445	16.5	22.2	>0.9	0.00	-0.12	1.67	1.67
15.5	2569	16.6	22.3	>0.9	0.00	-0.29	1.53	1.52
16.5	2694	16.4	22.4	>0.9	0.00	-0.38	1.45	1.45
17.5	2819	16.8	22.3	>0.9	0.01	-0.23	1.58	1.58
19.5	3068	16.8	22.3	>0.9	0.01	-0.25	1.56	1.56
20.5	3193	16.1	22.7	0.88	0.01	-0.47	1.42	1.42
21.5	3317	16.4	22.4	>0.9	0.01	-0.43	1.40	1.39
22.5	3442	16.5	23.1	>0.9	0.01	-0.21	1.77	1.76
23.5	3567	16.5	22.2	>0.9	0.01	-0.36	1.43	1.42
24.5	3706	16.6	22.5	>0.9				
25.5	3846	16.5	22.2	>0.9	0.01	-0.10	1.69	1.68
26.5	3985	16.6	22.4	>0.9	0.01	-0.28	1.55	1.54
27.5	4125	17.2	23.8	0.87	0.01	-0.14	1.98	1.97
28.5	4264	16.7	22.5	0.89	0.02	0.08	1.93	1.92
29.5	4404	16.5	23.2	>0.9				
30.0	4474	17.1	23.3	0.86	0.02	-0.12	1.90	1.88
31.5	4683	16.9	23.5	0.88	0.02	-0.25	1.81	1.79
32.5	4823	16.5	22.3	>0.9	0.02	-0.39	1.42	1.40
33.5	4962	17.2	24	0.86	0.02	-0.42	1.75	1.73
34.5	5102	16.9	23.4	>0.9	0.02	-0.21	1.83	1.81
35.5	5241	17	22.5	>0.9	0.02	-0.33	1.53	1.50
36.5	5381	17	23.6	0.89	0.03	-0.13	1.95	1.93
37.5	5520	16.8	23.4	0.89	0.03	-0.14	1.90	1.88
38.5	5660	16.6	23.3	0.89	0.03	-0.18	1.84	1.81
39.5	5800	16.8	23.4	0.87	0.03	-0.22	1.82	1.79
40.8	5895	17.7	24	0.83	0.03	-0.11	2.05	2.02
41.5	5936	16.2	22.5	>0.9	0.03	-0.27	1.58	1.55
42.5	5993	16.7	23.3	0.88	0.03	-0.10	1.92	1.89
43.5	6051	16.3	22.9	>0.9	0.03	-0.20	1.73	1.70
44.5	6109	16.4	22.9	>0.9	0.03	-0.10	1.84	1.80
45.5	6166	16.5	23.1	>0.9	0.04	-0.17	1.81	1.78
46.5	6224	16.5	23.2	0.88	0.04	0.38	2.38	2.34

APPENDIX

GEOFAR KF16								
depth [cm]	age [years BP]	SST _{wi} ndw [°C]	SST _{su} ndw [°C]	similarity	$\delta^{18}\text{O}_{\text{ice}}$ <i>Waelbroeck (2002)</i> [‰ SMOW]	$\delta^{18}\text{O}$ <i>G.ruber w.</i> [‰ V-PDB]	$\delta^{18}\text{O}_w$ <i>G.ruber w.</i> [‰ SMOW]	$\delta^{18}\text{O}_{w\text{-ice}}$ <i>G.ruber w.</i> [‰ SMOW]
47.5	6282	16.9	21.2	>0.9	0.04	-0.33	1.25	1.21
48.5	6340	16.3	22.4	>0.9	0.04	0.34	2.17	2.14
50.5	6455	15.2	21.4	0.87	0.04	0.31	1.93	1.89
51.5	6513	16	22	>0.9	0.04	-0.15	1.60	1.56
52.5	6570	15.8	22.3	>0.9	0.04	-0.19	1.62	1.58
54.5	6686	16.1	22.7	>0.9	0.05	-0.23	1.67	1.62
55.5	6744	16.1	22.2	>0.9	0.05	-0.07	1.73	1.68
57.5	6859	16.6	23	>0.9	0.05	-0.27	1.69	1.64
58.5	6917	16.4	22.3	0.89				
59.5	6974	16.4	22.8	0.89	0.05	-0.13	1.79	1.73
60.5	7032	16.8	23.3	0.87				
62.5	7148	16.9	22	>0.9	0.06	-0.20	1.55	1.49
65.5	7321	16.9	22	>0.9	0.06	-0.34	1.41	1.35
66.5	7379	16.7	21.9	>0.9	0.06	-0.23	1.50	1.43
67.5	7436	16.7	21.7	>0.9	0.06	-0.19	1.50	1.43
68.5	7494	16.8	23	0.85	0.07	-0.22	1.74	1.67
69.5	7552	17.1	21.8	0.89	0.07	-0.47	1.23	1.17
70.5	7609	16.7	23.3	0.89	0.07	-0.36	1.66	1.59
72.5	7725	17.2	21.8	>0.8	0.07	-0.38	1.32	1.25
73.5	7783	16.7	22.1	0.98	0.07	-0.15	1.62	1.55
74.5	7840	16.7	22.5	0.89	0.08	-0.18	1.67	1.60
75.5	7898	16.7	23.3	0.87	0.08	-0.40	1.62	1.55
75.5	7898	17	23.6	0.89	0.08	-0.40	1.69	1.61
77.5	8013	16.9	21.8	>0.9	0.08	-0.30	1.41	1.33
78.5	8071	16.6	22.5	0.89	0.09	-0.20	1.65	1.57
80.5	8138	16.8	23.2	0.88	0.09	-0.35	1.65	1.56
80.5	8138	18.4	24	0.8	0.09	-0.35	1.82	1.73
81.5	8163	16.7	24	>0.9				
82.5	8188	16.9	22	0.87	0.10	-0.09	1.66	1.56
83.5	8213	16.5	22.3	>0.9				
84.5	8238	16.5	22.3	>0.9	0.10	-0.62	1.19	1.09
85.5	8263	16.5	22.3	0.89				
85.5	8263	14.7	20.2	0.85				
86.5	8288	16.5	22.3	>0.9	0.10	-0.20	1.61	1.51
87.5	8324	16.5	22.3	>0.9	0.11	-0.17	1.64	1.54
88.5	8373	17.1	21.6	>0.9	0.11	-0.30	1.36	1.25
89.5	8422	16.8	22.2	0.89	0.12	-0.16	1.63	1.51
90.5	8471	17	22.2	0.78	0.12	-0.15	1.64	1.52
92.5	8568	16.8	22.2	>0.9	0.13	-0.27	1.52	1.39
94.5	8666	17	21.7	>0.9	0.14	-0.31	1.37	1.24
95.5	8714	17	21.7	0.85	0.14	-0.12	1.57	1.43
96.5	8763	17	23.5	>0.9	0.15	-0.15	1.92	1.77
100.5	8958	17.3	21.2	0.89	0.16	-0.06	1.52	1.36
102.5	9056	16.7	23.3	>0.9	0.17	-0.11	1.91	1.74
103.5	9104	17.5	21.3	>0.9	0.18	-0.20	1.40	1.23
105.5	9202	17.3	21.2	0.89	0.18	-0.11	1.47	1.28
106.5	9251	16.5	23.1	>0.9	0.19	-0.18	1.80	1.61

GEOFAR KF16								
depth [cm]	age [years BP]	SST _{wi} ndw [°C]	SST _{su} ndw [°C]	similarity	$\delta^{18}\text{O}_{\text{ice}}$ <i>Waelbroeck (2002)</i> [‰ SMOW]	$\delta^{18}\text{O}$ <i>G.ruber w.</i> [‰ V-PDB]	$\delta^{18}\text{O}_w$ <i>G.ruber w.</i> [‰ SMOW]	$\delta^{18}\text{O}_{w\text{-ice}}$ <i>G.ruber w.</i> [‰ SMOW]
108.5	9348	14.4	18.9	>0.9	0.20	-0.15	0.96	0.76
109.5	9397	17.3	21.5	0.83	0.20	-0.12	1.52	1.32
110.5	9446	17.3	21.5	>0.9	0.21	-0.10	1.55	1.34
112.5	9543	17.3	21.5	>0.9	0.21	-0.34	1.31	1.09
115.5	9690	17	21.2	0.88	0.23	0.01	1.59	1.36
117.5	9787	9.4	14	>0.9	0.24	0.16	0.24	0.00
119.5	9885	16.5	20.5	>0.9	0.25	0.00	1.44	1.18
120.5	9933	17.4	21.2	0.89				
122.5	10031	10.4	15	>0.9	0.27	-0.04	0.25	-0.02
124.5	10128	17.4	21.3	>0.9	0.28	-0.03	1.57	1.29
126.5	10226	17.2	21.3	>0.9	0.29	-0.05	1.55	1.26
130.5	10421	16.4	21.2	0.89	0.31	-0.01	1.57	1.26
135.5	10665	9.8	14.5	>0.9	0.34	0.04	0.22	-0.12
137.5	10705	14.2	18.9	>0.9	0.35	0.09	1.19	0.84
139.5	10727	14.6	19.2	0.88	0.35	-0.13	1.03	0.68
140.5	10738	11.3	16.6	>0.9	0.35			
141.5	10749	12.6	17.6	>0.9	0.35			
143.5	10770	13.8	19	>0.9	0.35	0.11	1.23	0.88
145.5	10792	14.7	19.7	>0.9	0.36	-0.06	1.21	0.85
150.5	10846	13.9	18.7	>0.9	0.36	-0.05	1.02	0.65
154.5	10890	9.4	14.1	>0.9	0.37	0.19	0.29	-0.08
160.5	10955	13.5	18.4	>0.9	0.37	0.46	1.46	1.08
170.5	11063	11.4	16.8	>0.9	0.39			
172.5	11085	10.1	15.1	>0.9	0.39	0.14	0.45	0.06
174.5	11106	13.5	18.8	>0.9				
176.5	11128	12.7	17.8	>0.9	0.40	0.15	1.02	0.63
180.5	11172	11.6	16.6	>0.9	0.40	0.06	0.68	0.28
184.5	11215	9.2	14.2	>0.9	0.41	0.19	0.31	-0.09
190.5	11280	12.5	17.4	>0.9				
196.5	11345	10.5	15.7	0.83	0.42	0.04	0.48	0.05

Table A 10a SIMMAX reconstructions and $\delta^{18}\text{O}_w$ and $\delta^{18}\text{O}_{w\text{-ice}}$ calculations MD08-3180

MD08-3180CQ				MD08-3180CQ			
depth [cm]	age [years BP]	SST _{wi} ndw [°C]	SST _{su} ndw [°C]	depth [cm]	age [years BP]	SST _{wi} ndw [°C]	SST _{su} ndw [°C]
70.25	7923	16.9	21.8	110.50	10608	16.2	20.4
75.25	8159	17.5	21.3	120.50	10771	11	15.8
76.25	8176	16.5	22.6	126.25	10864	15.5	20.8
77.25	8194	16.6	22.8	127.25	10881	16	21
78.25	8211	16.5	22.6	131.75	10954	14	19.3
80.25	8246	7.5	12	134.75	11003	11.9	17.1
81.25	8264	7.8	12.1	141.25	11108	13.5	18.8
81.75	8272	6.4	10.7	143.25	11141	11.2	17.1
85.25	8363	16.4	20.6	144.25	11157	14.3	19
90.25	9046	17.2	21.6	146.25	11189	13.1	18.6
100.25	10412	17.6	21.3	149.25	11238	13.8	18.5

APPENDIX

MD08-3180CQ				MD08-3180CQ			
depth [cm]	age [years BP]	SST _{wi} ndw[°C]	SST _{su} ndw[°C]	depth [cm]	age [years BP]	SST _{wi} ndw[°C]	SST _{su} ndw[°C]
152.5	11291	13.5	18.1	275.5	13411	16.7	21.1
155.5	11340	11.2	15.8	276.5	13439	13.6	18.9
159.5	11405	13.3	18.1	277.5	13467	13.9	19.6
160.5	11421	12.6	17.6	278.5	13495	14.1	19.4
161.5	11437	12	16.7	279.5	13523	13.7	19.1
163.5	11470	11.1	15.7	280.5	13551	12.9	18.3
165.5	11502	12.7	17.5	281.5	13579	13.3	18.8
166.5	11518	10.7	15.5	282.5	13607	14.7	20.3
167.5	11535	11.2	16.2	283.5	13635	13.8	19.4
168.5	11551	10.6	15.5	285.5	13691	14.9	20.4
169.5	11567	10.9	15.7	286.5	13719	13.8	19.2
170.5	11583	10.6	15.2	287.5	13747	14.4	20
172.5	11616	10.9	15.8	288.5	13774	14.4	20.1
173.5	11631	11.1	15.8	289.5	13802	13.6	19
175.5	11661	10.6	15.7	291.5	13858	11.5	16.8
180.5	11734	10.3	14.9	292.5	13886	12.8	18.1
185.5	11808	10.4	14.9	293.5	13914	11.9	17
190.5	11882	10.3	14.7	294.5	13942	13	18.4
195.5	11955	10.5	15	295.5	13970	13.2	18.9
200.5	12029	11.4	16.6	296.5	13998	13.7	19.2
205.5	12102	10.8	15.5	297.5	14026	12.7	18.2
210.5	12174	10.2	14.5	298.5	14054	14.4	20.1
213.5	12219	13.2	18.5	299.5	14082	12.9	18.4
216.5	12263	11.6	16.9	302.5	14165	13.4	19.1
218.5	12292	12.4	17.7	304.5	14221	13.1	18.8
220.5	12322	11.8	16.8	305.5	14248	11.4	16.5
223.5	12366	13.2	18.4	306.5	14276	14	19.7
225.5	12395	12	17	307.5	14304	13.7	19.2
228.5	12439	13.4	18.4	308.5	14332	13.2	18.5
230.5	12469	12.9	18.3	310.5	14387	13.5	19.2
232.5	12498	10.7	15.4	312.5	14442	12.9	18.7
235.5	12542	11.6	16.9	313.5	14470	10.4	15
238.5	12587	13.2	18.5	314.5	14498	11	15.8
242.5	12645	10.8	15.5	316.5	14553	10.1	14.9
245.5	12690	10.3	14.7	317.5	14581	12	17.1
248.5	12734	10.8	15.6	318.5	14608	12	17.3
250.5	12763	12	17.3	319.5	14636	10.7	15.5
252.5	12793	10.7	15.3	320.5	14657	10.1	14.5
255.5	12868	12.6	18.1	321.5	14670	11.2	16
257.5	12922	10.3	15.4	323.5	14696	10.1	14.5
258.5	12949	10.8	15.7	325.5	14723	7.8	11.4
260.5	13004	10.3	15.5	327.5	14750	9.9	14.3
263.5	13085	6.3	10	329.5	14776	9.6	13.8
264.5	13112	7.6	11.3	330.5	14789	6.4	9.8
265.5	13139	9.5	13.7	335.5	14856	5.9	9.5
267.5	13193	6.9	10.5	340.5	14922	5.7	9.1
268.5	13221	6.3	9.9	345.5	14988	7.2	10.8
269.5	13248	12.2	17.7	350.5	15055	6.1	9.6
271.5	13302	13.3	18.6	360.5	15188	8.3	12.4
272.5	13329	15.6	21.6	370.5	15320	6.2	9.8
273.5	13356	13.4	18.9	380.5	15453	7.2	10.9

Table A10b $\delta^{18}\text{O}_w$ and $\delta^{18}\text{O}_{w\text{-ice}}$ calculations based on SIMMAX reconstructions and $\delta^{18}\text{O}$ of *G. ruber* w. from core MD08-3180

MD08-3180							
depth [cm]	age [years BP]	SST _{su} ndw [°C]	$\delta^{18}\text{O}_{\text{ice}}$ <i>Waelbroeck (2002)</i> [‰ SMOW]	$\delta^{18}\text{O}$ <i>G.ruber</i> w. [‰ V-PDB]	$\delta^{18}\text{O}_w$ <i>G.ruber</i> w. [‰ SMOW]	$\delta^{18}\text{O}_{w\text{-ice}}$ <i>G.ruber</i> w. [‰ SMOW]	
127.5	10885	21	0.37	0.06	1.60	1.23	
149.5	11242	18.5	0.41	0.09	1.11	0.70	
152.5	11290	18.1	0.42	0.15	1.09	0.67	
155.5	11339	15.8	0.42	0.02	0.47	0.05	
160.5	11420	17.6	0.43	0.07	0.90	0.47	
165.5	11501	17.5	0.44	0.36	1.17	0.73	
166.5	11518	15.5	0.45	0.43	0.82	0.38	
168.5	11550	15.5	0.45	0.06	0.46	0.01	
170.5	11583	15.2	0.45	0.22	0.55	0.10	
250.5	12763	17.3	0.60	0.53	1.30	0.69	
255.5	12868	18.1	0.61	0.10	1.03	0.42	
263.5	13085	10	0.64	0.43	-0.33	-0.97	
265.5	13139	13.7	0.65	0.59	0.61	-0.04	
269.5	13248	17.7	0.66	0.59	1.44	0.78	
272.5	13329	21.6	0.67	0.24	1.90	1.23	
274.5	13383	18.5	0.68	0.48	1.50	0.82	
275.5	13411	21.1	0.68	0.57	2.13	1.45	
277.5	13467	19.6	0.69	0.03	1.27	0.59	
278.5	13495	19.4	0.69	0.49	1.70	1.01	
279.5	13523	19.1	0.69	0.43	1.57	0.88	
280.5	13551	18.3	0.70	0.38	1.35	0.66	
285.5	13691	20.4	0.71	0.50	1.92	1.21	
295.5	13970	18.9	0.75	0.55	1.66	0.91	
305.5	14248	16.5	0.77	0.70	1.30	0.53	
310.5	14387	19.2	0.79	0.61	1.78	0.99	
320.5	14657	14.5	0.81	0.59	0.77	-0.04	
325.5	14723	11.4	0.82	1.34	0.88	0.06	
330.5	14789	9.8	0.82	0.97	0.18	-0.65	
335.5	14856	9.5	0.83	0.94	0.08	-0.75	
340.5	14922	9.1	0.84	1.06	0.12	-0.71	
345.5	14988	10.8	0.84	1.19	0.61	-0.23	
350.5	15055	9.6	0.85	1.04	0.20	-0.65	
360.5	15188	12.4	0.86	1.42	1.17	0.31	
370.5	15320	9.8	0.87	1.46	0.66	-0.21	
380.5	15453	10.9	0.89	1.43	0.87	-0.02	
390.5	15586	21.9	0.89	1.42	3.15	2.25	
271.5	13302	18.6	0.67	0.20	1.24	0.57	
273.5	13356	18.9	0.67	0.04	1.14	0.47	
276.5	13439	18.9	0.68	0.22	1.33	0.64	

Table A10c $\delta^{18}\text{O}_w$ and $\delta^{18}\text{O}_{w\text{-ice}}$ calculations based on SIMMAX reconstructions and $\delta^{18}\text{O}$ of *G. bulloides* from core MD08-3180

MD08-3180							
depth [cm]	age [years BP]	SST _{su} ndw [°C]	$\delta^{18}\text{O}_{\text{ice}}$ <i>Waelbroeck (2002)</i> [‰ SMOW]	$\delta^{18}\text{O}$ <i>G.bulloides</i> [‰ V-PDB]	$\delta^{18}\text{O}_w$ <i>G.bulloides</i> [‰ SMOW]	$\delta^{18}\text{O}_{w\text{-ice}}$ <i>G.bulloides</i> [‰ SMOW]	
160.5	11420	17.6	0.43	0.83	1.66	1.22	
173.5	11631	15.8	0.46	1.14	1.60	1.14	
175.5	11661	15.7	0.46	1.42	1.85	1.39	
180.5	11734	14.9	0.47	1.76	2.03	1.56	
185.5	11808	14.9	0.48	1.58	1.85	1.37	
190.5	11882	14.7	0.49	1.51	1.73	1.24	
200.5	12029	16.6	0.51	1.71	2.34	1.83	
205.5	12102	15.5	0.52	1.89	2.28	1.76	

MD08-3180							
Depth [cm]	age [years BP]	SST _{su} ndw [°C]	$\delta^{18}\text{O}_{\text{ice}}$ <i>Waelbroeck</i> (2002) [‰ SMOW]	$\delta^{18}\text{O}$ <i>G. bulloides</i> [‰ V-PDB]	$\delta^{18}\text{O}_w$ <i>G. bulloides</i> [‰ SMOW]	$\delta^{18}\text{O}_{w\text{-ice}}$	<i>G. bulloides</i> [‰ SMOW]
220.5	12322	16.8	0.55	1.56	2.23		1.68
223.5	12366	18.4	0.55	1.72	2.72		2.17
225.5	12395	17	0.56	1.72	2.43		1.87
229.5	12454	18.4	0.56	1.71	2.71		2.14
230.5	12469	18.3	0.57	1.49	2.47		1.90
235.5	12542	16.9	0.58	1.66	2.35		1.77
238.5	12587	18.5	0.58	1.92	2.94		2.36
248.5	12734	15.6	0.60	1.57	1.99		1.39
250.5	12763	17.3	0.60	1.77	2.54		1.94
255.5	12868	18.1	0.61	1.57	2.51		1.89
260.5	13004	15.5	0.63	1.55	1.95		1.31
263.5	13085	10	0.64	1.28	0.52		-0.12
265.5	13139	13.7	0.65	1.21	1.23		0.58
269.5	13248	17.7	0.66	1.28	2.13		1.47
272.5	13329	21.6	0.67	1.46	3.12		2.45
274.5	13383	18.5	0.68	1.16	2.18		1.50
275.5	13411	21.1	0.68	1.07	2.63		1.95
277.5	13467	19.6	0.69	1.34	2.58		1.90
278.5	13495	19.4	0.69	1.17	2.38		1.69
279.5	13523	19.1	0.69	1.38	2.53		1.83
280.5	13551	18.3	0.70	0.95	1.92		1.23
285.5	13691	20.4	0.71	1.18	2.60		1.89
295.5	13970	18.9	0.75	1.37	2.47		1.72
305.5	14248	16.5	0.77	1.34	1.94		1.17
310.5	14387	19.2	0.79	1.53	2.70		1.91
320.5	14657	14.5	0.81	1.80	1.98		1.17
325.5	14723	11.4	0.82	2.23	1.77		0.95
330.5	14789	9.8	0.82	2.23	1.44		0.62
335.5	14856	9.5	0.83	1.64	0.78		-0.05
340.5	14922	9.1	0.84	1.91	0.97		0.13
345.5	14988	10.8	0.84	1.78	1.19		0.35
350.5	15055	9.6	0.85	2.24	1.40		0.55
360.5	15188	12.4	0.86	2.17	1.92		1.06
370.5	15320	9.8	0.87	2.48	1.69		0.81
380.5	15453	10.9	0.89	2.67	2.11		1.22
390.5	15586	21.9	0.89	2.55	4.28		3.39
232.5	12498	15.4	0.57	1.58	1.95		1.38
242.5	12645	15.5	0.59	1.63	2.02		1.43
271.5	13302	18.6	0.67	1.23	2.27		1.61
273.5	13356	18.9	0.67	1.13	2.23		1.56
276.5	13439	18.9	0.68	1.50	2.60		1.92

Table A11 U^{k}_{37} SST reconstructions from core MD08-3180 and $\delta^{18}\text{O}_w$ and $\delta^{18}\text{O}_{w\text{-ice}}$ calculations based on U^{k}_{37} SST and $\delta^{18}\text{O}$ reconstructions of *G. ruber w.* and *G. bulloides* from core MD08-3180 and GEOFAR KF16

depth [cm]	age [years BP]	U^{k}_{37} SST [°C]	$\delta^{18}\text{O}$ <i>G. ruber w.</i> [‰ V-PDB]	$\delta^{18}\text{O}$ <i>G. bulloides</i> [‰ V-PDB]	$\delta^{18}\text{O}_w$ <i>G. ruber w.</i> [‰ V-PDB]	$\delta^{18}\text{O}_w$ <i>G. bulloides</i> [‰ SMOW]	$\delta^{18}\text{O}_{w\text{-ice}}$ <i>G. ruber w.</i> [‰ SMOW]	$\delta^{18}\text{O}_{w\text{-ice}}$ <i>G. bulloides</i> [‰ SMOW]
5.25	1241	18.9	-0.30		0.80		0.80	
10.25	1786	18.8	-0.15		0.93		0.93	
15.25	2297	19.0	-0.27		0.86		0.86	
20.25	2809	19.5	-0.23		1.00		0.99	
25.25	3320	18.6	-0.43		0.60		0.60	
30.25	3832	18.5	-0.10		0.93		0.91	
35.25	4343	18.8	-0.12		0.95		0.93	
40.25	4854	19.2	-0.39		0.77		0.75	
45.25	5366	18.8	-0.13		0.95		0.93	

APPENDIX

depth [cm]	age [years BP]	U ^k ₃₇ SST [°C]	$\delta^{18}\text{O}$ <i>G.ruber</i> w. [‰ V-PDB]	$\delta^{18}\text{O}$ <i>G.bulloides</i> [‰ V-PDB]	$\delta^{18}\text{O}_w$ <i>G.ruber</i> w. [‰ V-PDB]	$\delta^{18}\text{O}_w$ <i>G. bulloides</i> [‰ SMOW]	$\delta^{18}\text{O}_{w-ice}$ <i>G.ruber</i> w. [‰ SMOW]	$\delta^{18}\text{O}_{w-ice}$ <i>G.bulloides</i> [‰ SMOW]
50.25	5877	18.8	-0.11		0.97		0.94	
55.25	6389	18.7	0.30		1.36		1.32	
60.25	6900	19.5	-0.13		1.09		1.04	
65.25	7412	18.9	-0.22		0.89		0.82	
70.25	7923	19.0	-0.30		0.83		0.75	
75.25	8159	17.9	-0.09		0.80		0.71	
80.25	8246	17.8	-0.62		0.25		0.15	
85.25	8363	19.9	-0.30		1.00		0.89	
90.25	9046	20.2	-0.11		1.25		1.08	
94.25	9592	19.8	-0.02		1.27		1.05	
95.25	9729	20.0	-0.06		1.26		1.03	
100.25	10412	19.2	-0.01		1.16		0.85	
105.25	10523	19.6	0.09		1.34		1.01	
110.25	10604	19.9	0.17		1.47		1.13	
115.25	10686	19.9	0.04		1.36		1.01	
120.25	10767	19.7	0.11		1.37		1.02	
125.25	10848	19.4	0.07		1.28		0.92	
130.25	10929	19.0	0.08		1.20		0.83	
135.25	11011	19.0	0.06		1.18		0.79	
140.25	11092	18.9	-0.03		1.07		0.68	
145.25	11173	18.1	0.33		1.26		0.86	
150.25	11254	18.4	0.22		1.22		0.80	
155.25	11336	18.3	0.02		1.00		0.58	
160.25	11417	18.4	0.07	0.83	1.07	1.82	0.63	1.39
165.25	11498	18.2	0.36		1.32		0.87	
170.25	11579	17.4	0.22		1.00		0.55	
175.25	11657	16.4		1.42		2.00		1.53
180.25	11731	15.1		1.76		2.08		1.61
185.25	11804	16.8		1.58		2.25		1.77
190.25	11878	15.0		1.51		1.79		1.30
195.25	11952	14.7		1.70		1.93		1.43
200.25	12025	14.7		1.71		1.95		1.44
205.25	12098	14.3		1.89		2.03		1.51
210.25	12171	14.2						
215.25	12244	14.5		1.73		1.91		1.37
220.25	12318	14.7		1.56		1.79		1.25
225.25	12391	14.5		1.72		1.90		1.34
230.25	12465	15.2		1.49		1.81		1.24
235.25	12539	15.5		1.66		2.05		1.48
240.25	12612	15.9		1.82		2.28		1.70
245.25	12686	15.8		1.63		2.10		1.50
250.25	12760	15.6	0.53	1.77	0.95	2.19	0.35	1.59
255.25	12861	18.7	0.10	1.57	1.16	2.64	0.55	2.03
260.25	12997	18.0		1.56		2.48		1.85
265.25	13132	18.2	0.59	1.21	1.55	2.17	0.90	1.53
270.25	13268	19.1	0.40	1.02	1.53	2.16	0.87	1.50
275.25	13404	19.4	0.57	1.07	1.78	2.28	1.10	1.60
280.25	13544	18.8	0.38	0.95	1.46	2.03	0.76	1.33
285.25	13684	17.9	0.50	1.18	1.39	2.06	0.68	1.35
290.25	13823	18.2	0.69	1.19	1.65	2.15	0.92	1.42
295.25	13963	18.3	0.55	1.37	1.53	2.35	0.79	1.60
300.25	14103	18.2	0.62	1.30	1.58	2.25	0.82	1.49
305.25	14242	17.2	0.70	1.34	1.46	2.09	0.68	1.32
310.25	14380	16.6	0.61	1.53	1.24	2.16	0.45	1.37
315.25	14518	18.2	1.18	1.79	2.15	2.75	1.35	1.95
320.25	14653	15.0	0.59	1.80	0.87	2.08	0.06	1.27
325.25	14720	13.8	1.34	2.23	1.37	2.26	0.55	1.45
330.25	14786	13.1	0.97	2.23	0.87	2.13	0.05	1.31
335.25	14852	13.6	0.94	1.64	0.94	1.64	0.11	0.81
340.25	14919	12.9	1.06	1.91	0.92	1.76	0.08	0.93
345.25	14985	13.9	1.19	1.78	1.24	1.83	0.40	0.99

APPENDIX

depth [cm]	age [years BP]	U ^k ₃₇ SST [°C]	δ ¹⁸ O <i>G. ruber</i> w. [‰ V-PDB]	δ ¹⁸ O <i>G. bulloides</i> [‰ V-PDB]	δ ¹⁸ O _w <i>G. ruber</i> w. [‰ V-PDB]	δ ¹⁸ O _w <i>G. bulloides</i> [‰ SMOW]	δ ¹⁸ O _{w-ice} <i>G. ruber</i> w. [‰ SMOW]	δ ¹⁸ O _{w-ice} <i>G. bulloides</i> [‰ SMOW]
350.25	15052	13.6	1.04	2.24	1.04	2.24	0.19	1.39
355.25	15118	13.5	1.70	2.23	1.67	2.19	0.82	1.34
360.25	15184	12.6	1.42	2.17	1.20	1.96	0.34	1.10
365.25	15251	12.6	1.63	2.38	1.41	2.16	0.54	1.29
370.25	15317	12.7	1.46	2.48	1.26	2.28	0.39	1.41
375.25	15383	12.9	1.56	2.50	1.41	2.35	0.53	1.47
380.25	15450	13.1	1.43	2.67	1.32	2.57	0.44	1.68
385.25	15516	12.7	1.64	2.68	1.45	2.49	0.56	1.60
390.25	15582	13.1	1.42	2.55	1.32	2.45	0.42	1.56
395.25	15649	13.6	1.81	2.51	1.79	2.49	0.90	1.60
grey	Data from S. Balmer (unpublished data)							
δ ¹⁸ _{ice}	After Waelbroeck (2002) recalculated using Analyseries							

Table A12 subsurface temperature and δ¹⁸O_w / δ¹⁸O_{w-ice} reconstructions from core GEOFAR KF16 based on data from *G. truncatulinoides*

GEOFAR KF16							
depth [cm]	age [years BP]	Mg/Ca <i>G. truncatulinoides</i> >315µm [mmol/mol]	SST <i>G. truncatulinoides</i> [°C]	δ ¹⁸ O <i>G. truncatulinoides</i> [‰ VPDB]	δ ¹⁸ O _w <i>G. truncatulinoides</i> [‰ SMOW]	δ ¹⁸ O _{ice} (Waelbroeck, 2002) [‰ SMOW]	δ ¹⁸ O _{w-ice} <i>G. truncatulinoides</i> [‰ SMOW]
2.5	524	1.66	13.32	1.00	0.94	0.00	0.94
2.5	524	1.68	13.49	1.00	0.98	0.00	0.98
72.5	7725	1.86	14.84	1.23	1.49	0.07	1.41
80.5	8250	1.79	14.32	1.18	1.33	0.09	1.24
80.5	8250	1.82	14.52	1.18	1.37	0.09	1.28
90.5	8471	1.66	13.32	1.18	1.12	0.12	1.00
100.5	8958	1.56	12.46	1.21	0.98	0.16	0.81
100.5	8958	1.59	12.73	1.21	1.03	0.16	0.87
110.5	9446	1.71	13.70	1.31	1.33	0.21	1.12
120.5	9933	1.59	12.69	1.40	1.21	0.26	0.95
120.5	9933	1.60	12.80	1.40	1.24	0.26	0.98
130.5	10421	1.50	11.98	1.30	0.96	0.31	0.65
130.5	10421	1.53	12.23	1.30	1.01	0.31	0.70
140.5	10738	1.66	13.31	1.43	1.37	0.35	1.02
140.5	10738	1.70	13.59	1.43	1.42	0.35	1.07
150.5	10846	1.67	13.35	1.49	1.44	0.36	1.08
150.5	10846	1.68	13.49	1.49	1.47	0.36	1.11
155.5	10900	1.52	12.16	1.49	1.19	0.37	0.82
155.5	10900	1.56	12.47	1.49	1.25	0.37	0.88
160.5	10955	1.74	13.95	1.41	1.48	0.37	1.11
165.5	11009	1.72	13.81	1.39	1.43	0.38	1.05
165.5	11009	1.74	13.93	1.39	1.46	0.38	1.08
175.5	11117	1.82	14.58	1.56	1.76	0.39	1.37
175.5	11117	1.90	15.13	1.56	1.88	0.39	1.49
190.5	11280	1.84	14.69	1.51	1.73	0.42	1.32
195.5	11334	1.88	14.99	1.39	1.68	0.42	1.26

Table A13 SST and $\delta^{18}\text{O}_w / \delta^{18}\text{O}_{w\text{-ice}}$ reconstructions from core MD08-3180 based on data from *G. ruber w.*

MD08-3180 CQ							
depth [cm]	age [years BP]	Mg/Ca <i>G. ruber w.</i> >315 μm [mmol/mol].	SST <i>G. ruber w.</i> [$^{\circ}\text{C}$]	$\delta^{18}\text{O}$ <i>G. ruber w.</i> [‰ VPDB]	$\delta^{18}\text{O}_w$ <i>G. ruber w.</i> [‰ SMOW]	$\delta^{18}\text{O}_{\text{ice}}$ (Waelbroeck, 2002) [‰ SMOW]	$\delta^{18}\text{O}_{w\text{-ice}}$ <i>G. ruber w.</i> [‰ SMOW]
150.5	11258	2.59	17.51				
269.5	13248	2.81	18.71	0.59	1.65	0.66	0.99
270.5	13275	2.62	17.70	0.40	1.25	0.66	0.59
272.5	13329	2.52	17.10	0.24	0.97	0.67	0.30
274.5	13383	2.72	18.21	0.48	1.44	0.68	0.76
276.5	13439	2.47	16.81	0.22	0.89	0.68	0.21
278.5	13495	2.74	18.30	0.49	1.47	0.69	0.78
280.5	13551	2.58	17.46	0.38	1.18	0.70	0.48
284.5	13663	2.48	16.90			0.71	
286.5	13719	2.48	16.87			0.72	
288.5	13774	2.44	16.67			0.72	
290.5	13830	2.43	16.61	0.69	1.32	0.73	0.59
292.5	13886	2.63	17.76			0.74	

Table A 14 SST and $\delta^{18}\text{O}_w / \delta^{18}\text{O}_{w\text{-ice}}$ reconstructions from core MD08-3180 based on data from *G. bulloides*

MD08-3180 CQ							
depth [cm]	age [years BP]	Mg/Ca <i>G. bulloides</i> >315 μm [mmol/mol].	SST <i>G. bulloides</i> [$^{\circ}\text{C}$]	$\delta^{18}\text{O}$ <i>G. bulloides</i> [‰ VPDB]	$\delta^{18}\text{O}_w$ <i>G. bulloides</i> [‰ SMOW]	$\delta^{18}\text{O}_{\text{ice}}$ (Waelbroeck, 2002) [‰ SMOW]	$\delta^{18}\text{O}_{w\text{-ice}}$ <i>G. bulloides</i> [‰ SMOW]
150.5	11258	3.60	18.65				
170.5	11583	2.93	16.15	1.41	1.94	0.45	1.49
180.5	11734	2.74	15.31	1.76	2.12	0.47	1.65
190.5	11882	2.32	13.28	1.51	1.44	0.49	0.95
200.5	12029	2.48	14.09	1.71	1.81	0.51	1.30
210.5	12174	2.38	13.62	1.72	1.72	0.53	1.20
212.5	12204	2.79	15.54	1.71	2.11	0.53	1.58
213.5	12219	2.63	14.83			0.53	
214.5	12233	2.44	13.93	1.77	1.84	0.54	1.30
215.5	12248	2.27	13.05	1.73	1.61	0.54	1.08
216.5	12263	2.33	13.33			0.54	
217.5	12277	2.45	13.97	1.64	1.72	0.54	1.18
217.5	12277	2.47	14.05			0.54	
218.5	12292	2.69	15.10			0.54	
219.5	12307	2.35	13.47	1.65	1.62	0.55	1.07
220.5	12322	2.63	14.80	1.56	1.81	0.55	1.26
223.5	12366	2.35	13.45	1.72	1.69	0.55	1.13
227.5	12425	2.65	14.93	1.64	1.92	0.56	1.36
228.5	12439	2.62	14.76			0.56	
230.5	12469	2.55	14.45	1.49	1.66	0.57	1.10
232.5	12498	2.52	14.29	1.58	1.72	0.57	1.15
233.5	12513	2.86	15.83	1.77	2.24	0.57	1.67
235.5	12542	2.29	13.14	1.66	1.57	0.58	0.99
237.5	12572	2.35	13.47	1.72	1.69	0.58	1.11
238.5	12587	2.43	13.87	1.92	1.97	0.58	1.39

MD08-3180 CQ							
depth [cm]	age [years BP]	Mg/Ca <i>G. bulloides</i> >315 μ m [mmol/mol].	SST <i>G. bulloides</i> [°C]	$\delta^{18}\text{O}$ <i>G. bulloides</i> [‰ VPDB]	$\delta^{18}\text{O}_w$ <i>G. bulloides</i> [‰ SMOW]	$\delta^{18}\text{O}_{\text{ice}}$ (Waelbroeck, 2002) [‰ SMOW]	$\delta^{18}\text{O}_{w\text{-ice}}$ <i>G. bulloides</i> [‰ SMOW]
240.5	12616	2.30	13.17	1.82	1.73	0.58	1.14
242.5	12645	2.64	14.86	1.63	1.89	0.59	1.30
243.5	12660	2.80	15.60	1.72	2.13	0.59	1.54
245.5	12690	2.31	13.24	1.63	1.56	0.59	0.97
247.5	12719	2.75	15.35	1.72	2.08	0.60	1.49
248.5	12734	2.43	13.86	1.57	1.62	0.60	1.03
250.5	12763	2.77	15.46	1.77	2.15	0.60	1.55
252.5	12793	2.83	15.73	1.48	1.92	0.61	1.32
254.5	12841	2.74	15.33	1.40	1.76	0.61	1.14
255.5	12868	3.34	17.75	1.57	2.43	0.61	1.82
255.5	12868	2.76	15.43	1.57	1.95	0.61	1.34
256.5	12895	2.69	15.11	1.38	1.69	0.62	1.07
257.5	12922	3.37	17.86	1.14	2.03	0.62	1.40
257.5	12922	3.90	19.63	1.14	2.40	0.62	1.77
258.5	12949	2.65	14.91	1.70	1.97	0.62	1.34
260.5	13004	2.47	14.08	1.57	1.67	0.63	1.04
260.5	13004	3.13	16.93	1.57	2.26	0.63	1.63
261.5	13031	3.57	18.55	1.27	2.30	0.63	1.67
262.5	13058	4.47	21.29				overprinted
263.5	13085	3.71	19.02				overprinted
264.5	13112	4.70	21.89				overprinted
266.5	13166	4.23	20.62				overprinted
268.5	13221	3.73	19.07				overprinted
272.5	13329	2.91	16.04	1.46	1.96	0.67	1.29
274.5	13383	3.60	18.64	1.16	2.21	0.68	1.53
276.5	13439	3.24	17.38	1.50	2.29	0.68	1.60
278.5	13495	2.50	14.23	1.17	1.30	0.69	0.61
280.5	13551	2.66	14.97	0.95	1.23	0.70	0.53
284.5	13663	2.54	14.42	1.31	1.48	0.71	0.77
286.5	13719	3.44	18.10	1.01	1.94	0.72	1.23
288.5	13774	2.93	16.15	1.14	1.67	0.72	0.94
290.5	13830	2.74	15.33	1.19	1.55	0.73	0.82
292.5	13886	2.94	16.20	1.29	1.83	0.74	1.09

Table A15 subsurface temperature and $\delta^{18}\text{O}_w / \delta^{18}\text{O}_{w\text{-ice}}$ reconstructions from core MD08-3180 based on data from *G. truncatulinoides*

MD08-3180 CQ							
depth [cm]	age [years BP]	Mg/Ca <i>G. truncatulinoides</i> >315 μ m [mmol/mol]	SST <i>G. truncatulinoides</i> [°C]	$\delta^{18}\text{O}$ <i>G. truncatulinoides</i> [‰ VPDB]	$\delta^{18}\text{O}_w$ <i>G. truncatulinoides</i> [‰ SMOW]	$\delta^{18}\text{O}_{\text{ice}}$ (Waelbroeck, 2002) [‰ SMOW]	$\delta^{18}\text{O}_{w\text{-ice}}$ <i>G. truncatulinoides</i> [‰ SMOW]
140.5	11096	1.57	12.60	1.62	1.41	0.39	1.02
145.5	11177	1.73	13.86	1.55	1.60	0.40	1.20
155.5	11340	1.89	15.03	1.31	1.60	0.42	1.18
160.5	11421	1.80	14.43	1.50	1.67	0.43	1.24
165.5	11502	1.91	15.17	1.37	1.70	0.44	1.25
178.5	11704	1.69	13.51	2.02	2.00	0.47	1.53
178.5	11704	1.71	13.71	2.02	2.04	0.47	1.58
180.5	11734	1.79	14.32	1.63	1.78	0.47	1.30

APPENDIX

MD08-3180 CQ							
depth [cm]	age [years BP]	Mg/Ca <i>G. truncatulinoides</i> >315 μ m [mmol/mol]	SST <i>G. truncatulinoides</i> [$^{\circ}$ C]	$\delta^{18}\text{O}$ <i>G. truncatulinoides</i> [‰ VPDB]	$\delta^{18}\text{O}_w$ <i>G. truncatulinoides</i> [‰ SMOW]	$\delta^{18}\text{O}_{\text{ice}}$ (Waelbroeck , 2002) [‰ SMOW]	$\delta^{18}\text{O}_{w\text{-ice}}$ <i>G. truncatulinoides</i> [‰ SMOW]
185.5	11808	1.78	14.28	2.00	2.14	0.48	1.66
187.5	11838	1.61	12.86	2.00	1.84	0.49	1.36
190.5	11882	1.77	14.14	1.95	2.06	0.49	1.57
195.5	11955	1.70	13.60	2.19	2.18	0.50	1.68
200.5	12029	1.66	13.31	2.29	2.23	0.51	1.72
204.5	12087	1.77	14.21	2.31	2.44	0.52	1.92
205.5	12102	1.77	14.18	2.04	2.16	0.52	1.64
207.5	12131	1.56	12.49	2.33	2.10	0.52	1.58
207.5	12131	1.58	12.61	2.33	2.13	0.52	1.60
210.5	12174	1.79	14.35	2.31	2.47	0.53	1.94
215.5	12248	1.59	12.71	2.07	1.88	0.54	1.34
215.5	12248	1.72	13.77	2.07	2.11	0.54	1.57
217.5	12277	1.85	14.75	1.99	2.23	0.54	1.68
217.5	12277	1.91	15.23	1.99	2.33	0.54	1.79
220.5	12322	1.57	12.58	1.83	1.62	0.55	1.07
220.5	12322	1.65	13.20	1.83	1.75	0.55	1.20
223.5	12366	1.81	14.48	1.87	2.05	0.55	1.50
227.5	12425	1.85	14.75	2.31	2.55	0.56	1.98
230.5	12469	1.84	14.67	1.93	2.15	0.57	1.58
230.5	12469	1.76	14.12	1.93	2.03	0.57	1.47
233.5	12513	1.62	12.95	2.32	2.19	0.57	1.61
233.5	12513	1.63	13.02	2.32	2.20	0.57	1.63
235.5	12542	1.75	14.05	1.78	1.87	0.58	1.30
237.5	12572	1.67	13.40	2.30	2.26	0.58	1.68
237.5	12572	1.83	14.60	2.30	2.51	0.58	1.93
240.5	12616	1.64	13.16	2.31	2.21	0.58	1.63
245.5	12690	1.74	13.96	2.40	2.48	0.59	1.88
250.5	12763	1.84	14.70	2.29	2.51	0.60	1.91
255.5	12868	1.80	14.44	1.99	2.17	0.61	1.55
260.5	13004	1.78	14.23	2.15	2.28	0.63	1.65
265.5	13139	1.76	14.11	1.88	1.98	0.65	1.33
270.5	13275	1.58	12.67	2.01	1.81	0.66	1.15
270.5	13275	1.94	15.43	2.01	2.39	0.66	1.72
275.5	13411	1.67	13.39	2.00	1.96	0.68	1.28
280.5	13551	1.89	15.09	1.81	2.12	0.70	1.42
285.5	13691	1.92	15.26	2.08	2.43	0.71	1.72
290.5	13830	1.82	14.56	1.88	2.08	0.73	1.35
295.5	13970	1.92	15.26	1.97	2.32	0.75	1.57
300.5	14110	1.95	15.50	2.02	2.42	0.76	1.66
305.5	14248	2.09	16.44	1.85	2.44	0.77	1.67
305.5	14248	2.13	16.65	1.85	2.49	0.77	1.71
310.5	14387	1.86	14.86	1.86	2.12	0.79	1.34
310.5	14387	1.89	15.09	1.86	2.17	0.79	1.39
315.5	14525	1.85	14.79	2.33	2.58	0.80	1.78
315.5	14525	1.91	15.23	2.33	2.67	0.80	1.87
320.5	14657	1.79	14.36	1.57	1.73	0.81	0.92
325.5	14723	1.63	13.02	2.59	2.47	0.82	1.65
330.5	14789	1.53	12.23	2.61	2.32	0.82	1.50
335.5	14856	1.71	13.70	2.51	2.53	0.83	1.70
340.5	14922	1.65	13.27	2.48	2.41	0.84	1.57

MD08-3180 CQ							
depth [cm]	age [years BP]	Mg/Ca <i>G. truncatulinoides</i> >315µm [mmol/mol]	SST <i>G. truncatulinoides</i> [°C]	$\delta^{18}\text{O}$ <i>G. truncatulinoides</i> [‰ VPDB]	$\delta^{18}\text{O}_w$ <i>G. truncatulinoides</i> [‰ SMOW]	$\delta^{18}\text{O}_{\text{ice}}$ (Waelbroeck, 2002) [‰ SMOW]	$\delta^{18}\text{O}_{w\text{-ice}}$ <i>G. truncatulinoides</i> [‰ SMOW]
345.5	14988	1.61	12.93	2.26	2.12	0.84	1.28
350.5	15055	1.74	13.96	2.69	2.77	0.85	1.92

Deepwater data

Table A 16 deepwater temperature and $\delta^{18}\text{O}_w / \delta^{18}\text{O}_{w\text{-ice}}$ reconstructions from core GEOFAR KF16 based on data from *C. wuellerstorfi*

GEOFAR KF16					
depth [cm]	age [years BP]	$\delta^{18}\text{O}$ <i>C. wuellerstorfi</i> corrigiert [‰ VPDB]	Mg/Ca <i>C. wuellerstorfi</i> >250µm [mmol/mol]	BWT <i>C. wuellerstorfi</i> Healey exp [°C]	$\delta^{18}\text{O}_w$ <i>C. wuellerstorfi</i> [‰ SMOW]
2.5	524	2.94	1.65	3.26	-0.27
6.5	1362	2.99	1.58	3.06	-0.27
8.5	1697	2.96	1.82	3.69	-0.14
9.5	1821	3.00	1.42	2.59	-0.38
10.5	1946	3.00	1.62	3.16	-0.23
11.5	2071	2.96	1.51	2.86	-0.35
13.5	2320	2.95	1.60	3.13	-0.29
14.5	2445	3.00	1.50	2.84	-0.32
17.5	2819	2.98	1.81	3.64	-0.14
18.5	2943	2.92	1.57	3.04	-0.35
21.5	3317	2.94	1.67	3.30	-0.26
22.5	3442	3.02	1.42	2.61	-0.35
23.5	3567	2.93	1.45	2.69	-0.42
24.5	3706	2.96	1.65	3.25	-0.26
30	4474	3.02	1.39	2.50	-0.38
32.5	4823	3.05	1.65	3.26	-0.16
33.5	4962	2.99	1.45	2.69	-0.36
39.5	5800	2.86	1.43	2.63	-0.50
53.5	6628	3.34	1.69	3.35	0.15
55.5	6744	3.00	1.57	3.03	-0.27
56.5	6801		1.50	2.84	
58.5	6917	2.88	1.58	3.06	-0.38
59.5	6974	2.95	1.67	3.30	-0.25
60.5	7032	3.04	1.64	3.23	-0.18
61.5	7090		1.59	3.09	
64.5	7263	2.92	1.74	3.49	-0.24
65.5	7321	3.06	1.51	2.85	-0.25
66.5	7379	2.95	1.47	2.75	-0.39
68.5	7494	2.98	1.58	3.07	-0.28
69.5	7552	3.01	1.64	3.22	-0.21
70.5	7609	3.07	1.69	3.35	-0.12
71.5	7667	3.04	1.52	2.91	-0.26
74.5	7840	2.88	1.51	2.87	-0.43
75.5	7898	3.10	1.71	3.41	-0.07
76.5	7956	2.89	1.59	3.09	-0.36
78.5	8071	3.13	1.66	3.29	-0.07
86.5	8288	2.99	1.74	3.48	-0.17
87.5	8324	3.07	1.55	2.98	-0.21
89.5	8422	3.14	1.57	3.05	-0.12
90.5	8471	3.12	1.47	2.74	-0.22
91.5	8519	3.07	1.67	3.31	-0.13
92.5	8568	3.15	1.63	3.21	-0.07
93.5	8617	2.97	1.55	2.99	-0.31
93.5	8617		1.84	3.72	
94.5	8666	3.10	1.51	2.87	-0.20

GEOFAR KF16					
depth [cm]	age [years BP]	$\delta^{18}\text{O}$ <i>C. wuellerstorfi</i> corrigiert [‰ VPDB]	Mg/Ca <i>C. wuellerstorfi</i> >250 μm [mmol/mol]	BWT <i>C. wuellerstorfi</i> Healey exp [°C]	$\delta^{18}\text{O}_w$ <i>C. wuellerstorfi</i> [‰ SMOW]
96.5	8763	3.11	1.71	3.41	-0.07
100.5	8958	3.14	1.62	3.18	-0.09
101.5	9007	3.12	1.67	3.30	-0.08
103.5	9104	3.04	1.59	3.09	-0.21
104.5	9153	3.06	1.55	2.97	-0.22
105.5	9202	3.02	1.58	3.06	-0.24
106.25	9239	3.11	1.34	2.34	-0.33
107.25	9287	3.12	1.78	3.58	-0.01
108.5	9348	3.01	1.65	3.25	-0.20
109.5	9397	3.05	1.62	3.17	-0.18
113.5	9592	3.04	1.73	3.45	-0.12
114.5	9641	3.05	1.74	3.49	-0.10
115.5	9690	2.99	1.42	2.59	-0.39
116.5	9738	2.98	1.58	3.05	-0.29
120.5	9933	3.04	1.84	3.73	-0.06
124.5	10128	3.05	1.61	3.14	-0.19
135.5	10665	3.02	1.65	3.25	-0.20

Table A 17 deepwater temperature and $\delta^{18}\text{O}_w / \delta^{18}\text{O}_{w\text{-ice}}$ reconstructions from core GEOFAR KF16 based on data from *M. barleanum*

GEOFAR KF16					
depth [cm]	age [years BP]	$\delta^{18}\text{O}$ <i>M. barleanum</i> 250-315 μm [‰ VPDB]	Mg/Ca <i>M. barleanum</i> [mmol/mol]	BWT <i>M. barleanum</i> Healey exp [°C]	$\delta^{18}\text{O}_w$ <i>M. barleanum</i> [‰ SMOW]
25.5	3846		1.46	2.7	
42.5	5993		1.52	2.9	
43.5	6051		1.24	2.0	
44.5	6109		1.56	3.0	
49.5	6397		1.70	3.4	
50.5	6455		1.78	3.6	
52.5	6570		1.52	2.9	
54.5	6686		1.61	3.2	
74.5	7840		1.22	1.9	
117.5	9787		1.63	3.2	
123.5	10080		1.52	2.9	
125.5	10177		1.57	3.0	
126.5	10226		1.59	3.1	
128.5	10323		1.61	3.1	
129.5	10372		1.67	3.3	
132.5	10518		1.71	3.4	
133.5	10567		1.67	3.3	
134.5	10616		1.60	3.1	
136.5	10694		1.63	3.2	
137.5	10705	2.67	1.75	3.5	-0.47
138.5	10716		1.65	3.3	
139.5	10727	2.64	1.64	3.2	-0.58
144.5	10781		1.64	3.2	
149.5	10835		1.74	3.5	
154.5	10890		1.51	2.9	

Table A 18 deepwater temperature and $\delta^{18}\text{O}_w / \delta^{18}\text{O}_{w\text{-ice}}$ reconstructions from core GEOFAR KF16 based on data from *M. affinis*

GEOFAR KF16							
depth [cm]	age [years BP]	$\delta^{18}\text{O}$ <i>M. affinis</i> 250-315 μm [‰ VPDB]	$\delta^{18}\text{O}$ <i>M. affinis</i> corr. 250-315 μm [‰ VPDB]	Mg/Ca <i>M. affinis</i> [mmol/mol]	Mg/Ca <i>M. affinis</i> corr. [mmol/mol]	BWT <i>M. affinis</i> Healey exp [°C]	$\delta^{18}\text{O}_w$ <i>M. affinis</i> [‰ SMOW]
40.75	5892			1.50	1.80	3.64	
50.5	6455			1.61	1.91	3.89	
127.5	10275			1.35	1.65	3.26	
136.5	10694			1.34	1.64	3.21	
140.5	10738	2.68	3.12				
142.5	10759			1.25	1.55	2.97	
144.5	10781			1.35	1.65	3.25	
145.5	10792			1.46	1.76	3.53	
146.5	10803			1.44	1.74	3.49	
147.5	10814			1.30	1.60	3.11	
148.5	10825			1.32	1.62	3.17	
149.5	10835	2.43	2.87	1.33	1.63	3.19	-0.36
154.5	10890	2.79	3.23				
155.5	10900			1.50	1.80	3.64	
156.5	10911	2.71	3.15				
158.5	10933	2.66	3.10				
162.5	10976			1.36	1.66	3.27	
163.5	10987			1.54	1.84	3.71	
164.5	10998	2.64	3.08	1.43	1.73	3.47	-0.08
165.5	11009	2.63	3.07	1.41	1.71	3.41	-0.11
166.5	11020	2.71	3.15	1.26	1.56	3.01	-0.12
167.5	11031	2.71	3.15	1.41	1.71	3.40	-0.03
168.5	11041	2.70	3.14				
169.5	11052	2.63	3.07	1.33	1.63	3.19	-0.15
170.5	11063	2.58	3.02	1.42	1.72	3.42	-0.15
172.5	11085	2.66	3.10				
173.5	11096	2.65	3.09				
174.5	11106	2.66	3.10	1.30	1.60	3.11	-0.15
175.5	11117	2.60	3.04	1.35	1.65	3.27	-0.17
176.5	11128	2.60	3.04	1.42	1.72	3.44	-0.12
178.5	11150	2.69	3.13	1.28	1.58	3.05	-0.13
179.5	11161	2.56	3.00	1.30	1.60	3.11	-0.25
182.5	11193	2.67	3.11				
183.5	11204	2.64	3.08	1.24	1.54	2.95	-0.20
184.5	11215	2.68	3.12	1.33	1.63	3.20	-0.11
185.5	11226	2.70	3.14	1.35	1.65	3.25	-0.08
186.5	11237	2.71	3.15	1.26	1.56	3.01	-0.12
187.5	11247	2.74	3.18	1.29	1.59	3.09	-0.07
192.5	11302	2.70	3.14	1.34	1.64	3.23	-0.08
194.5	11323	2.68	3.12	1.29	1.59	3.10	-0.13
195.5	11334	2.68	3.12	1.27	1.57	3.04	-0.14

Table A 19 deepwater temperature and $\delta^{18}\text{O}_w / \delta^{18}\text{O}_{w\text{-ice}}$ reconstructions from core MD08-3180 based on data from *M. barleanum*

MD08-3180CQ					
depth [cm]	age [years BP]	$\delta^{18}\text{O}$ <i>M. barleanum</i> 250-315 μm [‰ VPDB]	Mg/Ca <i>M. barleanum</i> [mmol/mol]	BWT <i>M. barleanum</i> Healey exp [°C]	$\delta^{18}\text{O}_w$ <i>M. barleanum</i> [‰ SMOW]
265.5	13142		1.45	2.7	
270.5	13279		1.72	3.4	
275.5	13416		1.49	2.8	
280.5	13555		1.44	2.7	
285.5	13694		1.45	2.7	
290.5	13833		1.41	2.6	
295.5	13972		1.48	2.8	
300.5	14111		1.46	2.7	
305.5	14249		1.41	2.6	
310.5	14387		1.26	2.1	

Table A 20 deepwater temperature and $\delta^{18}\text{O}_w / \delta^{18}\text{O}_{w\text{-ice}}$ reconstructions from core MD08-3180 based on data from *M. affinis*

MD08-3180 CQ							
depth [cm]	age [years BP]	$\delta^{18}\text{O}$ <i>M. affinis</i> 250-315 μm [‰ VPDB]	$\delta^{18}\text{O}$ <i>M. affinis</i> corr. 250-315 μm [‰ VPDB]	Mg/Ca <i>M. affinis</i> [mmol/mol]	Mg/Ca <i>M. affinis</i> corr. [mmol/mol]	BWT <i>M. affinis</i> Healey exp [°C]	$\delta^{18}\text{O}_w$ <i>M. affinis</i> [‰ SMOW]
157.5	11372			1.33	1.63	3.19	
158.5	11388	2.62	3.06	1.33	1.63	3.19	-0.17
159.5	11404	2.53	2.97				
160.5	11420	2.52	2.96	1.36	1.66	3.29	-0.24
162.5	11453	2.61	3.05	1.42	1.72	3.44	-0.11
166.5	11518	2.69	3.13	1.52	1.82	3.69	0.02
168.5	11550	2.63	3.07	1.36	1.66	3.28	-0.14
171.5	11599	2.73	3.17	1.35	1.65	3.24	-0.04
173.5	11631	2.65	3.09	1.28	1.58	3.06	-0.17
174.5	11645	2.85	3.29	1.33	1.63	3.21	0.06
175.5	11660	2.64	3.08	1.36	1.66	3.28	-0.12
176.5	11675	2.55	2.99	1.28	1.58	3.08	-0.27
177.5	11690	2.77	3.21	1.30	1.60	3.12	-0.04
178.5	11704	2.80	3.24	1.23	1.53	2.92	-0.06
180.5	11734			1.27	1.57	3.03	
183.5	11778			1.31	1.61	3.15	
185.5	11808			1.31	1.61	3.15	
187.5	11837	2.79	3.23	1.26	1.56	3.02	-0.04
188.5	11852			1.32	1.62	3.18	
189.5	11867			1.43	1.73	3.45	
190.5	11881			1.23	1.53	2.94	
191.5	11896	2.75	3.19				
195.5	11955			1.19	1.49	2.81	
197.5	11985			1.24	1.54	2.97	
198.50	11999			1.15	1.45	2.68	
200.50	12029	3.07	3.51	1.38	1.68	3.34	0.32
201.50	12044			1.19	1.49	2.80	
204.50	12087			1.22	1.52	2.90	
208.50	12145			1.17	1.47	2.74	
210.50	12174	2.77	3.21				
214.50	12233	2.80	3.24	1.16	1.46	2.73	-0.11
215.50	12248			1.54	1.84	3.71	
217.50	12277			1.20	1.50	2.85	
219.50	12307	2.95	3.39				
220.50	12322			1.23	1.53	2.93	
221.50	12336	3.02	3.46	1.22	1.52	2.91	0.16
223.50	12366			1.17	1.47	2.75	
225.50	12395	3.08	3.52	1.17	1.47	2.76	0.18
227.50	12425	2.98	3.42	1.29	1.59	3.08	0.17
229.50	12454	3.21	3.65	1.44	1.74	3.48	0.50
230.50	12469			1.17	1.47	2.75	
232.50	12498	3.05	3.49	1.16	1.46	2.72	0.14
233.50	12513	3.31	3.75	1.21	1.51	2.87	0.44
235.50	12542			1.26	1.56	3.01	
237.50	12572			1.21	1.51	2.86	
238.50	12587			1.23	1.53	2.93	
240.50	12616	3.16	3.60	1.18	1.48	2.77	0.27
242.50	12645	3.60	4.04	1.18	1.48	2.78	0.71
245.50	12690			1.41	1.71	3.41	
265.50	13142			1.18	1.48	2.79	
315.50	14526			1.28	1.58	3.06	
320.50	14657			1.52	1.82	3.67	
325.50	14723			1.24	1.54	2.94	
335.50	14856			1.19	1.49	2.80	
340.50	14922			1.19	1.49	2.82	
345.50	14988			1.41	1.71	3.41	

Table A21 planktonic stable isotope data of core MD08-3181

MD08-3181				MD08-3181			
depth (cm)	sampled intervall (cm)	$\delta^{18}\text{O}$	$\delta^{18}\text{O}$	depth (cm)	sampled intervall (cm)	$\delta^{18}\text{O}$	$\delta^{18}\text{O}$
		<i>G. ruber w.</i> >315 μm [‰ VPDB]	<i>G. bulloides</i> 315-400 μm [‰ VPDB]			<i>G. ruber w.</i> >315 μm [‰ VPDB]	<i>G. bulloides</i> 315-400 μm [‰ VPDB]
190.5	190-191		2.63	820.5	820-821		2.17
200.5	200-201		2.55	830.5	830-831	2.17	
210.5	210-211		2.75	840.5	840-841	1.49	
220.5	220-221		2.48	870.5	870-871	1.96	
230.5	230-231		2.41	910.5	910-911	1.73	
240.5	240-241		2.37	940.5	940-941	1.80	
250.5	250-251		2.49	980.5	980-981	1.77	
260.5	260-261		2.39	1010.5	1010-1011	1.43	
270.5	270-271		2.52	1020.5	1020-1021	1.67	
280.5	280-281		2.27	1030.5	1030-1031	1.96	
290.5	290-291		2.39	1040.5	1040-1041	1.82	
300.5	300-301		2.16	1050.5	1050-1051	1.94	
310.5	310-311		2.31	1060.5	1060-1061	1.91	
320.5	320-321		2.04	1070.5	1070-1071	1.71	
330.5	330-331		1.96	1080.5	1080-1081	1.81	
340.5	340-341		2.00	1090.5	1090-1091	1.74	
350.5	350-351		2.11	1100.5	1100-1101	1.96	
360.5	360-361		2.43	1110.5	1110-1111	2.03	
370.5	370-371		2.08	1120.5	1120-1121	1.75	
380.5	380-381		2.33	1130.5	1130-1131	1.70	
390.5	390-391		2.43	1140.5	1140-1141	1.80	
400.5	400-401		2.36	1150.5	1150-1151	1.79	
410.5	410-411		2.44	1160.5	1160-1161	2.31	
420.5	420-421		2.23	1170.5	1170-1171	1.62	
430.5	430-431		2.29	1180.5	1180-1181	1.74	
440.5	440-441		2.15	1200.5	1200-1201	1.98	
450.5	450-451		2.01	1210.5	1210-1211	1.93	
460.5	460-461		2.31	1220.5	1220-1221	1.89	
470.5	470-471		2.14	1230.5	1230-1231	1.28	
490.5	490-491		2.59	1240.5	1240-1241	1.77	
500.5	500-501		3.09	1250.5	1250-1251	1.79	
510.5	510-511		2.31	1280.5	1280-1281	1.83	
520.5	520-521		2.22	1290.5	1290-1291	2.00	
530.5	530-531		2.18	1300.5	1300-1301	1.71	
540.5	540-541		2.12	1310.5	1310-1311	1.82	
550.5	550-551		2.20	1320.5	1320-1321	1.96	
560.5	560-561		1.91	1330.5	1330-1331	1.52	
570.5	570-571		2.06	1340.5	1340-1341	1.73	
610.5	610-611		2.15	1350.5	1350-1351	1.84	
650.5	65-651		2.22	1360.5	1360-1361	1.86	
690.5	690-691		2.43	1370.5	1370-1371	1.68	
730.5	730-731		2.46	1380.5	1380-1381	1.69	
750.5	750-751		2.20	1390.5	1390-1391	1.74	
760.5	760-761		2.55	1400.5	1400-1401	1.54	1.86
770.5	770-771		2.03	1410.5	1410-1411	1.28	1.67
790.5	790-791		2.16	1420.5	1420-1421	1.33	2.00
800.5	800-801		2.43	1430.5	1430-1431	0.97	2.06
810.5	810-811		2.22	1440.5	1440-1441	1.34	2.00

APPENDIX

MD08-3181				MD08-3181			
depth (cm)	sampled intervall (cm)	$\delta^{18}\text{O}$	$\delta^{18}\text{O}$	depth (cm)	sampled intervall (cm)	$\delta^{18}\text{O}$	$\delta^{18}\text{O}$
		<i>G. ruber w.</i> >315 μm [‰ VPDB]	<i>G. bulloides</i> 315-400 μm [‰ VPDB]			<i>G. ruber w.</i> >315 μm [‰ VPDB]	<i>G. bulloides</i> 315-400 μm [‰ VPDB]
1450.5	1450-1451		2.32	2075.5	2075-2076	1.72	
1460.5	1460-1461		2.57	2085.5	2085-2086	1.51	
1470.5	1470-1471		2.49	2095.5	2095-2096	1.34	
1480.5	1480-1481		2.43	2105.5	2105-2106	1.55	
1490.5	1490-1491	1.09	2.45	2115.5	2115-2116	1.16	
1500.5	1500-1501	1.36	2.18	2125.5	2125-2126	1.19	
1510.5	1510-1511		2.35	2135.5	2135-2136	1.11	
1520.5	1520-1521	1.10	2.00	2145.5	2145-2146	1.46	
1530.5	1530-1531	1.14	2.05	2155.5	2155-2156	1.38	
1540.5	1540-1541	1.49	2.35	2175.5	2175-2176	1.38	
1550.5	1550-1551	1.23	2.00	2185.5	2185-2186	1.45	
1560.5	1560-1561	0.84	2.29	2195.5	2195-2196	1.33	
1570.5	1570-1571		2.26		2210	1.23	
1580.5	1580-1581		1.95	2210.5	2210-2211	1.27	
1610.5	1610-1611		2.06	2211.5	2211-2212	1.19	
1620.5	1620-1621	1.19	2.18	2212.5	2212-2213	1.21	
1630.5	1630-1631		2.18	2213.5	2213-2214	1.09	
1640.5	1640-1641		2.31	2214.5	2214-2215	1.03	
1650.5	1650-1651		2.57	2215.5	2215-2216	1.37	
1660.5	1660-1661		2.14	2216.5	2216-2217	1.11	
1670.5	1670-1671		2.19	2217.5	2217-2218	1.63	
1680.5	1680-1681		2.20	2218.5	2218-2219	1.47	
1690.5	1690-1691	1.09	2.00	2219.5	2219-2220	1.04	
1700.5	1700-1701	0.93	2.08		2220	1.48	
1710.5	1710-1711		2.36	2222.5	2222-2223	1.27	
1720.5	1720-1721		2.59	2223.5	2223-2224	1.32	
1740.5	1740-1741	1.48	2.36	2224.5	2224-2225	1.32	
1750.5	1750-1751	1.69	2.61	2225.5	2225-2226	1.24	
1760.5	1760-1761	1.60	2.60	2226.5	2226-2227	1.10	
1770.5	1770-1771		2.69	2227.5	2227-2228	1.37	
1780.5	1780-1781	1.46	2.51	2228.5	2228-2229	1.29	
1790.5	1790-1791		2.78	2229.5	2229-2230	1.31	
1800.5	1800-1801	1.71	2.64	2230.5	2230-2231	1.36	
1810.5	1810-1811	1.50	2.55	2231.5	2231-2232	1.24	
1820.5	1820-1821	1.19	2.35	2232.5	2232-2233	1.25	
1830.5	1830-1831		2.36	2233.5	2233-2234	1.14	
1840.5	1840-1841		2.33	2234.5	2234-2235	1.32	
1850.5	1850-1851	1.49	1.97	2235.5	2235-2236	1.07	
1860.5	1860-1861	1.04	1.90	2236.5	2236-2237	1.24	
1870.5	1870-1871	1.20	1.86	2237.5	2237-2238	1.08	
1880.5	1880-1881		1.78	2238.5	2238-2239	1.17	
1890.5	1890-1891	1.41	2.03	2239.5	2239-2240	0.98	
2005.5	2005-2006	1.59		2240.5	2240-2241	0.93	
2015.2				2241.5	2241-2242	0.93	
5	2015-2015,5	1.75		2242.5	2242-2243	0.98	
2025.5	2025-2026	1.36		2243.5	2243-2244	0.93	
2035.5	2035-2036	0.91		2244.5	2244-2245	0.92	
2044.5	2044-2045	1.17		2245.5	2245-2246	0.88	
2051.5	2051-2052	0.96		2246.5	2246-2247	0.83	
2055.5	2055-2056	0.95		2247.5	2247-2248	0.64	
2065.5	2065-2066	1.31					

APPENDIX

MD08-3181				MD08-3181			
depth (cm)	sampled intervall (cm)	$\delta^{18}\text{O}$	$\delta^{18}\text{O}$	depth (cm)	sampled intervall (cm)	$\delta^{18}\text{O}$	$\delta^{18}\text{O}$
		<i>G. ruber w.</i> >315 μm [‰ VPDB]	<i>G. bulloides</i> 315-400 μm [‰ VPDB]			<i>G. ruber w.</i> >315 μm [‰ VPDB]	<i>G. bulloides</i> 315-400 μm [‰ VPDB]
2248.5	2248-2249	0.55		2294.5	2294-2295	0.68	
2252.5	2252-2253	0.99		2295.5	2295-2296	0.78	
2253.5	2253-2254	0.33		2296.5	2296-2297	0.70	
2254.5	2254-2255	0.44		2297.5	2297-2298	0.57	
2255.5	2255-2256	0.46		2298.5	2298-2299	0.62	
2256.5	2256-2257	0.72		2299.5	2299-2300	0.69	
2257.5	2257-2258	0.50		2300.5	2300-2301	0.61	
2258.5	2258-2259	0.50		2301.5	2301-2302	0.70	
2259.5	2259-2260	0.44		2302.5	2302-2303	0.49	
2260.5	2260-2261	0.59		2303.5	2303-2304	0.51	
2261.5	2261-2262	0.55		2304.5	2304-2305	0.34	
2262.5	2262-2263	0.58		2305.5	2305-2306	0.38	
2263.5	2263-2264	0.47		2306.5	2306-2307	0.47	
2264.5	2264-2265	0.32		2307.5	2307-2308	0.39	
2265.5	2265-2266	0.33		2308.5	2308-2309	0.14	
2266.5	2266-2267	0.32		2309.5	2309-2310	0.54	
2267.5	2267-2268	-0.06		2310.5	2310-2311	0.26	
2268.5	2268-2269	0.00		2311.5	2311-2312	-0.06	
2269.5	2269-2270	0.10		2312.5	2312-2313	0.33	
2270.5	2270-2271	0.26		2313.5	2313-2314	0.20	
2271.5	2271-2272	-0.03		2314.5	2314-2315	0.33	
2272.5	2272-2273	-0.07		2315.5	2315-2316	0.21	
2273.5	2273-2274	0.14		2316.5	2316-2317	0.04	
2274.5	2274-2275	-0.04		2317.5	2317-2318		
2275.5	2275-2276	-0.01		2318.5	2318-2319	0.34	
2276.5	2276-2277	0.25		2319.5	2319-2320	-0.10	
2277.5	2277-2278	-0.01		2320.5	2320-2321	0.06	
2279.5	2279-2280	0.73		2321.5	2321-2322	0.15	
2280.5	2280-2281	0.48		2322.5	2322-2323	-0.19	
2281.5	2281-2282	0.41		2323.5	2323-2324	-0.11	
2282.5	2282-2283	0.67		2324.5	2324-2325	0.07	
2283.5	2283-2284	0.80		2325.5	2325-2326	-0.03	
2284.5	2384-2285	0.32		2326.5	2326-2327	-0.07	
2285.5	2285-2286	0.49		2327.5	2327-2328	0.06	
2286.5	2286-2287	0.58		2328.5	2328-2329	-0.00	
2287.5	2287-2288	0.56		2329.5	2329-2330	0.09	
2288.5	2288-2289	0.34		2330.5	2330-2331	0.11	
2289.5	2289-2290	0.61		2331.5	2331-2332	0.20	
2290.5	2290-2291	0.59		2332.5	2332-2333	0.11	
2291.5	2291-2292	0.47		2333.5	2333-2334	0.27	
2292.5	2292-2293	0.27		2334.5	2334-2335	0.58	
2293.5	2293-2294	0.54		2335.5	2335-2336	0.68	

Dipl. Geol. Janne Repschläger
Curriculum vitae

Private Address

Feldstr.76
24105 Kiel
0431 6693636
jrepschlaeger@yahoo.de

Working Address

Institute of Geosciences
Christian-Albrechts-University of Kiel
Ludewig-Meyn-Str. 10
24118 Kiel

Personal Information

Date of Birth: 06.10.1979
Place of Birth: Castrop-Rauxel, Germany
Citizenship: German
Gender: female
status: married, 4 children

Education

Since Jan. 2008	Ph.D. Euromarc AMOCINT Project: "Changes in AMOC over Holocene and previous interglacials- Mg/Ca temperature reconstructions of mixed layer and NADW in the subpolar and subtropical North Atlantic" at the Christian Albrechts University of Kiel
10/2011-11/2012	maternity leave
05/2009-06/2010	maternity leave
2006	Diploma thesis in Geology/ Palaeontology (supervisor: PD Dr. Mara Weinelt) "Chnges in the Demark strait overflow over MIS5e and glacial Inception"
05/2006-07/2006	Maternity leave (during Diploma thesis)
11/2004-04/2005	Maternity leave (during Diploma thesis)
2004	Geological Mapping in the area Vergon East (Southern French Alpes-Provence)
2002	Pre-diploma in Geology/ Palaeontology Christian-Albrechts-University of Kiel/ Germany
2000 – 2006	Studies of Geology/ Palaeontology Christian-Albrechts-University of Kiel/ Germany
1999	Abitur, Abalbert-Stifter-Gymnasium, Castrop-Rauxel
1990-1999	Abalbert-Stifter-Gymnasium, Castrop-Rauxel

Conferences

Repschläger, J.; Balmer, S.; Weinelt, M.; Sarnthein, M.; Andersen, N. and Schwab, C. (2012) Subtropical freshwater event at the onset of younger Dryas. GV & Sediment Meeting, Hamburg, Germany, September 23-28, 2012; Talk.

Repschläger, J.; Weinelt, M.; Kinkel, H.; Andersen, N.; Blanz, T.; Garbe-Schönberg, D. and Schwab, C.; (2011) Differences in Atlantic Meridional overturning circulation over Holocene and MIS5 - indications from the subtropical North Atlantic. Final EUROMARC Conference, Cascais, Portugal, February 7-9, 2011; Talk

Repschläger, J.; Weinelt, M.; Andersen, N.; Garbe-Schönberg, D. and Blanz, T. (2010), Early Holocene Evolution of AMOC: a view from the Central subtropical North Atlantic. 10th International Conference on Paleoceanography, August 29 - September 3rd, 2010; Poster.

Repschläger, J.; Weinelt, M.; Andersen, N. and Garbe-Schönberg D. (2009), Monitoring multi-decadal to multi-centennial variability of AMOC strength in the subtropical Northeast Atlantic over Holocene and Eemian. EGU Assembly 2009, Vienna 19-24 April 2009; Talk.

Repschläger, J.; Weinelt, M.; Andersen, N.; Garbe-Schönberg D. and G. Bartoli (2008), Comparison between interglacial AMOC strength in the Denmark strait and south of the Azores. 1st EUROMARC Conference, September 15-17, 2008; Poster.

Repschläger, J.; Weinelt, M.; Andersen, N.; Garbe-Schönberg D. and G. Bartoli (2005), Evolution of Denmark Strait Overflow over the Eemian and last glacial inception, GeoErlangen 2005, System Earth -Biosphere Coupling Regional Geology of Central Europe, September 24-29, 2005; Talk.

Publications

Schwab, C., Kinkel, H., Weinelt, M., and Repschläger, J. (2012), Coccolithophore paleoproductivity and ecology response to deglacial and Holocene changes in the Azores Current System; *Paleoceanography*, v. 27, p. PA3210.

Schwab, C., Kinkel, H., Weinelt, M., and Repschläger, J. (2012), Paleoenvironmental changes in the Azores region between 130 and 48 ka BP with special emphasizes on MIS 5e, *Quaternary Science Reviews*, resubmitted

Repschläger, J., Weinelt, M., Kinkel, H., Andersen, N., Blanz, N., and Schwab, C. (2014), Response of the central subtropical North Atlantic surface hydrography on Deglacial and Holocene AMOC changes; *Paleoceanography*, v. under revision

Participation on seagoing expeditions

2008	AMOCINT 168 RV Marion Dufresne cruise- core description, core sampling
2002	2002 RV Akademik Lavrentyev 29 cruise Sea of Okhotsk – student assistant pore water chemistry measurements

International experience

autumn 2003 study at University of Bergen, Norway